# GABA-Induced $Ca^{2+}$ Signaling in Rat Hippocampal Astrocytes

Inaugural-Dissertation

zur

Erlangung des Doktorgrades der

Mathematisch-Naturwissenschaftlichen Fakultät

der Heinrich-Heine-Universität Düsseldorf

vorgelegt von

Silke D. Meier

aus Aalen

September 2007

Aus dem Institut für Neurobiologie
der Heinrich-Heine-Universität Düsseldorf

Gedruckt mit der Genehmigung der
Mathematisch-Naturwissenschaftlichen Fakultät der
Heinrich-Heine-Universität Düsseldorf

Referentin: Prof. Dr. C. R. Rose

Koreferent: Prof. Dr. H.-W. Müller

Koreferent: Prof. Dr. A. Reichenbach

Tag der mündlichen Prüfung: 16.01.2008

## Introductory Remarks

Part of my PhD work, carried out in the Institute of Physiology at the LMU Munich and the Institute for Neurobiology at the HHU Düsseldorf, has already been published (Meier et al., 2006) or has been illustrated in manuscripts that are in revision (Bennay et al.) or have been submitted (Kafitz et al.). Therefore, the present work is confined to the description of my most recent study on "GABA-induced $Ca^{2+}$ Transients in Hippocampal Astrocytes". A manuscript describing these results will be submitted for publication in winter 2007. In addition, I included all reprints or submitted manuscripts in the appendix (page 122ff), where I also detail my contributions to each publication.

**Abstract**

GABA ($\gamma$-aminobutyric acid), the predominant inhibitory neurotransmitter in the mature mammalian brain, is excitatory for neurons during early development upon $GABA_A$ receptor activation. In astrocytes, GABA induces intracellular $Ca^{2+}$ transients by activation of both, $GABA_A$ and $GABA_B$ receptors. $GABA_B$ receptor-mediated $[Ca^{2+}]_i$ increases are involved in neuron-glia interaction by potentiating inhibitory synaptic transmission (Kang et al., 1998) and by causing heterosynaptic depression (Serrano et al., 2006). Given that $GABA_B$ receptors couple to $G_{i/o}$ proteins in neurons and inhibit presynaptic $Ca^{2+}$ channels, the observed $[Ca^{2+}]_i$ increase in astrocytes is an unexpected finding. Hence, the aims of the present study were (1) to elucidate the mechanism of GABA-induced $Ca^{2+}$ transients in astrocytes and (2) to establish a developmental profile of astrocytic $Ca^{2+}$ responses. To this end, I performed $Ca^{2+}$ imaging with Fura-2 in combination with whole-cell patch-clamp recordings in acute rat hippocampal slices. For the identification of astrocytes, I adapted a method which had originally been introduced for the identification of cortical astrocytes *in vivo* (Nimmerjahn et al., 2004). Astrocytes were stained with the red fluorescent dye sulforhodamine 101 (SR101). The specificity of SR101 for astrocytes in acute hippocampal slices at young postnatal stages (P03 and P15) was confirmed with electrophysiological recordings. Local pressure application of GABA (100 ms, 1 mM) to SR101-positive cells induced intracellular $Ca^{2+}$ transients, which were mediated by both $GABA_A$ and $GABA_B$ receptors. Muscimol, a specific $GABA_A$ receptor agonist, depolarized astrocytes and resulted in $Ca^{2+}$ influx through voltage-gated $Ca^{2+}$ channels, confirming earlier studies. This mechanism was the same throughout the developmental period investigated (P03 and P15). $GABA_B$ receptor activation, in contrast, resulted in delayed $Ca^{2+}$ transients that were due to G-protein activation and $Ca^{2+}$ release from $IP_3$-sensitive intracellular $Ca^{2+}$ stores. An interaction of $GABA_B$ receptors with metabotropic glutamate receptors, as has been described in the cerebellum (Hirono et al., 2001; Tabata et al., 2004), might also be the case in hippocampal astrocytes. While $GABA_A$R-activation induced $Ca^{2+}$ transients in 70-100% of astrocytes throughout development (P03 to P33$\pm$1), $GABA_B$-R-mediated $Ca^{2+}$ signaling exhibited a clear developmental profile. The amount of astrocytes responding with a $[Ca^{2+}]_i$ increase upon $GABA_B$ receptor-activation showed a bell-shaped distribution with a maximum of 60% of cells responding during the second postnatal week (P11 to P15). This developmental profile of $GABA_B$ receptor-mediated $Ca^{2+}$ transients suggests that astrocytes play a role during postnatal maturation of the hippocampal network.

**Zusammenfassung**

GABA ($\gamma$-Aminobuttersäure), der bedeutendste inhibitorische Neurotransmitter im adulten Gehirn, wirkt während früher Entwicklungsphasen über $GABA_A$-Rezeptoren exzitatorisch auf Neurone. In Astrozyten führt sowohl die Aktivierung von $GABA_A$- als auch $GABA_B$-Rezeptoren zu einer Erhöhung der intrazellulären Kalziumkonzentration ($[Ca^{2+}]_i$). Diese $Ca^{2+}$-Transienten können zur Transmitterfreisetzung führen, weshalb sie bei Glia-Neuron-Interaktionen eine Rolle spielen. Die Aktivierung von $GABA_B$-Rezeptoren in Astrozyten führt zu heterosynaptischer Depression (Serrano et al., 2006) sowie zur Potenzierung inhibitorischer Neurotransmission (Kang et al., 1998). Die durch $GABA_B$-Rezeptoraktivierung entstehenden $[Ca^{2+}]_i$-Erhöhungen in Astrozyten sind ungewöhnlich, da neuronale $GABA_B$-Rezeptoren an $G_{i/o}$-Proteine binden und in Neuronen allenfalls eine $[Ca^{2+}]_i$-Erniedrigung hervorrufen. Die vorliegende Studie hatte die Zielsetzung, den Mechanismus GABA-induzierter $Ca^{2+}$-Signale in Astrozyten des Hippokampus zu ergründen, und die entstehenden $[Ca^{2+}]_i$-Erhöhungen während der postnatalen Entwicklung zu charakterisieren. Hierzu wurden Fluoreszensmessungen mit Fura-2 durchgeführt, sowie elektrophysiologische Methoden angewendet. Für die Identifizierung von Astrozyten wurde eine Methode modifiziert, welche ursprünglich für die Identifizierung von kortikalen Astrozyten *in vivo* eingeführt worden war (Nimmerjahn et al., 2004): Astrozyten in akuten Hirnschnitten von 3 bis 33 Tage alten Ratten wurden durch Färbung mit Sulforhodamin 101 (SR101) identifiziert und die Spezifität von SR101 für Astrozyten mittels elektrophysiologischer Charakterisierung bestätigt. Lokale GABA-Applikationen (100 ms, 100 µM) lösten $[Ca^{2+}]_i$-Erhöhungen in Astrozyten aus, welche sowohl von $GABA_A$- als auch $GABA_B$-Rezeptoren vermittelt wurden. $GABA_A$-Rezeptoraktivierung mit Muscimol depolarisierte Astrozyten und führte zu einem $Ca^{2+}$-Einstrom durch spannungsabhängige $Ca^{2+}$-Kanäle. Dieser Mechanismus blieb während der gesamten Entwicklung erhalten und löste in 70-100% der Astrozyten $Ca^{2+}$-Transienten aus. $GABA_B$-Rezeptoraktivierung führte zu G-Proteinaktivierung und $IP_3$-vermittelter $Ca^{2+}$-Freisetzung aus intrazellulären Speichern. Eine Interaktion zwischen $GABA_B$-Rezeptoren und metabotropen Glutamatrezeptoren, wie im Zerebellum beschrieben (Hirono et al., 2001; Tabata et al., 2004), konnte nicht ausgeschlossen werden. Interessanterweise bestanden bei $GABA_B$-Rezeptor-abhängigen $[Ca^{2+}]_i$-Erhöhungen deutliche Unterschiede während der Entwicklung: Die Anzahl der reagierenden Zellen zeigte eine glockenförmige Verteilung, wobei während der zweiten postnatalen Woche (P11 bis P15) ein Maximum von ca. 60% aller Astrozyten reagierte. Diese Veränderungen implizieren eine Rolle von Astrozyten während der postnatalen Entwicklung neuronaler Netzwerke.

# Contents

## Abbreviations

| | |
|---|---|
| t-ACPD | trans-(1S,3R)-1-Amino-1,3-cyclopentanedicarboxylic acid (metabotropic glutamate receptor group I/II agonist) |
| $AlCl_3$ | aluminium chloride |
| $AlF_4^-$ | aluminium fluoride (G-protein activator) |
| AMPA | $\alpha$-Amino-3-hydroxy-5-methylisoxazole-4-propionic acid (AMPA/kainate receptor agonist) |
| DL-AP5 | DL-2-Amino-5-phosphonovaleric acid (selective NMDA receptor antagonist) |
| ATP | adenosine triphosphate (substrate for ATP-dependent enzyme systems) |
| $Ba^{2+}$ | barium ion |
| Bac | Baclofen ($GABA_B$ receptor agonist) |
| BAPTA | 1,2-Bis(2-aminophenoxy)ethane-N,N,N',N'-tetraacetic acid ($Ca^{2+}$ chelator) |
| Bic | Bicuculline ($GABA_A$ receptor antagonist) |
| BrdU | 5-Bromo-2'-deoxyuridine (Thymidine analog selectively incorporated into cellular DNA during S-phase; marks dividing cells) |
| BSA | bovine serum albumine |
| ℃ | degrees centrigrade |
| CA1; CA3 | cornu ammonis area 1; cornu ammonis area 3 |
| $Ca^{2+}$ | calcium ion |
| $CaCl_2$ | calcium chloride |
| CaM | calmodulin |
| $Cd^{2+}$ | cadmium ion (broad band inhibitor of voltage-gated $Ca^{2+}$ channels and neuronal transmitter release) |
| CGP55845 | (2S)-3-[[(1S)-1-(3,4-Dichlorophenyl)ethyl]amino-2-hydroxy-propyl](phenylmethyl)phosphinic acid (potent, selective $GABA_B$ receptor antagonist ($IC_{50}$ = 6 nM)) |
| CNQX | 6-Cyano-7-nitroquinoxaline-2,3-dione (competitive AMPA/kainate glutamate receptor antagonist) |
| CNS | central nervous system |
| $CO_2$ | carbondioxide |
| CPA | cyclopiazonic acid (inhibitor of the sarco-endoplasmic reticulum $Ca^{2+}$-pump) |

| | |
|---|---|
| CPPG | (RS)-$\alpha$-Cyclopropyl-4-phosphonophenylglycine (potent group II/III mGluR antagonist) |
| DAG | diacylglycerol |
| DIV | days in vitro |
| DMSO | dimethyl sulfoxide |
| DMEM | Dulbecco's Modified Eagle's Medium |
| E | embryonic day |
| EAAC1 | excitatory amino acid carrier 1 (human homolog is EAAT3) |
| EAAT | excitatory amino acid transporter |
| EGTA | Ethylene glycol-bis(2-aminoethylether)-N,N,N',N'-tetra-acetic acid ($Ca^{2+}$ chelator) |
| ENO | early network oscillation |
| ER | endoplasmic reticulum |
| $F_{xxx}$ | fluorescence emission at *xxx* nm |
| Fura-2-AM | Fura-2 acetoxymethyl ester (ratiometric calcium indicator, membrane-permeant form) |
| GABA | $\gamma$-aminobutyric acid (neurotransmitter) |
| $GABA_AR$ | $\gamma$-aminobutyric acid receptor type A (ionotropic) |
| $GABA_BR$ | $\gamma$-aminobutyric acid receptor type B (metabotropic) |
| GAD | glutamate decarboxylase |
| GAT | GABA transporter |
| GDP | giant depolarizing potential |
| GFAP | glial fibrillary acidic protein |
| GFAP-eGFP-mice | transgenic mice, expressing enhanced green fluorescent protein under control of the human GFAP promoter |
| GIRK | G protein-coupled inward rectifying $K^+$ channel |
| GLAST | glutamate-aspartate transporter (human homolog is EAAT1) |
| GLT-1 | glutamate transporter 1 (human homolog is EAAT2) |
| GluR | glutamate receptor |
| GTP | guanosine triphosphate |
| G-protein | guanine nucleotide binding protein |
| HEPES | 4-(2-Hydroxyethyl)piperazine-1-ethanesulfonic acid (pH buffer) |
| HR | HEPES-buffered saline |
| IEG | immediate early genes |
| $IP_3$ | inositol 1,4,5-trisphosphate |
| $K^+$ | potassium ion |

| | |
|---|---|
| KCC2 | $K^+/Cl^-$ co-transporter isoform 2 |
| KCl | potassium chloride |
| $K_d$ | dissociation constant |
| $\lambda$ | wavelength |
| LTP | long-term potentiation |
| M | molar |
| MAPK | mitogen-activated protein kinase |
| MCPG | (RS)-$\alpha$-Methyl-4-carboxyphenylglycine (competitive non-selective group I/II mGluR antagonist) |
| MEK | mitogen-activated/extracellular regulated kinase |
| $MgCl_2$ | magnesium chloride |
| mGluR | metabotropic glutamate receptor |
| $MgSO_4$ | magnesium sulfate |
| mM | millimolar |
| mosm | milliosmol |
| ms | millisecond |
| Musci | muscimol ($GABA_A$ receptor agonist) |
| µl | microliter |
| $Na^+$ | sodium ion |
| NaCl | sodium chloride |
| NaF | sodium fluoride |
| $NaHCO_3$ | sodium hydrogen carbonate |
| $NaH_2PO_4$ | sodium hydrogen phosphate |
| NG2(+) | positive for the chondroitin sulphate proteoglycan NG2 |
| $Ni^{2+}$ | nickel ion (non-selective inibitor of voltage-gated $Ca^{2+}$ channels) |
| NMDA | N-methyl-D-aspartate (agonist at NMDA-type glutamate receptors |
| NR | normal ringer (standard extracellular solution) |
| nm | nanometer |
| $O_2$ | oxygen |
| ORG | outward rectifying glia |
| PAG | phosphate-activated glutaminase |
| PBS | phosphate-buffered saline |
| PC | pyruvate carboxylase |
| $PIP_2$ | phosphatidylinositol 4,5-bisphosphate |

| | |
|---|---|
| PLC | phospholipase C |
| PR | "preparation ringer" (reduced calcium dissection solution) |
| P*xx* | postnatal day *xx* |
| Raf | raf protein kinase |
| Ras | p21 ras guanine nucleotide-binding protein |
| PPADS | 4-[[4-Formyl-5-hydroxy-6-methyl-3-[(phosphonooxy)methyl]-2-pyridinyl]azo]-1,3-benzenedisulfonic acid tetrasodium salt (selective P2 purinoceptor antagonist) |
| RyR | ryanodine receptor |
| s | second |
| SBFI | sodium-binding benzofuran isophthalate |
| SERCA | sarco-endoplasmic reticulum $Ca^{2+}$-ATPase |
| SR101 | sulforhodamine 101 (fluorescent dye) |
| TEA | Tetraethylammonium chloride ($K^+$ channel blocker) |
| TTX | tetrodotoxin (inhibitor of voltage-activated $Na^+$ channels) |

# 1 Introduction

In the present study I characterized GABA-evoked intracellular $Ca^{2+}$ ($[Ca^{2+}]_i$) increases in hippocampal astrocytes at early stages of postnatal development. Accordingly, this introduction aims at briefly reviewing the current knowledge on astrocytes, the hippocampus, and the neurotransmitter GABA, including changes that occur during development. Furthermore, I will detail aspects which have not been resolved, as yet, and I will elucidate the objectives of the present study.

## 1.1 Astrocytes

### 1.1.1 Astrocytes - A Historical Perspective

The neuropathologist Rudolf Virchow first used the word "neuroglia" (in German "Nervenkitt", derived from the greek word for glue) in 1856 to describe "connective tissue" in the central nervous system (CNS). Neuroglia, at that point, was assumed to merely shape the brain and hold neurons together. The word "astrocyte" first appeared around 1913 and was used by Ramón y Cajal to refer to fibrous and protoplasmic glia found in white and grey matter, respectively (Somjen, 1988; Kimelberg, 2004). In the 1920s two other glial cell types, oligodendrocytes and microglia, were identified. Oligodendrocytes, like astrocytes, are of ectodermal origin. Their main function is to build the myelin sheath of neurons (Haydon, 2001). Microglial cells, on the other hand, are of mesodermal origin and are the immunocompetent cells of the CNS (Farber and Kettenmann, 2005).

The first functions attributed to astrocytes, besides providing neurons with structural support, were of metabolic nature. It has been confirmed that astrocytes are involved in providing neurons with nutrients and a desirable ionic milieu, maintaining the blood-brain-barrier, as well as taking-up neurotransmitters (for review see Ransom et al., 2003). In the 1970s, neu-

rotransmitter receptors were found on astrocytes, but it took until the late 1980s to identify their physiological relevance. Since the 1990s it is well accepted that astrocytes respond to neurotransmitter, spilling over from neuronal synapses (see Fiacco and McCarthy, 2006, for review).

One reason for not recognizing glial cells as actively involved in the communication of the brain earlier was their inability to communicate via action potentials as neurons do. However, astrocytes are far from being silent. Activation of neurotransmitter receptors on astrocytes, in many cases, results in transient increases in their $[Ca^{2+}]_i$ (Jensen and Chiu, 1990; Nilsson et al., 1993; Pasti et al., 1997; Araque et al., 2002). These $[Ca^{2+}]_i$ increases might even spread as a $Ca^{2+}$ wave within the astrocytic network (Cornell-Bell et al., 1990; Verkhratsky et al., 1998). Such $[Ca^{2+}]_i$ increases can trigger the release of neurotransmitters from astrocytes and thereby enable astrocytes to modulate neuronal transmission (Araque et al., 1998; Perea and Araque, 2005; Pasti et al., 2001; Parpura et al., 1994; Zonta and Carmignoto, 2002). Other, more recent, findings include glial involvement in the control of synapse formation and function (Ullian et al., 2004) as well as adult neurogenesis (Gaughwin et al., 2006) and brain vascular tone (Zonta et al., 2003a; Volterra and Meldolesi, 2005; Gordon et al., 2007; Winship et al., 2007).

Along with the new roles of astrocytes identified under physiological conditions, alterations in astrocyte functions became obvious during pathological conditions (Seifert et al., 2006; Bachoo et al., 2004). Originally changes in astrocyte function, observed in brain pathologies, had been assumed to be secondary to changes in neuronal transmission. This view, however, was challenged by recent findings, which imply a role of astrocytes in the pathogenesis of CNS disorders such as gliomas, amyotrophic lateral sclerosis, and chronic temporal lobe epilepsy (Tashiro et al., 2002; Tian et al., 2005; Sontheimer, 2003; Volterra and Meldolesi, 2005; Holden, 2007; Nagai et al., 2007).

Interestingly, antiepileptic drugs reduce the ability of astrocytes to transmit $Ca^{2+}$ signals, leading to the conclusion that astrocytes, besides being involved in the genesis of epilepsy, are a key player in the pathways targeted by current antiepileptic drugs (Tian et al., 2005; Barbaro et al., 2004). Thus, better knowledge of astrocyte function and disfunction, might lead to future development of astrocyte-specific drugs, which likely will have fewer side effects (Tian et al., 2005).

### 1.1.2 The Problem of Astrocyte Identity

Astrocytes are small cells of 8 to 10 µm diameter with several small processes, often extending towards blood vessels (figure 12; Nimmerjahn et al., 2004; Zerlin and Goldman, 1997). Because morphological characteristics are not sufficient for clearly distinguishing astrocytes from other cell types, biochemical characteristics have been included in the definition. Traditionally, all cells containing intermediate filaments consisting of glial fibrillary acidic protein (GFAP) were considered astrocytes (Kimelberg, 2004; Nolte et al., 2001). Accordingly, the main method for identifying astrocytes has commonly been immunohistochemistry using antibodies directed against GFAP. In addition to GFAP, the $Ca^{2+}$ binding protein S100$\beta$ and the astrocyte-specific glutamate transporters glutamate-aspartate transporter (GLAST) and glutamate transporter 1 (GLT-1; Danbolt, 2001) have been used as protein markers to identify astrocytes in immunohistochemical studies (Raponi et al., 2007; Zhou et al., 2006; Namba et al., 2005; Liu et al., 2006). However, immunohistochemical studies are time-consuming and can only be performed in fixed tissue after performing physiological experiments.

For the identification of astrocytes in vital tissue, transgenic mice, expressing enhanced green fluorescent protein under control of the human GFAP promoter, can be used (GFAP-eGFP-mice, Nolte et al., 2001). Typically two distinct astrocyte populations can be identified in these mice:

firstly, gap-junction coupled protoplasmic astrocytes with high GFAP expression; and secondly, fibrous astrocytes with low GFAP content and additional expression of S100$\beta$ (Nolte et al., 2001; Wallraff et al., 2004; Matthias et al., 2003).

However, the use of GFAP as a marker for the identification of astrocytes is being challenged by findings that the level of GFAP expression not only varies among astrocytes but also changes during development (Verkhratsky et al., 1998). In addition, subtypes of astrocytes do not express GFAP (Walz and Lang, 1998; Walz, 2000) and GFAP expression is upregulated upon injury (Nolte et al., 2001; Walz and Lang, 1998). Further problems arise because molecular markers that clearly distinguish astrocytes from astrocyte precursor cells are still lacking (Zhou and Kimelberg, 2001), and many of the molecules are also expressed by cells of the neuronal lineage. In addition, astrocytes are a highly plastic cell type and astrocytes of different brain regions differ considerably concerning their gene expression profile (Bachoo et al., 2004). Thus, a combination of measures is required to clearly define and identify astrocytes (Kimelberg, 2004). This combination might consist of morphological, biochemical, and electrophysiological characteristics.

When carrying out electrophysiological recordings, astrocytes are characterized by their lack of action potential generation upon depolarization (Zhou et al., 2006). Similar to the GFAP-eGFP-mice, two subtypes of astrocytes can generally be identified according to their electrophysiological properties (Steinhauser et al., 1994; Kressin et al., 1995; Walz, 2000). In the hippocampus, the protoplasmic cells with high GFAP content seem to correspond to electrophysiologically "passive" cells; and the fibrous cells with low GFAP content have a "complex" current pattern (Matthias et al., 2003; Wallraff et al., 2004; Grass et al., 2004).

Complex cells (Steinhauser et al., 1994; Kressin et al., 1995) typically express voltage-gated delayed outward rectifyer $K^+$ currents (Nolte et al.,

2001), inward rectifying $K^+$ currents, as well as inactivating currents resembling A-type $K^+$ currents (Grass et al., 2004; Steinhauser et al., 1994; Walz, 2000). In addition most of these cells express small voltage-dependent $Na^+$ currents (Schools et al., 2003; Matthias et al., 2003). Hence, complex cells closely resemble outward rectifying glia (ORG) described by others (Schools et al., 2006; Grass et al., 2004). They typically lack gap junction coupling (Wallraff et al., 2004) and, in comparison to passive cells (see below), ORGs have a less negative resting membrane potential (-45 ±17.2 mV), a higher input resistance (870 ±705.7 MΩ), and a lower membrane capacitance (24.5 ±15.4 pF; Zhou et al., 2006).

This cell type has been shown to express ionotropic glutamate receptor currents, but no glutamate transporter currents (Zhang, 2001; Zhou and Kimelberg, 2001; Matthias et al., 2003). However, a large proportion of ORGs (83%) express transcripts of astrocyte-specific glutamate transporters (GLT-1 and GLAST), and moreover, 44% also express the neuronal glutamate transporter EAAC-1 (Matthias et al., 2003). To make the story even more complicated, some of these cells express NG2 immunoreactivity (Matthias et al., 2003), a marker commonly expressed by oligodendrocyte precursor cells (Kimelberg, 2004). Hence, ORGs seem to be a much more heterogeneous cell population than formerly thought. During development ORGs amount to roughly 70% of glial cells in the hippocampal CA1 region at P1 and are almost non-existent at P22. Accordingly they have been considered astrocyte precursor cells (Kressin et al., 1995; Walz, 2000; Zhou et al., 2006). Considering that ORGs share protein markers with neurons and oligodendrocytes, they might also be precursors for these cell types, though being positive for GFAP (Zhou et al., 2006).

Passive cells, above all else, express a large voltage- and time-independent potassium conductance. Further electrophysiological properties of passive cells are a highly negative resting membrane potential (-72.8

±8.3 mV), close to the equilibrium potential for $K^+$, as well as a low input resistance (6.3 ±12.2 MΩ), and high capacitance (2897.7 ±13041 pF) due to gap junction coupling (Zhou et al., 2006; Schools et al., 2006). Passive cells lack ionotropic glutamate receptors but express functional glutamate transporters. Thus, they are well-suited for taking-up glutamate which has been released into the synaptic cleft (Bergles and Jahr, 1997; Rothstein et al., 1996, Bennay et al., see appendix page 133). In conclusion, passive cells are commonly considered "classical", mature astrocytes (Steinhauser et al., 1994; Zhou et al., 2006; Schools et al., 2006). In addition, these passive astrocytes express metabotropic glutamate receptors as well as receptors for GABA, ATP, and others (see below). During development passive astrocytes appear around P4 and their amount increases gradually until they make up roughly 90% of glial cells at P22 (Zhou et al., 2006).

Recently, a new method for the identification of astrocytes has been introduced *in vivo*: cortical cells, which (1) had a morphology typical for protoplasmic astrocytes, (2) were gap-junction coupled, and (3) overlapped with GFAP-positive cells in GFAP-eGFP-mice were found to stain specifically with the fluorescent indicator dye sulforhodamine 101 (SR101; Nimmerjahn et al., 2004) . In addition, SR101-labeled cells in the molecular layer of the hippocampus exhibited passive membrane properties (Jourdain et al., 2007), typical for mature astrocytes (Steinhauser et al., 1994; Schools et al., 2006). These results indicate that staining with SR101 might be useful for the identification of classical astrocytes in acute hippocampal slices.

In the present study, this technique was adapted for use in acute hippocampal slices of newborn (P03), juvenile (P07 to P15), and adult rats (P21 and P33±1). The astrocytic identity of SR101-positive cells was confirmed with electrophysiological recordings, in which SR101-positive cells in the stratum radiatum did not express voltage-gated $Na^+$ channels (see also results; and Kafitz et al., appendix page 123ff) and had properties typical

for classical astrocytes (cf. Schools et al., 2006).

### 1.1.3 $Ca^{2+}$ Signaling in Astrocytes

$Ca^{2+}$ is an important intracellular messenger, controlling a variety of cellular functions (for review, see Petersen, 2005; Carafoli, 2002; Verkhratsky et al., 1998). Cellular responses mediated by $Ca^{2+}$ can be in a short (microseconds to milliseconds), intermediate (seconds to minutes) or long (hours to days) time range and often last much longer than the initial $Ca^{2+}$ transients. In a short time range $Ca^{2+}$ triggers transmitter release and directly changes the agonist affinity of receptors and ion channels. In the case of the $GABA_B$ receptor, lack of extracellular $Ca^{2+}$ decreases the affinity of the receptor to GABA, but not to baclofen (Wise et al., 1999). Similarly the affinity of the ryanodine and $IP_3$ receptors depend on $[Ca^{2+}]_i$ (Berridge et al., 2003; Hamilton, 2005). In the intermediate time range, $Ca^{2+}$ regulates the functional activity of enzymes, such as calmodulin-dependent protein kinase, protein phosphatase, and adenylate cyclase, resulting in protein phosphorylation or dephosphorylation (see also figure 1). Long-term effects of $Ca^{2+}$ are largely due to modulation of gene expression (1) by directly interacting with transcription factors or (2) by activating small guanine nucleotide-binding proteins (Ras proteins), leading to modulation of gene expression by triggering phoshorylation events (Finkbeiner and Greenberg, 1996; Verkhratsky et al., 1998).

The extracellular concentration of free $Ca^{2+}$ is in the millimolar (1-2 mM) range and the concentration in intracellular stores, as for example the endoplasmic reticulum (ER), is in the high micromolar range ($\sim$100 to 150 µM; Golovina and Blaustein, 2000; Berridge et al., 2000). In contrast, the concentration of free $Ca^{2+}$ in the cytosol $[Ca^{2+}]_i$ is very low, typically between 50 and 200 nM (Verkhratsky et al., 1998). There are two main pathways mediating cytosolic $[Ca^{2+}]$ increases in astrocytes: (1) influx from

the extracellular space and (2) release from intracellular stores (figure 1; see Verkhratsky et al., 1998, for review).

In general, $Ca^{2+}$ influx from the extracellular space is mediated by voltage-gated $Ca^{2+}$ channels, $Ca^{2+}$-permeable ligand-gated ("ionotropic") channels, and nonspecific cation channels ("store-operated channels") in the plasma membrane. Release from intracellular stores, such as the ER, is triggered by activation of metabotropic receptors and is considered the primary mechanism for increasing $[Ca^{2+}]_i$ in astrocytes (Berridge, 1997; Verkhratsky et al., 1998). Many different neurotransmitter receptors are coupled to heterotrimeric $G_{q/11}$ proteins (consisting of $G_\alpha$ and $G_{\beta\gamma}$ subunits) and stimulate the release of $Ca^{2+}$ from intracellular stores. Upon receptor activation, the G-protein is cleaved and typically $G_\alpha$ activates phospholipase C (PLC; Wettschureck and Offermanns, 2005). PLC cleaves phosphatidylinositol 4,5-bisphosphate ($PIP_2$) into inositol 1,4,5-trisphosphate ($IP_3$) and diacylglycerol (DAG). $IP_3$ then binds to the $IP_3$ receptor ($IP_3R$) on the ER membrane and triggers the efflux of $Ca^{2+}$ from the ER lumen into the cytosol (Verkhratsky et al., 1998).

A second mechanism releasing $Ca^{2+}$ from intracellular stores is mediated by ryanodine receptors (RyR; Berridge et al., 2000) and is denoted $Ca^{2+}$-induced $Ca^{2+}$ release. In astrocytes, this signaling cascade triggers $Ca^{2+}$ release from a spacially separated compartment in the ER (Golovina and Blaustein, 2000).

To prevent cytotoxicity, cells have to employ mechanisms that reduce the $[Ca^{2+}]_i$ to basal levels (Guerini et al., 2005). Plasma membrane bound $Ca^{2+}$ pumps transport $Ca^{2+}$ back to the extracellular space and into intracellular compartments such as the ER (sarco-endoplasmic reticulum $Ca^{2+}$ ATPase, SERCA); and in addition, $Na^+$ / $Ca^{2+}$ exchangers replace intracellular $Ca^{2+}$ with extracellular $Na^+$ (Blaustein and Lederer, 1999; Golovina et al., 1996). $Ca^{2+}$ binding proteins, for instance calmodulin or calbindin,

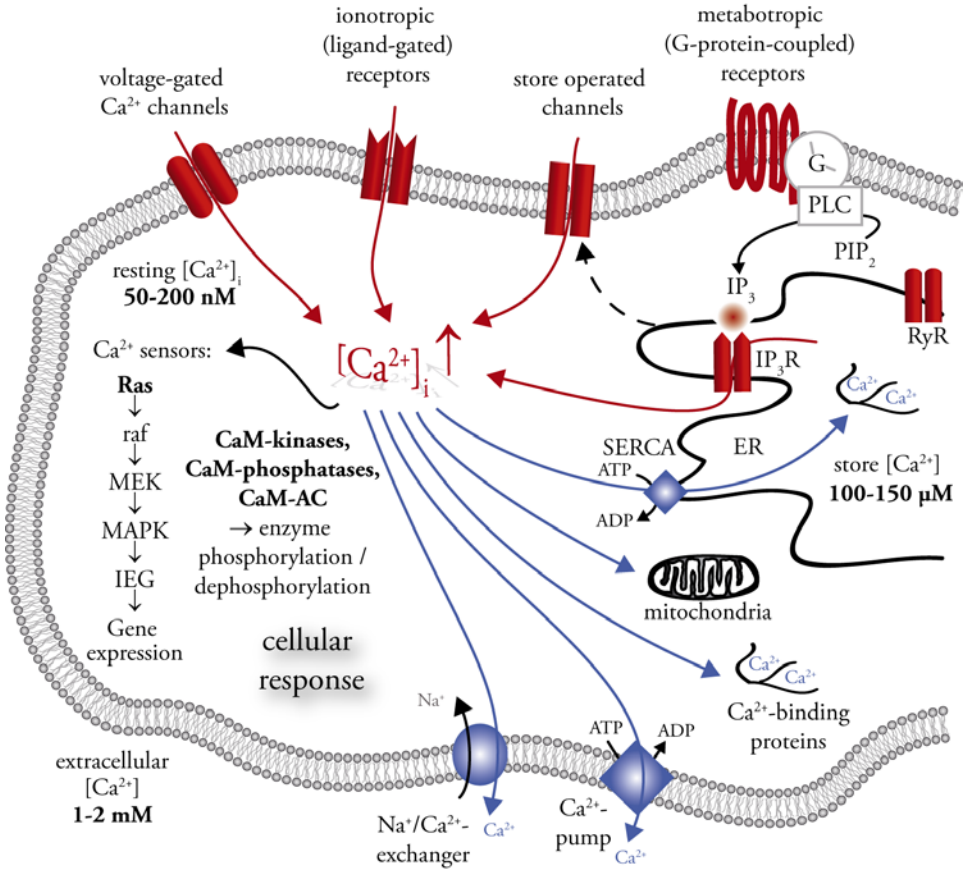


**Figure 1: Scheme illustrating $Ca^{2+}$ Homeostasis and Signaling Cascades in Astrocytes**

$Ca^{2+}$ homeostasis in astrocytes is very complex. $Ca^{2+}$ influx and release pathways are shown in red. In classical astrocytes, $[Ca^{2+}]_i$ increases are primarily due to $Ca^{2+}$ release from intracellular stores upon activation of metabotropic receptors. Cellular actions are in a short, intermediate or long time range, and include changes in enzyme activity upon phosphorylation or dephosphorylation as well as changes in gene expression. Mechanisms reducing $[Ca^{2+}]_i$ to basal levels are shown in blue and mainly rely on $Ca^{2+}$ pumps and the $Ca^{2+}/Na^{+}$ exchanger. See text for further details; after Verkhratsky et al. (1998).

ER, endoplasmic reticulum; G, heterotrimeric G protein; $IP_3$(R), inositol 1,4,5-trisphosphate (receptor); $PIP_2$, phosphatidylinositol 4,5-bisphosphate; PLC, phospholipase C; RyR, ryanodine receptor / $Ca^{2+}$-gated $Ca^{2+}$ channel; SERCA, sarco-endoplasmic reticulum $Ca^{2+}$-ATPase.
**$Ca^{2+}$ sensors**: CaM, calmodulin; CaM kinase, $Ca^{2+}$/calmodulin-dependent protein kinase; CaM AC, $Ca^{2+}$/calmodulin-dependent-adenylate cyclase; CaM-phosphatase, $Ca^{2+}$/calmodulin-dependent-protein phosphatase; Ras, p21ras guanine nucleotide-binding proteins; Raf, raf protein kinase; MEK, mitogen-activated/extracellular regulated kinase; MAPK, mitogen-activated protein kinase; IEG, immediate early genes.

bind $Ca^{2+}$ once it enters the cytosol and consequently, by buffering $Ca^{2+}$, shape both amplitude and time course of $Ca^{2+}$ transients (Berridge et al., 2003; Barski et al., 2003).

Astrocytes can respond to many different neurotransmitters, neurohormones and neuromodulators with increases in $[Ca^{2+}]_i$ (for review see Verkhratsky et al., 1998). In comparison to electrical information processing by neurons, $Ca^{2+}$ signaling in astrocytes is some orders of magnitude slower and might even be several seconds delayed, in particular when metabotropic receptors are involved (Wang et al., 2006; Kang et al., 1998). Glutamate receptor activation can result in periodic $[Ca^{2+}]_i$ increases (Parri and Crunelli, 2001; Zonta and Carmignoto, 2002; Haydon and Carmignoto, 2006) in astrocytes. By changing the frequency of these $Ca^{2+}$ oscillations, astrocytes discriminate between different levels and patterns of synaptic activity (Zonta and Carmignoto, 2002; Haydon and Carmignoto, 2006). However, $Ca^{2+}$ oscillations in astrocytes also occur independent of neuronal activity (Nett et al., 2002) and may influence neuronal networks by triggering the release of glutamate (Parri and Crunelli, 2001).

In addition to displaying oscillatory activity, $[Ca^{2+}]_i$ increases have been reported to propagate within astrocytes (intracellular $Ca^{2+}$ wave) and even to neighboring cells within the astrocytic network (intercellular $Ca^{2+}$ wave Cornell-Bell et al., 1990; Verkhratsky and Kettenmann, 1996). The two main hypotheses explaining intercellular $Ca^{2+}$ waves are (1) $IP_3$ diffusion through gap junctions and (2) ATP release and extracellular diffusion to adjacent cells (Schipke et al., 2002; Peters et al., 2003), both of which in a regenerative or non-regenerative fashion cause $[Ca^{2+}]_i$ increases in neighboring astrocytes. In astrocytes in acute slices $Ca^{2+}$ transients are often localized to cellular microdomains and if they spread to neighboring cells (Schipke et al., 2002), the range is severely reduced compared to cultures (Haydon and Carmignoto, 2006; Nett et al., 2002; Parri and Crunelli, 2001).

This discrepancy has been attributed to a faster cleavage of ATP into the inhibitory adenosine by extracellular endonucleotidases in the intact tissue (Haydon and Carmignoto, 2006).

The range over which astrocytic $Ca^{2+}$ waves travel *in vivo* is not known in detail. In the cortex, astrocytic $Ca^{2+}$ transients are observed *in vivo* (Aguado et al., 2002; Nimmerjahn et al., 2004) and astrocytic activity is correlated (Hirase et al., 2004), however, spontaneous $Ca^{2+}$ waves merely spread to a few neighboring astrocytes (Nimmerjahn et al., 2004). The hippocampus, due to its location, is difficult to assess *in vivo* with the current techniques. Given that each astrocyte in the hippocampus contacts up to 140,000 synapses (Bushong et al., 2002), release of glutamate from a single astrocyte might synchronize neuronal activity (see section 1.1.4 Angulo et al., 2004) without a $Ca^{2+}$ wave travelling through the astrocytic network.

### 1.1.4 Neuron-Glia and Glia-Neuron Interaction

Astrocytes are located in close proximity to neuronal synapses. In area CA1 of the hippocampus, two thirds of the axon-dendritic spines are associated with processes of astrocytes (Ventura and Harris, 1999; Witcher et al., 2007). This spatially close relationship with sites of neuronal transmitter release puts astrocytes into a perfect position not only for taking up neurotransmitter (Bergles and Jahr, 1997, Bennay et al., see appendix page 133ff), but also for modulating synaptic transmission (Auld and Robitaille, 2003). Besides expressing neurotransmitter transporters, astrocytes express a plethora of neurotransmitter receptors (Verkhratsky et al., 1998) which enables them to respond to neuronal activity with increases in their $[Ca^{2+}]_i$ (Porter and McCarthy, 1996; Schipke and Kettenmann, 2004).

In addition to their close association with neuronal synapses, astrocytic processes form endfeet on brain capillaries and arterioles (Haydon and Carmignoto, 2006; Schipke and Kettenmann, 2004). Active neurons have a

higher energy and oxygen demand than inactive ones, which is why blood flow is generally inreased locally in areas of increased activity - a mechanism called functional hyperemia (Fiacco and McCarthy, 2006; Winship et al., 2007; Zonta et al., 2003a). Because the neuronal network is not in direct contact with the vascular system, an intermediate system is needed which senses neuronal activity and relays this information to the brain microcirculation (Haydon and Carmignoto, 2006).

Glutamate-mediated $Ca^{2+}$ oscillations in astrocytes not only correlate with neuronal activity but also regulate the secretion of vasoactive substances by astrocytes (Zonta et al., 2003b). In brain slices, both vasodilation mediated by prostaglandin $E_2$ (cyclooxygenase 1 pathway; Zonta et al., 2003a) and vasoconstriction by 20-hydroxyeicosatetraenoic acid (phospholipase $A_2$-arachidonic acid pathway; Mulligan and MacVicar, 2004) have been described. Takano et al. (2006) in a very elegant set of experiments *in vivo* showed that increasing $[Ca^{2+}]_i$ in astrocytic endfeet reversibly increases arteriole diameter. Hence, by sensing neuronal activity and passing this information on to blood vessels, astrocytes interconnect two systems which otherwise would not be connected (see also Fellin and Carmignoto, 2004; Gordon et al., 2007; Haydon and Carmignoto, 2006; Winship et al., 2007).

Besides releasing vasoactive substances, astrocytes can actively influence the neuronal network by releasing neuroactive substances (Parri and Crunelli, 2001; Haydon, 2001). These substances, also referred to as "gliotransmitters", include classical neurotransmitters such as glutamate and GABA (Liu et al., 2000) but also ATP, D-serine, hormones and nitric oxide (Haydon and Carmignoto, 2006; Schipke and Kettenmann, 2004).

Physiological $[Ca^{2+}]_i$ increases in astrocytes trigger the release of glutamate by vesicular exocytosis (Bezzi et al., 2004; Chen et al., 2005; Jourdain et al., 2007; Zhang et al., 2004; Domercq et al., 2006; Parpura et al., 1994).

However, other release mechanisms such as hemi-channels (Ye et al., 2003), anion transporters and $P2X_7$ receptors (Duan et al., 2003) may also play a role (Haydon and Carmignoto, 2006).

$Ca^{2+}$-dependent glutamate release by astrocytes (Bezzi et al., 2004), resulting in modulation of the neuronal network, has been observed both in cultures (Araque et al., 1998; Parpura et al., 1994) and in acute brain slices (Fiacco and McCarthy, 2004; Jourdain et al., 2007). However, not every $Ca^{2+}$ transient in astrocytes triggers the release of neuroactive substances (Fiacco et al., 2007). More work needs to be carried out to determine the circumstances and prerequisites of gliotransmitter release by astrocytes under physiological conditions.

By releasing glutamate, astrocytes synchronize populations of neurons, which themselves are not connected (Angulo et al., 2004; Carmignoto and Fellin, 2006). Moreover, astrocytes can control synaptic strength: at excitatory synapses between perforant path afferents and granule cells in the dentate gyrus, glutamate, released from astrocytes, activates extrasynaptic N-methyl-D-aspartate (NMDA) receptors of granule cells and consequently increases synaptic transmitter release (Jourdain et al., 2007).

Astrocytes not only excite neurons but also potentiate inhibitory synaptic transmission by release of glutamate. GABA, released from interneurons in the hippocampus, causes $GABA_B$ receptor-dependent $[Ca^{2+}]_i$ increases in astrocytes. These $[Ca^{2+}]_i$ increases trigger the release of glutamate by astrocytes, which activates NMDA receptors on inhibitory interneurons and consequently causes an increase in the frequency of miniature inhibitory postsynaptic currents (mIPSC) in CA1 pyramidal neurons (Kang et al., 1998, see also section 1.3.2; and figure 6).

In the hippocampus, strengthening a population of synapses is associated with a depression of inactive neighboring synapses, a phenomenon called heterosynaptic depression (Lynch et al., 1977; Scanziani et al., 1996).

Such a depression of synaptic connections increases the contrast between potentiated and inactive synapses (Lynch et al., 1977) and is necessary to ensure stable transmission within the neuronal network (Abbott and Nelson, 2000). Astrocytes contribute to both homo- and heterosynaptic depression by release of ATP (see also section 1.3.2; Pascual et al., 2005; Zhang et al., 2003; Serrano et al., 2006). Because ATP is quickly degraded to the inhibitory adenosine by extracellular endonucleotidases, adjacent synapses are inhibited (Pascual et al., 2005; Zhang et al., 2003). Both potentiation of inhibitory synaptic transmission and heterosynaptic depression are mediated by astrocytic $GABA_B$ receptors and will be discussed in more detail in section 1.3.2.

Importantly, astrocytes are not only involved in modulation of synaptic transmission, but also influence the morphological and functional maturation of the neuronal network. Astrocytes can stimulate neurogenesis from oligodendrocyte precursor cells (Gaughwin et al., 2006) and adult neural stem cells (Song et al., 2002). Moreover, they can function as precusor cells for neurons themselves (Ma et al., 2005; Kriegstein, 2005), and are involved in synaptogenesis (Slezak and Pfrieger, 2003; Elmariah et al., 2005). During development astrocytes increase the number of mature, functional synapses on neurons (Ullian et al., 2001) and are required for maintenance of synaptic strength *in vitro* (Beattie et al., 2002).

## 1.2 The Hippocampus

The hippocampus is an area of the brain involved in learning and memory. Notably, its function is not information storage, but processing and consolidation of information which is stored in other brain areas (Lavenex et al., 2007). The hippocampus, a paired structure, which is located in the medial temporal lobe of each hemisphere is part of the limbic system. Together with its neighboring cortical regions, the dentate gyrus, entorhinal cortex

and subiculum, the hippocampus composes the "hippocampal formation".

Neuronal cell bodies are organized in distinct layers and the hippocampal network remains largely intact when the hippocampus is cut into sections perpendicular to its long axis (see also figures 2 and 7 on pages 2 and 36, respectively). The hippocampus receives and integrates inputs via the so-

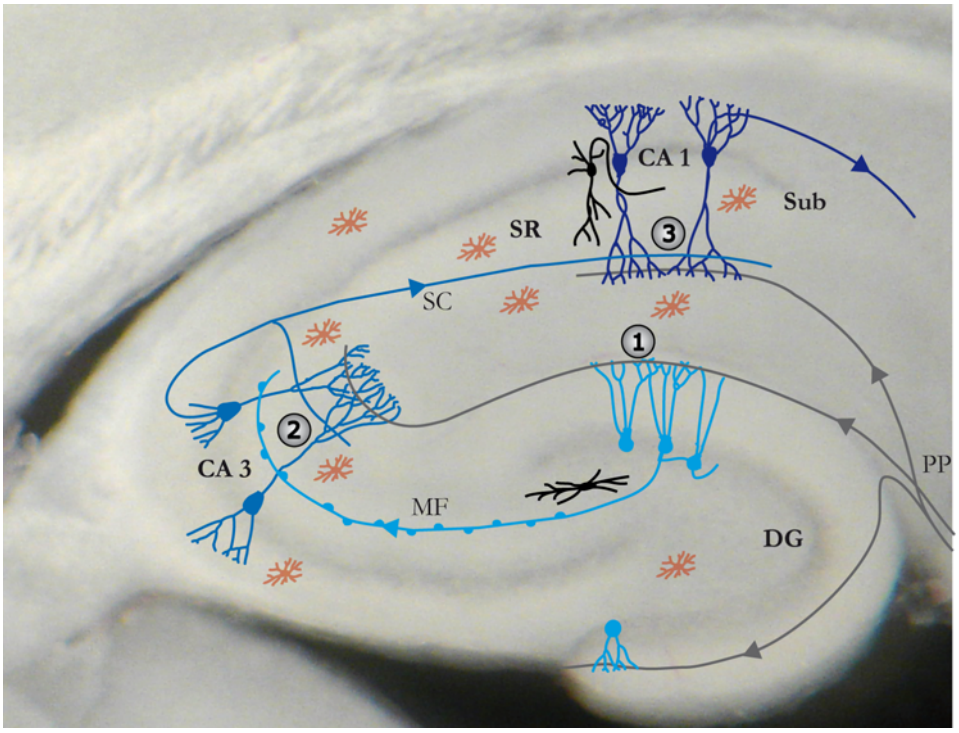


**Figure 2: The Trisynaptic Hippocampal Network Remains Largely Intact in Brain Slice Preparations**

Axons from pyramidal cells in the entorhinal cortex project via the perforant path (PP) to dentate gyrus (DG) granule cells (blue; **1**). Axons of granule cells are called mossy fibers (MF) and form glutamatergic synapses with CA3 pyramidal cells (light blue; **2**). CA3 pyramidal cells finally project as excitatory Schaffer collaterals (SC) to apical dendrites of CA1 pyramidal cells (dark blue; **3**) and from here via the Subiculum (Sub) back to deep layers of the entorhinal cortex. Astrocytes (red) and inhibitory interneurons (black) modulate information processed by the principal cells.

CA1 and CA3, cornu ammonis (hippocampus) area 1 and 3, respectively; SR, stratum radiatum.

called trisynaptic circuit described in the following (figure 2). First, axons

from the entorhinal cortex are projecting as the perforant path to dentate gyrus granule cells. Second, granule cell axons, called mossy fibers, form synapses with pyramidal cells in the CA3 region of the hippocampus. Finally, Schaffer collaterals, the axons of CA3 pyramidal neurons, contact apical dendrites of CA1 pyramidal cells, whose axons project back to deep layers of the entorhinal cortex. In addition, morphologically diverse inhibitory interneurons and astrocytes modulate information processed by pyramidal and granule cells.

The hippocampal network, similar to other brain regions, is not yet fully developed at birth (Lavenex et al., 2007): (1) glutamatergic synaptic signals are exclusively NMDA receptor mediated, since functional AMPA receptors are not present until the end of the first postnatal week (Leinekugel, 2003); (2) $GABA_A$ receptor activation is excitatory until around P15 in most neurons (see also section 1.3.1; Garaschuk et al., 1998); and (3) postsynaptic inhibition mediated by $GABA_B$ receptors is not functional (see section 1.3.1; Gaiarsa et al., 1995).

Spontaneous oscillatory activity is present during all developmental stages and adulthood but varies in duration and frequency (see below; Ben-Ari, 2001; Rivera et al., 2005; Leinekugel, 2003). Giant depolarizing potentials (GDPs; Ben-Ari, 2001), also referred to as early network oscillations (ENOs; Garaschuk et al., 1998), are responsible for most of the synaptic activity in immature neurons. At these early stages of development (P1 to ∼P10, in rats), the neuronal firing pattern is generally of longer duration (0.5-3 s) and slower frequency (about 0.1 Hz; Ben-Ari, 2001). Neuronal discharges are associated with $Ca^{2+}$ oscillations in the entire population of pyramidal neurons and interneurons (Garaschuk et al., 1998). This pattern disappears around P10 while adult patterns, ripples (150-200 Hz) or theta (5-10 Hz) with superimposed gamma (30-80 Hz) oscillations, appear progressively during the second postnatal week (Leinekugel et al., 2002).

During development, neurogenesis (embryonic day (E) 12 to birth, in rats) precedes the development of astrocytes, and oligodendrocytes are the last cell type to develop (Rowitch, 2004). The described patterns of oscillatory activity change in parallel with the maturation of the neuronal network. At birth, 80% of CA1 pyramidal neurons do not exhibit dendrites or synaptic connections (Ben-Ari, 2001). As the network matures, the dendritic tree increases and GABAergic and glutamatergic synapses form sequentially (Ben-Ari, 2002). Hence, GDPs are largely mediated by $GABA_A$ receptor activation. GABA is still excitatory at that point in development (see section 1.3.1) and acts in synergy with NMDA receptor activation. At the end of the second postnatal week, axons and dendrites reach adult-like characteristics (Ben-Ari, 2001), glutamatergic synapses are formed, and GABA is becoming inhibitory.

The ability of the brain to change in structure and function is referred to as plasticity (Lledo et al., 2006). In the hippocampus, homo- and heterosynaptic forms of plasticity are encountered. While in homosynaptic plasticity, such as long-term potentiation (LTP), active inputs are potentiated, inputs other than the potentiated synapses are modulated in heterosynaptic plasticity (Bailey et al., 2000). In addition to synaptic plasticity, adult neurogenesis is regarded as a form of plasticity as well, considering that new neurons are integrated into the existing neuronal network (Lledo et al., 2006).

Besides the olfactory bulb, the hippocampus is the only brain region in mammals, including humans, in which adult neurogenesis occurs (Doetsch et al., 1999; Doetsch, 2003; Seri et al., 2001; Laywell et al., 2000; Zhang, 2001). In the subgranular zone (SGZ) of the hippocampal dentate gyrus, new neurons are generated throughout life from GFAP-positive progenitor cells (Seri et al., 2001; Ganat et al., 2006). Interestingly, neuronal maturation in adult hippocampus closely resembles hippocampal development (Esposito et al., 2005; Piatti et al., 2006). The functional significance of

the integration of new neurons into the hippocampal network is not known in detail. Excitatory activity promotes neuron production from progenitor cells (Deisseroth et al., 2004), and it is likely that adult neurogenesis aids the organism in adapting to its ever changing environment (Lledo et al., 2006).

## 1.3 The Neurotransmitter GABA

### 1.3.1 Effects of GABA on Neurons

The neurotransmitter $\gamma$-aminobutyric acid (GABA, figure 3) is the predominant inhibitory neurotransmitter in the mature mammalian CNS. The cellular actions of GABA are mediated by both ionotropic ($GABA_A$ and $GABA_C$) and metabotropic ($GABA_B$) receptors (Kaila, 1994; Chebib and Johnston, 1999; Bettler et al., 2004).

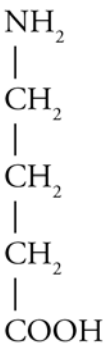


**Figure 3: GABA**

$GABA_A$ and $GABA_C$ receptors are anion channels, consisting of 5 subunits (Chebib and Johnston, 1999; Mohler, 2006). They are permeable to $Cl^-$ and to a lesser extent to $HCO_3^-$, the relative permeability of $HCO_3^-$ versus $Cl^-$ being 0.2 to 0.3 (Kaila, 1994). Ionotropic GABA receptors are both phasically activated by GABA, released from presynaptic neurons, and tonically activated by ambient GABA (figure 4; Ge et al., 2007). Ambient GABA results from diffusion from GABAergic synapses (Glykys and Mody, 2007) as well as from non-synaptic release from neurons and possibly astrocytes (Demarque et al., 2002; Liu et al., 2000). Phasic (synaptic) activation is mediated by high concentrations of GABA (0.3 to 1 mM) for short periods of time (<1 ms; Mozrzymas et al., 2003; Nusser et al., 2001). The concentration of ambient GABA is much lower and activates extrasynaptic receptors with a different subunit composition (Mohler, 2006;

Farrant and Nusser, 2005; Mody and Pearce, 2004). Once released into the synaptic cleft, astrocytes take up GABA, convert it back into glutamine and return it to the neuron (Bak et al., 2006; Liang et al., 2006). To a lesser extent, presynaptic neurons also take up GABA directly.

Upon $GABA_A$ and $GABA_C$ receptor activation, adult neurons are hyperpolarized due to chloride influx, whereas immature neurons are depolarized due to chloride efflux (Eilers et al., 2001). This developmental switch takes place postnatally following the expression of a $K^+/Cl^-$ co-transporter (KCC2) in the second postnatal week, which reduces the intracellular $Cl^-$ concentration in neurons (Rivera et al., 1999).

$GABA_B$ receptors are classical metabotropic receptors, predominantly coupled to $G_{1\alpha}$ and $G_{o\alpha}$ type G proteins (Bettler et al., 2004; Campbell et al., 1993). They are for the most part localized extrasynaptically on both glutamatergic and GABAergic neurons. The predominant $GABA_B$ receptor in the CNS is a heterodimer consisting of the $GABA_{B1}$ and $GABA_{B2}$ subunits (Jones et al., 1998; Bettler et al., 2004). According to Kaupmann et al. (1998) $GABA_{B1}$ is essential for agonist binding and $GABA_{B2}$ for binding to the G protein.

$GABA_B$ receptor-mediated inhibition is exerted by two main mechanisms (figure 4): (1) presynaptic inhibition of $Ca^{2+}$ channels, resulting in a reduction of neuronal transmitter release and (2) postsynaptic activation of G protein-coupled inward rectifying potassium (GIRK) channels, resulting in slow IPSCs due to efflux of $K^+$ (Luscher et al., 1997; Couve et al., 2000; Bowery et al., 2002; Couve et al., 2004). While presynaptic $GABA_B$ receptor-dependent inhibition in the hippocampus is functional at birth (Caillard et al., 1998), postsynaptic inhibition progressively develops during the first postnatal week (Gaiarsa et al., 1995).

Synaptic transmission between hippocampal interneurons and their target cells is mainly mediated by $GABA_A$ receptor activation (Scanziani, 2000;

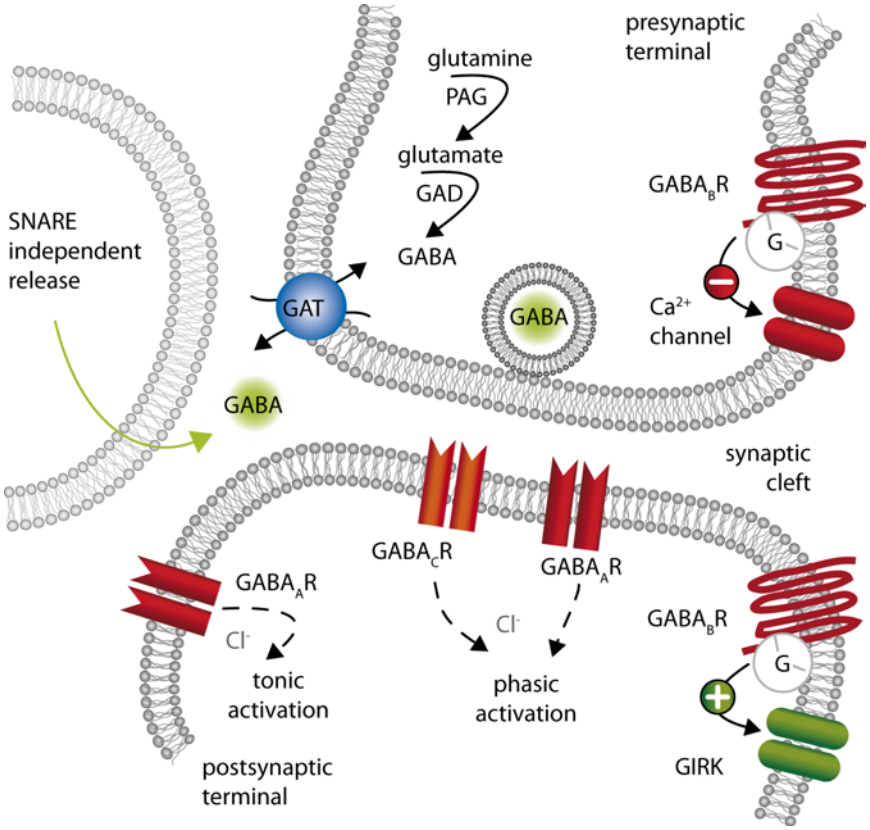


**Figure 4: GABA-Mediated Signaling in Neurons**

Neurons lack the enzyme pyruvate carboxylase (PC); consequently they cannot synthesize glutamate and GABA from glucose. Therefore, glutamine is transferred from astrocytes to neurons, where the enzyme phosphate-activated glutaminase (PAG) synthesizes the excitatory neurotransmitter glutamate. In inhibitory neurons (illustrated here), glutamate is then converted into GABA by the enzyme glutamate decarboxylase (GAD). Once released into the synaptic cleft, GABA phasically activates ionotropic $GABA_A$ and $GABA_C$ receptors. Extrasynaptic ionotropic receptors are tonically activated by ambient GABA, spilling over from the synaptic cleft or released by non-synaptic mechanisms from neurons and glial cells. $GABA_B$ receptors are metabotropic receptors and are located extrasynaptically. Presynaptic $GABA_B$ receptors inhibit $Ca^{2+}$ channels and hence transmitter release, while postsynaptic $GABA_B$ receptors activate G-protein coupled inward rectifying potassium (GIRK) channels; modified after Ge et al. (2007).

G, G protein; GABA, $\gamma$-aminobutyric acid; $GABA_AR$ and $GABA_CR$, ionotropic GABA receptors; $GABA_BR$, metabotropic GABA receptor; GAT, GABA transporter

Buhl et al., 1994). $GABA_B$ receptors, due to their extrasynaptic location, are activated when GABA uptake is inhibited or after simultaneous release of GABA from several interneurons (Scanziani, 2000).

Among other functions during development (see below), $GABA_A$ receptor activation appears to promote its own developmental switch from excitation to inhibition by inducing the expression of KCC2 (Ganguly et al., 2001; Leitch et al., 2005). This view, however, is debated because antagonists of $GABA_A$ receptors had no effect on the time course of KCC2 upregulation in other studies (Ludwig et al., 2003; Titz et al., 2003).

$GABA_B$ receptor activation is involved in the modulation of synaptic transmission and neuronal excitability (Kornau, 2006) as well as the modulation of rhythmic activity in the hippocampus (Leung and Shen, 2007; Scanziani, 2000). Furthermore, $GABA_B$ receptor activation plays a role in the induction of LTP in the hippocampus (Davies et al., 1991). During high-frequency transmission, GABA reduces its own release by activating presynaptic $GABA_B$ autoreceptors. As a consequence, the postsynaptic membrane is depolarized sufficiently to relieve the $Mg^{2+}$ block of NMDA receptors, enabling the induction of NMDA receptor-dependent LTP (Davies et al., 1991).

Studies in $GABA_{B1}$- and $GABA_{B2}$-deficient mice suggest that heterodimeric $GABA_{B1/B2}$ receptors are necessary for normal emotional behavior (Mombereau et al., 2005). In addition, $GABA_{B1}$-deficient mice suffer from spontaneous seizures, hyperlocomotor activity, hyperalgesia, and memory impairment (Schuler et al., 2001), fitting well with the hypothesis that hypoactivity of the GABAergic system is linked to the pathophysiology of epilepsy (Tosetti et al., 2004; Prosser et al., 2001) as well as possibly depression, anxiety, stress, and sleep disorders (Bettler et al., 2004).

In addition to its role in neurotransmission, GABA acts as a trophic substance (Owens and Kriegstein, 2002) as which it not only plays a mor-

phogenetic role during embryonic and postnatal development (Varju et al., 2001), but also regulates multiple steps of adult neurogenesis. In the developing nervous system GABA modulates precursor proliferation, migration, and maturation (LoTurco et al., 1995; Ben-Ari, 2002; Owens and Kriegstein, 2002; Behar et al., 1996). Likewise, in the adult CNS, GABA regulates differentiation and synaptic integration of precursor cells (Liu et al., 2005; Tozuka et al., 2005; Wang et al., 2005; Ge et al., 2006, 2007; Kriegstein, 2005).

Parallel to neurotransmission, the trophic actions of GABA are mainly mediated by $GABA_A$ and $GABA_B$ receptors. Proliferation and morphological development mediated by $GABA_A$ receptor activation largely depend on membrane depolarizations and/or influx of extracellular $Ca^{2+}$ (Maric et al., 2001; Cancedda et al., 2007). The signaling pathway involved in $GABA_B$ receptor-mediated modulation of migration of cortical neurons is less clear (Lopez-Bendito et al., 2003).

### 1.3.2 Effects of GABA on Astrocytes

Like neurons, astrocytes express both ionotropic and metabotropic GABA receptors as well as GABA transporters (Gadea and Lopez-Colome, 2001). $GABA_A$ receptor activation is depolarizing (Kettenmann et al., 1984), in both mature and immature astrocytes, and induces intracellular $Ca^{2+}$ transients (Nilsson et al., 1993; Fraser et al., 1995; Bernstein et al., 1996). $GABA_B$ receptor activation, in contrast to neurons, also induces intracellular $Ca^{2+}$ transients (figure 5; Nilsson et al., 1993; Kang et al., 1998).

As discussed above (see sections 1.1.3 and 1.1.4), $Ca^{2+}$ is an important second messenger and is essential for glia-neuron interaction. Elevations of $[Ca^{2+}]_i$ in astrocytes trigger the release gliotransmitters which signal back to neurons and hence modulate synaptic transmission (see also section 1.1.4; Haydon, 2001; Volterra and Steinhäuser, 2004; Volterra and

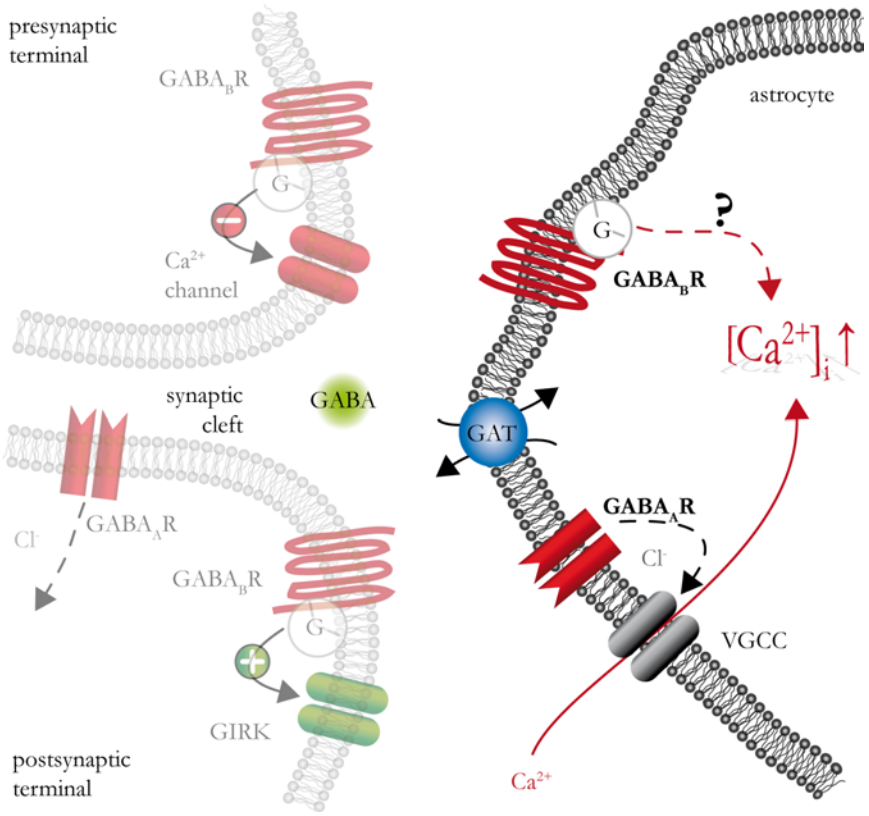


**Figure 5: GABA-Mediated Signaling in Astrocytes**

Similar to neurons, astrocytes express ionotropic $GABA_A$ and metabotropic $GABA_B$) receptors (cf. figure 4), as well as GABA transporters (GAT). $GABA_A$ receptor activation causes a depolarization and $Ca^{2+}$ influx though voltage-gated $Ca^{2+}$ channels (VGCC). $GABA_B$ receptor activation also causes a $[Ca^{2+}]_i$ increase, the origin of which, however, is less clear.

G, G protein; GIRK, G protein-coupled inward rectifying potassium channel.

Meldolesi, 2005).

Recently, new evidence has emerged that activation of astrocytic $GABA_B$ receptors in the hippocampus underlies a form of neuronal plasticity called heterosynaptic depression (see also section 1.1.4; Serrano et al., 2006; Lynch et al., 1977). The signaling cascade was described as follows (figure 6): First, glutamate, released at potentiated Schaffer collateral to CA1 pyramidal neuron synapses, activates NMDA receptors of interneurons. Second, interneurons release GABA which activates $GABA_B$ receptors of adjacent astrocytes, resulting in $[Ca^{2+}]_i$ increases. Finally, astrocytes release ATP and previously inactive synapses are inhibited because extracellular endonucleotidases quickly degrade ATP to the inhibitory adenosine.

Additionally, $GABA_B$ receptors have been proposed to mediate an activity-dependent decrease in the failure rate of unitary inhibitory postsynaptic currents (figure 6; Kang et al., 1998). GABA released by interneurons activates $GABA_B$ receptors on astrocytes and causes a $[Ca^{2+}]_i$ increase. Subsequently the astrocyte releases glutamate and activates NMDA receptors on interneurons, resulting in GABA release and a decrease in the failure rate of their synapse. As a consequence, the frequency of mIPSCs in CA1 pyramidal neurons is increased.

Hence, GABA-induced $Ca^{2+}$ signaling in hippocampal astrocytes plays an important role in neuron-glia interaction. However, the mechanism of $GABA_B$ receptor-induced $[Ca^{2+}]_i$ increases is still unclear.

## 1.4 Aims of this Study

Given that $GABA_B$ receptors couple to $G_{i/o}$ proteins (cf. section 1.3.1 Bettler et al., 2004; Campbell et al., 1993) and inhibit presynaptic $Ca^{2+}$ channels in neurons (Misgeld et al., 1995), the $[Ca^{2+}]_i$ increase observed in astrocytes is an unexpected finding. It has been suggested to be due to $Ca^{2+}$ influx from the extracellular space (Kang et al., 1998), a mechanism which

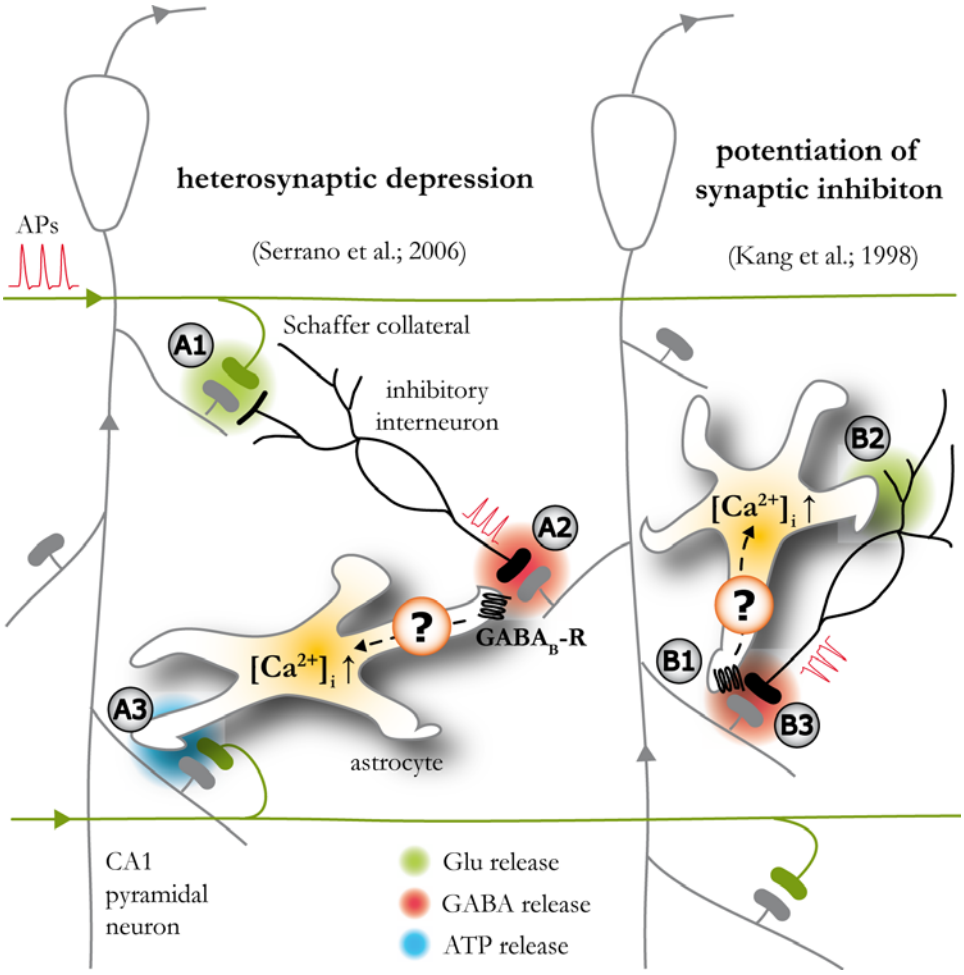


**Figure 6: Astrocytes Modulate Inhibitory Synaptic Transmission Upon Activation of GABA$_B$ Receptors**

**A1**: Glutamate is released at a potentiated Schaffer collateral to CA1 synapse and activates NMDA receptors of interneurons. **A2**: Interneurons release GABA resulting in activation of astrocytic GABA$_B$ receptors and subsequent $[Ca^{2+}]_i$ increases in astrocytes. **A3**: Astrocytes release ATP resuling in inhibition of previously unpotentiated inputs because ATP is degraded to the inhibitory adenosine by extracellular ectonucleotidases.
**B1**: GABA, released by interneurons in this second example also causes activation of astrocytic GABA$_B$ receptors and subsequent $[Ca^{2+}]_i$ increases in astrocytes. **B2**: In this scenario, however, astrocytes release glutamate whereby they re-activate interneurons. **B3**: This re-activation causes the interneurons to release more GABA, which consequently reduces the failure rate of unitary inhibitory synaptic currents.

The mechanism of the GABA$_B$ receptor-induced $[Ca^{2+}]_i$ increase in astrocytes is unclear.

is rather unusual, considering that $GABA_B$ receptors belong to the family of metabotropic receptors (cf. section 1.1.3). The cellular mechanisms of $GABA_B$ receptor-induced $[Ca^{2+}]_i$ increases in astrocytes, however, have not been investigated in detail.

$GABA_A$ receptor-induced $Ca^{2+}$ signals have largely been studied in cell cultures or acutely isolated cells (see also section 1.3.2; Fraser et al., 1995; Kirchhoff and Kettenmann, 1992). Considering that astrocytes are a very diverse and highly plastic cell type, results from cell cultures have to be interpreted with caution (Kimelberg et al., 1997). A major concern is the possible misexpression of proteins which are not normally expressed in astrocytes *in vivo* (Haydon and Carmignoto, 2006). In some studies, $GABA_A$ receptor expression has been reported to be absent (Bureau et al., 1995) or downregulated with in vitro ageing (Tateishi et al., 2006). A further concern when working with cultures is that the *in vitro* age does not necessarily correspond to the *in vivo* age. Acute isolation of astrocytes avoids these problems, however, acutely isolated cells have lost many of their fine processes and their location within the hippocampal network is no longer preserved (Kimelberg et al., 2000). Therefore, the first goal of this study was to elucidate the mechanisms by which $GABA_A$- and $GABA_B$ receptors elicit $[Ca^{2+}]_i$ increases in hippocampal astrocytes in acute slices.

The expression of $GABA_B$ receptors appears to vary developmentally in astrocytes (Fritschy et al., 2004) but to date no functional conclusions have been drawn from this finding. $GABA_B$ receptor activation in astrocytes is involved in glia-neuron interaction (see sections 1.1.4 and 1.3.2) but it is not known at which point in time during embryonic or postnatal development these mechanisms begin to develop. Considering the transformations the hippocampal network undergoes during the first two postnatal weeks (see section 1.2), this question is crucial for a better understanding of early postnatal development. Thus, the second goal of this study was to establish a

developmental profile of GABA-evoked $Ca^{2+}$ responses in astrocytes.

In order to identify astrocytes in acute tissue slices, I adapted a method previously introduced for staining cortical astrocytes *in vivo* (Nimmerjahn et al., 2004). Astrocytes were stained with the red fluorescent dye sulforhodamine 101 (SR101). The specificity of SR101 for astrocytes in acute hippocampal slices at young postnatal stages (P03, P15) was confirmed according to morphological, electrophysiological, and immunohistochemical criteria (see also Kafitz et al., appendix page 123ff; immunohistochemistry performed by Jonathan Stephan). To investigate the cellular mechanisms of $GABA_A$ - and $GABA_B$ receptor-induced $[Ca^{2+}]_i$ increases, I performed wide-field imaging of intracellular $Ca^{2+}$ transients along with whole-cell patch-clamp recordings in astrocytes of acute hippocampal slices. The origin of $[Ca^{2+}]_i$ increases was characterized with pharmacological tools. In addition, the functional responses of astrocytes to GABAergic stimulation were compared during development. To this end, I pressure-applied the $GABA_A$- and $GABA_B$ receptor agonists muscimol and baclofen, respectively, to SR101-positive astrocytes from postnatal day 3 to 34 and characterized the resulting $[Ca^{2+}]_i$ increases in six different age groups (P03, P07, P11, P15, P21$\pm$1, P33$\pm$1).

# 2 Materials and Methods

## 2.1 Model Systems

All experiments were carried out on rat hippocampal astrocytes. For the most part, astrocytes *in situ*, in acute hippocampal slices, were used. In addition, some experiments were performed in primary astrocyte cultures.

### 2.1.1 Primary Astrocyte Cultures

Cultured astrocytes were obtained from one to two day old Wistar rats as described previoulsy (Rose, 2003). Rat pups were decapitated, the brain was removed, and the meninges were carefully taken off in ice-cold PBS (phosphate-buffered saline). Both hippocampi were quickly dissected out and incubated for 20 to 40 minutes at 36℃ in 10 ml papain solution, consisting of PBS supplemented with 1 mg/ml papain (21 U/ml; Sigma-Aldrich), 1.5 mM $CaCl_2$, 0.5 mM Na-EDTA, and 5 mM L-Cysteine (Sigma-Aldrich). The enzyme papain breaks down extracellular matrix proteins by cleaving protein bonds and, thus, loosens connections between cells. This reaction was stopped by replacing the papain solution with glial medium (contents see below) supplemented with trypsin inhibitor (1.5 mg/ml; Sigma-Aldrich) and BSA (bovine serum albumine; 1.5 mg/ml; Sigma-Aldrich) and further incubation for about 20 minutes at 36℃. After washing twice in standard glial medium, cells were mechanically dissociated by careful tritruation with fire-polished Pasteur pipettes of decreasing tip diameter. Cells were plated at a density of 9 x $10^3$ astrocytes per $cm^2$ onto glass coverslips (12 mm diameter) coated with poly-D-lysine (400 µg/ml, Sigma-Aldrich) and laminin (9 µg/ml, Sigma-Aldrich). Cells were allowed to adhere to the coverslip in an incubator at 36℃ with a 5% $CO_2$/95% air atmosphere before they were transferred into 24-well plates containing standard glial medium. Every three to four days, astrocytes were fed by replacing all medium with

fresh glial medium consisting of Dulbecco's Modified Eagle Medium F-12 (DMEM, Invitrogen) supplemented with 10% FBS (Invitrogen or Gibco), 20 mM Glucose, 2 mM Glutamax (Invitrogen) and 0.5% G5 supplement (Gibco). Confluent cultures were used for experiments after 8 to 14 days *in vitro* and consisted of ≥95% GFAP positive cells.
Cultures used in this study were kindly provided by Dr. Tony Kelly.

### 2.1.2 Acute Hippocampal Slices

Wistar rats from postnatal day (P) 3 to 34 (P0 referring to the day of birth) were decapitated and the brain was removed while being submerged in ice-cold ringer solution. Animals older than P11 were anesthetized with $CO_2$ prior to decapitation and those older than P14 were generally dissected using a modified standard extracellular solution (PR) containing 0.5 mM $Ca^{2+}$ and 6 mM $Mg^{2+}$ (see table 1 on page 49 for composition of all extracellular solutions). Unless stated otherwise, experiments were carried out on slices of P15 animals, which were obtained as described previously (Meier et al., 2006; Edwards et al., 1989) with a few modifications: In order to keep dendrites of CA1 pyramidal neurons in the stratum radiatum largely intact, 250 µm thick slices were generally cut at an angle to the midline (see figure 7), with a Microm HM650 V vibratome (Microm, Walldorf, Germany; settings: speed 8 to 10; vibration 50 to 60 Hz; amplitude of lateral blade movement 1.0 to 1.2; Wilkinson Sword Classic blade). As soon as all slices were collected into cutting solution at 34°C, sulforhodamine 101 (0.5 - 1 µM) was added and slices were protected from light. After an incubation period of 20 minutes, slices were transferred to standard extracellular solution and kept at elevated temperature for an additional 10 minutes before they were transferred to room temperature (20 to 24°C) and used for up to 9 hours. During experiments, a grid consisting of nylon threads glued to a U-shaped platinum wire was put on top of the slices in the recording chamber, in or-

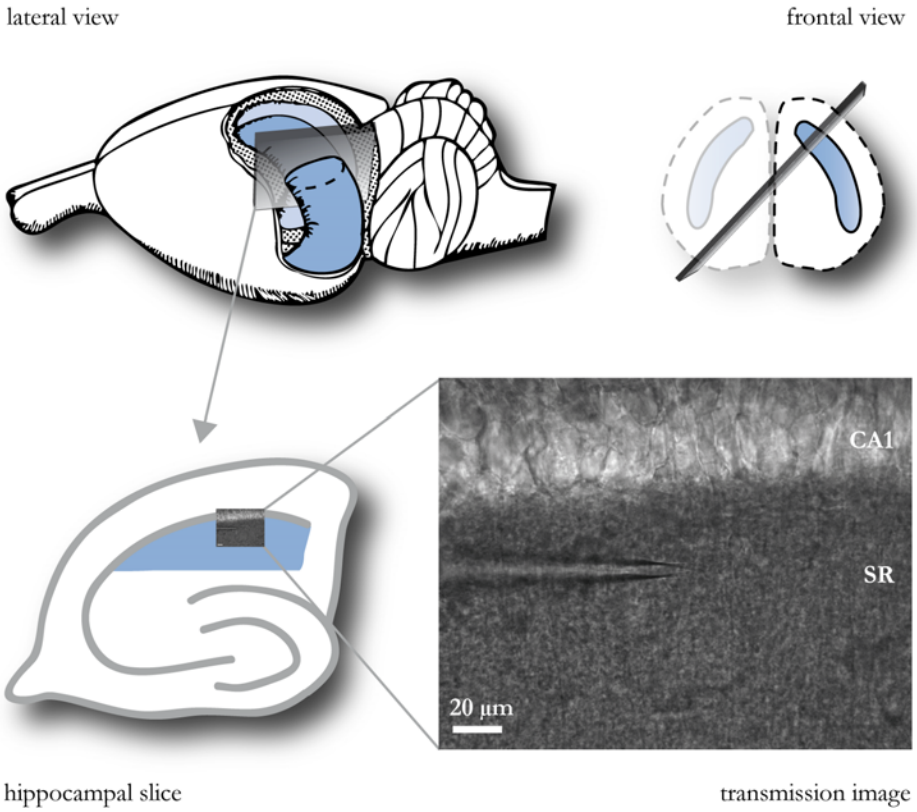


**Figure 7: Orientation of Hippocampal Slices**

Hippocampal slices were cut at an angle to the midline as depicted in the **top** panels. **Bottom left**: Astrocytes in the stratum radiatum (blue area) were used in this study. **Bottom right**: transmission image of parts of area CA1 and the stratum radiatum including a typical application pipette.

CA1, cornu ammonis area 1; SR, stratum radiatum.

der to fix the slices in place. Slices were constantly perfused with standard extracellular solution (NR) at a rate of about 1 ml/min using a peristaltic pump (Ismatec IPC, Wertheim-Mondfeld, Germany).

#### Astrocyte Identification with SR101

SR 101 is an inert indicator dye which has previously been used for identification of cortical astrocytes *in vivo* (Nimmerjahn et al., 2004). The acute hippocampal slices were incubated with SR101 (0.5 - 1 µM) for 20 minutes during the slicing procedure (see page 35). Since the spectra of SR101 fluorescence (see figure 8 for excitation and emission spectrum) are shifted to longer wavelengths as compared to the spectra of fura-2 (figure 10), which was used for $Ca^{2+}$ imaging, the imaging set-up (see section 2.2.2) was equipped with two different filter sets, one for $Ca^{2+}$ imaging and the other one for identification of astrocytes. For astrocyte identification, SR101 fluorescence was excited at 575 nm for 50 to 500 ms and fluorescence emission was collected above 590 nm (see also Kafitz et al., page 123ff).

## 2.2 Techniques

Responses of astrocytes to GABA, muscimol and baclofen were assessed by applying ratiometric $Ca^{2+}$ imaging with the fluorescent indicator fura-2 and whole-cell patch-clamp recordings.

### 2.2.1 $Ca^{2+}$ Imaging Principles

The concentration of free $Ca^{2+}$ ions generally is very low within cells: whereas the extracellular $Ca^{2+}$ concentration is around 2 mM, the intracellular concentration is a factor of more than $10^4$ less and varies between 50 and 200 nM (see also section 1.1.3). Given that the concentration of other ions ($Na^+$, $K^+$, $Mg^{2+}$) within cells is considerably higher than that of $Ca^{2+}$, and $Ca^{2+}$ transients may be less than 20 nM in amplitude, the

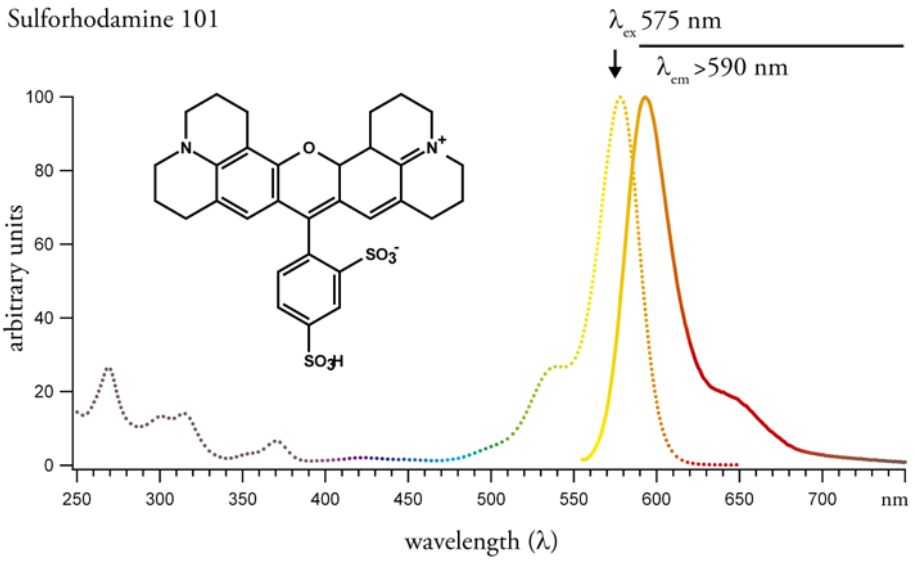


**Figure 8: Molecular Structure and Spectra of Sulforhodamine 101**
The indicator was excited at 575 nm and emission was collected above 590 nm. Dotted line, excitation spectrum; solid line, emission spectrum; data from Invitrogen.

ideal tool for measuring $[Ca^{2+}]_i$ is highly sensitive and specific for $Ca^{2+}$. Fluorescent indicator dyes have proven a valuable tool for measuring such small concentration changes (Tsien et al., 1985; Grynkiewicz et al., 1985).

There are many different fluorescent probes with different properties on the market. Most $Ca^{2+}$ indicators are derivatives of the $Ca^{2+}$ chelator BAPTA (1,2-Bis(2-aminophenoxy)ethane-N,N,N',N'-tetraacetic acid; Adams, 2005) and consist of an aromatic ring system, the double bonds of which are responsible for the characteristic fluorescence properties of the dye. The $K_d$ of a $Ca^{2+}$ indicator is a measure for its affinity to $Ca^{2+}$. In general, a specific indicator can be used when the expected signal is in the range of 0.1 to 10 times the $K_d$ of the dye. Upon binding $Ca^{2+}$, the indicator undergoes a conformational change resulting in a change in fluorescence intensity. Additionally, some indicator dyes exhibit a change in their fluorescence spectrum and are called dual excitation or dual emission indicators depending on whether the spectral shift occurs in the absorption or emission

spectrum, respectively.

Unfortunately the ideal indicator with 100% specificity does not exist: most $Ca^{2+}$ indicators do indeed bind other physiological divalent cations like $Mg^{2+}$ or $Zn^{2+}$, and are influenced by pH or unphysiological divalent ions as for example $Ba^{2+}$, $Ni^{2+}$, or $Cd^{2+}$. For fura-2, which was used in this study, many of these interactions are known (Marchi et al., 2000; Haugland, 2005) and must be taken into consideration by the experimenter. In case the properties of an indicator are not known, the substance has to be tested under physiological conditions to ensure its suitability for a given experiment (cf. Meier et al., 2006). As an example of which properties to look at, I previously examined the suitability of a new fluorescent indicator dye for measuring $Na^+$ transients in the physiological range (Meier et al., 2006, see also page 146ff).

### Fura-2 and Ratiometric $Ca^{2+}$ Imaging

Fura-2 is a dual excitation indicator with a $K_d$ of ∼224 nM in the presence of 1 mM $Mg^{2+}$ (according to the manufacturer), which makes it well suited for measuring $[Ca^{2+}]_i$ changes in the physiological range. The advantage of dual excitation ratiometric indicators is the possibility to excite with two alternating wavelengths and to calculate the ratio of fluorescence emission. Such ratio values are independent of dye concentration, optical path length, and illumination intensity, and when calibrated (see section 2.2.1 on page 43) the ratio renders concentrations rather than mere changes in fluorescence (see also Meier et al., 2006, ; Bennay et al., page 133ff).

Fura-2 is polar and therefore unable to pass cell membranes. If a large number of cells is to be loaded simultaneously, the AM form of the dye can be used: here the carboxylates are masked as acetoxymethyl (AM) esters and the substance can pass cell membranes. Once intracellular, ubiquitous esterases cleave the AM esters and the indicator is converted back into its

polar and $Ca^{2+}$-sensitive form (see figure 9).

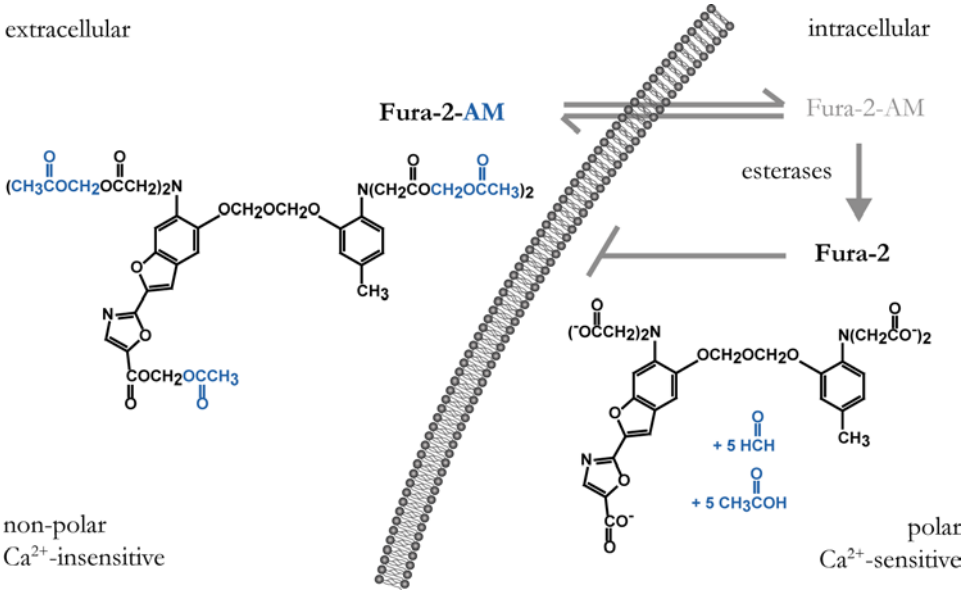


**Figure 9: Loading Cells with Fura-2-AM**

Carboxyl groups rendering the indicator polar are masked as acetoxymethyl esters. Once inside the cell, AM-esters are cleaved by ubiqutous esterases and the substance is trapped inside the cells; modified from Haugland (2005).

In all experiments fura-2 was excited at the isosbestic point (∼356 nm) and at 380 nm (figure 10). Theoretically, calculating a ratio with excitation wavelenghts of 340 and 380 nm would render bigger ratio changes. However, the optical system is not well-suited for wavelength below 350 nm and measurements do in fact become noisier (personal observations). Advantages of using the isosbestic point include: (1) cell swelling can be determined, (2) artefacts owing to the pressure application can clearly be seen and (3) bleaching can be assessed much easier. Particularly in slices from very young animals, pressure artefacts can become a problem. Figure 11 shows an example of such an artefact and illustrates the principle of ratiometric imaging. Importantly, the pressure application itself does not result in $[Ca^{2+}]_i$ increase in astrocytes.

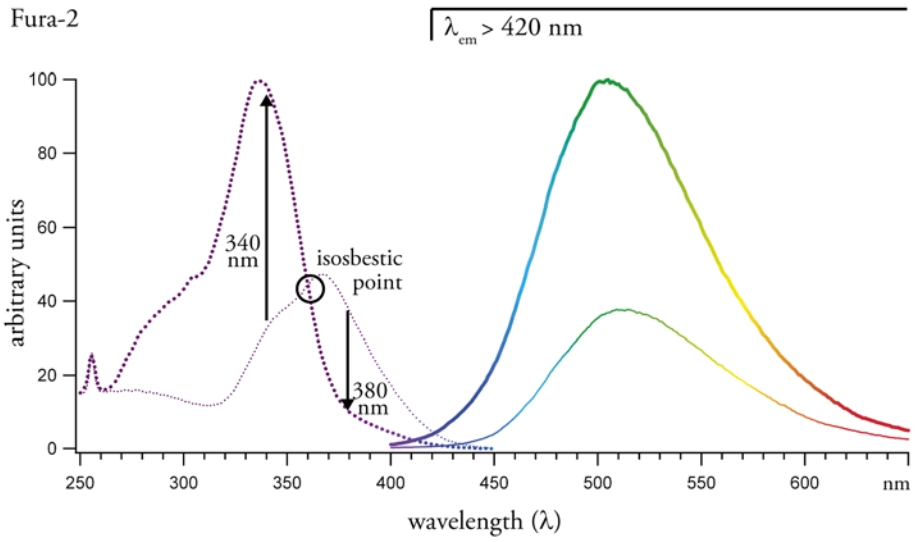


**Figure 10: Absorption and Emission Spectra of Fura-2**

The diagram illustrates the excitation (dotted line) and emission (solid line) spectrum of fura-2 at a high [$Ca^{2+}$] (thick lines) and under $Ca^{2+}$-free conditions (thin lines). At the isosbestic point (∼360 nm), fluorescence emission is independent of [$Ca^{2+}$] (circle). When exciting with wavelengths below the isosbestic point, fluorescence emission increases with increases in [$Ca^{2+}$]. Conversely, when exciting with wavelengths above the isosbestic point, fluorescence emission decreases with increases in [$Ca^{2+}$] (arrows). Note that fluorescence emission is proportional to fluorescence absorption; data from Invitrogen.

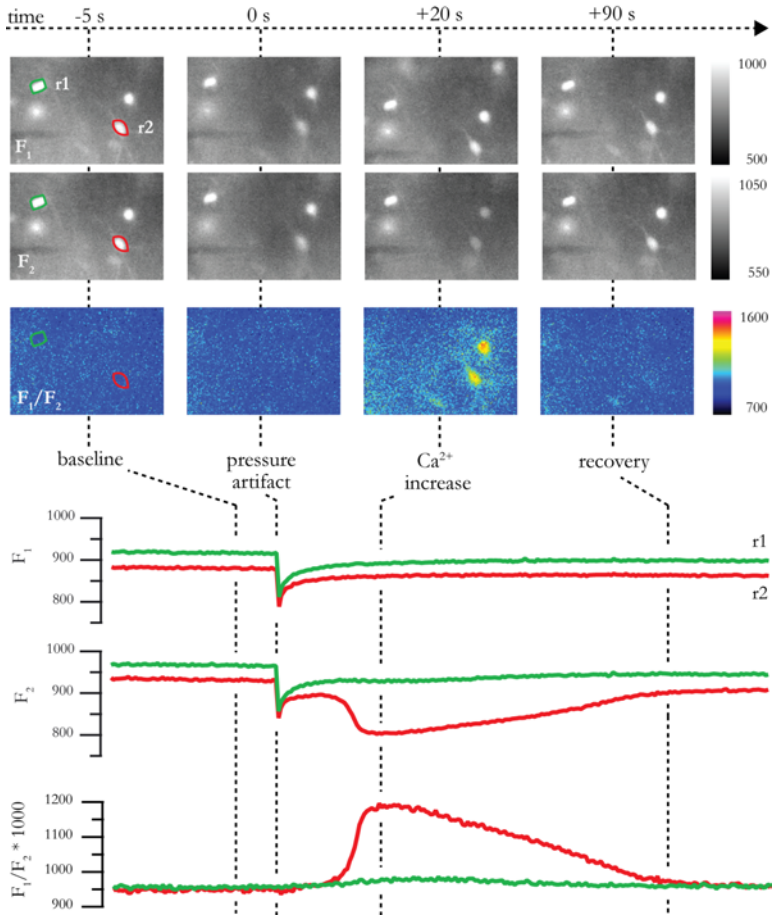


**Figure 11: Principle of Ratiometric Imaging**

**Top**: The black and white rows of images labeled $\mathbf{F_1}$ **and** $\mathbf{F_2}$ are images taken at the isosbestic point (∼360 nm for fura-2) and the ion-sensitive wavelength (380 nm), respectively. Fluorescence intensity is color-coded, the brighter (white) the color, the higher the fluorescence intensity (arbitrary units). Astrocytes in the stratum radiatium of a hippocampal brain slice which have taken up the indicator appear as white spots. The colored row of images resulted from calculating the ratio of $F_1$ and $F_2$ and conseqently codes concentrations (here blue corresponds to low ion concentrations, and pink to high ion concentrations). Note that single cells cannot be distinguished anymore because the ion concentration ($[Ca^{2+}]$, when using fura-2) is the same in all areas loaded with the indicator.
**Bottom**: Intensity values recorded in the regions of interest (r1 and r2) depicited in the first $F_1$ image. At the time 0 s, a decrease in fluorescence is observed both in $F_1$ and $F_2$ because the cells are moved out of focus due to the pressure application (see also 2nd image column from left). This so-called pressure artifact is cancelled out in the ratio of $F_1$ and $F_2$ (bottom). At time point 20 s a decrease in flourescence intensity is observed in two cells in $F_2$ (middle), but not in $F_1$. It is due to an increase in $[Ca^{2+}]_i$ of cell 2 (r2) and a neighboring cell and can be seen as increase in fluorescence ratio (bottom, and colored images) which subsequently recovers to baseline (time 90 s).

### Calibration of Fura-2 Signals

Because the excitation spectrum of fura-2 is shifted upon binding $Ca^{2+}$, the ratio (R) of the fluorescence emission ($F_1$ and $F_2$) at two different excitation wavelengths $\lambda_1$ and $\lambda_2$, respectively, is sufficient to convert ratio values into $Ca^{2+}$ concentrations. Fluorescence emission depends on the amount of $Ca^{2+}$-free and $Ca^{2+}$-bound dye in the sample and can be described by the following equations for wavelength $\lambda_1$ and $\lambda_2$, respectively.

$$F_1 = S_{f1}c_f + S_{b1}c_b \tag{1a}$$

$$F_2 = S_{f2}c_f + S_{b2}c_b \tag{1b}$$

$c_f$ and $c_b$ are the concentrations of $Ca^{2+}$-free and $Ca^{2+}$-bound indicator, respectively. $S_{f1}$, $S_{f2}$, $S_{b1}$, and $S_{b2}$ are proportionality coefficients for the two excitation wavelengths and the free and bound forms of the dye, respectively, which take into consideration that the emitted fluorescence - besides being dependent on the number of dye molecules - is dependend on intrinsic properties of the dye and the optical system. Such influences are illumination intensity, photon collection efficiency of the optical set-up, quantum efficiency of the detector, dye absorption coefficient and quantum yield. Given that $Ca^{2+}$ binds to the dye with a 1:1 stoichiometry, the relation of bound to free dye depends on $Ca^{2+}$ concentration and effective dissociation constant ($K_d$) of the dye and can be described as follows:

$$c_b = c_f \frac{[Ca^{2+}]}{K_d} \tag{2}$$

The fluorescence ratio R is the ratio $F_1/F_2$, which together with equation (2) yields:

$$R = \frac{S_{f1} + S_{b1}\frac{[Ca^{2+}]}{K_d}}{S_{f2} + S_{b2}\frac{[Ca^{2+}]}{K_d}} \tag{3}$$

For the $Ca^{2+}$ concentration the calibration equation ends up to be:

$$[Ca^{2+}] = K_d \left(\frac{S_{f2}}{S_{b2}}\right) \left(\frac{R - \frac{S_{f1}}{S_{f2}}}{\frac{S_{b1}}{S_{b2}} - R}\right) \tag{4}$$

$S_{f1}/S_{f2}$ is the limiting value of R at zero [$Ca^{2+}$] and therefore is considered $R_{min}$; and $S_{b1}/S_{b2}$ is the limiting value of R at saturated [$Ca^{2+}$] and is considered $R_{max}$. Consequently equation (4) can also be written as

$$[Ca^{2+}] = K_d \left(\frac{S_{f2}}{S_{b2}}\right) \left(\frac{R - R_{min}}{R_{max} - R}\right) \tag{5}$$

which is the standard calibration equation established by Grynkiewicz et al. (1985) for ratiometric indicators. $S_{f2}/S_{b2}$ is often referred to as $\beta$, and $\beta K_d$ is also known as the apparent $K_d$ ($K_{d_{app}}$).

A calibration of fura-2-loaded primary astrocyte cultures, using 10 µM ionomycin as $Ca^{2+}$ ionophore rendered the following calibration equation for measurements with fura-2:

$$[Ca^{2+}] = 1398.2 \left(\frac{R - 0.6}{6.0 - R}\right) nM \tag{6}$$

This equation was used for converting all ratio values measured with the system into $[Ca^{2+}]_i$. However, one has to keep in mind, that such a calibration of fura-2 fluorescence can only be an estimate of [$Ca^{2+}$] within cells. Therefore, in pharmacological experiments, carried out in one and the same cell, ratio values were not converted into $[Ca^{2+}]_i$ but are given as changes in fluorescence ratio in arbitrary units (a.u.) as measured by the system.

### 2.2.2 $Ca^{2+}$ Imaging in Acute Hippocampal Slices

Cells were loaded with the ratiometric $Ca^{2+}$ indicator fura-2 by pressure injection of fura-2-AM into the slice (Meier et al., 2006; Stosiek et al., 2003, ; Bennay et al., page 133ff). A 5 mM stock solution of fura-2-AM in 20%

Pluronic acid / DMSO was diluted in HEPES buffered saline (as used for cell cultures, but without glucose) to yield a final concentration of 500 µM. A 2 to 3 MΩ micropipette, filled with the solution, was inserted into the stratum radiatum close to area CA1 and fura-2-AM was pressure-applied for 2 to 10 s per region at 8 psi using a picospritzer II (General Valve/Parker Hanifin, Flein/Heilbronn, Germany). Experiments were started at least one hour after loading, in order to allow for resorption of the dye and to enable cleavage of the AM-ester (see figure 9). The extracellular solution contained 500 nM TTX in order to block neuronal activity, unless stated otherwise. Astrocyte cultures were loaded for 90 minutes at room temperature in HEPES-buffered saline containing 15 µM fura-2-AM. Experiments were started no earlier than half an hour after loading and coverslips were continuously perfused with HEPES-buffered saline.

Changes in fura-2 fluorescence were measured using a widefield epifluorescence system (TILL photonics, Martinsried, Germany) attached to an upright microscope (Zeiss, Oberkochen, Germany; Axioskop; Olympus 40x , N.A. 0.8 (LUMPlanFL) water-immersion objective (Olympus Europe, Hamburg, Germany)). Fura-2 fluorescence was excited at the isosbestic point (∼356 nm) and at 380 nm for 10 to 50 ms using a monochromator (Poly I or Poly V, TILL photonics, Martinsried, Germany) and fluorescence emission above 420 nm was detected with a CCD-camera (TILL Imago super-VGA; TILL photonics, Martinsried, Germany). TILLvisION (versions 4.0.1.3 and 4.5.18) software was used for image acquisition as well as ratio calculation. Fluorescence intensity was averaged in regions of interest corresponding to cell somata, and background was subtracted offline before calculation of the ratio. In order to standardize the background correction procedure, 50 and 30 % of the average fluorescence in an area of interest around the measured cells were taken as background and threshold, respectively. Acquisition rates were 1-2 Hz unless stated otherwise and only cells staining positive for SR101

were included in the analysis ($\lambda_{ex}$, 575 nm; $\lambda_{em}$ >590 nm, see section 2.1.2 for details). Agonists were pressure applied using fine micropipettes (Hilgenberg, Waldkappel, Germany) placed at a distance of about 15 µm from cell somata (picospritzer II, 8 psi). Antagonists were added to the standard extracellular solution from stock solutions and washed in for several minutes.

### 2.2.3 Patch-Clamp Principles

The patch-clamp technique offers the possibility to measure membane potential or membrane currents of a single cell (in whole-cell recordings and perforated patches) or current across a patch of membrane (in cell-attached or inside-/outside-out configurations; Hamill et al., 1981). The patch-clamp amplifier allows to measure voltage and to inject current through the same pipette.

Besides the different configurations mentioned above, there are two essentially different modes: voltage clamp and current clamp. In current-clamp mode, the amount of current injected into the cell is kept constant and changes in membrane potential are measured. In voltage-clamp mode, the membrane potential of the cell is kept constant and equal to the command potential, which allows measurement of electric current resulting from ion fluxes across the plasma membrane. Because the patch-clamp amplifier injects the amount of current, necessary for keeping the potential of the cell at the command potential, influx of positive ions into a cell in whole-cell-mode is shown as negative current (downward deflection) and an outflow of positive ions as positive current. Consequently, negative currents measured in whole-cell-voltage clamp mode, can either be due to influx of positive ions or to outflow of negative ions. Vice versa, positive currents are due to influx of negative ions or outflow of positive ions. One possibility to determine the kind of ions involved is the measurement of the reversal potential which can be calculated with the Goldman equation depending on the permeability of

the respective ions.

### 2.2.4 Patch-Clamp in Acute Hippocampal Slices

Somatic whole-cell patch-clamp recordings were carried out as described earlier (Meier et al., 2006; Edwards et al., 1989), using an Axopatch 200A or 200B amplifier (Molecular Devices, Sunnyvale, CA, USA) coupled to a personal computer via a digidata 1322A interface (Molecular Devices, Sunnyvale, CA, USA). Fine borosilicate glass pipettes (Hilgenberg, Waldkappel, Germany) of 1.5 to 3 MΩ resistance, filled with standard intracellular solution (refer to section 2.3.1 for composition) were lowered into the slice. While approaching the cell to be measured, a small amount of continuous pressure was applied. During the whole procedure the amplifier was set to voltage-clamp mode and test pulses of 5 to 10 mV (either positive or negative, generated by the "seal test" feature of PClamp 8.2 software; Molecular Devices, Sunnyvale, CA, USA) were applied. Once the pipette had approached the cell an indentation could be seen and the resistance increased. After correcting the offset, the pressure was released and the cell membrane formed a tight seal (resistance 1 to 10 GΩ) with the patch-pipette (cell attached configuration). The holding potential was adjusted to -85 mV, the expected membrane potential of astrocytes, before suction was applied and the pipette gained access to the cytosol. A correction for liquid junction potentials was not applied. IV curves were acquired at 10 kHz and lowpass-filtered at 5 kHz using PClamp 8.2 software. P/N leak subtraction was carried out online by measuring hyperpolarizing prepulses (amplitude -10 mV) before starting the voltage-step protocol. TTX (500 nM) was added to the standard extracellular solution only after obtaining an IV curve and was allowed to wash in for several minutes before agonists were applied. Muscimol was pressure-applied, using a picospritzer II (General Valve/Parker Hanifin, Flein/Heilbronn, Germany) coupled to standard

micropipettes placed at a distance of approximately 15 µm from the cell somata. Current and voltage responses upon agonist application were acquired at 1 kHz.

## 2.3 Solutions and Chemicals

### 2.3.1 Intracellular Solution

The intracellular solution used for whole-cell patch-clamp recordings contained in mM: 120 K-Gluconate, 32 KCl, 10 HEPES, 4 NaCl, 0.16 EGTA, 4 Mg-ATP, 0.4 Na-GTP, pH 7.3 (KOH). After preparation the solution was kept in 1 ml aliquots at -20°C and used for a maximum of 10 days. Once thawed, intracellular solution was kept on ice and was used for a maximum of a day.

### 2.3.2 Extracellular Solutions

The composition of extracellular solutions is shown in table 1. Concentrated stock solutions of transmitters and blockers were obtained according to table 2 (page 50) and kept at -20°C until use. Blockers were generally bath applied and dissolved in NR prior to use while substances applied with micropipettes were dissolved in HR and used for several weeks.

In oder to obtain $AlF_4^-$, 10 mM NaCl in the extracellular solution was replaced with NaF and the solution was supplemented with 10 µM $AlCl_3$ (Klein et al., 1998). Additionally, extracellular $Ca^{2+}$ was reduced to 1 mM ($Mg^{2+}$ as substitute), in both NaF and control applications.

Nominally $Ca^{2+}$-free solution (0 $Ca^{2+}$) was obtained by substituting $Ca^{2+}$ for $Mg^{2+}$ and adding 200 µM Ethylene glycol-bis(2-aminoethylether)-N,N,N',N'-tetraacetic acid (EGTA) as $Ca^{2+}$ chelator. All other substances were prepared as stock solutions (see table 2) and added to the extracellular solution prior to use.

**Table 1: Composition of Extracellular Solutions**

| ingredients (in mM) | HR (HEPES buffered saline) | NR (normal ringer) | PR (preparation ringer, reduced $Ca^{2+}$) |
|---|---|---|---|
| NaCl | 125 | 125 | 125 |
| KCl | 3 | 2.5 | 2.5 |
| $CaCl_2$ | 2 | 2 | 0.5 |
| $NaH_2PO_4$ | 1.25 | 1.25 | 1.25 |
| $NaHCO_3$ | | 26 | 26 |
| HEPES | 25 | | |
| $MgCl_2$ | | 1 | 6 |
| $MgSO_4$ | 2 | | |
| Glucose | 10 | 20 | 20 |
| pH | 7.4 (with NaOH) | 7.4 when bubbled with 95%$O_2$ / 5% $CO_2$ | 7.4 when bubbled with 95% $O_2$ / 5% $CO_2$ |
| osmolarity | ∼300 | ∼310 | ∼315 |

HR was used for cell culture experiments and for dilution of pipette solutions, NR refers to the standard extracellular solution which was used for all experiments in the acute slices. PR was used for the dissection of P14 and older animals. It contained less $Ca^{2+}$ and more $Mg^{2+}$ in order to reduce neuronal activity during the slicing procedure.

### 2.3.3 Chemicals and Stock Solutions

Receptor agonists and antagonists were dissolved in $\sigma$-$H_2O$ (Sigma-Aldrich, Taufkirchen, Germany; W3500), DMSO (Sigma-Aldrich; D5879), or other solvents, as recommended by the manufacturer. Supplier, order number, concentration of stock solution, solvent, as well as final concentration of each substance are detailed in table 2.

**Table 2: Chemicals and Stock Solutions**

| substance | order number | stock solution concentration | diluted in | final concentration |
|---|---|---|---|---|
| $AlCl_3$ | 06220 [1] | 100 mM | $\sigma$-$H_2O$ | 10 µM |
| DL-AP5 | A5282[1] | 50 mM | 70 mM $NaHCO_3$ | 100 µM |
| $BaCl_2$ x 2 $H_2O$ | B0750[1] | 100 mM | $\sigma$-$H_2O$ | 1 mM |
| Baclofen | B5399 [1] | 10 mM | HCl to dissolve; 10 mM HEPES | 50 - 500 µM |
| Bicuculline | B6889 [1] | 10 mM | $\sigma$-$H_2O$ | 50 µM |
| $CdCl_2$ | 20899 [1] | 10 mM | $\sigma$-$H_2O$ | 100 µM |
| CNQX | C127[1] | 50 mM | DMSO | 10 - 20 µM |
| CGP55845 | 1248[2] | 10 mM | DMSO | 3 µM |
| CPA | 239805[4] | 30 mM | DMSO | 10 µM |
| CPPG | 0972[2] | 10 mM | 0.1 N NaOH | 10 µM |
| Fura-2-AM | MFP F1221[3] | 5 mM | 20% Pluronic /DMSO | 15 - 500 µM |
| GABA | A2129[1] | 100 mM | $\sigma$-$H_2O$, 100 mM HEPES, pH 7.4 | 0.5 to 1 mM |
| Ionomycin | I0634[1] | 1 mM | DMSO | 10 µM |
| MCPG | 0336[2] | 50 mM | 0.11 M NaOH | 1 mM |
| Muscimol | M1523[1] | 20 mM | $\sigma$-$H_2O$ | 500 µM |
| NaF | 0285[5] | | | 10 mM |
| $NiCl_2$ x 6 $H_2O$ | 1.06717[4] | 1 M | $\sigma$-$H_2O$ | 2 mM |
| Pluronic F-127 | P6867[3] | 20% (2 mg/ml) | DMSO | 0.06% - 2% |
| PPADS | P178[1] | 10 mM | $\sigma$-$H_2O$ | 20 µM |
| SR101 | S7635[1] | 1.65 mM | $\sigma$-$H_2O$ | 0.5 - 1 µM |
| t-ACPD | 0187[2] | 10 mM | $\sigma$-$H_2O$, NaOH | 100 µM |

*continued on next page*

| substance | order number | stock solution concentration | diluted in | final concentration |
|---|---|---|---|---|
| TTX | 00061[6] or T550[7] | 10 mM | $\sigma$-$H_2O$ | 500 nM |
| U73122 | 1268[2] | 5 mM | DMSO | 5 to 10 µM |

[1] Sigma-Aldrich, Taufkirchen, Germany: www.sigmaaldrich.com

[2] Tocris, Eching, Germany: www.tocris.com

[3] Invitrogen, Karlsruhe, Germany: www.invitrogen.com

[4] Merck, Darmstadt, Germany: www.merck.de

[5] J.T.Baker, Deventer, Netherlands: www.mallbaker.com

[6] Biotrend Chemikalien, Cologne, Germany: www.biotrend.com

[7] Alomone Labs, Jerusalem, Israel: www.alomone.com

## 2.4 Data Analysis and Illustrations

Imaging experiments were analyzed using IgorPro software (version 5, WaveMetrics Inc., Lake Oswego, OR, USA). Histograms show average ratio changes of two consecutive applications, except for experiments with CPA and CGP55845 where only one application was performed.

The number of cells reacting to the $GABA_A$ and $GABA_B$ receptor agonists muscimol and baclofen, respectively, was determined with a routine written in IgorPro. Cut-off values were chosen according to $Ca^{2+}$ responses observed in control applications of each substance. Astrocytes were considered to respond to muscimol, if the ratio within 15 seconds after application increased by more than 2 standard deviations of noise measured before the application. Baclofen-induced $Ca^{2+}$ transients were more variable and generally slower in onset; therefore cells were considered to react if the peak ratio increased more than 3 standard deviations of noise between 10-120 s after application. Cells were considered oscillating and were not included in the analysis, if the standard deviation of baseline values within 25 seconds before the application exceeded 3 standard deviations of standard noise.

All illustrations were made with Illustrator (version CS2, Adobe Sys-

tems GmbH, Munich, Germany) and both ImageJ (National Institutes of Health, USA) and Photoshop (version CS2, Adobe Systems GmbH, Munich, Germany) were used for images. Illustrated $Ca^{2+}$ imaging traces were low-pass-filtered using the moving average smoothing function provided in IgorPro (5 point box smoothing). Baseline values were not preserved in most illustrations to allow for better comparison of signal amplitudes, unless a systematic change in baseline was illustrated (cf. figure 19). Patch-clamp data was analyzed in Clampfit (version 8.2; Molecular Devices, Sunnyvale, CA, USA) and IgorPro. Three consecutive applications were averaged and lowpass-filtered for illustrations.

## 2.5 Statistical Analyses

Statistical analyses were carried out with the routines provided in Igor Pro (version 6.0; Wavemetrics Inc., Lake Oswego, OR, USA). Considering that each cell was tested under control and drug conditions, statistical significance was assessed with the paired t-test and the Wilcoxon signed rank test at a significance level of 0.05. Each experiment was performed in at least three slices of at least two different animals; n refers to the number of tested cells. Baclofen applications in drug conditions were compared to 87.1 % of control, considering that consecutive applications decreased in amplitude (see figure 21).

# 3 Results

## 3.1 Identification of Astrocytes

The red fluorescent indicator sulforhodamine 101 (SR101, 100 µM) has been introduced previously, by Nimmerjahn et al. (2004), to specifically label all protoplasmic astrocytes close to the application site in intact neocortex of rats at postnatal day (P) 13 and older. During my work, I established a procedure for labeling astrocytes with SR101 in acute slices and assessed the usefulness of SR101 as astrocyte marker in hippocampal slices at young postnatal ages (P03 to P15; see also Kafitz et al., page 123ff). Slices were stained at 34°C with 0.5 - 1 µM sulforhodamine 101 for 20 minutes, immediately after sectioning the brain (see also section 2.1.2 on page 35).

Somata as well as primary processes of astrocytes could clearly be distinguished in the widefield epifluorescence system (figure 12A), when exciting SR101 at 575 nm and collecting fluorescence emission above 590 nm. Fine cellular processes were resolved using two-photon-laser scanning microscopy, where SR101 fluorescence was excited at 850 nm (see figure 12B). SR101-labeled cells had a morphology typical for astrocytes: cell bodies were about 10 µm in diameter and had several fine processes, some of which extended towards blood vessels (figure 12B). In fact, blood vessels could clearly be discriminated, consistent with the idea, that they are enclosed by endfeet of astrocyte processes (Zonta et al., 2003a; Simard et al., 2003). The pyramidal cell bodies, in contrast to the stratum radiatum, were not stained with SR101 and the CA1 layer appeared as a black, non-fluorescent band with the exception of a few small-sized cell somata and a few cellular processes reaching through the area (figure 12A,B; Kafitz et al., page 123, figure 1).

To confirm that SR101-stained hippocampal cells were indeed astrocytes, some cells were characterized electrophysiologically with respect to their membrane properties and their ability to generate action potentials

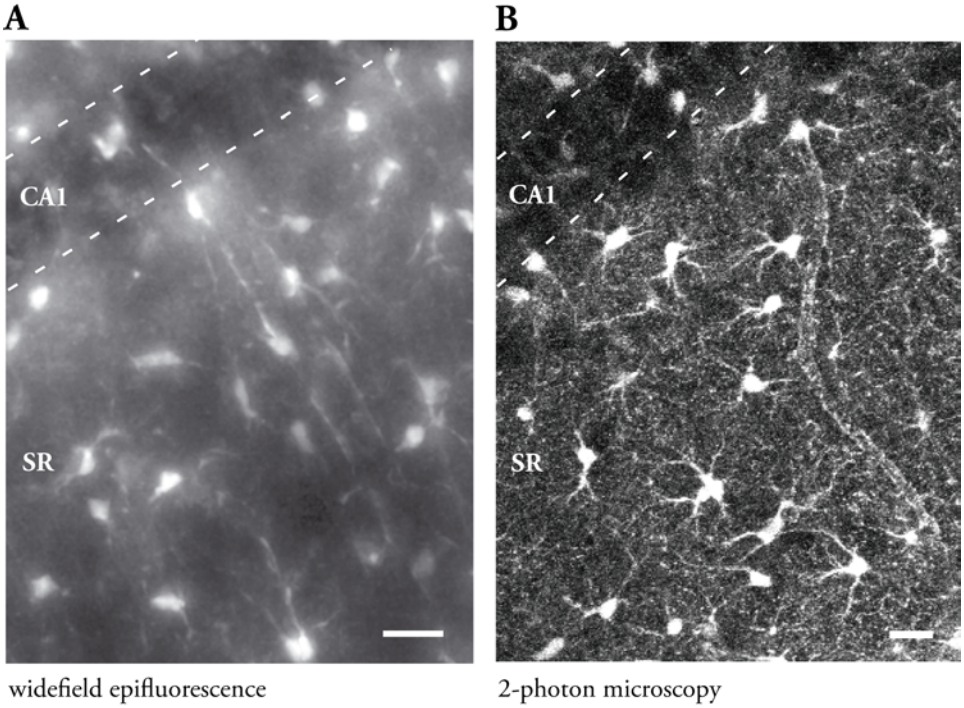


**Figure 12: SR101-Positive Cells Have a Morphology Typical for Astrocytes**

SR101-positive cells had a diameter of ∼10 µm and their fine processes frequently extended towards blood vessels (both P15, rat hippocampus). Astrocytes in the stratum radiatum (SR) were used for experiments.
**A**: SR101 staining as seen in the widefield epifluorescence system: the pyramidal cell layer (CA1, outlined by dashed lines) can clearly be seen as non-fluorescent band (upper left corner) - maximal intensity projection of 15 images taken while focussing through the slice. $\lambda_{ex}$: 575 nm; emission collected above 590 nm.
**B**: SR101 staining documented with two-photon laser scanning microscopy: small astrocytic processes can clearly be distinguished. Custom build two-photon microscope based on an Olympus Fluoview 300 system (Olympus Europe, Hamburg, Germany) coupled to a Mai-Tai broad band laser (Spectraphysics, Darmstadt, Germany); $\lambda_{ex}$: 850 nm, emission collected between 610 nm and 630 nm; z-projection of 15 optical sections at a distance of 1.0 µm, zoom 1.0; scale bars 20 µm.

(see also Bergles and Jahr, 1997; Steinhäuser et al., 1992; Zhou et al., 2006). All SR101-positive cells at P03 and P15 which were characterized electrophysiologically exhibited properties typical for astrocytes (n = 9 at P03, n = 11 at P15). First, their resting membrane potential was highly negative (P03: -84.2 ± 3.5 mV; P15: -85.5 ± 2.3 mV); second, they had low input resistances, especially at P15 (P03: 46.1 ± 19.7 MΩ; P15: 4.0 ± 1.4 MΩ); and finally, their capacitance was high (P03: 61.7 ± 17.4 pF; P15: 115.3 ± 41.9 pF; see also Kafitz et al., page 123ff).

In agreement with the developmental profile established by Zhou et al. (2006), all recorded cells at P03 (n=9/9; figure 13A) exhibited a non-linear IV-relationship. In contrast, the majority (∼70%) of astrocytes investigated at P15 had a linear IV-relationship and corresponded to typical passive astrocytes described earlier (n= 8/11; figure 13B; 5 of these cells were depolarized up to +55 mV, the other 6 only to +25 mV owing to overload of the amplifier). The remaining three cells recorded at P15 had non-linear IV-relationships, similar to the cells recorded at P03, also being in line with the results from Zhou et al. (2006, ; see also Kafitz et al.). In addition, none of the SR101-labeled cells exhibited voltage-dependent sodium currents (n = 20) and none elicited action potentials when depolarized to a membrane potential of up to + 50 mV (n = 5, not shown). In conclusion, in juvenile and adult rat hippocampus, the SR101-positive subpopulation of cells corresponded to classical astrocytes with a high potassium conductance and lack of voltage-gated sodium channels.

In order to perform $Ca^{2+}$ imaging experiments, slices were co-loaded with the $Ca^{2+}$-sensitive indicator dye fura-2 by pressure injection of fura-2-AM (∼500 µM) into the stratum radiatum. In general, more cells were loaded with fura-2 than with SR101, as fura-2, in contrast to SR101, was also taken up by neurons and small cells with astrocyte morphology in the stratum radiatum (figures 14A, P03; and 15A + B P15). When co-loaded with

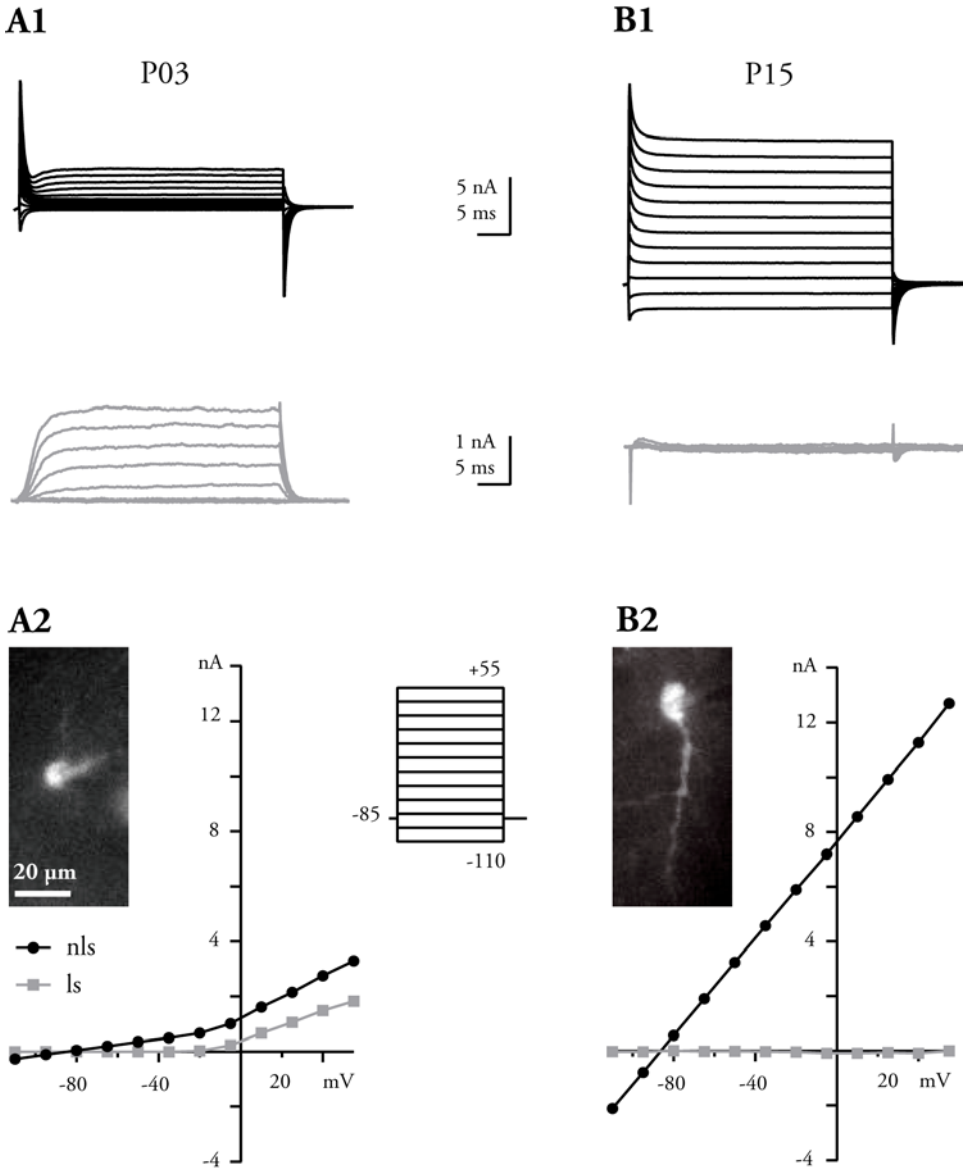


**Figure 13: SR101-Positive Cells Have Astrocytic Properties at P03 and P15**

SR101-positive cells at P3 (**A**) and P15 (**B**) were voltage-clamped at -85 mV and voltage was stepped from -110 to +55 mV (see bottom **insert**).
**A1, B1**: Non-leak-subtracted (nls; black) and leak-subtracted (ls; grey) traces, representative for the respective age (n = 9 and 11 at P03 and P15, respectively).
**A2, B2**: Current measured 10 ms after initiation of the voltage-step plotted versus voltage is unlinear in young cells (A2), typical for immature astrocytes. At P15 (B2), most cells show a linear IV-relationship, typical for mature astrocytes.
**Inserts**: SR101 fluorescence of the recorded cells, scale bar valid for both images.

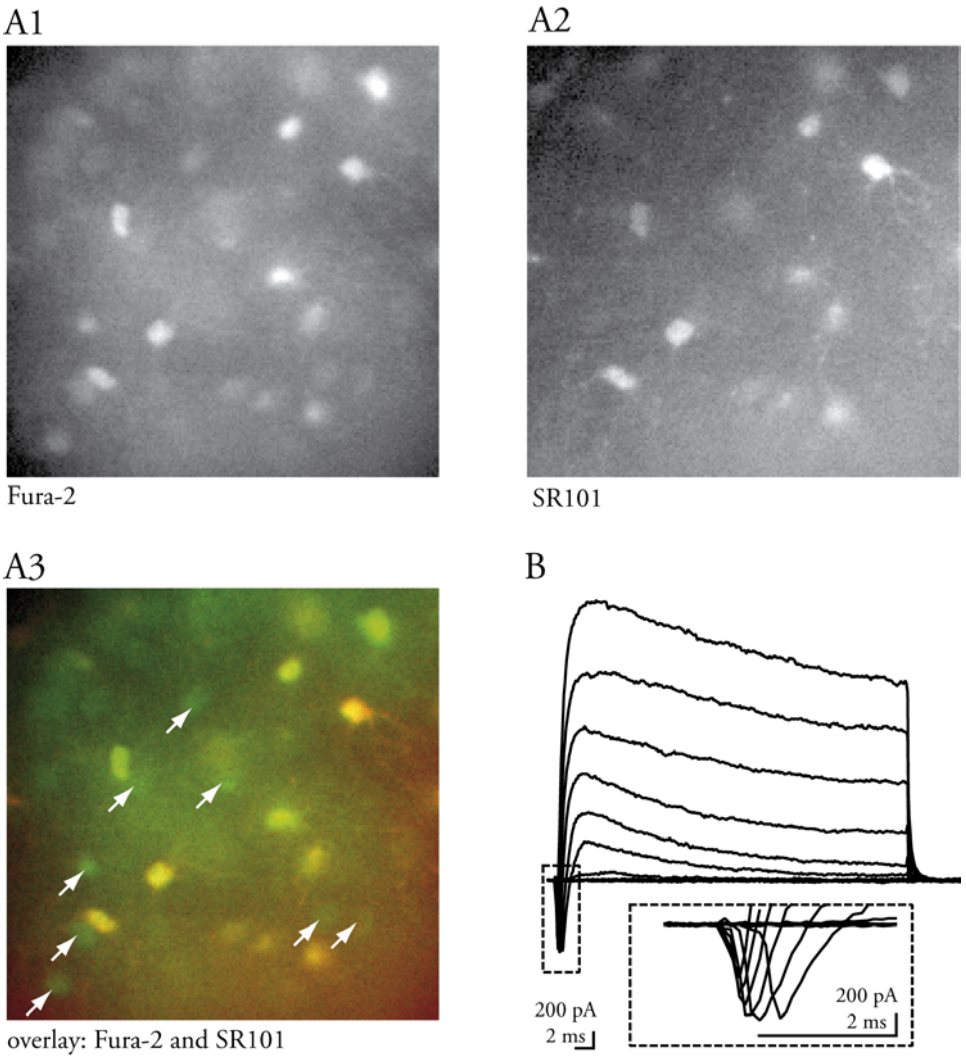


**Figure 14: SR101-Negative Cells at P03 Likely Correspond to Immature Glial Cells**

**A**: Fura-2-AM (**A1**) and SR101 (**A2**) stainings of rat hippocampal slices at P03. Overlay of fFura-2 and SR101 fluorescence (**A3**); note that there are many small cells in the stratum radiatum (arrows) which are stained with fura-2, but not with SR101. Their number amounted to roughly 55% of all cells with astrocyte morphology in the stratum radiatum.
**B**: Leak-subtracted IV-curves of SR101-negative cells at P03 reveal inward currents resembling voltage-gated $Na^+$ currents; same voltage-step-protocol as in figure 13).

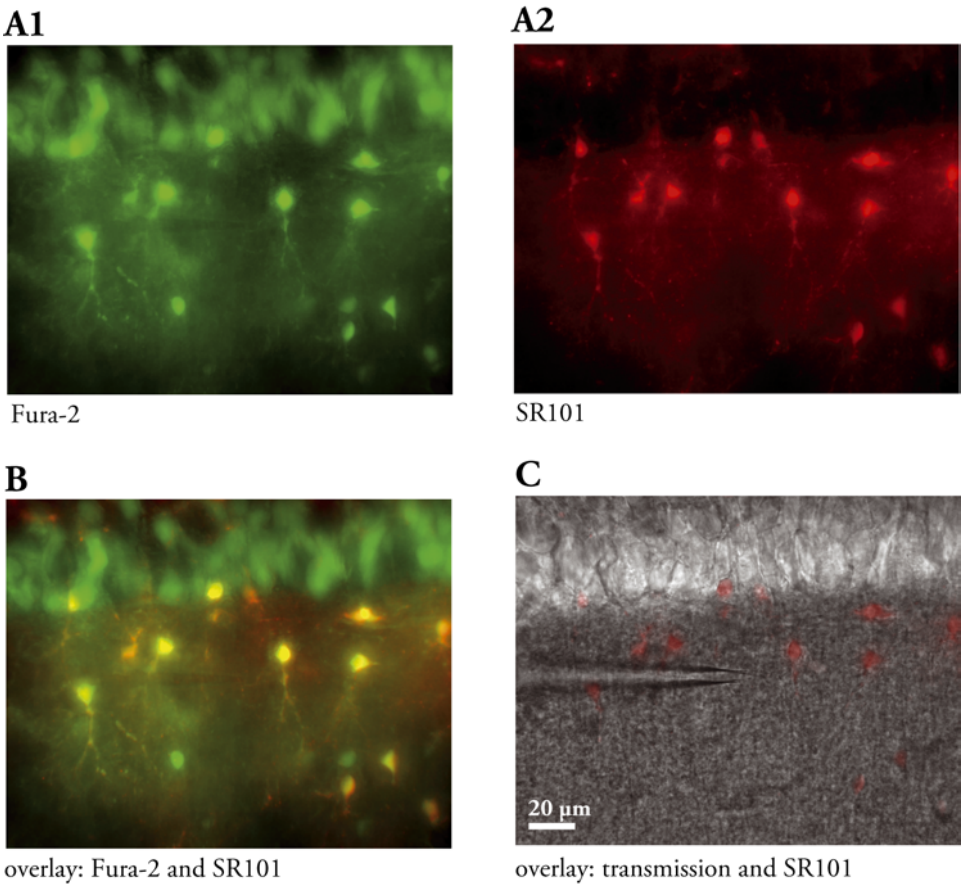


**Figure 15: Almost All Fura-2-Positive Cells with Astrocyte Morphology are Labeled with SR101 at P15**

**A**: Images taken with the widefield epifluorescence system showing typical fura-2 (**A1**) and SR101(**A2**) fluorescence; maximal intensity projections of five images each.
**B**:Overlay of fura-2 and SR101 fluorescence. Roughly 90% of cells with astrocyte morphology (as determined by staining with fura-2 or the $Na^+$ indicator dye SBFI) were also stained with SR101. Note that CA1 pyramidal cells are not stained with SR101, whereas most cells in the stratum radiatum are yellow, denoting colocalization of fura-2 and SR101.
**C**: The transmitted light image is overlaid with a contrast enhanced image of SR101 fluorescence depicting localization of astrocytic cell bodies. Additionally, the typical size and location of the application pipette is shown.

fluorescent indicator dyes for either $Na^+$ (SBFI) or $Ca^{2+}$ (fura-2), roughly 90% of indicator-loaded cells with astrocyte morphology in the stratum radiatum at P15 were positive for SR101 whereas at P03 this fraction was only about 55%. Four of these young SR101-negative cells were characterized electrophysiologically (see also Kafitz et al., page 123ff for a more thorough characterization of SR101-negative cells). Their properties varied considerably from those of SR101-positive cells at the same age: (1) their resting membrane potential was less negative (-48.1 ± 4.0 mV), (2) their input resistance was much higher (between 350 and 4000 MΩ), (3) their membrane capacitance was lower (21.1 ± 2.8 pF), and (4) all of them exhibited fast-inactivating inward currents, most likely representing voltage-gated $Na^+$ currents (figure 14B; n = 4). Nevertheless, none of the SR101-negative cells elicited action potentials upon depolarization up to +50 mV (n=3). Hence, SR101-negative cells with astrocyte morphology in the stratum radiatum presumably correspond to cells previously referred to as outward rectifying glia (ORG; Zhou et al., 2006).

Immunohistochemical stainings with an antibody directed against glial fibrillary acidic protein (GFAP) revealed that 80% of SR101-positive cells at P15 were positive for GFAP (Kafitz et al., page 123ff, immunohistochemistry carried out by Jonathan Stephan).

Taken together, these experiments validate staining with SR101 as a tool for identification of astrocytes in the acute slice. At P15, most cells with astrocyte morphology were stained, whereas at P03 a large proportion of cells, morphologically resembling astrocytes, was not stained with SR101. The fraction of non-SR101-stained cells with astrocyte morphology likely corresponded to another subpopulation of glial cells, the proportion of which decreases during maturation (Zhou et al., 2006). The SR101-labeled subpopulation of cells exhibited astrocytic properties as confirmed with patch-clamp recordings and immunohistochemistry for GFAP (Kafitz

et al., page 123ff). While SR101-positive cells at P03 exhibited a non-linear IV-relationship, they resembled classical passive astrocytes at P15 (see also discussion, section 4.1).

## 3.2 GABA-Induced $Ca^{2+}$ Signaling

$Ca^{2+}$ transients in astrocytes are implied in neuron-glia interaction, as astrocytes release gliotransmitters such as adenosine triphosphate (ATP), glutamate, and $\gamma$-aminobutyric acid (GABA) by which they influence the neuronal network (see also section 1.1.4; Kang et al., 1998; Serrano et al., 2006; Zhang et al., 2003; Liu et al., 2000). The mechanism of GABA-induced $Ca^{2+}$ transients in hippocampal astrocytes has not been elucidated in detail. In the present study, increases in $[Ca^{2+}]_i$ of hippocampal astrocytes in acute brain slices upon activation of GABA receptors were investigated by pressure application of GABA (0.5 - 1 mM; 100 - 500 ms) with micropipettes onto SR101-positive astrocytes in the stratum radiatum (see figure 15 for identification of astrocytes as well as typical size and location of application pipette). Changes in $[Ca^{2+}]_i$ were measured with the fluorescent $Ca^{2+}$ indicator dye fura-2 (see section 2.2.1 for details). 500 nM TTX was added to the extracellular solution to block neuronal activity, unless stated otherwise. Astrocytes at P15 exhibited $[Ca^{2+}]_i$ increases of up to 80 nM when challenged with GABA (figure 16). The average $[Ca^{2+}]_i$ increase was 45 nM from a resting $[Ca^{2+}]_i$ of $\sim$75 nM (n = 8). $Ca^{2+}$ transients started about 1 s after application and peaks were reached after $\sim$20 s (n = 8).

Astrocytes express both ionotropic and metabotropic GABA receptors (Fraser et al., 1995; MacVicar et al., 1989; Charles et al., 2003b; Oka et al., 2006). Their involvement in the GABA-induced $Ca^{2+}$ transient was investigated by application of specific receptor antagonists. The $GABA_A$ receptor antagonist bicuculline (50 µM; Fraser et al., 1995) partially blocked GABA-induced $Ca^{2+}$ signals in astrocytes (45% reduction; n = 8). CGP55845 (3

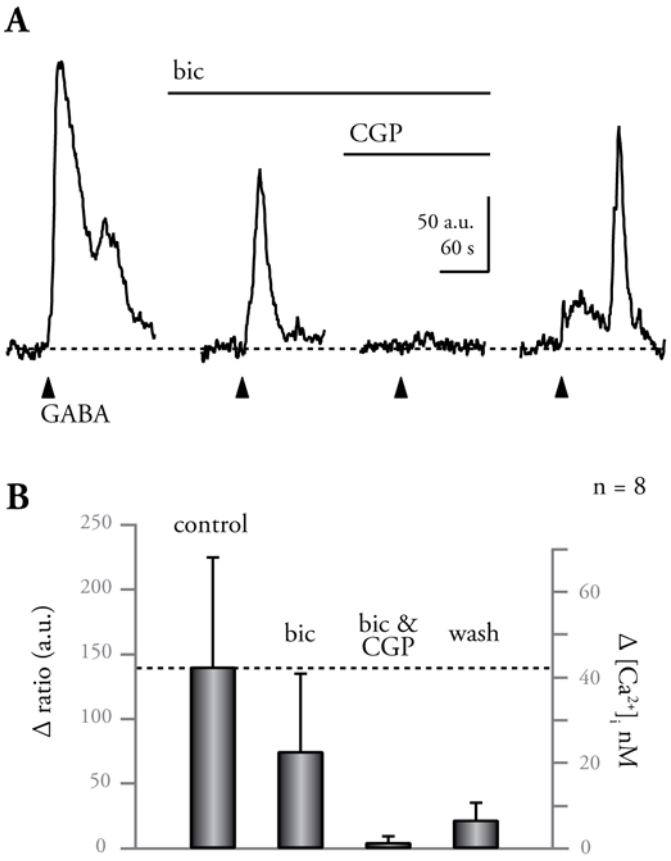


**Figure 16: GABA-Induced $Ca^{2+}$ Transients in Astrocytes are Mediated by both $GABA_A$ and $GABA_B$ Receptors**

**A**: Changes in the fura-2 ratio elicited by GABA (100 ms, 1 mM) were partially blocked by the $GABA_A$ receptor agonist bicuculline (50 µM; bic). The remainder of the signal was blocked by the $GABA_B$ receptor antagonist CGP55845 (3 µM; CGP). After washing out the drugs, the signal recovered partially.
**B**: Bar chart showing mean change in fura-2 ratio (left axis; a.u. = arbitrary units corresponding to change in ratio) and corresponding $[Ca^{2+}]_i$ increase (right axis, n= 8), peaks were measured approximately 20 s after GABA application, error bars correspond to standard deviation (S.D.); resting $[Ca^{2+}]_i$ was $\sim$ 75 nM.

µM), a specific $GABA_B$ receptor antagonist (Davies et al., 1993), blocked the remaining signals virtually completely (n = 8). After washout of bicuculline and CGP55845 the responses recovered to about 20% of control (figure 16; n = 8). Because the $GABA_B$ receptor antagonist was largely irreversible (see below), this partial recovery could be attributed to the activation of $GABA_A$ receptors. These results show that the GABA-induced $Ca^{2+}$ transient in mature astrocytes was mediated by both $GABA_A$ and $GABA_B$ receptors.

## 3.3 Mechanism of $GABA_A$ Receptor-Mediated $[Ca^{2+}]_i$ Increases

In subsequent experiments the mechanisms of $GABA_A$ and $GABA_B$ receptor-mediated $[Ca^{2+}]_i$ increases were investigated in detail using specific receptor agonists for each receptor type: $GABA_A$ receptors were activated by muscimol and $GABA_B$ receptors with the specific $GABA_B$ receptor agonist baclofen.

Muscimol (100 ms, 500 µM), when pressure-applied with fine micropipettes at a distance of 10 to 20 µm from the soma of an astrocyte, instantaneously caused small $[Ca^{2+}]_i$ increases of up to 20 nM (see also section 3.5). The peak $[Ca^{2+}]_i$ was reached 4-6 seconds after application (P03: 3.9 ± 2.7 s, n = 65 ; P15: 5.8 ± 3.4 s, n = 62).

In whole-cell voltage-clamp recordings, all of the cells tested exhibited large inward currents when challenged with 500 µM muscimol for 50 ms (n= 19; 8 at P03, figure 17A1; and 11 at P15, figure 17B1). 50 µM bicuculline, a selective $GABA_A$ receptor antagonist, reversibly blocked this current (figure 17, A1 and B1; n=7, 2 at P03 and 5 at P15). In current clamp mode, astrocytes were strongly depolarized upon $GABA_A$ receptor activation with muscimol (n=6; 2 at P03 and 4 at P15, figures 17 A1 and B2, respectively). The membrane potential depolarized by more than 60 mV from a typical

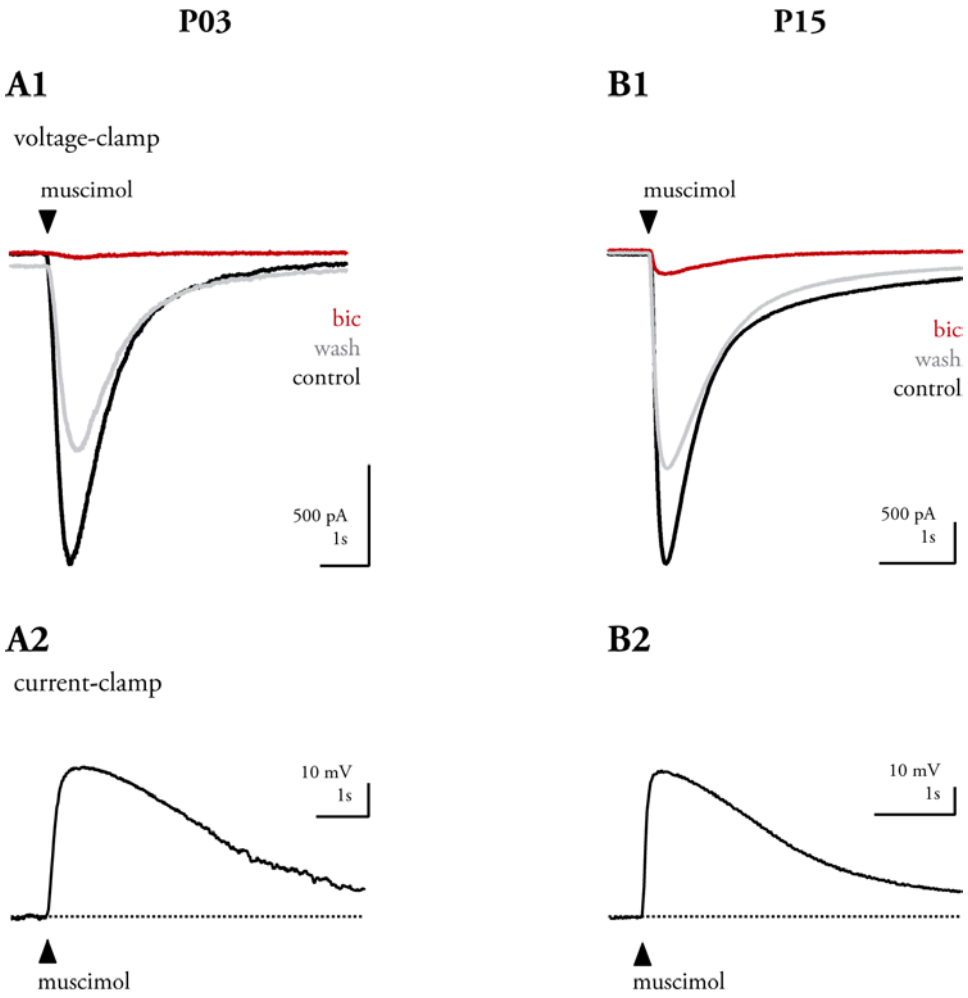


**Figure 17: Muscimol Induced Inward Currents and a Membrane Depolarization at P03 and P15**

**A1, B1**: Inward currents induced by muscimol (50 ms, 500 µM; n = 8 and 11 at P03 and P15, respectively) were reversibly blocked by bicuculline (50 µM) at P03 (**A1**, n = 2) and P15 (**B1**, n = 5).
**A2, B2**: Current-clamp recordings revealed large membrane depolarizations of astrocytes at P03 (**A2**, n = 2) and P15 (**B2**, n = 4) upon application of muscimol.

resting potential of -85 mV, and reached values of up to -20 mV. These results are consistent with opening of $Cl^-$ channels and subsequent efflux of $Cl^-$ upon $GABA_A$ receptor activation, as described earlier (MacVicar et al., 1989).

The origin of the $GABA_A$ receptor-mediated $[Ca^{2+}]_i$ increase was investigated further with pharmacological tools. As expected, bicuculline (50 µM) reversibly blocked muscimol-induced $Ca^{2+}$ transients at P03 and P15 (n = 7 each; figure 18). Additionally, perfusion with nominally $Ca^{2+}$- free extracellular solution (see section 2.3) blocked the $Ca^{2+}$ transient (n = 4 and 5 at P03 and P15, respectively; figure 18). Thus, $Ca^{2+}$ influx from the extracellular space was underlying the $[Ca^2]_i$ increase.

The involvement of voltage-activated $Ca^{2+}$ channels in the signaling cascade had been implied in a previous studie in acutely isolated astrocytes (Fraser et al., 1995). To test this possibility, I applied muscimol in the presence of 2 mM $Ni^{2+}$, an unselective blocker of voltage-activated $Ca^{2+}$ channels. In both, P03 and P15 astrocytes, $Ni^{2+}$ reversibly blocked the muscimol-induced $Ca^{2+}$ transient (n = 3 and 7, respectively; figure 18), suggesting involvement of voltage-gated $Ca^{2+}$ channels.

To collect further evidence for the involvement of voltage-gated $Ca^{2+}$ channels, experiments with $Ba^{2+}$ were performed. Besides being permeable for $Ca^{2+}$, voltage-activated $Ca^{2+}$ channels are permeable for other divalent ions. $Ba^{2+}$, in comparison to $Ca^{2+}$, slows the rate of channel inactivation and even has a higher permeability than $Ca^{2+}$ through most voltage-gated $Ca^{2+}$ channels (Carmignoto et al., 1998). Because fura-2 is also sensitive to $Ba^{2+}$ (Haugland, 2005), muscimol (100 ms 500 µM) was applied in the presence of 1 mM $Ba^{2+}$ (n = 8), expecting that the Fura-2 ratio would increase more than with $Ca^{2+}$ alone. The results of this experiment have to be interpreted with caution, as $Ba^{2+}$ shifted the baseline ratio, mimicking an increase in $[Ca^{2+}]_i$. The signals elicited by muscimol in the presence of

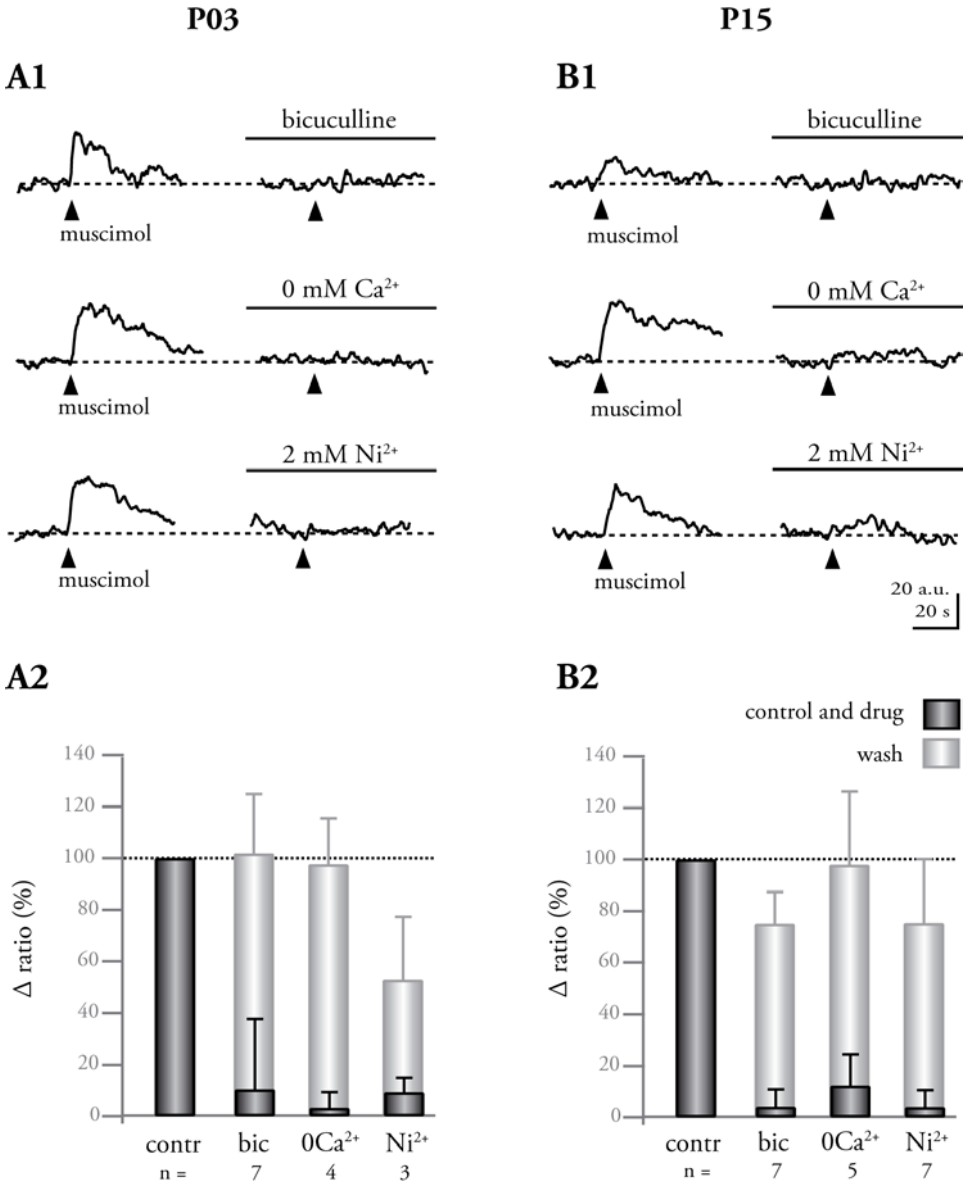


**Figure 18: The Pharmacological Profile of Muscimol-Induced $Ca^{2+}$ Increases is Similar Throughout Development**

Pharmacology at P03 (**A**) and P15 (**B**). **A1, B1**: $[Ca^{2+}]_i$ increases elicited with muscimol (100 ms 500 µM) were almost completely blocked by 50 µM bicuculline, 0 mM $Ca^{2+}$ / 200 µM EGTA or 2 mM $Ni^{2+}$, being consistent with $Ca^{2+}$ influx through voltage-gated $Ca^{2+}$ channels.
**A2, B2**: Bar charts quantifying muscimol-induced $[Ca^{2+}]_i$ increases in the presence of drugs and after wash-out, normalized to previous control applications in the same cells.

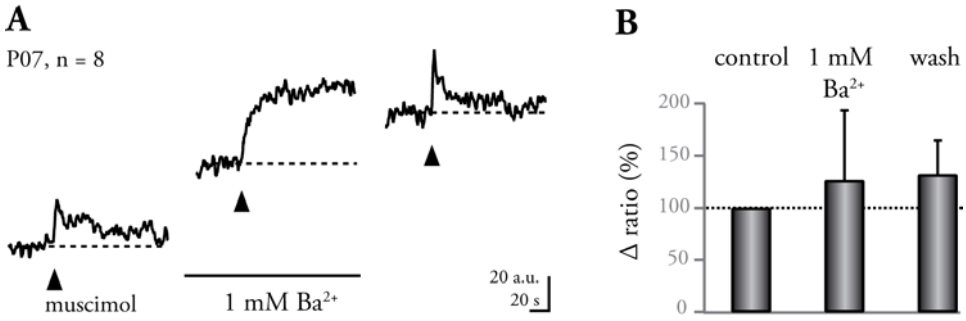


**Figure 19: $Ba^{2+}$ Changes Amplitude and Time Course of Muscimol-Induced $Ca^{2+}$ Transients**

**A**: The muscimol-induced (100 ms, 500 µM) ratio change is present in 1 mM $Ba^{2+}$, however, $Ba^{2+}$ seems to have long lasting influences on fura-2 fluorescence (P07; n=8).
**B**: Bar chart quantifying the observed ratio increase in the presence of and after $Ba^{2+}$.

$Ba^{2+}$ were larger than in the absence of $Ba^{2+}$ (figure 19). However, the time course of the $Ca^{2+}$ transients elicited in $Ba^{2+}$ differed from that of the control application, and the signal did not recover to baseline (n=8, P07; figure 19A). The change in the kinetic of the signal was reversible after wash-out of $Ba^{2+}$, but the change in baseline did not recover, indicating a long-term effect of $Ba^{2+}$ either on $Ca^{2+}$ homeostasis in astrocytes or on fura-2.

The pharmacological profiles of $GABA_A$ receptor-mediated $[Ca^{2+}]_i$ increases at P03 and P15 are summarized in figure 18 (A2 and B2, respectively). The mechanism of $GABA_A$ receptor-mediated $[Ca^{2+}]_i$ increases in astrocytes was identical during development from P03 to P15.

Accordingly, these results confirm that $GABA_A$ receptor-mediated $[Ca^{2+}]_i$ increases in both juvenile and adult rat hippocampal astrocytes were due to depolarization and subsequent $Ca^{2+}$ influx through voltage-gated $Ca^{2+}$ channels.

## 3.4 Mechanism of $GABA_B$ Receptor-Mediated $[Ca^{2+}]_i$ Increases

### 3.4.1 Characteristics of $Ca^{2+}$ Responses

$GABA_B$ receptor-mediated $Ca^{2+}$ responses in SR101-positive hippocampal astrocytes were examined, using the specific $GABA_B$ receptor agonist baclofen. When baclofen (100 ms, 500 µM) was pressure-applied onto acute hippocampal slices of P15 animals, ∼55% of astrocytes (n=35/65) responded with a $[Ca^{2+}]_i$ increase that was several seconds delayed and typically reached its peak about 30 seconds after the application (31.4 s ± 9.6 s; n = 201 applications in 35 cells).

The amplitudes and time courses of baclofen-evoked $Ca^{2+}$ transients varied among neighboring cells and did not correlate with the distance from the pipette (figure 20). Hence, individual cells respond differently to $GABA_B$ receptor activation, and amplitudes of $[Ca^{2+}]_i$ increases elicited by baclofen did not only depend on the concentration of baclofen. $Ca^{2+}$ increases were in the range of 5 to 270 nM and the average increase was 45 ±50 nM. Lower concentrations of baclofen (500 ms, 50 µM) also elicited $Ca^{2+}$ transients in astrocytes, which varied between 10 nM and 105 nM (n = 6; P15; not shown).

Interestingly, a variability in amplitude and time course of $[Ca^{2+}]_i$ increases was also observed when one and the same cell was repetitively challenged with baclofen at an interval of six minutes (see figure 21 for sample responses). Consequently, I generally averaged two consecutive applications under either control or drug conditions. Repetitive applications exhibited a small run-down in the amplitudes of baclofen-induced $[Ca^{2+}]_i$ increases (figure 21B): the mean amplitudes of the third and fourth application amounted to ∼87% of the first two applications (n=32; figure 21B2, second bar), and that of the fifth and sixth to ∼79% (n=15; figure 21B2, third bar).

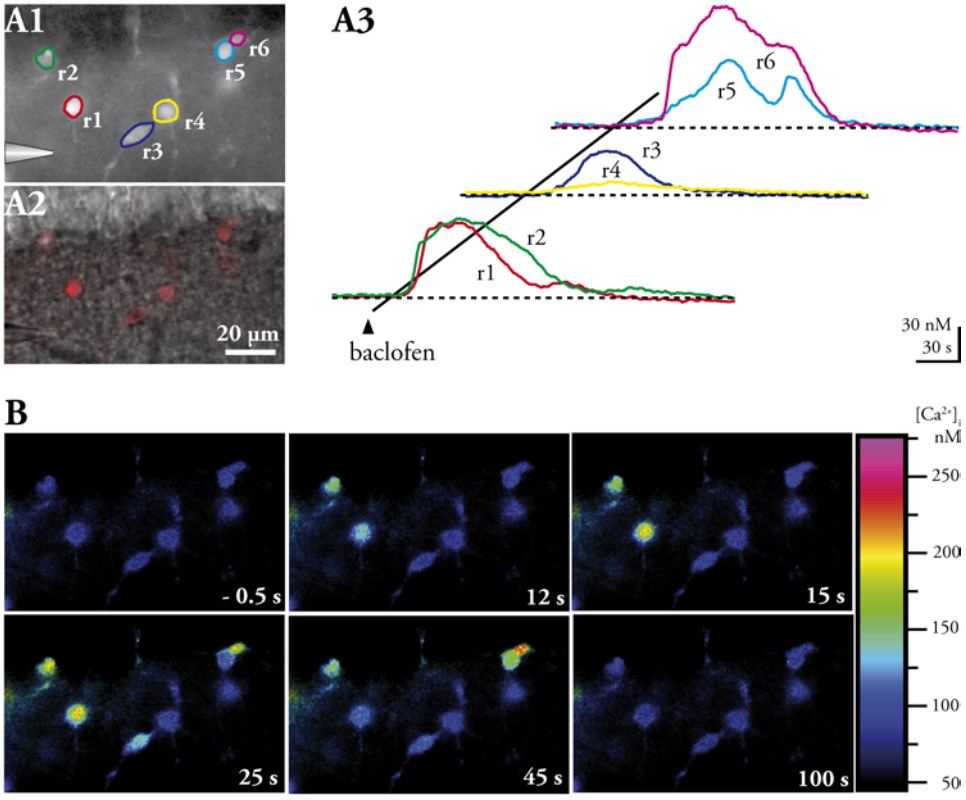


**Figure 20: Amplitudes of Baclofen-Induced $[Ca^{2+}]_i$ Increases in Astrocytes Did Not Correlate with the Distance from the Pipette**

**A**: $Ca^{2+}$ transients elicited with baclofen (100 ms, 500 µM) in an acute slice. Traces (A3) show changes in $[Ca^{2+}]_i$ in regions of interest (r1 to r6) depicted in A1. The solid line denotes the time point at which baclofen was applied. The location of the application pipette is illustrated in A1 and A2; the transmission image (A2) is overlayed with contrast enhanced SR101 fluorescence to show location of cell bodies.

**B**: Color coded images of $[Ca^{2+}]_i$ (see scale bar). Ratio images have been converted into $[Ca^{2+}]_i$ and were overlayed with a mask obtained from SR101 fluorescence in order to show changes in $[Ca^{2+}]_i$ selectively in SR101-positive cells (P15).

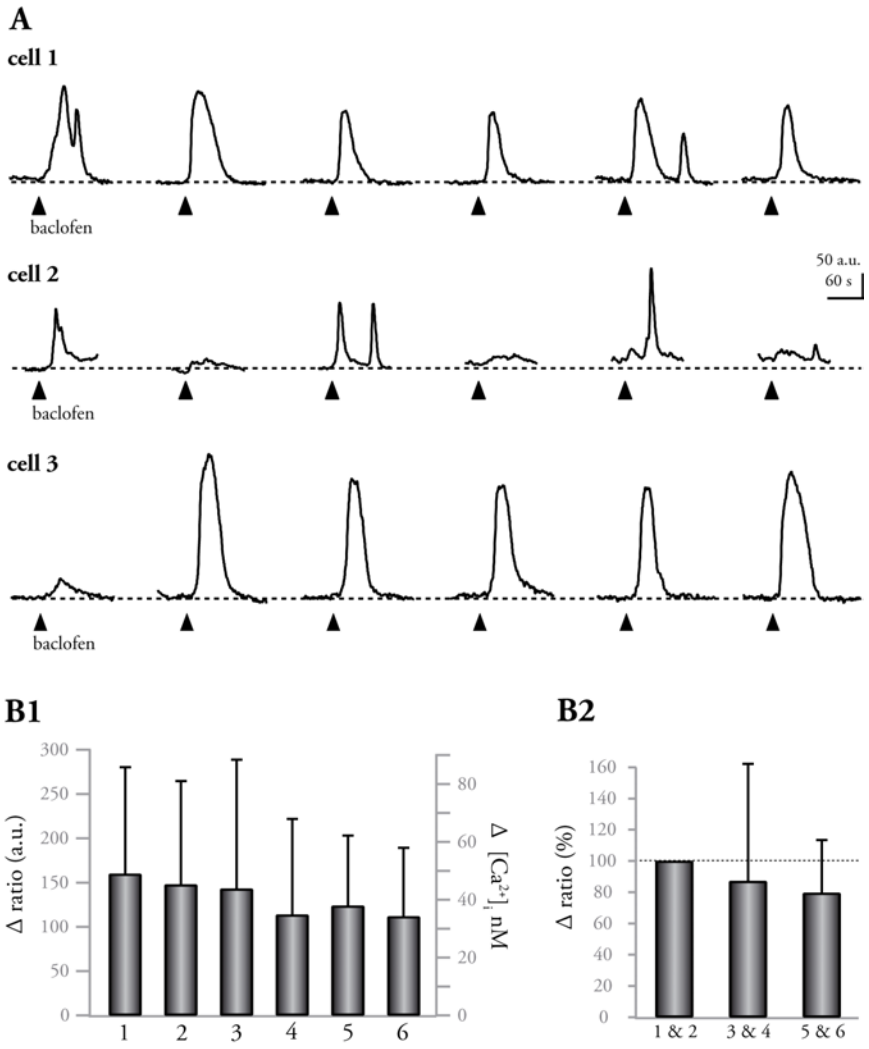


**Figure 21: Baclofen Induced $Ca^{2+}$ Increases in Astrocytes in the Acute Slice**

**A**: Responses of three different cells (cell 1-3) to six consecutive baclofen applications (100 ms, 500 µM) at an interval of six minutes. The $Ca^{2+}$ transients did vary both in amplitude and time course.
**B**: Quantification of baclofen-induced $[Ca^{2+}]_i$ increases. The left bar chart (B1) shows mean ratio changes and corresponding $[Ca^{2+}]_i$ increases induced by the single baclofen applications. In pharmacological experiments, two applications under each condition were generally averaged. The right bar chart (B2) depicts the observed run-down of baclofen-induced $[Ca^{2+}]_i$ increases under this paradigm. Each bar corresponds to averaged mean values of two consecutive applications. The second and third bars are normalized to the average of the first two applications. Numbers refer to application numbers; error bars depict standard deviation (S.D.).

Next, I investigated baclofen-induced $[Ca^{2+}]_i$ increases in primary cultures of hippocampal astrocytes. After 8 to 14 days in vitro (DIV), astrocytes were typically distributed in a monolayer and most cells were spread out over large distances. $GABA_B$ receptor activation with baclofen (10 s, 500 µM) evoked $[Ca^{2+}]_i$ increases in only a few cells in cultures (DIV 8-14). Altogether, 25 out of more than 315 cells reacted (<8%). On one coverslip (DIV 11) 24 out of 143 cells responded with a $[Ca^{2+}]_i$ increase, whereas on the remaining five coverslips (DIV 8, 11 and 14) only one out of more than 172 cells reacted. Typically, consecutive baclofen applications elicited only small changes in $[Ca^{2+}]_i$ (not shown).

However, in contrast to the acute slice, small cellular processes could be resolved in cultured cells with the monochromator-based widefield imaging system. In the few cells that responded, baclofen (10 s, 500 µM) typically elicited intracellular $Ca^{2+}$ waves which started in the periphery of astrocytes and only sometimes invaded the soma (figure 22).

Owing to the small number of responding cells as well as the unreliability of repetitive signals in cultures, all subsequent experiments were performed in acute slices.

### 3.4.2 Direct vs. Indirect Activation of Astrocytes

Given that in acute slices the hippocampal network remains largely intact (see section 1.2 and figure 2), interactions of astrocytes with other cell types cannot be excluded. In addition, drugs applied onto intact slices activate not only astrocytic receptors, but also receptors of other cell types which subsequently might release "glioactive" substances. Therefore, the next subset of experiments aimed at elucidating whether astrocytic $[Ca^{2+}]_i$ increases upon $GABA_B$ receptor activation were due to a direct or indirect activation of astrocytes. A pharmacological approach was chosen to answer this question.

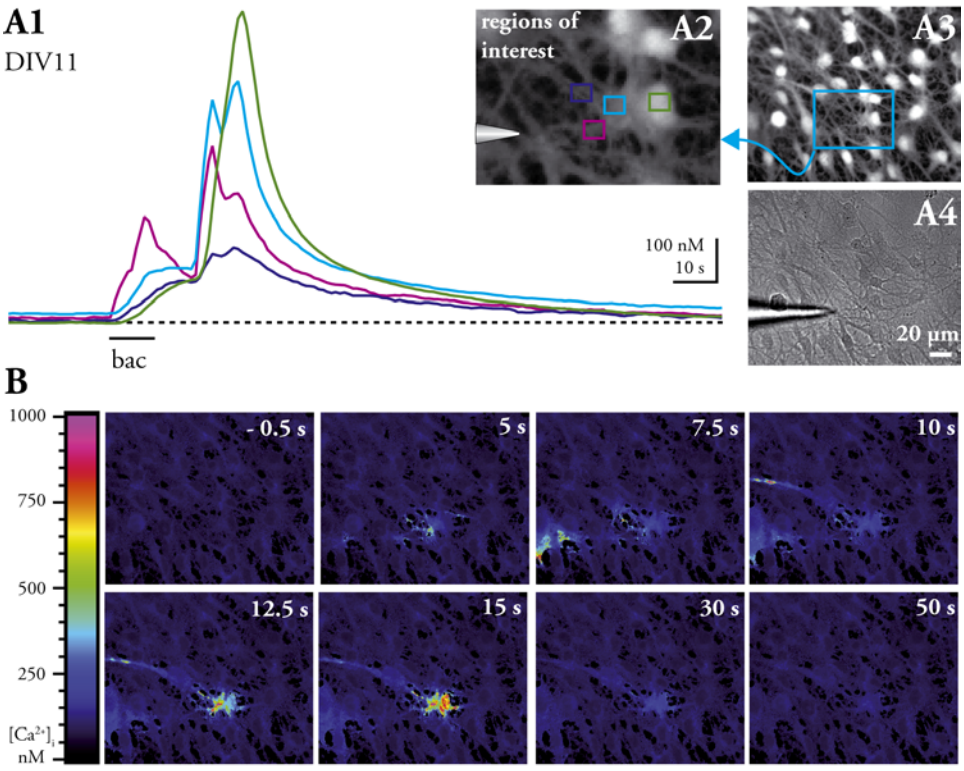


**Figure 22: Baclofen Induced Intracellular $Ca^{2+}$ Waves in Cultured Astrocytes**

**A**: $Ca^{2+}$ transients (A1) measured in the regions depicted in A2 (which also illustrates the position of the application pipette); A3, fluorescence image of astrocytes in culture loaded with fura-2; A4, transmission image of cultured astrocytes, note the position of the application pipette at the left; DIV, days *in vitro*.
**B**: Color-coded $[Ca^{2+}]_i$ images, showing a typical response to baclofen in cell culture; time after application is indicated in each image.

The specific $GABA_B$ receptor antagonist CGP55845 (3 µM; n = 9) blocked baclofen-induced $Ca^{2+}$ signals virtually completely (figure 23), indicating that $[Ca^{2+}]_i$ increases were indeed mediated by activation of $GABA_B$ receptors. To investigate whether astrocytic $[Ca^{2+}]_i$ increases elicited by baclofen were secondary to neuronal activity, I compared baclofen-induced $[Ca^{2+}]_i$ increases in the absence and presence of TTX (500 nM). Blocking neuronal action potential firing and subsequent transmitter release with 500 nM TTX did not reduce the baclofen-induced $Ca^{2+}$ signal in astrocytes (n = 14; figure 23; no TTX in extracellular solution during control applications).

In addition to blocking action potential generation with TTX, synaptic transmitter release is impeded by blocking high voltage-activated $Ca^{2+}$ channels (Araque et al., 2002). A possible influence of neuronal transmitter release on the baclofen-induced $Ca^{2+}$ signal was examined by blocking neuronal transmitter release with 100 µM $Cd^{2+}$. However, similar to the experiments with $Ba^{2+}$, $Cd^{2+}$ caused the fura-2 ratio to increase continuously (n = 8), mimicking an increase in baseline $[Ca^{2+}]_i$. Additional increases in the fura-2 ratio could clearly be evoked by baclofen (100 ms, 500 µM; n = 8; not shown). These ratio changes likely reflected $[Ca^{2+}]_i$ increases induced by $GABA_B$ receptor activation, however, quantification was not attempted owing to the interaction of $Cd^{2+}$ with fura-2 (Marchi et al., 2000; Haugland, 2005) and / or $Ca^{2+}$ homeostasis (Marchi et al., 2000).

To further investigate a possible involvement of voltage-gated $Ca^{2+}$ channels in the baclofen-induced $[Ca^{2+}]_i$ increase in astrocytes, I applied baclofen in the presence of $Ni^{2+}$, which is an unspecific inhibitor of voltage-gated $Ca^{2+}$ channels. $Ni^{2+}$ (2 mM) neither altered the $Ca^{2+}$ transient substantially (n = 6; figure 23), nor had any influence on fura-2 fluorescence, despite being a divalent ion.

Taken together these data indicate that baclofen-induced $[Ca^{2+}]_i$ increases in astrocytes did not depend on neuronal activity and transmitter

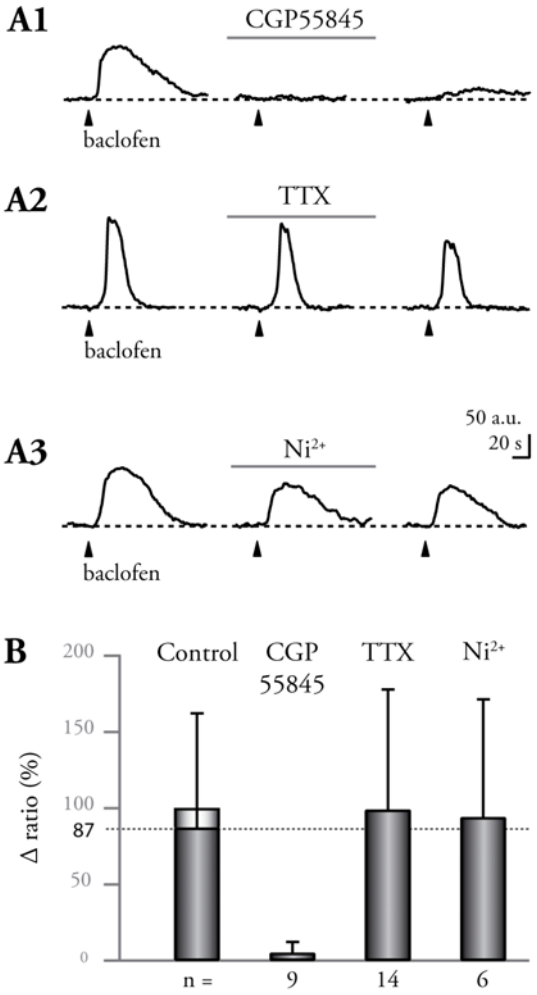


**Figure 23: Mechanism of $GABA_B$ Receptor-Induced $[Ca^{2+}]_i$ Increases**

**A**: Baclofen-induced (100 ms, 500 µM) $Ca^{2+}$ transients in astrocytes were blocked by the $GABA_B$ receptor antagonist CGP55845 (3 µM; A1). Neither TTX (500 nM; A2) nor $Ni^{2+}$ (2 mM; A3) considerably altered the amplitude of $GABA_B$ receptor-mediated $[Ca^{2+}]_i$ increases.
**B**: Bar chart quantifying baclofen-evoked $[Ca^{2+}]_i$ increases of all experiments. Baclofen applications in the presence of drugs are compared to 87% of control as the $[Ca^{2+}]_i$ increased caused by consecutive applications decreased in amplitude (cf. figure 21).

release. Furthermore, voltage-gated $Ca^{2+}$ channels were not involved in the signaling pathway of $GABA_B$ receptor-mediated $[Ca^{2+}]_i$ increases in hippocampal astrocytes.

### 3.4.3 $Ca^{2+}$ Influx vs. $Ca^{2+}$ Release

The next step was to determine whether $Ca^{2+}$ influx from the extracellular space or $Ca^{2+}$ release from intracellular stores is underlying the the $GABA_B$ receptor-induced $[Ca^{2+}]_i$ increase. To this end, experiments in nominally $Ca^{2+}$-free extracellular solution were performed.

In addition to baclofen, a control substance, trans-(1S,3R)-1-Amino-1,3-cyclopentanedicarboxylic acid (t-ACPD; 100 ms, 100 µM), was applied to ensure that intracellular stores did not deplete and were capable of releasing $Ca^{2+}$. t-ACPD activates metabotropic glutamate receptors in astrocytes and thereby releases $Ca^{2+}$ from $IP_3$-sensitive intracellular stores (Floyd et al., 2001). In nominally $Ca^{2+}$-free saline, the amplitudes of $Ca^{2+}$ transients evoked by either substance were strongly reduced (see figure 24A1; n =13 and 4 for baclofen and t-ACPD, respectively). Interestingly, $Ca^{2+}$-free extracellular solution reduced both $Ca^{2+}$ transients alike. In addition, when reperfusing with $Ca^{2+}$-containing solution (2 mM $Ca^{2+}$, 1 mM $Mg^{2+}$) both signals were restored to roughly 50% of control after ∼17 minutes (figure 24A1). In contrast, muscimol-induced $Ca^{2+}$ signals, mediated by $Ca^{2+}$ influx from the extracellular space, were completely restored within 8 to 10 minutes of reperfusion (n = 16; cf. figure 18).

The reduction of the t-ACPD-induced signal implies that intracellular $Ca^{2+}$ stores in astrocytes rapidly deplete in the absence of extracellular $Ca^{2+}$. Taken together, the data obtained in nominally $Ca^{2+}$-free extracellular solution suggest that baclofen acted onto the same cellular compartment as t-ACPD. Hence, $GABA_B$ receptor activation in astrocytes likely causes $Ca^{2+}$ release from inositol-1,4,5-trisphosphate ($IP_3$)-sensitive intracellular

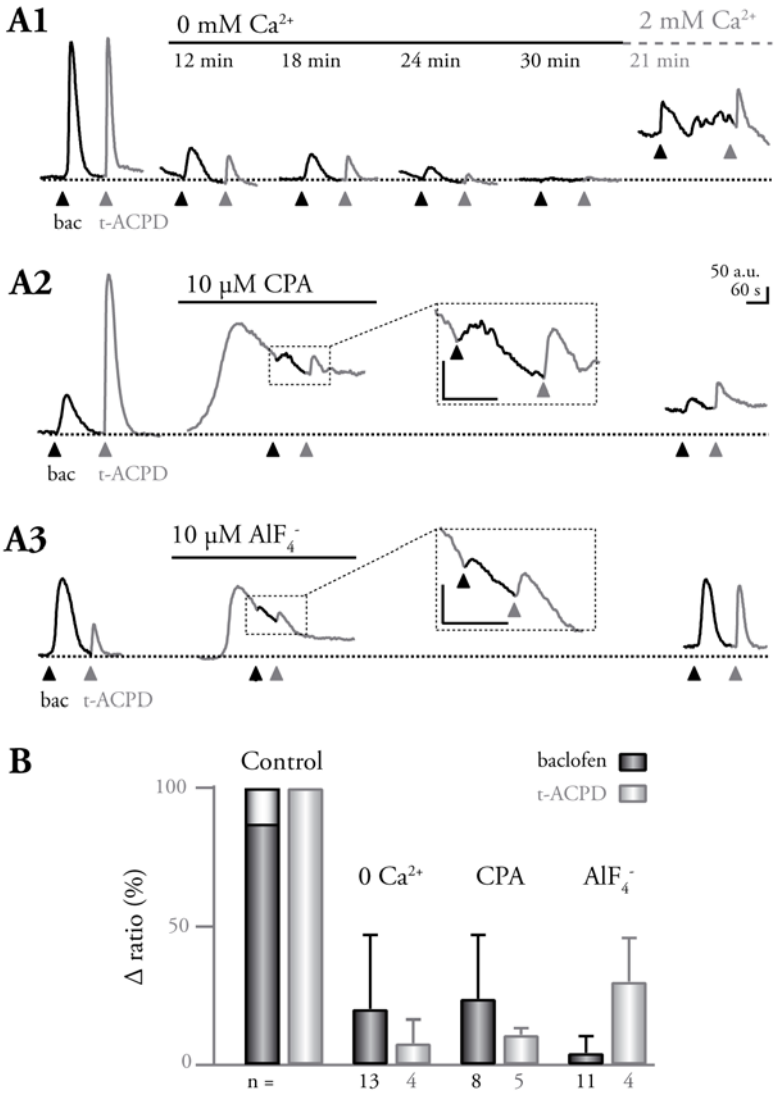


**Figure 24: GABA$_B$ Receptors Activate G Proteins and Cause $Ca^{2+}$ Release from Intracellular Stores**

Baclofen-induced (100 ms, 500 µM) $[Ca^{2+}]_i$ increases are compared to $Ca^{2+}$ transients elicited by t-ACPD (100 ms, 100 µM), a metabotropic glutamate receptor agonist.

**A**: When omitting extracellular $Ca^{2+}$, both transients are reduced in the same manner (A1). 10 µM cyclopiazonic acid (CPA) caused a $[Ca^{2+}]_i$ increase due to leakage of $Ca^{2+}$ from intracellular stores. $[Ca^{2+}]_i$ increases evoked by baclofen and t-ACPD were strongly reduced under this paradigm (A2). In addition, activation of heterotrimeric G-proteins with 10 µM $AlF_4^-$ reversibly prevented further $[Ca^{2+}]_i$ increases evoked by either baclofen or t-ACPD (A3).

**B**: Mean ratio changes evoked by baclofen and t-ACPD were normalized to control and quantified in a bar chart.

stores.

To test this hypothesis, I made use of the drug cyclopiazonic acid (CPA). CPA reduces the $Ca^{2+}$ content in intracellular stores by reversibly inhibiting the sarco-endoplasmic-reticulum $Ca^{2+}$ ATPase (SERCA pump). When the SERCA pump is inhibited, intracellular $Ca^{2+}$ stores are not refilled (see also section 1.1.3 and figure 1) and as $Ca^{2+}$ constantly leaks out of the intracellular $Ca^{2+}$ stores, they deplete and a $[Ca^{2+}]_i$ increase is observed (Dallwig et al., 2000). CPA (10 µM), which was applied in the presence of 2 mM extracellular $Ca^{2+}$, caused a marked $[Ca^{2+}]_i$ increase in hippocampal astrocytes. During depletion of intracellular $Ca^{2+}$ stores, $[Ca^{2+}]_i$ increases elicited by either baclofen (n = 8) or t-ACPD (n = 5; control for depletion of stores) were reduced by 70% and 90%, respectively (figure 24A2, B), again suggesting that baclofen induced $Ca^{2+}$ release from intracellular $Ca^{2+}$ stores.

Two distinct endoplasmic reticulum $Ca^{2+}$ stores exist in astrocytes (Golovina and Blaustein, 2000). One is sensitive to ryanodine and caffeine, the other one to $IP_3$. Because CPA does not interfere with the ryanodine-sensitive pool (Tanaka and Tashjian, 1993), $IP_3$ is likely involved in the $GABA_B$ receptor-mediated $[Ca^{2+}]_i$ increase. $IP_3$ production is commonly linked to phospholipase C (PLC) activation (see also section 1.1.3; Verkhratsky et al., 1998). Accordingly, I attempted to block PLC-dependent $IP_3$ production with the membrane permeable PLC blocker U73122 . Again, t-ACPD was used as a control substance to ensure that U73122 indeed blocked PLC-dependent $[Ca^{2+}]_i$ increases. However, the t-ACPD-induced control signal was not considerably influenced by U73122 (5 and 10 µM) in the acute slice (n = 4, not shown). Given that, in primary astrocyte cultures, U73122 (5 µM) almost completely blocked t-ACPD-induced $Ca^{2+}$ signals (n = 10; experiments performed together with Claudia Roderigo), I concluded that the drug did not reliably reach its target in the acute slice.

In cell cultures PLC involvement in the $GABA_B$ receptor-mediated $[Ca^{2+}]_i$ increase could not be assessed owing to the small number of responding cells and the strong run down of the baclofen-induced $Ca^{2+}$ signal (see page 70).

$IP_3$ is typically produced intracellularly following activation of G protein-coupled signaling cascades. $IP_3$ activates $IP_3$ receptors on the endoplasmic reticulum (see also section 1.1.3) and $Ca^{2+}$ is released. To test for G protein involvement in the $GABA_B$ receptor-mediated signaling cascade, I activated heterotrimeric G proteins with $AlF_4^-$ ($NaF/AlCl_3$, see also solutions on page 48; Chen and Penington, 2000; Wittinghofer, 1997) and tested whether further increases in $[Ca^{2+}]_i$ could be evoked by baclofen. Again, t-ACPD served as a control for G protein activation. As expected, the activation of G proteins with $AlF_4^-$ (10 µM, n = 11) induced a $[Ca^{2+}]_i$ increase and largely precluded further $[Ca^{2+}]_i$ increases upon application of either baclofen (n = 11) or t-ACPD (n = 4). Evoked signals were reduced by 95% and 70%, respectively (figure 24 A3, B). In conclusion, the signaling cascade releasing $Ca^{2+}$ from intracellular stores upon $GABA_B$ receptor activation likely involves G proteins.

Taken together, the above experiments indicate that $GABA_B$ receptor activation induces $Ca^{2+}$ release from $IP_3$-sensitive intracellular stores via a G protein-dependent mechanism.

### 3.4.4 Cross-Talk with the $GABA_B$ Receptor

Astrocytic $[Ca^{2+}]_i$ increases are evoked by activation of many different neurotransmitter receptors. Because $Ca^{2+}$ is their common second messenger, different receptors influence the functional state of the cell by converging onto the same effector proteins (see also Verkhratsky et al., 1998). Interplay between different receptors can occur much earlier in the signaling cascade as well. Both interactions at the receptor level via protein-protein-interaction and at different levels of the G-protein transduction pathways activated

by metabotropic receptors have been described earlier (Selbie and Hill, 1998; Tabata and Kano, 2006). Glutamate, for example, enhances $GABA_A$ receptor-mediated responses in the cortex (Stelzer and Wong, 1989); and $GABA_B$ receptor activation in the cerebellum postsynaptically augments metabotropic glutamate receptor (mGluR) type 1-mediated currents and $[Ca^{2+}]_i$ increases in Purkinje cells (Hirono et al., 2001; Tabata and Kano, 2006). In order to test for receptor interactions with the $GABA_B$ receptor in hippocampal astrocytes, I examined baclofen-induced $Ca^{2+}$ signals in the presence of different non-$GABA_B$ receptor antagonists.

Neither the $GABA_A$ receptor blocker bicuculline (50 µM; n=20) nor the broad spectrum purinergic receptor antagonist PPADS (20 µM; n=12) influenced amplitude or time course of baclofen-induced $[Ca^{2+}]_i$ increase (figure 25A1, A2, B; p= 0.509 and 0.769, respectively, paired t-test). Antagonists of ionotropic glutamate receptors (figure 25A3, B; 10-20 µM CNQX plus 100 µM DL-AP5; n = 10, p= 0.386) slightly, but not significantly, increased the baclofen-induced $Ca^{2+}$ signal. The competitive group I/II mGluR antagonist MCPG (figure 25B; 1 mM; n = 14), reduced the baclofen-induced $Ca^{2+}$ signal to ∼58% of control (p = 0.036; paired t-test; 11/14 cells reduced). However, when combining MCPG with the group II/III mGluR antagonist CPPG (figure 25A4, B; 1 mM MCPG plus 10 µM CPPG; n = 9) the resulting reduction (remaining signal ∼66%; 7/9 cells reduced) was not significant (p = 0.149, paired t-test). The Wilcoxon signed rank test, which is used for non-parametric samples rendered similar results.

Because these experiments suggested a possible interaction between metabotropic glutamate receptors and $GABA_B$ receptors, an additional set of experiments was performed. The metabotropic glutamate receptor agonist t-ACPD was applied in the presence of low concentrations of baclofen, which themselves did not increase $[Ca^{2+}]_i$. In the presence of baclofen (1 µM), the t-ACPD-induced $Ca^{2+}$ transient, on average, was increased to

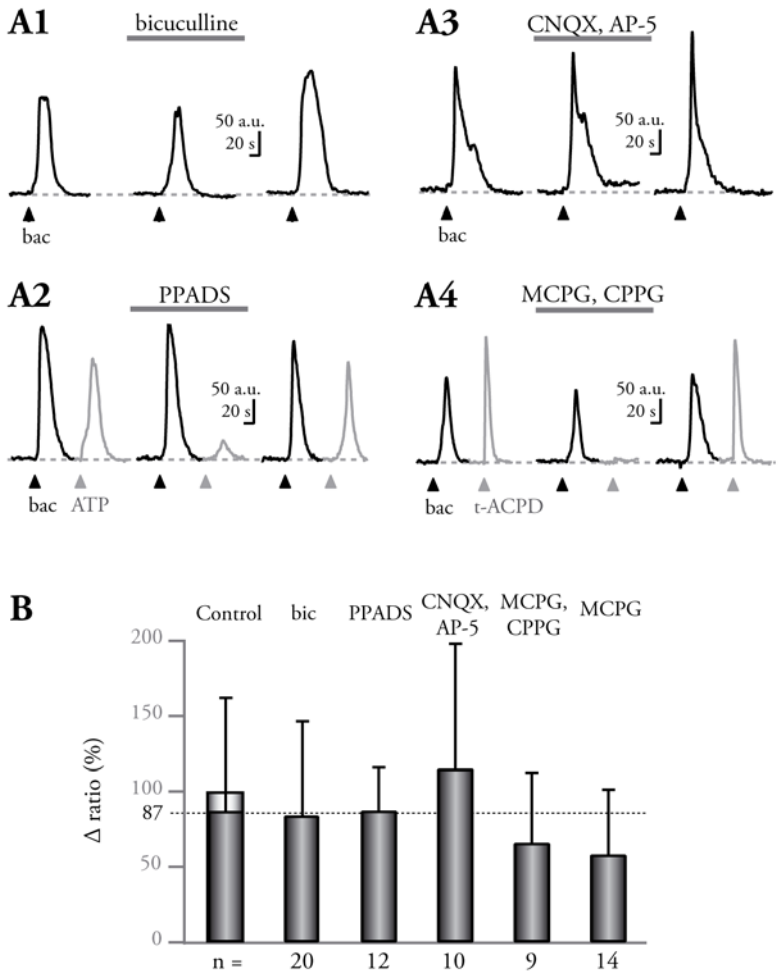


**Figure 25: Cross-Talk of $GABA_B$ Receptors with Metabotropic Glutamate Receptors Cannot Be Excluded**

**A**: Baclofen-induced $Ca^{2+}$ transients were not considerably altered by the $GABA_A$ receptor antagonist bicuculline (50 µM; A1; p= 0.509), the purinoreceptor antagonist PPADS (20 µM; A2, p= 0.769), and antagonists of ionotropic glutamate receptors (10-20 µM CNQX plus 100 µM DL-AP-5; A3, p= 0.386). The metabotropic glutamate receptor (mGluR) agonists MCPG (1 mM) plus CPPG (10 µM) reduced the baclofen-induced $Ca^{2+}$ signal, however, this reduction was only significant in MCPG (1 mM) alone (B; p= 0.149 and p = 0.036, respectively). In the experiments with PPADS, ATP (100 ms, 10 µM) served as a control whereas in the experiments with mGluR antagonists, t-ACPD (100 ms, 100 µM) was applied as control. Because bicuculline as well as CNQX and AP-5 were known to reliably work in the slice, experiments with these substances were performed without application of a control substance.
**B**: Bar chart quantifying baclofen-induced $[Ca^{2+}]_i$ increases of all experiments. An additional bar shows the remaining signal when baclofen was applied in the presence of the non-selective group I/II mGluR antagonist MCPG (1 mM) alone. Bars depict averaged mean values of two consecutive applications + S.D.; n= 9-20 cells as indicated below each bar.

127% of control (figure 26; n = 11; p = 0.012, paired t-test). However, the enhancement of the $[Ca^{2+}]_i$ increase was variable between the different cells and in 3/11 cells, the $Ca^{2+}$ signal was not augmented.

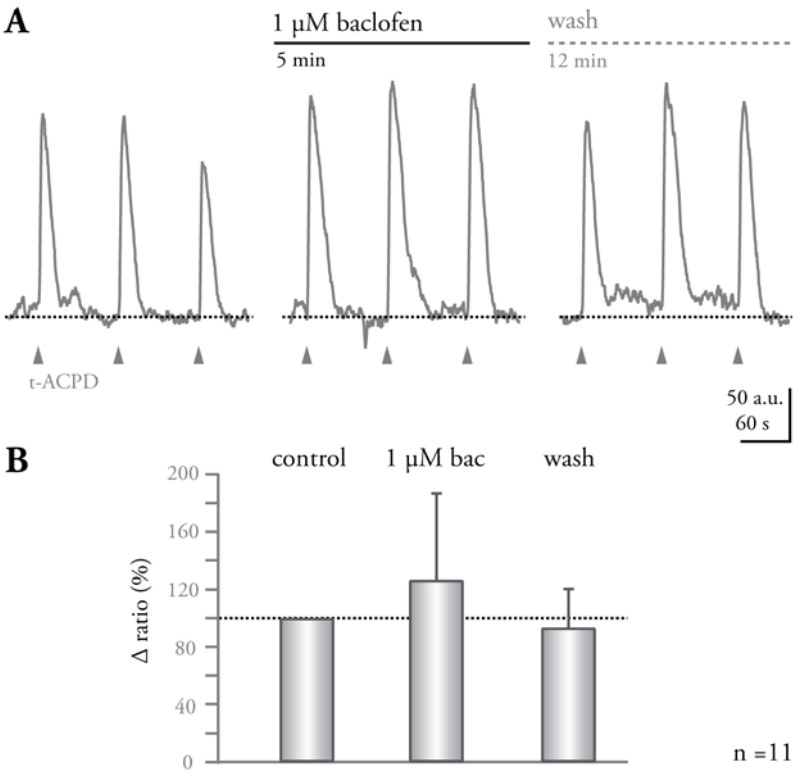


**Figure 26: Metabotropic Glutamate Receptor Mediated Calcium Increases are Slightly Enhanced by Baclofen**

**A**:$Ca^{2+}$ transients elicited by the group I/II metabotropic glutamate receptor agonist t-ACPD (100 ms, 100 µM) were slighty enhanced in the presence of 1 µM baclofen, which itself did not increase $[Ca^{2+}]_i$.
**B**: Bar chart quantifying the observed ratio changes. Three consecutive applications were averaged under each condition.

This result supports an interaction of metabotropic glutamate and $GABA_B$ receptors or cross-talk between their signaling pathways. However, the results also show that baclofen-induced $Ca^{2+}$ transients were not primarily dependent on such interactions.

### 3.5 Developmental Profile

It is well established that ionotropic GABAergic transmission in neurons undergoes large changes during postnatal development (for review see Ben-Ari, 2002). To study the developmental profile of GABA-induced $Ca^{2+}$ signals in astrocytes, I compared the responses of astrocytes to GABAergic activation between P03 and P33±1 (figure 27). The $GABA_A$ receptor agonist muscimol (100 ms, 500 µM) generally elicited only small $[Ca^{2+}]_i$ increases of less than 20 nM at all developmental stages investigated (P03, P07, P11, P15, P21±1, and P33±1; figure 27). The $GABA_B$ receptor agonist baclofen (figure 27; 100 ms, 500 µM) induced $[Ca^{2+}]_i$ increases of 45 nM on average but elicited $Ca^{2+}$ transients of more than 150 nM in several cells (∼5%).

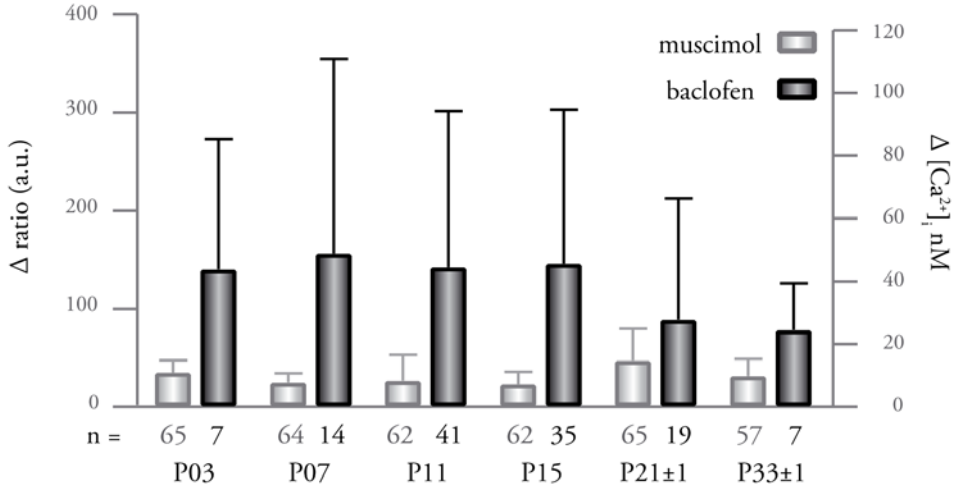


**Figure 27: Mean $Ca^{2+}$ Increases Induced by Muscimol and Baclofen**

The bar chart depicts the mean increases in ratio (left axis) and $[Ca^{2+}]_i$ (right axis) elicited in astrocytes between P03 and P33±1 by baclofen (100 ms, 500 µM) and muscimol (100 ms, 500 µM).

Next, I assessed the number of cells responding with a $[Ca^{2+}]_i$ increase upon activation of ionotropic or metabotropic GABA receptors (figure 28). The percentage of cells exhibiting a $[Ca^{2+}]_i$ increase when challenged with muscimol (100 ms, 500 µM) ranged between 70% and 100% throughout the

developmental period investigated (P03 to P33±1). In contrast, the number

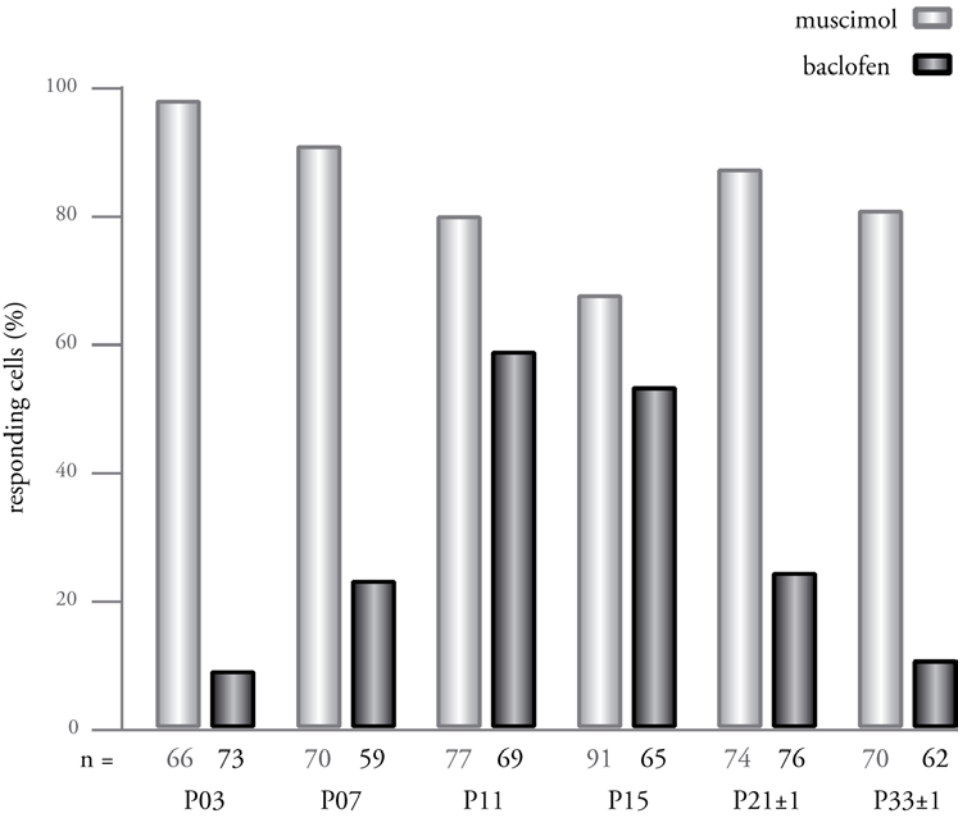


**Figure 28: GABA$_B$ Receptor-Activation Shows a Clear Developmental Profile**

The bar chart depicts the amount of SR101 positive astrocytes between P03 and P33±1 reacting with a $[Ca^{2+}]_i$ increase when challenged with baclofen (100 ms, 500 µM) or muscimol (100 ms, 500 µM).

of cells responding with a $[Ca^{2+}]_i$ increase when challenged with baclofen differed considerably between the investigated age groups: At the end of the second postnatal week (P11 to P15) a maximum of 60% of astrocytes responded with a $[Ca^{2+}]_i$ increase, whereas at the end of the first and third week (P07 and P21±1) only 25% of cells reacted. Less than 10% of SR101-positive cells responded to baclofen at P03 and P33±1.

Hence, baclofen-induced $Ca^{2+}$ responses in astrocytes exhibited a clear developmental profile. The majority of astrocytes reacted with $[Ca^{2+}]_i$ in-

creases upon $GABA_B$ receptor activation at a time during postnatal development when synapses begin to be established. In conclusion $GABA_B$ receptor-mediated $Ca^{2+}$ signaling in astrocytes might play a role during postnatal maturation of the hippocampal network (see also section 4.4).

# 4 Discussion

## 4.1 Identification of Astrocytes Using SR101

The fluorescent indicator sulforhodamine 101 (SR101) has been found to specifically label astrocytes in the neocortex of juvenile and adult rodents *in vivo* (Nimmerjahn et al., 2004). For the present study, I adapted this method for acute hippocampal slices and for the first time confirmed the specificity of SR101 for glial cells not only in mature rats (P15) but also in newborn (P03) animals. All cells labeled with SR101 clearly had astrocytic properties concerning both morphology and electrophysiological characteristics.

According to previous studies (Steinhäuser et al., 1992; Zhou et al., 2006; Wallraff et al., 2004), at least two different subtypes of astrocytes can be identified in acute slices, depending on their electrophysiological properties, "passive" and "complex" cells, the latter also being referred to as "outward rectifying glia" (ORG, see also section 1.1.2). SR101-positive cells corresponded to classical passive astrocytes, exhibiting a high $K^+$ conductance and lacking voltage-gated $Na^+$ channels (see also Kafitz et al., page 123ff). Most SR101-negative cells with astrocyte morphology, exhibited small inward currents resembling voltage-gated sodium channels, and because they did not generate action potentials upon depolarization, corresponded to ORG cells (Zhou et al., 2006). ORG cells, likely corresponding to immature glia or precursor cells (Kressin et al., 1995; Walz, 2000; Zhou et al., 2006), were not found among the SR101-positive subpopulation.

Interestingly, the proportion of SR101-positive cells with astrocyte morphology in the stratum radiatum increased with age (see also Kafitz et al., page 123ff). At P03, only ∼55% of presumed astrocytes in the stratum radiatum were SR101-positive, whereas at P15 this fraction amounted to ∼90%. According to the literature, the amount of ORG cells *in situ* decreases with age, and mature astrocytes have largely passive membrane properties and do

not express voltage-gated $Na^+$ channels (Steinhauser et al., 1994; Kressin et al., 1995; Zhou et al., 2006). Considering that the number of SR101-negative cells, resembling ORG cells, decreases with age and that SR101-positive cells largely have passive membrane properties, SR101 apparently marks mature astrocytes. In addition, at P15, 80% of SR101-positive cells were positive for GFAP in immunohistochemical studies (Kafitz et al., page 123ff).

Importantly, in patch-clamp and $Ca^{2+}$ imaging recordings, SR101-positive cells did not differ in their properties from classical astrocytes in unstained slices (cf. Schools et al., 2006; Zhou et al., 2006; Nimmerjahn et al., 2004). Therefore, SR101 proves a suitable tool for identifiying classical astrocytes in vital tissue.

Besides electrophysiology, the first method for identification of astrocytes in acute slices was introduced by Dallwig and Deitmer (2002) who showed that astrocytes, but not neurons, react with a $[Ca^{2+}]_i$ increase when challenged with reduced $K^+$ solution (<1 mM). However, only 86 % of astrocytes (identified by postrecording staining with a marker for the $Ca^{2+}$-binding protein S100$\beta$) react with a $[Ca^{2+}]_i$ increase when challenged with low $K^+$ solution. In addition, a considerable fraction of S100$\beta$ -negative cells respond as well. Staining with SR101, in contrast, allows us to identify virtually all classical astrocytes in a certain brain region (Nimmerjahn et al., 2004). In addition, SR101 staining proves useful for a pre-recording identification of astrocytes, not only when $Ca^{2+}$ measurements are to be carried out but also for $Na^+$ or pH measurements, electrophysiological recordings, and even morphological studies.

In addition, SR101-staining is less labor-intensive than post-recording methods, as for instance immunohistochemical stainings, and ensures that experiments are carried out on the cell type under investigation. Moreover, staining with SR101 takes little extra time and besides requiring filter sets

suitable for red light it is a very inexpensive method.

In contrast to astrocyte identification using GFAP as molecular marker, SR101 stainings can easily be carried out in either rats or mice and possibly other mammals, which to this end do not have to be genetically modified. Furthermore, the SR101-positive subpopulation has defined properties and evidently is less diverse than the GFAP-positive subpopulation (see also section 1.1.2).

Taken together, staining acute rat hippocampal slices with SR101 is a very useful means for identification of astrocytes in imaging and electrophysiological experiments. SR101-positive cells, in comparison to GFAP-positive cells, are a much more defined subpopulation of astrocytes, which completely lack voltage-gated $Na^+$ channels, and likely correspond to classical astrocytes.

## 4.2 GABA-Induced $Ca^{2+}$ Signaling

The main goals of this study were to elucidate the cellular mechanisms of GABA-mediated $Ca^{2+}$ signaling in hippocampal astrocytes *in situ* and to assess the cellular responses of astrocytes at different postnatal ages.

### 4.2.1 $GABA_A$ Receptor-Mediated $Ca^{2+}$ Signaling

As expected from earlier experiments in cell cultures and acutely dissociated cells (Nilsson et al., 1993; Fraser et al., 1995), muscimol, a $GABA_A$ receptor agonist, depolarized SR101-positive astrocytes in acute hippocampal slices and elicited $Ca^{2+}$ transients in SR101-positive cells from P03 to P34. Because bicuculline, $Ni^{2+}$, and $Ca^{2+}$-free extracellular solution largely and reversibly blocked muscimol-induced $Ca^{2+}$ transients (cf. figure 18), $GABA_A$ receptor activation presumably caused $Ca^{2+}$-influx from the extracellular space through voltage-gated $Ca^{2+}$ channels. The suggested signaling pathway, depolarization-induced opening of voltage-gated $Ca^{2+}$ channels, is

in accordance with previous studies (Kettenmann et al., 1984; Kettenmann and Schachner, 1985; Fraser et al., 1995; Bernstein et al., 1996; Pastor et al., 1995). I did not observe differences in the pharmacological profile of $GABA_A$ receptor-mediated $[Ca^{2+}]_i$ increases between P03 and P15, indicating that their mechanism is identical from early development to adulthood. This finding is in line with reports stating that astrocytes, unlike neurons (see section 1.3.1), exhibit a high intracellular $Cl^-$ concentration throughout development (Bekar et al., 1999; Bekar and Walz, 2002; Kanaka et al., 2001), owing to the lack of KCC2.

Despite evidence supporting opening of voltage-gated $Ca^{2+}$ channels following GABA-induced depolarizations (this study, Fraser et al., 1995), the existence of voltage-gated $Ca^{2+}$ channels in astrocytes is still being debated (Carmignoto et al., 1998). In the hippocampus L-type $Ca^{2+}$ channels were found on astrocytes using immunohistochemistry (Westenbroek et al., 1998), and in cultured rat cortical astrocytes, evidence for L-, N- and R-type $Ca^{2+}$ channels was found, with both electrophysiological and molecular techniques (D'Ascenzo et al., 2004). However, functional studies of voltage-gated $Ca^{2+}$ channels in astrocytes rendered opposing results. While voltage-gated $Ca^{2+}$ currents could not be isolated in some studies (Carmignoto et al., 1998), currents of small amplitude that exhibited a quick run-down were found in others (Akopian et al., 1996). The latter two studies were carried out in acute slices, however, both focussed on cells with a complex current pattern.

In other studies (Kang et al., 1998; Jourdain et al., 2007), depolarization-induced $[Ca^{2+}]_i$ increases in astrocytes have been attributed to $Ca^{2+}$ release from intracellular stores, as they were blocked after depletion of intracellular $Ca^{2+}$ stores with antagonists of SERCA pumps. Modulation of the $IP_3$ receptor by changes in the membrane potential (Imtiaz et al., 2002; Jourdain et al., 2007) could underly this finding. These $[Ca^{2+}]_i$ increases however, were caused by repetitive current injections resulting in depolarizations of up

to +50 mV. Muscimol-induced depolarizations, in contrast, depolarized the membrane potential to $\sim$ -20 mV, and according to their pharmacological profile likely caused $[Ca^{2+}]_i$ increases by activation of voltage-gated $Ca^{2+}$ channels.

Interestingly, $[Ca^{2+}]_i$ increases evoked in astrocytes in acute slices by depolarization with 50 mM $K^+$ solution (Dallwig and Deitmer, 2002) were shown to be due to activation of metabotropic glutamate receptors, secondary to depolarization-induced neuronal transmitter release (Carmignoto et al., 1998). However, their time of onset, in contrast to muscimol-induced $Ca^{2+}$ transients, was several seconds delayed, again indicating that $GABA_A$ receptor-mediated $[Ca^{2+}]_i$ increases are mediated by a different mechanism.

Even though the pharmacology of muscimol-induced $[Ca^{2+}]_i$ increases clearly supported the involvement of voltage-gated $Ca^{2+}$channels in the observed $[Ca^{2+}]_i$ transients (cf. figures 13 and 18), I did not detect voltage-gated $Ca^{2+}$ currents in my electrophysiological recordings. This discrepancy could be due to the fact that neither the voltage-step-protocol nor the intra- or extracellular solutions were specifically designed to isolate $Ca^{2+}$ currents. Owing to the massive $K^+$ conductance exhibited by SR101-positive astrocytes, a possible $Ca^{2+}$ conductance could have easily been masked (Bordey et al., 2000). In experiments specifically designed to isolate voltage-activated $Ca^{2+}$ currents, the potassium conductance is usually blocked with $Cs^+$ or Tetraethylammonium ($TEA^+$); and $Ba^{2+}$ is used as charge carrier instead of $Ca^{2+}$, rendering bigger currents (D'Ascenzo et al., 2004; Carmignoto et al., 1998; Akopian et al., 1996, see also page 64).

In my experiments, both the enhancement of the fluorescence ratio with $Ba^{2+}$ and the block with $Ni^{2+}$, in addition to the fast time of onset, supported the involvement of voltage-gated $Ca^{2+}$ channels in the $GABA_A$ receptor-mediated $Ca^{2+}$ signal.

### 4.2.2 $GABA_B$ Receptor-Mediated $Ca^{2+}$ Signaling

#### Mechanism of $[Ca^{2+}]_i$ increases

GABA causes elevations in $[Ca^{2+}]_i$ of astrocytes not only by activation $GABA_A$ receptors but also by activation of $GABA_B$ receptors. The specific $GABA_B$ receptor agonist baclofen elicited $Ca^{2+}$ transients in hippocampal astrocytes both in primary culture and in acute slices (P03 to P34). Considering that $GABA_B$ receptors are inhibitory in neurons, it is unlikely, that $[Ca^{2+}]_i$ increases in astrocyte of acute slices were secondary to activation of neuronal $GABA_B$ receptors. In addition, drugs interfering with the neuronal release machinery did not alter astrocytic $Ca^{2+}$ signaling. Both, the number of astrocytes responding and the amplitudes of $Ca^{2+}$ signals were not altered when blocking action potential firing with TTX. Moreover, $GABA_B$ receptor-mediated $[Ca^{2+}]_i$ increases could also be evoked in astrocytes when neuronal transmitter release was blocked with $Cd^{2+}$ (100 µM). Thus baclofen, directly activates astrocytic $GABA_B$ receptors and baclofen-induced $Ca^{2+}$ transients are independent of neuronal activity and transmitter release. These findings are in line with the results from Kang et al. (1998), who previously described $GABA_B$ receptor-mediated $[Ca^{2+}]_i$ increases in rat hippocampal astrocytes from P08 to P13.

Considering that neuronal $GABA_B$ receptors couple to $G_{i/o}$ proteins and, besides activating postsynaptic $K^+$ channels, inhibit presynaptic $Ca^{2+}$ channels (Bowery et al., 2002), the observed $[Ca^{2+}]_i$ increase in astrocytes is a surprising finding. Because $Ca^{2+}$ transients could not be elicited in the absence of extracellular $Ca^{2+}$, the $[Ca^{2+}]_i$ increase had been attributed to $Ca^{2+}$ influx from the extracellular space (Kang et al., 1998). My results confirm the reduction of $GABA_B$ receptor-induced $[Ca^{2+}]_i$ increases when superfusing the slice with $Ca^{2+}$-free extracellular saline. However, under this condition, intracellular $Ca^{2+}$ stores were depleted as well (cf. figure

24). Two of my observations substantiate the notion that $GABA_B$ receptor activation in astrocytes causes $Ca^{2+}$ release from intracellular $Ca^{2+}$ stores: Firstly, the long time of recovery after re-perfusion with $Ca^{2+}$-containing saline until the baclofen-induced $[Ca^{2+}]_i$ increase was restored, and secondly the strong reduction of the baclofen-induced $Ca^{2+}$ signal when depleting $IP_3$-sensitive intracellular $Ca^{2+}$ stores with CPA. In conclusion, my data suggest that $GABA_B$ receptor activation in astrocytes activates G proteins which mediate $Ca^{2+}$ release from $IP_3$-sensitive intracellular stores.

### Differences Underlying Neuronal and Glial Responses

Remarkably, $GABA_B$ receptor activation in neurons and astrocytes differs considerably concerning the modulation of $[Ca^{2+}]_i$: while $Ca^{2+}$ channels and transmitter release are inhibited in presynaptic neurons, $[Ca^{2+}]_i$ is increased in astrocytes and might result in gliotransmitter release (Kang et al., 1998; Serrano et al., 2006). But how does the same receptor mediate such opposing responses? Neurons and astrocytes might express different $GABA_B$ receptor subtypes or splice variants. However, functional $GABA_B$ receptors seem to be obligate heterodimers consisting of $GABA_{B1}$ and $GABA_{B2}$ subunits (Bowery et al., 2002; Mohler and Fritschy, 1999; Jones et al., 1998). While $GABA_{B1}$ is responsible for agonist binding (Kaupmann et al., 1998), $GABA_{B2}$ is necessary for G protein coupling and for trafficking the receptor complex out of the ER (Couve et al., 2000; Bowery et al., 2002).

The only receptor diversity described so far arises from the expression of $GABA_{B1a}$ and $GABA_{B1b}$ receptor subtypes due to differential promoter usage (Bowery et al., 2002; Steiger et al., 2004). In the hippocampus, at the synapse between Schaffer collaterals and CA1 pyramidal neurons, $GABA_{B1a}$-containing heteroreceptors are localized presynaptically and inhibit glutamate release, whereas $GABA_{B1b}$-containing receptors are mainly localized postsynaptically and mediate postsynaptic inhibition by activation

of $K^+$ conductances (Vigot et al., 2006).

Interestingly, most reports stating the importance of $GABA_{B2}$ subunits for obtaining functional receptors assessed typical neuronal responses such as inhibition of presynaptic $Ca^{2+}$ channels or activation of postsynaptic $K^+$ conductances (for review, see Bowery et al., 2002; Marshall et al., 1999). While one study found evidence for both $GABA_{B1}$ receptor variants as well as $GABA_{B2}$ subunits on hippocampal astrocytes *in situ* (Charles et al., 2003a), others reported that hippocampal astrocytes *in situ* express exclusively the $GABA_{B1}$ subunit (Fritschy et al., 2004; Lopez-Bendito et al., 2004). Similarly, astrocytes in the cerebellum only express $GABA_{B1}$ immunoreactivity (Lujan and Shigemoto, 2006). Thus, astrocytes and neurons seem to differ in their $GABA_B$ receptor subunit composition, which might result in a $[Ca^{2+}]_i$ increase in astrocytes rather than an inhibition of $Ca^{2+}$ channels.

Functional evidence for the possible existence of $GABA_B$ receptors other than $GABA_{B1/B2}$ heterodimers is originating from the analysis of knockout animals. In $GABA_{B2}$ double knockout (B2-/-) mice, $GABA_{B1}$ receptor activation G-protein dependently *inhibited* a postsynaptic $K^+$ conductance (Gassmann et al., 2004). This response is untypical, considering that the $GABA_B$ heterodimer in neurons *activates* a $K^+$ conductance postsynaptically, yet, it shows that the $GABA_{B1}$ subunit is able to exit the ER even in absence of the $GABA_{B2}$ subunit and can become a functional receptor at the plasma membrane. Whether the $GABA_{B1}$ subunit becomes functional alone or in combination with other proteins is not known (Bettler et al., 2004; Marshall et al., 1999).

Other explanations for the differential responses observed in neurons and glial cells might be found further downstream in the signaling pathway. $GABA_B$ receptors of neurons and astrocytes might differ in the G protein they are coupled to; or G proteins might control different effector

system. Upon dissociation of $G_{q/11}$ proteins, $G_\alpha$ typically activates PLC$\beta$, resulting in $IP_3$ production and subsequent $Ca^{2+}$ release from intracellular $Ca^{2+}$ stores (see section 1.1.3 Wettschureck and Offermanns, 2005). $G_\alpha$ subunits of $G_{i/o}$ proteins, that $GABA_B$ receptors are known to couple to, typically inhibit adenylate cyclase (Wettschureck and Offermanns, 2005). However, $G_{\beta\gamma}$ subunits of $G_{i/o}$ proteins, have been described to activate PLC$\beta_2$ in leukocytes (Camps et al., 1992; Katz et al., 1992). Similarly, when $\alpha_2$-adrenoceptors are expressed at high levels in fibroblasts, $G_{\alpha i}$ associated $\beta\gamma$ subunits activate PLC (Milligan, 1993), whereby it likely depends on the amount of $G_{\beta\gamma}$ released, whether PLC$\beta$ is activated (Milligan, 1993). $G_{\beta\gamma}$-mediated PLC$\beta$ activation has not been described in astrocytes, as yet, but it might well account for the $[Ca^{2+}]_i$ increase observed in hippocampal astrocytes.

**Receptor Cross-Talk**

Because many G protein-coupled receptors eventually converge onto the same effector proteins, interactions of different metabotropic signaling pathways are a common finding (Selbie and Hill, 1998). $G_i$-coupled receptor stimulation can enhance $G_q$-mediated PLC activation and $[Ca^{2+}]_i$ increases. This augmentation of $G_q$-mediated responses is often accompanied by a small direct stimulation of PLC by the $\beta\gamma$-subunits of $G_i$-coupled receptors (Selbie and Hill, 1998). In cerebellar Purkinje cells, $GABA_B$ receptor activation enhances membrane currents and $[Ca^{2+}]_i$ increases induced by the metabotropic glutamate receptor agonist t-ACPD (Hirono et al., 2001; Tabata et al., 2004); but also enhancement of $GABA_A$ receptor-mediated responses or AMPA receptor-dependent $[Ca^{2+}]_i$ increases has been described (Tabata and Kano, 2006). Modulatory actions of the $GABA_B$ receptor on glutamatergic signaling in the cerebellum are exerted by both, the classical $G_{i/o}$ pathway as well as direct interactions between $GABA_B$ receptors and

mGluR1 (Tabata and Kano, 2006).

A certain degree of interaction between $GABA_B$ receptors and metabotropic glutamate receptors might be the case in hippocampal astrocytes according to the experiments performed in the present study. Firstly, MCPG, an agonist of group I/II metabotropic glutamate receptors, reduced the baclofen-induced $[Ca^{2+}]_i$ increase by ∼30%, and secondly, t-ACPD-induced $[Ca^{2+}]_i$ increases were slightly enhanced (∼25% increase) in the presence of low concentrations of baclofen. However, both effects were only observed in ∼75% of astrocytes. In addition, the reduction of the baclofen-induced $[Ca^{2+}]_i$ increase was not significant when MCPG was combined with CPPG, an antagonist of group II/III metabotropic glutamate receptors. In a previous study by Kang et al. (1998), MCPG (0.5 mM) reduced the number of astrocytes reacting with a $Ca^{2+}]_i$ increase when stimulated with baclofen but did not have any influence on the amplitude of the baclofen-induced $Ca^{2+}$ signal. In contrast to the present study, Kang et al. (1998) used a lower concentration of MCPG (0.5 vs. 1 mM) and, in addition, pressure-applied baclofen for a longer period of time (seconds vs. 100 ms), which could have severely diluted MCPG.

Taken together, my experiments do not rule out an interaction between metabotropic glutamate receptors and $GABA_B$ receptors. Probing for receptor interactions, however, is complicated by the fact that interactions can take place at different levels in one and the same cell, but especially in acutes slices, receptors on other cell types are activated as well. When washing-in baclofen or t-ACPD, receptors on both neurons and astrocytes, and possibly oligodendrocytes or oligodendrocyte precursor cells (Luyt et al., 2007) are activated. Thus, the putative interaction will have to be confirmed under more defined experimental conditions to ensure that the augmentation of t-ACPD-induced $[Ca^{2+}]_i$ increases was due to a specific interaction of $GABA_B$ receptors with metabotropic glutamate receptors in astrocytes.

## 4.3 Developmental Changes

The majority of hippocampal astrocytes (70 to 100%) reacted with a $[Ca^{2+}]_i$ increase upon $GABA_A$ receptor activation from early postnatal development (P03) to adulthood (P33±1). In contrast, $GABA_B$ receptor-dependent $[Ca^{2+}]_i$ increases showed an as yet undescribed bell-shaped distribution during development, with a majority of cells (about 60 %) reacting during the second and at the beginning of the third postnatal week.

In neurons, presynaptic inhibition upon $GABA_B$ receptor activation is functional at birth, while postsynaptic inhibition through activation of slow IPSPs progressively develops during the first postnatal week (Gaiarsa et al., 1995). This delayed maturation was ascribed to (1) the absence of $GABA_B$ receptors or $K^+$ channels, (2) an absence of G proteins, or (3) uncoupling of the G proteins at early postnatal stages (Gaiarsa et al., 1995). While baclofen stimulates GTP$\gamma$S binding in rat spinal cord of P07 and P14 animals, no such stimulation is observed in older animals, leading to the conclusion that in adult rat spinal cord, $GABA_B$ receptors might not be coupled to G proteins (Moran et al., 2001). Another factor influencing GABAergic transmission might be a changing affinity for GABA. In early postnatal development the affinity of baclofen at $GABA_{B1a}$ and $GABA_{B1b}$ receptors is 10-fold lower than in adult rat brain and gradually increases with aging (Malitschek et al., 1998) until the maximal affinity is reached at P60.

In hippocampal (Lopez-Bendito et al., 2004; Fritschy et al., 2004) and cerebellar (Lujan and Shigemoto, 2006) astrocytes, differential expresssion of $GABA_B$ receptor subunits has been reported. In all three studies, astrocytes were shown to express exclusively $GABA_{B1}$ immunoreactivity transiently during development. In the hippocampus $GABA_B$ receptor expression was most pronounced from P05 to P20, with a maximum at P10 and in the cerebellum from P07 to P12. These expression profiles correspond to the developmental differences in $Ca^{2+}$ signaling described in this study. Hence,

it is tempting to speculate that differential expression of $GABA_{B1}$ receptors is underlying both the mechanism of $GABA_B$ receptor-induced $[Ca^{2+}]_i$ increases as well as the developmental profile of $[Ca^{2+}]_i$ increases (see also figure 28). Whether a changing affinity of agonists at the $GABA_B$ receptor or changes in G protein coupling also play a role in $GABA_B$ receptor-mediated reponses in hippocampal astrocytes remains to be elucidated.

## 4.4 Functional Implications

In neurons, $GABA_B$ receptor activation causes inhibition, presynaptically by inhibition of $Ca^{2+}$ channels and reduction of synaptic vesicle priming (Sakaba and Neher, 2003), and postsynaptically by activation of $K^+$ conductances (see Bowery et al., 2002, for review). In astrocytes, on the other hand, $GABA_B$ receptor activation causes cytosolic $[Ca^{2+}]_i$ increases (this study; Nilsson et al., 1993) and subsequent release of glutamate and/or ATP (Kang et al., 1998; Serrano et al., 2006). Both ATP and glutamate activate inhibitory interneurons (Kang et al., 1998; Kawamura et al., 2004). Furthermore, ATP, degraded to adenosine by extracellular endonucleotidases, acts inhibitory upon activating pre- and postsynaptic A1 receptors (Zhang et al., 2003; Serrano et al., 2006). Thus, the apparently opposing responses in astrocytes and neurons upon $GABA_B$ receptor activation, $[Ca^{2+}]_i$ increase in astrocytes versus inhibition of $Ca^{2+}$ conductances in neurons, in the end both have an inhibitory effect.

Interestingly, glutamate released by astrocytes upon $GABA_BR$ activation acts inhibitory due to activation of GABA-releasing interneurons. Astrocytes have been described to release other excitatory substances, such as D-serine, a cofactor at NMDA receptors, as well; but excitatory neuronal transmission secondary to astrocytic $GABA_B$ receptor activation has not been observed as yet.

The release of gliotransmitters by astrocytes not only modulates synap-

tic transmission but also influences neuron and synapse development. Both ATP and glutamate, which can be released from astrocytes upon stimulation, are trophic substances during development (Neary et al., 1996; Di Giorgi-Gerevini et al., 2005) and, interestingly,$[Ca^{2+}]_i$ increases upon $GABA_B$ receptor activation in astrocytes conicide with the time of dendrite and spine (Ben-Ari, 2001) as well as synapse development. Especially the inhibitory network undergoes massive changes during the first three weeks of postnatal development. There is a 45% reduction in the number of GABAergic neurons in the stratum radiatum of mouse hippocampus between P05 and P15 (Danglot et al., 2006) and dendrites of interneurons progressivly mature until around P20.

Many of the trophic actions of glutamate are mediated by mGluR5 receptors, which are the only mGluRs expressed in dividing (BrdU+) neuroprogenitors in the subventricular zone and in the dentate gyrus (Di Giorgi Gerevini et al., 2004). Interestingly, mGluR5 in the hippocampus, similar to $GABA_B$ receptors in astrocytes, is most abundandly expressed during development and decreases to adult levels after the second postnatal week (Carmelo Romano, 1996). Thus astrocytes might actively influence proliferating cells in the juvenile hippocampus by releasing glutamate upon $GABA_B$ receptor activation. Moreover, $GABA_B$ receptor-induced $Ca^{2+}$ signaling in astrocytes might be re-activated during pathological conditions, when astrocytes become "reactive", a change in the functional state of the cells that goes along with changes in their gene expression profile. If so, astrocytes might stimulate neuronal progenitor cells to develop into neurons and enhance their integration into the neuronal network upon brain injury.

Besides the integration of new neurons, other activity-dependent forms of plasticity exist in the hippocampus (see also section 1.2). Hebbian plasticity, activity-dependent strengthening of synapses, is considered the basic principle underlying learning and memory (Martin et al., 2000). Along with

the potentiation of active sets of synapses, inactive inputs are inhibited. This mechanism, also referred to as heterosynaptic depression (Lynch et al., 1977), is supposed to increase the contrast between potentiated and inactive inputs. In addition heterosynaptic depression is proposed as a means to stabilize total synaptic weights, after LTP is induced in a set of synapses (Royer and Pare, 2003). This coordination of synaptic strength across multiple synapses, is required to ensure stable transmission within the network (Abbott and Nelson, 2000).

Astrocytes are in a perfect position for mediating heterosynaptic depression because they sense neuronal activity and each astrocyte is in close association with roughly 140.000 synapses (Bushong et al., 2004). By releasing gliotransmitters, astrocytes connect populations of neurons which otherwise are not connected. Interestingly, $GABA_B$ receptor-mediated $[Ca^{2+}]_i$ increases resulting in transmitter release of astrocytes are tens of seconds delayed compared to receptor activation (see also figure 21; Kang et al., 1998; Serrano et al., 2006). This time course is also reflected in heterosynaptic depression exerted by astrocytes upon release of ATP (see also page 31).

Given that astrocytic modulation of the neuronal network upon $GABA_B$ receptor activation is implied in learning and memory formation it is interesting to know, whether astrocytes in other brain regions than the hippocampus express a similar developmental profile. In the cerebellum, for instance, immunohistochemical studies show a similar expression profile of $GABA_B$ receptors in astrocytes (Lujan and Shigemoto, 2006), supporting the notion, that astrocytic $GABA_B$ receptor mediated signaling might be similar in other brain areas.

The involvement of $GABA_B$ receptor dependent inhibiton on the neuronal network becomes apparent in $GABA_B$ receptor knockout mice. Absence of the $GABA_{B1a}$ subunit results in impaired synaptic plasticity and hippocampus-dependent memory (Vigot et al., 2006) and both $GABA_{B1}$

and $GABA_{B2}$ deficient mice were found to be more anxious than wild-type and showed anti-depressant like behavior in behavioral tests (Mombereau et al., 2005). Unfortunately, astrocyte-specific $GABA_B$ receptor knockout animals do not exist, as yet.

These thoughts lead to two further interesting questions along these lines: (1) in which way would a lack of astrocytic $GABA_B$ receptor-mediated signaling influence the development of the neuronal network and, hence, influence learning and memory, and (2) would $GABA_B$ receptor expression in astrocytes at later stages of development, when they are not normally expressed, lead to alterations of neuronal transmission. Both questions are complex and certainly require targeted genetic manipulations, possibly in an inducible fashion, in order to be answered.

According to the developmental profile of $Ca^{2+}$ responses in astrocytes, heterosynaptic depression and potentiation of inhibition by astrocytes can only occur during the second and at the beginning of the third postnatal week. The significance of these developmental differences remains to be elucidated. However, these early developmental stages appear to be particularly important in setting the basis for cognitive abilities in later life (Munakata et al., 2004).

## 4.5 Conclusions and Perspectives

In conclusion, my results show, that SR101 is a suitable tool for the identification of astrocyte in acute hippocampal slices if cells in vital, unfixed tissue are to be analyzed. SR101 staining can be combined with physiological measurements using fluorescent indicator dyes or electrophysiological recordings since astrocytic properties are not altered.

$GABA_A$ receptor activation depolarizes astrocytes and results in $Ca^{2+}$ influx presumably through voltage gated $Ca^{2+}$ channels (figure 29), confirming earlier studies. $GABA_B$ receptor activation, in contrast to previ-

ously published work, causes release of $Ca^{2+}$ from $IP_3$-sensitive intracellular $Ca^{2+}$ stores by a G-protein-dependent mechanism (figure 29). While 70%

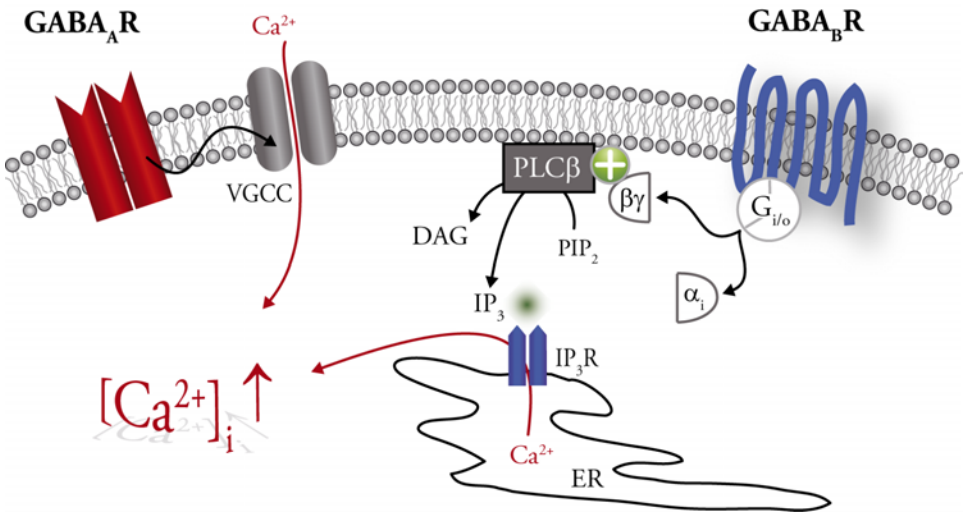


**Figure 29: Model of GABA-Induced $[Ca^{2+}]_i$ Increases in Astrocytes**

The conducted experiments resulted in the following model for GABA-induced $Ca^{2+}$ transients in hippocampal astrocytes: **$GABA_A$ receptor activation** causes a membrane depolarization which results in $Ca^{2+}$ influx through voltage-gated $Ca^{2+}$ channels. **$GABA_B$ receptor activation** activates G-proteins and causes $Ca^{2+}$ release from $IP_3$-sensitive intracellular $Ca^{2+}$ stores. $GABA_B$ receptor-mediated $[Ca^{2+}]_i$ increases were predominantly observed at the end of the second postnatal week, indicating a role of astrocytes for the formation of neuronal networks in the hippocampus.

DAG, diacylglycerol; ER, endoplasmic reticulum; $IP_3$(R), inositol 1,4,5-trisphosphate (receptor); $PIP_2$, phosphatidylinositol 4,5-bisphosphate; PKC, protein kinase C; PLC, phospholipase C; VGCC, voltage-gated $Ca^{2+}$ channel.

to 100% of astrocytes react with a $[Ca^{2+}]_i$ increase upon $GABA_A$ receptor activation throughout development (P03 to P33), the amount of cells reacting to baclofen changes considerably during development. During the time of synapse formation, up to 60% of astrocytes respond to $GABA_B$ receptor activation with an increase in $[Ca^{2+}]_i$. Given that astrocytes are able to release both neurotransmitters and neurotrophic substances, these results imply an important role of astrocytes during the development of the hippocampal network.

It remains to be elucidated which receptor subtypes mediate $GABA_B$ receptor mediated $[Ca^{2+}]_i$ increases in astrocytes, and whether alterations in the receptor subunit composition cause the differential responses observed during development. Both questions could be investigated by employing GABA $_{B1a/B1b}$ and $GABA_{B2}$ knockout animals.

Additional variation could be due to differences in G protein coupling or the subsequent signaling cascade. Pharmacological tools have proven difficult to use in acute slices because they might not be readily available at their target. In addition, there are no drugs available that discriminate between astrocytic and neuronal receptors. One possibility to avoid these limitations is the introduction of drugs via patch-pipettes into the astrocytic network. In particular, experiments with the $IP_3$ receptor antagonist heparin or the GTP analogues GTP$\gamma$S and GDP$\beta$S might render interesting results. Last but not least, the use of G protein knock-out animals could provide important information as to which G proteins are involved in the $GABA_B$ receptor induced $[Ca^{2+}]_i$ increases in astrocytes. However, given that the $GABA_B$ receptor-mediated $Ca^{2+}$signal is rather variable, and that receptor interactions with other receptors might occur, the results of these experiments might be difficult to interpret, considering that the modulation of G protein signaling pathways also interferes with metabotropic glutamate receptor signaling.

High-resolution two-photon imaging close to synapses in the intact tissue will certainly add interesting information as to the spatial extend of baclofen-induced $Ca^{2+}$ transients in astrocytes. Whether $Ca^{2+}$ transients, restricted to cellular microdomains, such as observed in cell cultures, play a role in modulation of the neuronal network can certainly be answered with this technique, when performed in combination with whole-cell patch-clamp recordings.

## Acknowledgements

I gratefully acknowledge Prof. Dr. Christine R. Rose for her superb supervision, her encouragement, and the time and effort she put into teaching me her way of research, including all the basics about imaging, electrophysiology and research in general. I am particularly grateful for having had the opportunity to participate in the "Neurobiology" course at the MBL which gave me wonderful insight into state-of-the-art techniques and cutting-edge research. I would also like to take the opportunity to thank Prof. Dr. Hans-Werner Müller for offering to examine this work and the DFG for financially supporting this project.

I am indebted to Peter and Tony for long hours of proof-reading and helpful comments on earlier versions of this thesis, and to Claudia and Karl for help with the illustrations. Claudia and Simone, in particular, I would like to acknowledge for their talented organization of the daily lab work, their planning ahead, and help wherever need be. Thanks also to Marion for bridging the gap between me and everything related to administration. Also, I would like to thank all my colleagues and former colleagues in Munich and Düsseldorf for putting up with me and having created a great atmosphere to work in.

There are lots of other people I would like to thank because this work would not have been possible without them. Above all, I would like to thank Sascha, without whom my life would be very sad and boring, and my parents, Inge and Hans-Jürgen, for their constant support in every possible way. Last but not least I would like to thank my sister Elke, the extended family, and all my friends for being friends, and supporting me, each in their own way.

# 5 References


Abbott LF and Nelson SB (2000): Synaptic plasticity: Taming the beast. *Nat Neurosci*, 3 Suppl:1178–83.

Adams SR (2005): *Imaging in Neuroscience and Development: A Laboratory Manual*. Cold Spring Harbor Press.

Aguado F, Espinosa-Parrilla JF, Carmona MA, and Soriano E (2002): Neuronal activity regulates correlated network properties of spontaneous calcium transients in astrocytes in situ. *J Neurosci*, 22(21):9430–44.

Akopian G, Kressin K, Derouiche A, and Steinhäuser C (1996): Identified glial cells in the early postnatal mouse hippocampus display different types of Ca2+ currents. *Glia*, 17(3):181–94.

Angulo MC, Kozlov AS, Charpak S, and Audinat E (2004): Glutamate released from glial cells synchronizes neuronal activity in the hippocampus. *J Neurosci*, 24(31):6920–7.

Araque A, Martin ED, Perea G, Arellano JI, and Buno W (2002): Synaptically released acetylcholine evokes Ca2+ elevations in astrocytes in hippocampal slices. *J Neurosci*, 22(7):2443–50.

Araque A, Parpura V, Sanzgiri RP, and Haydon PG (1998): Glutamate-dependent astrocyte modulation of synaptic transmission between cultured hippocampal neurons. *Eur J Neurosci*, 10(6):2129–42.

Auld DS and Robitaille R (2003): Glial cells and neurotransmission: An inclusive view of synaptic function. *Neuron*, 40(2):389–400.

Bachoo RM, Kim RS, Ligon KL, Maher EA, Brennan C, Billings N, Chan S, Li C, Rowitch DH, Wong WH, and DePinho RA (2004): Molecular diversity of astrocytes with implications for neurological disorders. *PNAS*, 101(22):8384–8389.

Bailey CH, Giustetto M, Huang YY, Hawkins RD, and Kandel ER (2000): Is heterosynaptic modulation essential for stabilizing hebbian plasiticity and memory. *Nat Rev Neurosci*, 1(1):11–20.

Bak LK, Schousboe A, and Waagepetersen HS (2006): The glutamate/gaba-glutamine cycle: Aspects of transport, neurotransmitter homeostasis and ammonia transfer. *Journal of Neurochemistry*, 98(3):641–653.

Barbaro NM, Takahashi DK, and Baraban SC (2004): A potential role for astrocytes in mediating the antiepileptic actions of furosemide in vitro. *Neuroscience*, 128(3):655–663.

Barski JJ, Hartmann J, Rose CR, Hoebeek F, Morl K, Noll-Hussong M, De Zeeuw CI, Konnerth A, and Meyer M (2003): Calbindin in cerebellar purkinje cells is a critical determinant of the precision of motor coordination. *J Neurosci*, 23(8):3469–77.

Beattie EC, Stellwagen D, Morishita W, Bresnahan JC, Ha BK, Von Zastrow M, Beattie MS, and Malenka RC (2002): Control of synaptic strength by glial TNFalpha. *Science*, 295(5563):2282–2285.

Behar TN, Li YX, Tran HT, Ma W, Dunlap V, Scott C, and Barker JL (1996): GABA stimulates chemotaxis and chemokinesis of embryonic cortical neurons via calcium-dependent mechanisms. *J Neurosci*, 16(5):1808–18.

Bekar LK, Jabs R, and Walz W (1999): GABAa receptor agonists modulate K+ currents in adult hippocampal glial cells in situ. *Glia*, 26(2):129–38.

Bekar LK and Walz W (2002): Intracellular chloride modulates A-type potassium currents in astrocytes. *Glia*, 39(3):207–16.

Ben-Ari Y (2001): Developing networks play a similar melody. *Trends in Neurosciences*, 24(6):353–360.

Ben-Ari Y (2002): Excitatory actions of gaba during development: The nature of the nurture. *Nat Rev Neurosci*, 3(9):728–39.

Bergles DE and Jahr CE (1997): Synaptic activation of glutamate transporters in hippocampal astrocytes. *Neuron*, 19(6):1297–308.

Bernstein M, Lyons SA, Moller T, and Kettenmann H (1996): Receptor-mediated calcium signalling in glial cells from mouse corpus callosum slices. *J Neurosci Res*, 46(2):152–63.

Berridge MJ (1997): Elementary and global aspects of calcium signalling. *J Exp Biol*, 200(2):315–319.

Berridge MJ, Bootman MD, and Roderick HL (2003): Calcium signalling: Dynamics, homeostasis and remodelling. *Nat Rev Mol Cell Biol*, 4(7):517–29.

Berridge MJ, Lipp P, and Bootman MD (2000): The versatility and universality of calcium signalling. *Nat Rev Mol Cell Biol*, 1(1):11–21.

Bettler B, Kaupmann K, Mosbacher J, and Gassmann M (2004): Molecular structure and physiological functions of GABA(B) receptors. *Physiol Rev*, 84(3):835–67.

Bezzi P, Gundersen V, Galbete JL, Seifert G, Steinhäuser C, Pilati E, and Volterra A (2004): Astrocytes contain a vesicular compartment that is competent for regulated exocytosis of glutamate. *Nat Neurosci*, 7(6):613–20.

Blaustein MP and Lederer WJ (1999): Sodium/calcium exchange: Its physiological implications. *Physiol Rev*, 79(3):763–854.

Bordey A, Hablitz JJ, and Sontheimer H (2000): Reactive astrocytes show enhanced inwardly rectifying K+ currents in situ. *Neuroreport*, 11(14):3151–5.

Bowery NG, Bettler B, Froestl W, Gallagher JP, Marshall F, Raiteri M, Bonner TI, and Enna SJ (2002): International union of pharmacology. xxxiii. mammalian gamma-aminobutyric acid(b) receptors: Structure and function. *Pharmacol Rev*, 54(2):247–64.

Buhl EH, Halasy K, and Somogyi P (1994): Diverse sources of hippocampal unitary inhibitory postsynaptic potentials and the number of synaptic release sites. *Nature*, 368(6474):823–828.

Bureau M, Laschet J, Bureau-Heeren M, Hennuy B, Minet A, Wins P, and Grisar T (1995): Astroglial cells express large amounts of GABAa receptor proteins in mature brain. *Journal of Neurochemistry*, 65(5):2006–2015.

Bushong EA, Martone ME, and Ellisman MH (2004): Maturation of astrocyte morphology and the establishment of astrocyte domains during postnatal hippocampal development. *International Journal of Developmental Neuroscience*, 22(2):73–86.

Bushong EA, Martone ME, Jones YZ, and Ellisman MH (2002): Protoplasmic astrocytes in CA1 stratum radiatum occupy separate anatomical domains. *J. Neurosci.*, 22(1):183–192.

Caillard O, McLean HA, Ben-Ari Y, and Gaiarsa JL (1998): Ontogenesis of presynaptic gabab receptor-mediated inhibition in the CA3 region of the rat hippocampus. *J Neurophysiol*, 79(3):1341–1348.

Campbell V, Berrow N, and Dolphin AC (1993): GABA(B) receptor modulation of Ca2+ currents in rat sensory neurones by the G protein G(0): Antisense oligonucleotide studies. *J Physiol*, 470(1):1–11.

Camps M, Carozzi A, Schnabel P, Scheer A, Parker PJ, and Gierschik P (1992): Isozyme-selective stimulation of phospholipase C-beta 2 by G protein beta gamma-subunits. *Nature*, 360(6405):684–6.

Cancedda L, Fiumelli H, Chen K, and Poo MM (2007): Excitatory gaba action is essential for morphological maturation of cortical neurons in vivo. *J Neurosci*, 27(19):5224–35.

Carafoli E (2002): Calcium signaling: A tale for all seasons. *Proc Natl Acad Sci U S A*, 99(3):1115–22.

Carmelo Romano ANVdPKLO (1996): Enhanced early developmental expression of the metabotropic glutamate receptor mGluR5 in rat brain: Protein, mRNA splice variants, and regional distribution. *The Journal of Comparative Neurology*, 367(3):403–412.

Carmignoto G and Fellin T (2006): Glutamate release from astrocytes as a non-synaptic mechanism for neuronal synchronization in the hippocampus. *Journal of Physiology-Paris*, 99(2-3):98–102.

Carmignoto G, Pasti L, and Pozzan T (1998): On the role of voltage-dependent calcium channels in calcium signaling of astrocytes in situ. *J. Neurosci.*, 18(12):4637–4645.

Charles KJ, Calver AR, Jourdain S, and Pangalos MN (2003a): Distribution of a GABA(B)-like receptor protein in the rat central nervous system. *Brain Res*, 989(2):135–46.

Charles KJ, Deuchars J, Davies CH, and Pangalos MN (2003b): GABA b receptor subunit expression in glia. *Mol Cell Neurosci*, 24(1):214–23.

Chebib M and Johnston GAR (1999): The 'abc' of GABA receptors: A brief review. *Clinical and Experimental Pharmacology and Physiology*, 26(11):937–940.

Chen X, Wang L, Zhou Y, Zheng LH, and Zhou Z (2005): "kiss-and-run" glutamate secretion in cultured and freshly isolated rat hippocampal astrocytes. *J. Neurosci.*, 25(40):9236–9243.

Chen Y and Penington NJ (2000): Competition between internal AlF(4)(-) and receptor-mediated stimulation of dorsal raphe neuron g-proteins coupled to calcium current inhibition. *J Neurophysiol*, 83(3):1273–82.

Cornell-Bell AH, Finkbeiner SM, Cooper MS, and Smith SJ (1990): Glutamate induces calcium waves in cultured astrocytes: Long-range glial signaling. *Science*, 247(4941):470–473.

Couve A, Calver AR, Fairfax B, Moss SJ, and Pangalos MN (2004): Unravelling the unusual signalling properties of the GABA(B) receptor. *Biochem Pharmacol*, 68(8):1527–36.

Couve A, Moss SJ, and Pangalos MN (2000): GABA(B) receptors: A new paradigm in G protein signaling. *Mol Cell Neurosci*, 16(4):296–312.

Dallwig R and Deitmer JW (2002): Cell-type specific calcium responses in acute rat hippocampal slices. *J Neurosci Methods*, 116(1):77–87.

Dallwig R, Vitten H, and Deitmer JW (2000): A novel barium-sensitive calcium influx into rat astrocytes at low external potassium. *Cell Calcium*, 28(4):247–59.

Danbolt NC (2001): Glutamate uptake. *Progress in Neurobiology*, 65(1):1–105.

Danglot L, Triller A, and Marty S (2006): The development of hippocampal interneurons in rodents. *Hippocampus*, 16(12):1032–60.

D'Ascenzo M, Vairano M, Andreassi C, Navarra P, Azzena GB, and Grassi C (2004): Electrophysiological and molecular evidence of L-(Cav1), N-(Cav2.2), and R- (Cav2.3) type Ca2+ channels in rat cortical astrocytes. *Glia*, 45(4):354–63.

Davies CH, Pozza MF, and Collingridge GL (1993): CGP 55845a: A potent antagonist of GABA(B) receptors in the CA1 region of rat hippocampus. *Neuropharmacology*, 32(10):1071–1073.

Davies CH, Starkey SJ, Pozza MF, and Collingridge GL (1991): GABA(B) autoreceptors regulate the induction of LTP. *Nature*, 349(6310):609–611.

Deisseroth K, Singla S, Toda H, Monje M, Palmer TD, and Malenka RC (2004): Excitation-neurogenesis coupling in adult neural stem/progenitor cells. *Neuron*, 42(4):535–52.

Demarque M, Represa A, Becq H, Khalilov I, Ben-Ari Y, and Aniksztejn L (2002): Paracrine intercellular communication by a Ca2+- and snare-independent release of GABA and glutamate prior to synapse formation. *Neuron*, 36(6):1051–61.

Di Giorgi-Gerevini V, Melchiorri D, Battaglia G, Ricci-Vitiani L, Ciceroni C, Busceti CL, Biagioni F, Iacovelli L, Canudas AM, Parati E, De Maria R, and Nicoletti F (2005): Endogenous activation of metabotropic glutamate receptors supports the proliferation and survival of neural progenitor cells. *Cell Death Differ*, 12(8):1124–33.

Di Giorgi Gerevini VD, Caruso A, Cappuccio I, Ricci Vitiani L, Romeo S, Della Rocca C, Gradini R, Melchiorri D, and Nicoletti F (2004): The mGlu5 metabotropic glutamate receptor is expressed in zones of active neurogenesis of the embryonic and postnatal brain. *Developmental Brain Research*, 150(1):17–22.

Doetsch F (2003): The glial identity of neural stem cells. *Nat Neurosci*, 6(11):1127–34.

Doetsch F, Caille I, Lim DA, Garcia-Verdugo JM, and Alvarez-Buylla A (1999): Subventricular zone astrocytes are neural stem cells in the adult mammalian brain. *Cell*, 97(6):703–716.

Domercq M, Brambilla L, Pilati E, Marchaland J, Volterra A, and Bezzi P (2006): P2Y1 receptor-evoked glutamate exocytosis from astrocytes: Control by tumor necrosis factor-alpha and prostaglandins. *J Biol Chem*, 281(41):30684–96.

Duan S, Anderson CM, Keung EC, Chen Y, and Swanson RA (2003): P2x7 receptor-mediated release of excitatory amino acids from astrocytes. *J Neurosci*, 23(4):1320–8.

Edwards FA, Konnerth A, Sakmann B, and Takahashi T (1989): A thin slice preparation for patch clamp recordings from neurones of the mammalian central nervous system. *Pflugers Arch*, 414(5):600–12.

Eilers J, Plant TD, Marandi N, and Konnerth A (2001): GABA-mediated Ca2+ signalling in developing rat cerebellar purkinje neurones. *J Physiol*, 536(Pt 2):429–37.

Elmariah SB, Oh EJ, Hughes EG, and Balice-Gordon RJ (2005): Astrocytes regulate inhibitory synapse formation via Trk-mediated modulation of postsynaptic GABAa receptors. *J Neurosci*, 25(14):3638–50.

Esposito MS, Piatti VC, Laplagne DA, Morgenstern NA, Ferrari CC, Pitossi FJ, and Schinder AF (2005): Neuronal differentiation in the adult hippocampus recapitulates embryonic development. *J. Neurosci.*, 25(44):10074–10086.

Farber K and Kettenmann H (2005): Physiology of microglial cells. *Brain Research Reviews*, 48(2):133–143.

Farrant M and Nusser Z (2005): Variations on an inhibitory theme: Phasic and tonic activation of GABA(a) receptors. *Nat Rev Neurosci*, 6(3):215–29.

Fellin T and Carmignoto G (2004): Neurone-to-astrocyte signalling in the brain represents a distinct multifunctional unit. *J Physiol*, 559(Pt 1):3–15.

Fiacco TA, Agulhon C, Taves SR, Petravicz J, Casper KB, Dong X, Chen J, and McCarthy KD (2007): Selective stimulation of astrocyte calcium in situ does not affect neuronal excitatory synaptic activity. *Neuron*, 54(4):611–26.

Fiacco TA and McCarthy KD (2004): Intracellular astrocyte calcium waves in situ increase the frequency of spontaneous ampa receptor currents in CA1 pyramidal neurons. *J Neurosci*, 24(3):722–32.

Fiacco TA and McCarthy KD (2006): Astrocyte calcium elevations: Properties, propagation, and effects on brain signaling. *Glia*, 54(7):676–690.

Finkbeiner S and Greenberg ME (1996): Ca2+-dependent routes to ras: Mechanisms for neuronal survival, differentiation, and plasticity? *Neuron*, 16(2):233–236.

Floyd CL, Rzigalinski BA, Weber JT, Sitterding HA, Willoughby KA, and Ellis EF (2001): Traumatic injury of cultured astrocytes alters inositol (1,4,5)-trisphosphate-mediated signaling. *Glia*, 33(1):12–23.

Fraser DD, Duffy S, Angelides KJ, Perez-Velazquez JL, Kettenmann H, and MacVicar BA (1995): GABAa/benzodiazepine receptors in acutely isolated hippocampal astrocytes. *J. Neurosci.*, 15(4):2720–2732.

Fritschy JM, Sidler C, Parpan F, Gassmann M, Kaupmann K, Bettler B, and Benke D (2004): Independent maturation of the GABA(B) receptor subunits GABA(B1) and GABA(B2) during postnatal development in rodent brain. *J Comp Neurol*, 477(3):235–52.

Gadea A and Lopez-Colome AM (2001): Glial transporters for glutamate, glycine, and GABA: Ii. GABA transporters. *J Neurosci Res*, 63(6):461–8.

Gaiarsa JL, Tseeb V, and Ben-Ari Y (1995): Postnatal development of pre- and postsynaptic GABA(B)-mediated inhibitions in the CA3 hippocampal region of the rat. *J Neurophysiol*, 73(1):246–55.

Ganat YM, Silbereis J, Cave C, Ngu H, Anderson GM, Ohkubo Y, Ment LR, and Vaccarino FM (2006): Early postnatal astroglial cells produce multilineage precursors and neural stem cells in vivo. *J. Neurosci.*, 26(33):8609–8621.

Ganguly K, Schinder AF, Wong ST, and Poo M (2001): GABA itself promotes the developmental switch of neuronal gabaergic responses from excitation to inhibition. *Cell*, 105(4):521–32.

Garaschuk O, Hanse E, and Konnerth A (1998): Developmental profile and synaptic origin of early network oscillations in the CA1 region of rat neonatal hippocampus. *J Physiol (Lond)*, 507(1):219–236.

Gassmann M, Shaban H, Vigot R, Sansig G, Haller C, Barbieri S, Humeau Y, Schuler V, Muller M, Kinzel B, Klebs K, Schmutz M, Froestl W, Heid J, Kelly PH, Gentry C, Jaton AL, Van der Putten H, Mombereau C, Lecourtier L, Mosbacher J, Cryan JF, Fritschy JM, Luthi A, Kaupmann K, and Bettler B (2004): Redistribution of GABA(B)(1) protein and atypical GABA(B) responses in GABA(B)(2)-deficient mice. *J. Neurosci.*, 24(27):6086–6097.

Gaughwin PM, Caldwell MA, Anderson JM, Schwiening CJ, Fawcett JW, Compston DAS, and Chandran S (2006): Astrocytes promote neurogenesis from oligodendrocyte precursor cells. *European Journal of Neuroscience*, 23(4):945–956.

Ge S, Goh ELK, Sailor KA, Kitabatake Y, Ming Gl, and Song H (2006): GABA regulates synaptic integration of newly generated neurons in the adult brain. *Nature*, 439(7076):589–593.

Ge S, Pradhan DA, Ming GL, and Song H (2007): GABA sets the tempo for activity-dependent adult neurogenesis. *Trends Neurosci*, 30(1):1–8.

Glykys J and Mody I (2007): The main source of ambient GABA responsible for tonic inhibition in the mouse hippocampus. *J Physiol*, 582(3):1163–1178.

Golovina VA, Bambrick LL, Yarowsky PJ, Krueger BK, and Blaustein MP (1996): Modulation of two functionally distinct Ca2+ stores in astrocytes: Role of the plasmalemmal Na/Ca exchanger. *Glia*, 16(4):296–305.

Golovina VA and Blaustein MP (2000): Unloading and refilling of two classes of spatially resolved endoplasmic reticulum Ca(2+) stores in astrocytes. *Glia*, 31(1):15–28.

Gordon GR, Mulligan SJ, and MacVicar BA (2007): Astrocyte control of the cerebrovasculature. *Glia*, 55(12):1214–21.

Grass D, Pawlowski PG, Hirrlinger J, Papadopoulos N, Richter DW, Kirchhoff F, and Hulsmann S (2004): Diversity of functional astroglial properties in the respiratory network. *J. Neurosci.*, 24(6):1358–1365.

Grynkiewicz G, Poenie M, and Tsien RY (1985): A new generation of Ca2+ indicators with greatly improved fluorescence properties. *J Biol Chem*, 260(6):3440–50.

Guerini D, Coletto L, and Carafoli E (2005): Exporting calcium from cells. *Cell Calcium*, 38(3-4):281–289.

Hamill OP, Marty A, Neher E, Sakmann B, and Sigworth FJ (1981): Improved patch-clamp techniques for high-resolution current recording from cells and cell-free membrane patches. *Pflugers Arch*, 391(2):85–100.

Hamilton SL (2005): Ryanodine receptors. *Cell Calcium*, 38(3-4):253–260.

Haugland RP (2005): *The Handbook. A Guide to Fluorescent Probes and Labeling Technologies.* 10 ed.

Haydon PG (2001): Glia: Listening and talking to the synapse. *Nat Rev Neurosci*, 2(3):185–93.

Haydon PG and Carmignoto G (2006): Astrocyte control of synaptic transmission and neurovascular coupling. *Physiol. Rev.*, 86(3):1009–1031.

Hirase H, Qian L, Bartho P, and Buzsaki G (2004): Calcium dynamics of cortical astrocytic networks in vivo. *PLoS Biol*, 2(4):E96.

Hirono M, Yoshioka T, and Konishi S (2001): GABA(B) receptor activation enhances mglur-mediated responses at cerebellar excitatory synapses. *Nat Neurosci*, 4(12):1207–1216.

Holden C (2007): Neuroscience: Astrocytes secrete substance that kills motor neurons in ALS. *Science*, 316(5823):353a–.

Imtiaz MS, Smith DW, and van Helden DF (2002): A theoretical model of slow wave regulation using voltage-dependent synthesis of inositol 1,4,5-trisphosphate. *Biophys J*, 83(4):1877–90.

Jensen AM and Chiu SY (1990): Fluorescence measurement of changes in intracellular calcium induced by excitatory amino acids in cultured cortical astrocytes. *J Neurosci*, 10(4):1165–75.

Jones KA, Borowsky B, Tamm JA, Craig DA, Durkin MM, Dai M, Yao WJ, Johnson M, Gunwaldsen C, Huang LY, Tang C, Shen Q, Salon JA, Morse K, Laz T, Smith KE, Nagarathnam D, Noble SA, Branchek TA, and Gerald C (1998): GABA(B) receptors function as a heteromeric assembly of the subunits GABA(B)R1 and GABA(B)R2. *Nature*, 396(6712):674–9.

Jourdain P, Bergersen LH, Bhaukaurally K, Bezzi P, Santello M, Domercq M, Matute C, Tonello F, Gundersen V, and Volterra A (2007): Glutamate exocytosis from astrocytes controls synaptic strength. *Nat Neurosci*, 10(3):331–9.

Kaila K (1994): Ionic basis of GABAa receptor channel function in the nervous system. *Prog Neurobiol*, 42(4):489–537.

Kanaka C, Ohno K, Okabe A, Kuriyama K, Itoh T, Fukuda A, and Sato K (2001): The differential expression patterns of messenger rnas encoding K-Cl cotransporters (KCC1,2) and Na-K-2Cl cotransporter (NKCC1) in the rat nervous system. *Neuroscience*, 104(4):933–946.

Kang J, Jiang L, Goldman SA, and Nedergaard M (1998): Astrocyte-mediated potentiation of inhibitory synaptic transmission. *Nat Neurosci*, 1(8):683–92.

Katz A, Wu D, and Simon MI (1992): Subunits beta gamma of heterotrimeric G protein activate beta 2 isoform of phospholipase C. *Nature*, 360(6405):686–9.

Kaupmann K, Malitschek B, Schuler V, Heid J, Froestl W, Beck P, Mosbacher J, Bischoff S, Kulik A, Shigemoto R, Karschin A, and Bettler B (1998): GABA(B)-receptor subtypes assemble into functional heteromeric complexes. *Nature*, 396(6712):683–687.

Kawamura M, Gachet C, Inoue K, and Kato F (2004): Direct excitation of inhibitory interneurons by extracellular ATP mediated by P2Y1 receptors in the hippocampal slice. *J. Neurosci.*, 24(48):10835–10845.

Kettenmann H, Backus KH, and Schachner M (1984): Aspartate, glutamate and [gamma]-aminobutyric acid depolarize cultured astrocytes. *Neuroscience Letters*, 52(1-2):25–29.

Kettenmann H and Schachner M (1985): Pharmacological properties of gamma-aminobutyric acid-, glutamate-, and aspartate-induced depolarizations in cultured astrocytes. *J. Neurosci.*, 5(12):3295–3301.

Kimelberg HK (2004): The problem of astrocyte identity. *Neurochem Int*, 45(2-3):191–202.

Kimelberg HK, Cai Z, Rastogi P, Charniga CJ, Goderie S, Dave V, and Jalonen TO (1997): Transmitter-induced calcium responses differ in astrocytes acutely isolated from rat brain and in culture. *Journal of Neurochemistry*, 68(3):1088–1098.

Kimelberg HK, Cai Z, Schools G, and Zhou M (2000): Acutely isolated astrocytes as models to probe astrocyte functions. *Neurochemistry International*, 36(4-5):359–367.

Kirchhoff F and Kettenmann H (1992): GABA triggers a [Ca2+]i increase in murine precursor cells of the oligodendrocyte lineage. *Eur J Neurosci*, 4(11):1049–1058.

Klein J, Vakil M, Bergman F, Holler T, Iovino M, and Loffelholz K (1998): Glutamatergic activation of hippocampal phospholipase D: Postnatal fading and receptor desensitization. *Journal of Neurochemistry*, 70(4):1679–1685.

Kornau HC (2006): GABA(B) receptors and synaptic modulation. *Cell and Tissue Research*, 326(2):517–533.

Kressin K, Kuprijanova E, Jabs R, Seifert G, and Steinhäuser C (1995): Developmental regulation of Na+ and K+ conductances in glial cells of mouse hippocampal brain slices. *Glia*, 15(2):173–87.

Kriegstein AR (2005): Constructing circuits: Neurogenesis and migration in the developing neocortex. *Epilepsia*, 46(s7):15–21.

Lavenex P, Banta Lavenex P, and Amaral DG (2007): Postnatal development of the primate hippocampal formation. *Dev Neurosci*, 29(1-2):179–92.

Laywell ED, Rakic P, Kukekov VG, Holland EC, and Steindler DA (2000): Identification of a multipotent astrocytic stem cell in the immature and adult mouse brain. *Proc Natl Acad Sci U S A*, 97(25):13883–8.

Leinekugel X (2003): Developmental patterns and plasticities: The hippocampal model. *Journal of Physiology-Paris*, 97(1):27–37.

Leinekugel X, Khazipov R, Cannon R, Hirase H, Ben-Ari Y, and Buzsaki G (2002): Correlated bursts of activity in the neonatal hippocampus in vivo. *Science*, 296(5575):2049–52.

Leitch E, Coaker J, Young C, Mehta V, and Sernagor E (2005): GABA type-A activity controls its own developmental polarity switch in the maturing retina. *J Neurosci*, 25(19):4801–5.

Leung LS and Shen B (2007): GABA(B) receptor blockade enhances theta and gamma rhythms in the hippocampus of behaving rats. *Hippocampus*, 17(4):281–91.

Liang SL, Carlson GC, and Coulter DA (2006): Dynamic regulation of synaptic GABA release by the glutamate-glutamine cycle in hippocampal area CA1. *J. Neurosci.*, 26(33):8537–8548.

Liu QY, Schaffner AE, Chang YH, Maric D, and Barker JL (2000): Persistent activation of GABAa receptor/Cl- channels by astrocyte-derived GABA in cultured embryonic rat hippocampal neurons. *J Neurophysiol*, 84(3):1392–1403.

Liu X, Bolteus AJ, Balkin DM, Henschel O, and Bordey A (2006): GFAP-expressing cells in the postnatal subventricular zone display a unique glial phenotype intermediate between radial glia and astrocytes. *Glia*, 54(5):394–410.

Liu X, Wang Q, Haydar TF, and Bordey A (2005): Nonsynaptic GABA signaling in postnatal subventricular zone controls proliferation of GFAP-expressing progenitors. *Nat Neurosci*, 8(9):1179–87.

Lledo PM, Alonso M, and Grubb MS (2006): Adult neurogenesis and functional plasticity in neuronal circuits. *Nat Rev Neurosci*, 7(3):179–193.

Lopez-Bendito G, Lujan R, Shigemoto R, Ganter P, Paulsen O, and Molnar Z (2003): Blockade of GABA(B) receptors alters the tangential migration of cortical neurons. *Cereb Cortex*, 13(9):932–42.

Lopez-Bendito G, Shigemoto R, Kulik A, Vida I, Fairen A, and Lujan R (2004): Distribution of metabotropic GABA receptor subunits GABA(B)1a/b and GABA(B)2 in the rat hippocampus during prenatal and postnatal development. *Hippocampus*, 14(7):836–48.

LoTurco JJ, Owens DF, Heath MJ, Davis MB, and Kriegstein AR (1995): GABA and glutamate depolarize cortical progenitor cells and inhibit DNA synthesis. *Neuron*, 15(6):1287–98.

Ludwig A, Li H, Saarma M, Kaila K, and Rivera C (2003): Developmental up-regulation of KCC2 in the absence of GABAergic and glutamatergic transmission. *Eur J Neurosci*, 18(12):3199–206.

Lujan R and Shigemoto R (2006): Localization of metabotropic GABA receptor subunits GABA(B)1 and GABA(B)2 relative to synaptic sites in the rat developing cerebellum. *European Journal of Neuroscience*, 23(6):1479–1490.

Luscher C, Jan LY, Stoffel M, Malenka RC, and Nicoll RA (1997): G protein-coupled inwardly rectifying K+ channels (GIRKs) mediate postsynaptic but not presynaptic transmitter actions in hippocampal neurons. *Neuron*, 19(3):687–695.

Luyt K, Slade TP, Dorward JJ, Durant CF, Wu Y, Shigemoto R, Mundell SJ, Varadi A, and Molnar E (2007): Developing oligodendrocytes express functional GABA(B) receptors that stimulate cell proliferation and migration. *Journal of Neurochemistry*, 100(3):822–840.

Lynch GS, Dunwiddie T, and Gribkoff V (1977): Heterosynaptic depression: A postsynaptic correlate of long-term potentiation. *Nature*, 266(5604):737–739.

Ma DK, Ming Gl, and Song H (2005): Glial influences on neural stem cell development: Cellular niches for adult neurogenesis. *Current Opinion in Neurobiology*, 15(5):514–520.

MacVicar BA, Tse FW, Crichton SA, and Kettenmann H (1989): GABA-activated Cl- channels in astrocytes of hippocampal slices. *J Neurosci*, 9(10):3577–83.

Malitschek B, Ruegg D, Heid J, Kaupmann K, Bittiger H, Frostl W, Bettler B, and Kuhn R (1998): Developmental changes of agonist affinity at GABA(B)r1 receptor variants in rat brain. *Mol Cell Neurosci*, 12(1-2):56–64.

Marchi B, Burlando B, Panfoli I, and Viarengo A (2000): Interference of heavy metal cations with fluorescent Ca2+ probes does not affect Ca2+ measurements in living cells. *Cell Calcium*, 28(4):225–31.

Maric D, Liu QY, Maric I, Chaudry S, Chang YH, Smith SV, Sieghart W, Fritschy JM, and Barker JL (2001): GABA expression dominates neuronal lineage progression in the embryonic rat neocortex and facilitates neurite outgrowth via GABA(a) autoreceptor/Cl- channels. *J Neurosci*, 21(7):2343–60.

Marshall FH, Jones KA, Kaupmann K, and Bettler B (1999): GABA(B) receptors - the first 7TM heterodimers. *Trends in Pharmacological Sciences*, 20(10):396–399.

Martin SJ, Grimwood PD, and Morris RG (2000): Synaptic plasticity and memory: An evaluation of the hypothesis. *Annu Rev Neurosci*, 23:649–711.

Matthias K, Kirchhoff F, Seifert G, Huttmann K, Matyash M, Kettenmann H, and Steinhäuser C (2003): Segregated expression of AMPA-type glutamate receptors and glutamate transporters defines distinct astrocyte populations in the mouse hippocampus. *J. Neurosci.*, 23(5):1750–1758.

Meier SD, Kovalchuk Y, and Rose CR (2006): Properties of the new fluorescent Na(+) indicator CoroNa Green: Comparison with SBFI and confocal Na(+) imaging. *J Neurosci Methods*.

Milligan G (1993): Mechanisms of multifunctional signalling by G protein-linked receptors. *Trends Pharmacol Sci*, 14(6):239–44.

Misgeld U, Bijak M, and Jarolimek W (1995): A physiological role for GABA(B) receptors and the effects of baclofen in the mammalian central nervous system. *Prog Neurobiol*, 46(4):423–62.

Mody I and Pearce RA (2004): Diversity of inhibitory neurotransmission through GABAa receptors. *Trends in Neurosciences*, 27(9):569–575.

Mohler H (2006): GABA(a) receptor diversity and pharmacology. *Cell Tissue Res*, 326(2):505–16.

Mohler H and Fritschy JM (1999): GABA(B) receptors make it to the top–as dimers. *Trends Pharmacol Sci*, 20(3):87–9.

Mombereau C, Kaupmann K, Gassmann M, Bettler B, van der Putten H, and Cryan JF (2005): Altered anxiety and depression-related behaviour in mice lacking GABA(B)(2) receptor subunits. *Neuroreport*, 16(3):307–10.

Moran JM, Enna SJ, and McCarson KE (2001): Developmental regulation of GABA(B) receptor function in rat spinal cord. *Life Sci*, 68(19-20):2287–95.

Mozrzymas JW, Zarmowska ED, Pytel M, and Mercik K (2003): Modulation of GABAa receptors by hydrogen ions reveals synaptic GABA transient and a crucial role of the desensitization process. *J. Neurosci.*, 23(22):7981–7992.

Mulligan SJ and MacVicar BA (2004): Calcium transients in astrocyte endfeet cause cerebrovascular constrictions. *Nature*, 431(7005):195–9.

Munakata Y, Casey BJ, and Diamond A (2004): Developmental cognitive neuroscience: Progress and potential. *Trends in Cognitive Sciences*, 8(3):122–128.

Nagai M, Re DB, Nagata T, Chalazonitis A, Jessell TM, Wichterle H, and Przedborski S (2007): Astrocytes expressing als-linked mutated SOD1 release factors selectively toxic to motor neurons. *Nat Neurosci*, 10(5):615–22.

Namba T, Mochizuki H, Onodera M, Mizuno Y, Namiki H, and Seki T (2005): The fate of neural progenitor cells expressing astrocytic and radial glial markers in the postnatal rat dentate gyrus. *European Journal of Neuroscience*, 22(8):1928–1941.

Neary JT, Rathbone MP, Cattabeni F, Abbracchio MP, and Burnstock G (1996): Trophic actions of extracellular nucleotides and nucleosides on glial and neuronal cells. *Trends Neurosci*, 19(1):13–8.

Nett WJ, Oloff SH, and McCarthy KD (2002): Hippocampal astrocytes in situ exhibit calcium oscillations that occur independent of neuronal activity. *J Neurophysiol*, 87(1):528–37.

Nilsson M, Eriksson PS, Ronnback L, and Hansson E (1993): GABA induces Ca2+ transients in astrocytes. *Neuroscience*, 54(3):605–14.

Nimmerjahn A, Kirchhoff F, Kerr JN, and Helmchen F (2004): Sulforhodamine 101 as a specific marker of astroglia in the neocortex in vivo. *Nat Methods*, 1(1):31–37.

Nolte C, Matyash M, Pivneva T, Schipke CG, Ohlemeyer C, Hanisch UK, Kirchhoff F, and Kettenmann H (2001): GFAP promoter-controlled eGFP-expressing transgenic mice: A tool to visualize astrocytes and astrogliosis in living brain tissue. *Glia*, 33(1):72–86.

Nusser Z, Naylor D, and Mody I (2001): Synapse-specific contribution of the variation of transmitter concentration to the decay of inhibitory postsynaptic currents. *Biophys J*, 80(3):1251–61.

Oka M, Wada M, Wu Q, Yamamoto A, and Fujita T (2006): Functional expression of metabotropic GABA(B) receptors in primary cultures of astrocytes from rat cerebral cortex. *Biochemical and Biophysical Research Communications*, 341(3):874–881.

Owens DF and Kriegstein AR (2002): Is there more to GABA than synaptic inhibition? *Nat Rev Neurosci*, 3(9):715–27.

Parpura V, Basarsky TA, Liu F, Jeftinija K, Jeftinija S, and Haydon PG (1994): Glutamate-mediated astrocyte-neuron signalling. *Nature*, 369(6483):744–7.

Parri HR and Crunelli V (2001): Pacemaker calcium oscillations in thalamic astrocytes in situ. *Neuroreport*, 12(18):3897–900.

Pascual O, Casper KB, Kubera C, Zhang J, Revilla-Sanchez R, Sul JY, Takano H, Moss SJ, McCarthy K, and Haydon PG (2005): Astrocytic purinergic signaling coordinates synaptic networks. *Science*, 310(5745):113–116.

Pasti L, Volterra A, Pozzan T, and Carmignoto G (1997): Intracellular calcium oscillations in astrocytes: A highly plastic, bidirectional form of communication between neurons and astrocytes in situ. *J Neurosci*, 17(20):7817–30.

Pasti L, Zonta M, Pozzan T, Vicini S, and Carmignoto G (2001): Cytosolic calcium oscillations in astrocytes may regulate exocytotic release of glutamate. *J Neurosci*, 21(2):477–84.

Pastor A, Chvatal A, Sykova E, and Kettenmann H (1995): Glycine- and GABA-activated currents in identified glial cells of the developing rat spinal cord slice. *Eur J Neurosci*, 7(6):1188–98.

Perea G and Araque A (2005): Glial calcium signaling and neuron-glia communication. *Cell Calcium*, 38(3-4):375–382.

Peters O, Schipke CG, Hashimoto Y, and Kettenmann H (2003): Different mechanisms promote astrocyte Ca2+ waves and spreading depression in the mouse neocortex. *J Neurosci*, 23(30):9888–96.

Petersen OH (2005): Ca2+ signalling and Va2+-activated ion channels in exocrine acinar cells. *Cell Calcium*, 38(3-4):171–200.

Piatti VC, Esposito MS, and Schinder AF (2006): The timing of neuronal development in adult hippocampal neurogenesis. *Neuroscientist*, 12(6):463–468.

Porter JT and McCarthy KD (1996): Hippocampal astrocytes in situ respond to glutamate released from synaptic terminals. *J Neurosci*, 16(16):5073–81.

Prosser HM, Gill CH, Hirst WD, Grau E, Robbins M, Calver A, Soffin EM, Farmer CE, Lanneau C, and Gray J (2001): Epileptogenesis and enhanced prepulse inhibition in GABA(B)1-deficient mice. *Molecular and Cellular Neuroscience*, 17(6):1059–1070.

Ransom B, Behar T, and Nedergaard M (2003): New roles for astrocytes (stars at last). *Trends in Neurosciences*, 26(10):520–522.

Raponi E, Agenes F, Delphin C, Assard N, Baudier J, Legraverend C, and Deloulme JC (2007): S100b expression defines a state in which gfap-expressing cells lose their neural stem cell potential and acquire a more mature developmental stage. *Glia*, 55(2):165–77.

Rivera C, Voipio J, and Kaila K (2005): Two developmental switches in gabaergic signalling: The K+-Cl- cotransporter KCC2 and carbonic anhydrase cavii. *J Physiol (Lond)*, 562(1):27–36.

Rivera C, Voipio J, Payne JA, Ruusuvuori E, Lahtinen H, Lamsa K, Pirvola U, Saarma M, and Kaila K (1999): The K+/Cl- co-transporter KCC2 renders GABA hyperpolarizing during neuronal maturation. *Nature*, 397(6716):251–5.

Rose CR (2003): High-resolution Na+ imaging in dendrites and spines. *Pflugers Arch*, 446(3):317–21.

Rothstein JD, Dykes-Hoberg M, Pardo CA, Bristol LA, Jin L, Kuncl RW, Kanai Y, Hediger MA, Wang Y, Schielke JP, and Welty DF (1996): Knockout of glutamate transporters reveals a major role for astroglial transport in excitotoxicity and clearance of glutamate. *Neuron*, 16(3):675–86.

Rowitch DH (2004): Glial specification in the vertebrate neural tube. *Nat Rev Neurosci*, 5(5):409–19.

Royer S and Pare D (2003): Conservation of total synaptic weight through balanced synaptic depression and potentiation. *Nature*, 422(6931):518–522.

Sakaba T and Neher E (2003): Direct modulation of synaptic vesicle priming by GABA(B) receptor activation at a glutamatergic synapse. *Nature*, 424(6950):775–8.

Scanziani M (2000): GABA spillover activates postsynaptic GABA(B) receptors to control rhythmic hippocampal activity. *Neuron*, 25(3):673–81.

Scanziani M, Malenka RC, and Nicoll RA (1996): Role of intercellular interactions in heterosynaptic long-term depression. *Nature*, 380(6573):446–450.

Schipke CG, Boucsein C, Ohlemeyer C, Kirchhoff F, and Kettenmann H (2002): Astrocyte Ca2+ waves trigger responses in microglial cells in brain slices. *FASEB J.*, 16(2):255–257.

Schipke CG and Kettenmann H (2004): Astrocyte responses to neuronal activity. *Glia*, 47(3):226–32.

Schools GP, Zhou M, and Kimelberg HK (2003): Electrophysiologically "complex" glial cells freshly isolated from the hippocampus are immunopositive for the chondroitin sulfate proteoglycan NG2. *J Neurosci Res*, 73(6):765–77.

Schools GP, Zhou M, and Kimelberg HK (2006): Development of gap junctions in hippocampal astrocytes: Evidence that whole cell electrophysiological phenotype is an intrinsic property of the individual cell. *J Neurophysiol*, 96(3):1383–92.

Schuler V, Luscher C, Blanchet C, Klix N, Sansig G, Klebs K, Schmutz M, Heid J, Gentry C, Urban L, Fox A, Spooren W, Jaton AL, Vigouret J, Pozza M, Kelly PH, Mosbacher J, Froestl W, Kaslin E, Korn R, Bischoff S, Kaupmann K, van der Putten H, and Bettler B (2001): Epilepsy, hyperalgesia, impaired memory, and loss of pre- and postsynaptic GABA(B) responses in mice lacking GABA(B(1)). *Neuron*, 31(1):47–58.

Seifert G, Schilling K, and Steinhäuser C (2006): Astrocyte dysfunction in neurological disorders: A molecular perspective. *Nat Rev Neurosci*, 7(3):194–206.

Selbie LA and Hill SJ (1998): G protein-coupled-receptor cross-talk: The fine-tuning of multiple receptor-signalling pathways. *Trends Pharmacol Sci*, 19(3):87–93.

Seri B, Garcia-Verdugo JM, McEwen BS, and Alvarez-Buylla A (2001): Astrocytes give rise to new neurons in the adult mammalian hippocampus. *J. Neurosci.*, 21(18):7153–7160.

Serrano A, Haddjeri N, Lacaille JC, and Robitaille R (2006): GABAergic network activation of glial cells underlies hippocampal heterosynaptic depression. *J. Neurosci.*, 26(20):5370–5382.

Simard M, Arcuino G, Takano T, Liu QS, and Nedergaard M (2003): Signaling at the gliovascular interface. *J. Neurosci.*, 23(27):9254–9262.

Slezak M and Pfrieger FW (2003): New roles for astrocytes: Regulation of CNS synaptogenesis. *Trends in Neurosciences*, 26(10):531–535.

Somjen GG (1988): Nervenkitt: Notes on the history of the concept of neuroglia. *Glia*, 1(1):2–9.

Song H, Stevens CF, and Gage FH (2002): Astroglia induce neurogenesis from adult neural stem cells. *Nature*, 417(6884):39–44.

Sontheimer H (2003): Malignant gliomas: Perverting glutamate and ion homeostasis for selective advantage. *Trends in Neurosciences*, 26(10):543–549.

Steiger JL, Bandyopadhyay S, Farb DH, and Russek SJ (2004): CAMP response element-binding protein, activating transcription factor-4, and upstream stimulatory factor differentially control hippocampal GABA(B)R1a and GABA(B)R1b subunit gene expression through alternative promoters. *J Neurosci*, 24(27):6115–26.

Steinhauser C, Kressin K, Kuprijanova E, Weber M, and Seifert G (1994): Properties of voltage-activated Na+ and K+ currents in mouse hippocampal glial cells in situ and after acute isolation from tissue slices. *Pflugers Arch*, 428(5-6):610–20.

Steinhäuser C, Berger T, Frotscher M, and Kettenmann H (1992): Heterogeneity in the membrane current pattern of identified glial cells in the hippocampal slice. *Eur J Neurosci*, 4(6):472–484.

Stelzer A and Wong RKS (1989): GABAa responses in hippocampal neurons are potentiated by glutamate. *Nature*, 337(6203):170–173.

Stosiek C, Garaschuk O, Holthoff K, and Konnerth A (2003): In vivo two-photon calcium imaging of neuronal networks. *Proc Natl Acad Sci U S A*, 100(12):7319–24.

Tabata T, Araishi K, Hashimoto K, Hashimotodani Y, van der Putten H, Bettler B, and Kano M (2004): Ca2+ activity at GABA(B) receptors constitutively promotes metabotropic glutamate signaling in the absence of GABA. *Proc Natl Acad Sci U S A*, 101(48):16952–7.

Tabata T and Kano M (2006): GABA(B) receptor-mediated modulation of glutamate signaling in cerebellar purkinje cells. *Cerebellum*, 5(2):127–33.

Takano T, Tian GF, Peng W, Lou N, Libionka W, Han X, and Nedergaard M (2006): Astrocyte-mediated control of cerebral blood flow. *Nat Neurosci*, 9(2):260–267.

Tanaka Y and Tashjian AH (1993): Functional identification and quantitation of three intracellular calcium pools in Gh4C1 cells: Evidence that the caffeine-responsive pool is coupled to a thapsigargin-resistant, ATP-dependent process. *Biochemistry*, 32(45):12062–12073.

Tashiro A, Goldberg J, and Yuste R (2002): Calcium oscillations in neocortical astrocytes under epileptiform conditions. *J Neurobiol*, 50(1):45–55.

Tateishi N, Shimoda T, Manako Ji, Katsumata S, Shinagawa R, and Ohno H (2006): Relevance of astrocytic activation to reductions of astrocytic GABAa receptors. *Brain Research*, 1089(1):79–91.

Tian GF, Azmi H, Takano T, Xu Q, Peng W, Lin J, Oberheim N, Lou N, Wang X, Zielke HR, Kang J, and Nedergaard M (2005): An astrocytic basis of epilepsy. *Nat Med*, 11(9):973–81.

Titz S, Hans M, Kelsch W, Lewen A, Swandulla D, and Misgeld U (2003): Hyperpolarizing inhibition develops without trophic support by GABA in cultured rat midbrain neurons. *J Physiol*, 550(Pt 3):719–30.

Tosetti P, Bakels R, Colin-Le Brun I, Ferrand N, Gaiarsa JL, and Caillard O (2004): Acute desensitization of presynaptic GABA(B)-mediated inhibition and induction of epileptiform discharges in the neonatal rat hippocampus. *Eur J Neurosci*, 19(12):3227–34.

Tozuka Y, Fukuda S, Namba T, Seki T, and Hisatsune T (2005): GABAergic excitation promotes neuronal differentiation in adult hippocampal progenitor cells. *Neuron*, 47(6):803–15.

Tsien RY, Rink TJ, and Poenie M (1985): Measurement of cytosolic free Ca2+ in individual small cells using fluorescence microscopy with dual excitation wavelengths. *Cell Calcium*, 6(1-2):145–57.

Ullian EM, Christopherson KS, and Barres BA (2004): Role for glia in synaptogenesis. *Glia*, 47(3):209–16.

Ullian EM, Sapperstein SK, Christopherson KS, and Barres BA (2001): Control of synapse number by glia. *Science*, 291(5504):657–661.

Varju P, Katarova Z, Madarasz E, and Szabo G (2001): GABA signalling during development: New data and old questions. *Cell Tissue Res*, 305(2):239–46.

Ventura R and Harris KM (1999): Three-dimensional relationships between hippocampal synapses and astrocytes. *J. Neurosci.*, 19(16):6897–6906.

Verkhratsky A and Kettenmann H (1996): Calcium signalling in glial cells. *Trends Neurosci*, 19(8):346–52.

Verkhratsky A, Orkand RK, and Kettenmann H (1998): Glial calcium: Homeostasis and signaling function. *Physiol Rev*, 78(1):99–141.

Vigot R, Barbieri S, Brauner-Osborne H, Turecek R, Shigemoto R, Zhang YP, Lujan R, Jacobson LH, Biermann B, and Fritschy JM (2006): Differential compartmentalization and distinct functions of GABA(B) receptor variants. *Neuron*, 50(4):589–601.

Volterra A and Meldolesi J (2005): Astrocytes, from brain glue to communication elements: The revolution continues. *Nat Rev Neurosci*, 6(8):626–40.

Volterra A and Steinhäuser C (2004): Glial modulation of synaptic transmission in the hippocampus. *Glia*, 47(3):249–57.

Wallraff A, Odermatt B, Willecke K, and Steinhäuser C (2004): Distinct types of astroglial cells in the hippocampus differ in gap junction coupling. *Glia*, 48(1):36–43.

Walz W (2000): Controversy surrounding the existence of discrete functional classes of astrocytes in adult gray matter. *Glia*, 31(2):95–103.

Walz W and Lang MK (1998): Immunocytochemical evidence for a distinct GFAP-negative subpopulation of astrocytes in the adult rat hippocampus. *Neurosci Lett*, 257(3):127–30.

Wang LP, Kempermann G, and Kettenmann H (2005): A subpopulation of precursor cells in the mouse dentate gyrus receives synaptic GABAergic input. *Mol Cell Neurosci*, 29(2):181–9.

Wang X, Lou N, Xu Q, Tian GF, Peng WG, Han X, Kang J, Takano T, and Nedergaard M (2006): Astrocytic Ca(2+) signaling evoked by sensory stimulation in vivo. *Nat Neurosci*, 9(6):816–23.

Westenbroek RE, Bausch SB, Lin RC, Franck JE, Noebels JL, and Catterall WA (1998): Upregulation of L-type Ca2+ channels in reactive astrocytes after brain injury, hypomyelination, and ischemia. *J Neurosci*, 18(7):2321–34.

Wettschureck N and Offermanns S (2005): Mammalian G proteins and their cell type specific functions. *Physiol Rev*, 85(4):1159–204.

Winship IR, Plaa N, and Murphy TH (2007): Rapid astrocyte calcium signals correlate with neuronal activity and onset of the hemodynamic response in vivo. *J. Neurosci.*, 27(23):6268–6272.

Wise A, Green A, Main MJ, Wilson R, Fraser N, and Marshall FH (1999): Calcium sensing properties of the GABA(B) receptor. *Neuropharmacology*, 38(11):1647–56.

Witcher MR, Kirov SA, and Harris KM (2007): Plasticity of perisynaptic astroglia during synaptogenesis in the mature rat hippocampus. *Glia*, 55(1):13–23.

Wittinghofer A (1997): Signaling mechanistics: Aluminum fluoride for molecule of the year. *Current Biology*, 7(11):R682–R685.

Ye ZC, Wyeth MS, Baltan-Tekkok S, and Ransom BR (2003): Functional hemichannels in astrocytes: A novel mechanism of glutamate release. *J Neurosci*, 23(9):3588–96.

Zerlin M and Goldman JE (1997): Interactions between glial progenitors and blood vessels during early postnatal corticogenesis: Blood vessel contact represents an early stage of astrocyte differentiation. *The Journal of Comparative Neurology*, 387(4):537–546.

Zhang JM, Wang HK, Ye CQ, Ge W, Chen Y, Jiang ZL, Wu CP, Poo MM, and Duan S (2003): ATP released by astrocytes mediates glutamatergic activity-dependent heterosynaptic suppression. *Neuron*, 40(5):971–82.

Zhang Q, Pangrsic T, Kreft M, Krzan M, Li N, Sul JY, Halassa M, Van Bockstaele E, Zorec R, and Haydon PG (2004): Fusion-related release of glutamate from astrocytes. *J Biol Chem*, 279(13):12724–33.

Zhang SC (2001): Defining glial cells during CNS development. *Nature Reviews Neuroscience*, 2(11):840–843.

Zhou M and Kimelberg HK (2001): Freshly isolated hippocampal CA1 astrocytes comprise two populations differing in glutamate transporter and AMPA receptor expression. *J. Neurosci.*, 21(20):7901–7908.

Zhou M, Schools GP, and Kimelberg HK (2006): Development of GLAST(+) astrocytes and NG2(+) glia in rat hippocampus CA1: Mature astrocytes are electrophysiologically passive. *J Neurophysiol*, 95(1):134–143.

Zonta M, Angulo MC, Gobbo S, Rosengarten B, Hossmann KA, Pozzan T, and Carmignoto G (2003a): Neuron-to-astrocyte signaling is central to the dynamic control of brain microcirculation. *Nat Neurosci*, 6(1):43–50.

Zonta M and Carmignoto G (2002): Calcium oscillations encoding neuron-to-astrocyte communication. *J Physiol Paris*, 96(3-4):193–8.

Zonta M, Sebelin A, Gobbo S, Fellin T, Pozzan T, and Carmignoto G (2003b): Glutamate-mediated cytosolic calcium oscillations regulate a pulsatile prostaglandin release from cultured rat astrocytes. *J Physiol*, 553(Pt 2):407–14.

# A Lists of Figures and Tables

## List of Figures



## List of Tables

# B Publications

In the following I have attached reprints or submitted manuscripts of publications I contributed to during my time as a PhD student.

## B.1 Meier et al., in Preparation

### $GABA_B$ Receptor Activation in Astrocytes Causes $Ca^{2+}$ Release from Intracellular Stores - A Response which Varies Developmentally

Silke D. Meier, Karl W. Kafitz, and Christine R. Rose

This manuscript contains the most relevant data of the present work and will be submitted in 2007.

My contributions:

- experimental design, together with C.R.R.
- all experimental work and illustration thereof
- data analysis and statistics
- writing of the first draft

## B.2 Kafitz et al., Submitted

### Developmental Profile and Properties of Sulforhodamine 101-Labeled Glial Cells in Acute Brain Slices of Rat Hippocampus

Karl W. Kafitz*, Silke D. Meier*, Jonathan Stephan*, and Christine R. Rose

* these authors equally contributed to this work

My contributions:

- experimental design, together with K.W.K and C.R.R.
- establishing the procedure for staining acute slices with SR101
- analysis of the staining pattern of SR101 in comparison to SBFI, together with J.S. (figures 1 and 2)
- electrophysiological recordings of SR101-positive cells at P03 and P15 and SR101-negative cells at P03 (part of the experimental data illustrated in table I and figures 3 and 4)
- $Ca^{2+}$ imaging experiments and illustration thereof (figure 6)
- discussion of the manuscript

# Developmental Profile and Properties of Sulforhodamine 101-Labeled Glial Cells in Acute Brain Slices of Rat Hippocampus

**Karl W. Kafitz*, Silke D. Meier*, Jonathan Stephan* and Christine R. Rose**

Institute for Neurobiology, Geb. 26.02.00, Universitaetsstrasse 1, Heinrich Heine University of Duesseldorf, 40225 Duesseldorf, Germany

* These authors equally contributed to this study.

**The reliable identification of astrocytes for physiological measurements was always time-consuming and difficult. Recently, the fluorescent dye sulforhodamine 101 (SR101) was reported to label cortical glial cells *in vivo* (Nimmerjahn et al., 2004). We adapted this technique for use in acute hippocampal slices at early postnatal stages (postnatal days 3, 7, 15) and describe a procedure for double-labeling of SR101 and conventional ion-selective dyes. Using whole-cell patch-clamp, imaging and immunohistochemistry, we characterized the properties of SR101-positive versus SR101-negative cells in the stratum radiatum. Our data show that SR101, in contrast to Fura-2 or SBFI, only stains a subset of glial cells. Throughout development, SR101-positive and SR101-negative cells differ in their basic membrane properties. Furthermore, SR101-positive cells undergo a developmental switch from variably rectifying to passive between P3 and P15 and lack voltage-gated $Na^+$ currents. At P15, the majority of SR101-positive cells is positive for GFAP. In summary, our data demonstrate that SR101 selectively labels a subpopulation of glial cells in the early postnatal hippocampus that shows the typical developmental changes and characteristics of classical astrocytes. Owing to its reliability and uncomplicated handling, we expect that this technique will be outstandingly helpful in future investigations studying astrocytes in the developing brain.**

***Key words*: astrocyte, sulforhodamine 101, hippocampus, imaging, electrophysiology, GFAP, SBFI, Fura-2**

## 1. Introduction

During the last decade it has been firmly established that astrocytes are not purely supportive for neuronal function, but also modulate the synaptic communication between neurons (Araque et al., 1999; Fiacco et al., 2007; Haydon and Carmignoto, 2006; Kang et al., 1998; Nedergaard, 1994; Newman and Volterra, 2004; Parri et al., 2001; Parri and Crunelli, 2007; Pascual et al., 2005; Schipke and Kettenmann, 2004; Serrano et al., 2006; Verkhratsky et al., 1998; Volterra and Meldolesi, 2005). Recent studies demonstrated that astroglia also plays a central role in the regulation of blood vessel diameter during neuronal activity (Metea and Newman, 2006; Mulligan and MacVicar, 2004; Takano et al., 2006; Zonta et al., 2003). The analysis of astrocytes in the intact tissue with electrophysiological and high-resolution imaging techniques, however, was always hampered by the problem of a reliable identification of this cell type. The identification of astrocytes based solely on morphological criteria, such as somatic size and cellular architecture, hosts the chance to mistakenly include small-sized neurons (Kimelberg, 2004). Immunohistochemical stainings of markers such as glial fibrillary acidic protein (GFAP) or the $Ca^{2+}$-binding protein S-100$\beta$, can only be performed after the experiment, are time-consuming and often do not allow an undeniable identification of the cells analyzed in physiological experiments. To overcome this problem, transgenic mice, in which enhanced green fluorescent protein (EGFP) is expressed under the human GFAP promoter have been raised (Hirrlinger et al., 2006; Nolte et al., 2001; Zhuo et al., 1997). However, because astrocytes show very diverse levels of GFAP-expression (Kimelberg, 2004), this approach enables the identification of only a subset of astrocytes. Many studies reported that glial cells take up the membrane-permeable forms of $Ca^{2+}$ indicator dyes such as Fura-2 or Fluo-4 much better than neurons (e. g. Dallwig and Deitmer, 2002; Wang et al., 2006), and astrocytes were thus often identified based on the emission patterns of the indicator dyes used. This approach was extended by Dallwig and Deitmer (2002), who have described that neurons and astrocytes in acute brain slices differ in their response to changes in the external potassium concentration. Still, this approach can only identify about 80% of astrocytes and necessitates performing additional $Ca^{2+}$-imaging experiments. Recently, the fluorescent dye sulforhodamine 101 (SR101) was reported as a powerful tool for specific labeling of cortical glial cells in the intact brain of juvenile and adult rodents (Nimmerjahn et al., 2004; Wang et al., 2006). In the present study we adapted this technique for use in an acute tissue slice preparation of the early postnatal rat hippocampus. Because in the CA1 region of the rodent hippocampus, astrocytes undergo considerable changes in channel complement and passive membrane properties during postnatal development (Bordey and Sontheimer, 1997; Kressin et al., 1995; Zhou et al., 2006), we performed the study at

different early postnatal stages (postnatal days 3, 7, 15). Using whole-cell patch clamp, imaging techniques and immunohistochemistry, we show that the percentage of SR101-positive cells in the *stratum radiatum* increases during development. Furthermore, SR101-positive cells lack voltage-gated $Na^+$ currents and change from variably rectifying to passive cells between P3 and P15. At P15, the majority of SR101-labeled cells is positive for the astrocytic marker GFAP. Thus, our data demonstrate that SR101 selectively labels a subset of glial cells in the early postnatal hippocampus that shows typical characteristics of classical astrocytes.

## 2. Methods

### 2.1. Tissue preparation and labeling with SR101

Experiments were carried out on acute tissue slices (250 µm) of rat hippocampi harvested at postnatal days 3, 7, and 15 as described earlier (Meier et al., 2006). In brief, animals were decapitated and the hippocampi were rapidly removed. Slices of P3 and P7 animals were sectioned in ice-cold normal artificial cerebrospinal fluid (ACSF; in mM: 125 NaCl, 2.5 KCl, 2 $CaCl_2$, 1 $MgCl_2$, 1.25 $NaH_2PO_4$, 26 $NaHCO_3$ and 20 glucose, bubbled with 95% $O_2$ and 5% $CO_2$; pH 7.4). Following sectioning, slices were kept at 34°C for 20 minutes in ACSF that contained 0.5 - 1 µM sulforhodamine 101 (SR101), followed by a 10 min incubation in normal ACSF at 34°C. Slices of P15 rats were sectioned and post-incubated with SR101 in ACSF with a reduced $Ca^{2+}$ concentration (in mM: 125 NaCl, 2.5 KCl, 0.5 $CaCl_2$, 6 $MgCl_2$, 1.25 $NaH_2PO_4$, 26 $NaHCO_3$ and 20 glucose, bubbled with 95% $O_2$ and 5% $CO_2$; pH 7.4). Afterwards, all slices were kept at room temperature until they were used for experiments, which were also performed at room temperature. Unless stated otherwise, all chemicals were purchased from Sigma Aldrich Co. (Taufkirchen, Germany).

### 2.2. Determination of the density of SR101-labeled cells

For determination of the amount of SR101-positive cells on the total number of cells exhibiting glial morphology, slices were double-labeled with SR101 and the ester form of sodium-binding benzofuran isophthalate (SBFI; 800 µM), a conventional $Na^+$-selective fluorescent dye that exhibits similar properties as Fura-2 (Meier et al., 2006). To this end, SBFI-AM (800 µM) was repeatedly (1-5 s duration each) pressure injected through a fine-tipped glass microelectrode into the stratum radiatum (Stosiek et al., 2003). Injection was followed by a 45-60 min wash in normal ACSF at room temperature to allow for diffusion and de-esterification of the dye. Stacks of images (31 optical sections at 1 or 1.5 µm thickness) were then taken at a custom build two-photon laser scanning microscope (excitation wavelength at 850 nm) based on an Olympus FV300 system (Olympus Europe, Hamburg, Germany), coupled to a Mai-Tai Broadband laser (Spectra Physics, Darmstadt, Germany) and equipped with two fluorescence detection channels. Fluorescence emission of SBFI was collected between 400 and 590 nm, emission of SR101 was detected between 610 and 630 nm. Maximum intensity projections and analyses of the staining patterns were performed at montages of image stacks using "ImageJ"-software.

### 2.3. Electrophysiology and Immunohistochemistry

Somatic whole-cell recordings were obtained at an upright microscope (Nikon Eclipse E600FN, 60x water immersion objective, N.A. 1.00, Nikon Europe, Düsseldorf, Germany) using an EPC10 amplifier (HEKA Elektronik, Lambrecht, Germany). "PatchMaster"-software (HEKA Elektronik, Lambrecht, Germany) was used for data acquisition. Some recordings were carried out at a Zeiss Axioscope (Zeiss, Jena Germany, 40x water immersion objective, N.A. 0.80, Olympus Europe, Hamburg, Germany) using an Axopatch 200A (Molecular Devices, Sunnydale, CA) and "PClamp 8.2"-software for data acquisition. The pipette solution contained (in mM): 120 K-$MeSO_3$ or K-gluconate, 32 KCl, 10 HEPES (N-(2-Hydroxyethyl)piperazine-N'-(2-ethanesulfonic acid), 4 NaCl, 4 Mg-ATP and 0.4 $Na_3$-GTP, 0.1 Alexafluor 488 (Molecular Probes/Invitrogen, Karlsruhe, Germany), pH 7.30. Cells were generally held at membrane potentials of -85 mV. To separate passive conductances from voltage-gated currents, online leak subtraction (P/4) was performed. Data were processed and analyzed by employing "IGOR Pro"-Software (WaveMetrics, Inc., Lake Oswego, OR). Following electrophysiological recordings, images of fluorescence emission of SR101-labeled (excitation wavelength: 587 nm, emission detected above 602 nm) and Alexa-filled (excitation wavelength: 488 nm, emission detected between 495-575 nm) cells were captured by a CCD camera (Spot RT KE, Diagnostic Instruments Inc., Sterling Hights, MI) and "Spot"-software attached to the microscope. Slices were immediately fixed over night at 4°C in paraformaldehyde and immunohistochemically processed for GFAP (dilution 1:100; DAKO Z0334, Hamburg, Germany) as reported earlier (Kafitz and Greer, 1998; Kafitz et al., 1999). Labeled slices were coverslipped and documented as described above. Images of the immunohistochemistry were corrected for shrinkage caused by fixation by a factor of 4.67 and overlaid employing "Adobe Photoshop"-software.

### 2.4. $Ca^{2+}$ imaging

Conventional, wide-field fluorescence imaging was performed using a variable scan digital imaging system (TILL Photonics, Martinsried, Germany) attached to an upright microscope (Axioskop, Zeiss, Jena, Germany, 40x water immersion objective, N.A. 0.80, Olympus Europe, Hamburg, Germany) and a CCD camera as a sensor (TILL Imago SVGA, TILL Photonics, Martinsried, Germany). To this end, after confirmation of successful SR101-staining (excitation wavelength: 575 nm; detection of emission: >590 nm), cells were additionally dye-loaded with the $Ca^{2+}$-selective dye Fura-2 (Fura-2-AM, 500 µM); employing the protocol described above for SBFI. For wide-field imaging of Fura-2, background-corrected fluorescence signals (>410 nm) were collected from defined regions of interest after alternate excitation at 356 nm and 380 nm and the fluorescence ratio (F356/380) was calculated. Images were acquired at 2 Hz and analyzed off-line using "IGOR Pro"-Software (WaveMetrics, Inc., Lake Oswego, OR). ATP was applied by a Picospritzer II (General Valve/Parker Hanifin, Flein/Heilbronn, Germany) coupled to standard micropipettes (Hilgenberg, Waldkappel, Germany) placed at a distance of approximately 10-20 µm to a given cell.

### 2.5. Statistics

Unless otherwise specified, data are expressed as means ± s.e.m.. Data were statistically analyzed by the Kolmogorov-Smirnov-test for normal distribution and the t-test.

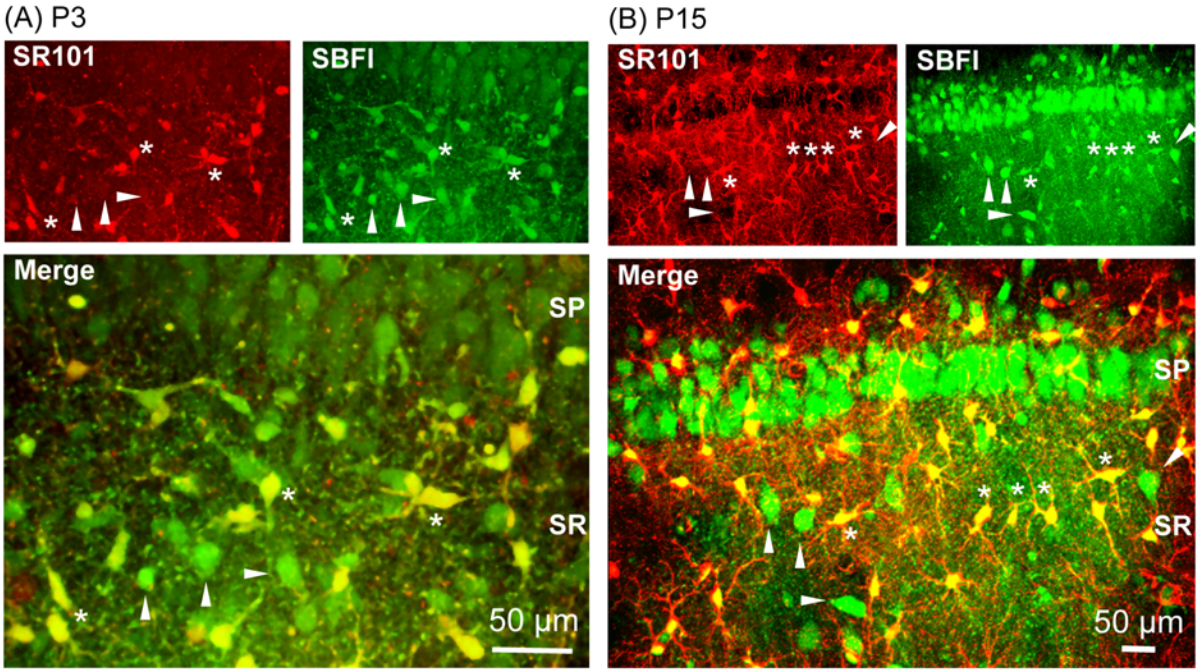


**Fig. 1**. Labeling pattern of SR101 versus SBFI-AM in the hippocampal CA1 region. Fluorescence images, taken at a two-photon laser-scanning microscope, of acute slices from postnatal day P3 (A) and P15 (B) rats, double-stained with SR101 (upper left panels) and SBFI-AM (upper right panels). The lower, enlarged panels show the merged fluorescence images. SP: stratum pyramidale; SR: stratum radiatum. Asterisks mark double-labeled cells located in the stratum radiatum; arrowheads point out cells which are exclusively stained by SBFI. Note that putative pyramidal neurons in the stratum pyramidale are also stained with SBFI, but not with SR101.

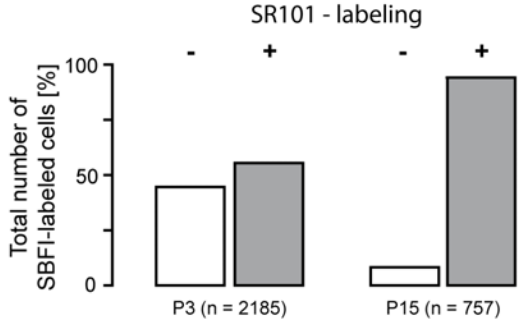


**Fig. 2**. Quantification of the percentage of SR101-negative (white bars) and SR101-postive (grey bars) cells on the total number of small-sized SBFI-labeled cells located in the stratum radiatum in P3 (n = 22 slices; 2185 cells) and P15 rats (n = 11 slices; 757 cells).

## 3. Results

### 3.1. Labeling pattern of acute hippocampal slices with SR101 and SR101/SBFI-AM

Incubation of cells in solutions containing 10-20 µM of the membrane-permeable acetoxymethyl ester (AM) forms of ion-selective fluorescent dyes such as the $Ca^{2+}$-sensitive dye Fura-2 or the $Na^{+}$-sensitive dye SBFI enables the loading and analysis of many cells at a time (e. g. Rose and Ransom, 1996; 1997). In acute brain slices, it was observed consistently that this staining protocol results in a fairly selective staining of astrocytes, and consequently, their primary identification in the intact tissue was often based on this specific staining pattern (e. g. Dallwig and Deitmer, 2002; Wang et al., 2006). Using bolus loading (injection of the AM-form of fluorescent dyes into the extracellular space) instead of bath incubation, in contrast, results in a good quality staining of neurons as well as astroglia (Meier et al., 2006; Stosiek et al., 2003). Injection of dyes thus enables the study of both astrocytes and neurons at the same time. However, dye-loaded neurons, such as interneurons with small somata in the stratum radiatum of the hippocampus, might be falsely identified as astrocytes based on this staining technique. To overcome this problem, we adapted a protocol for application of the red fluorescent dye SR101, which was reported to stain astrocytes in the intact cortex of rodents (Nimmerjahn et al., 2004), for use in acute slices of the rat hippocampus during early postnatal development. SR101 is excited around 575 nm and its emission can be collected above 590 nm, making it suitable for use in combination with many available ion-selective dyes. We found that incubation of the slices right after their preparation in ACSF con-

taining in 500 nM - 1 µM SR101 for 20 minutes at high temperature (34℃), resulted in an optimal staining of cells that was maintained for more than eight hours. The staining pattern of SR101 in slices obtained from animals at postnatal day 3 (P3, Fig. 1A), P7 (not shown), as well as P15 (Fig. 1B), excluded virtually all cells of the stratum pyramidale, clearly indicating that SR101 exclusively labeled glial cells throughout development in this preparation. To portray cells additional to SR101-positive ones in these preparations, we performed a second labeling with the $Na^+$-selective fluorescent dye SBFI-AM, which (like Fura-2) is excited in the UV range. SBFI-AM was directly injected into the stratum radiatum, followed by a period of 45-60 min incubation in ACSF to allow for diffusion of the dye into the cells and sufficient de-esterification. At all developmental stages investigated (P3, P7 and P15), and in contrast to SR101, SBFI-AM labeled cells in the stratum pyramidale (presumably CA1 pyramidal neurons) as well as SR101-negative cells in the stratum radiatum with large somata that presumably represented interneurons or ectopic pyramidal neurons (Fig. 1A, B). SBFI-AM labeling in the stratum radiatum also included small-sized SR101-negative cells that morphologically resembled astrocytes as judged by the size and shape of their somata and primary processes (Fig. 1A, B). Interestingly, the percentage of SR101-positive cells on the total number of small-sized SBFI-loaded cells with glial morphology changed during postnatal development. At P15 (n=757 cells in 11 slices), roughly 90% of these SBFI-stained cells were also SR101-positive, whereas at P3 (n=2185 cells in 22 slices) only about 50% of them were labeled with SR101 (Fig. 2). Taken together, these results demonstrate that SR101 stains cells with glial morphology in acute tissue slices of the rat hippocampus. Presumptive neurons are completely spared. In addition, we found a clear developmental profile of the staining pattern for SR101. Whereas the SR101-labeling comprised the vast majority of cells with glial morphology in P15 animals, only about half of such cells were stained by SR101 at P3.

### 3. 2. Electrophysiological characterization of SR101-positive and SR101-negative cells

In the CA1 region of the rodent hippocampus, several types of astrocytes were described based on their electrophysiological properties (Bordey and Sontheimer, 2000; D'Ambrosio et al., 1998; Kressin et al., 1995; Steinhauser et al., 1994b; Zhou and Kimelberg, 2001). Moreover, astrocytes undergo considerable changes in channel complement and passive membrane properties during early postnatal development (Bordey and Sontheimer, 1997; Kressin et al., 1995; Zhou et al., 2006). Therefore, we characterized the electrophysiological properties of SR101-positive and SR101-negative cells with glial morphology in the stratum radiatum by performing patch-clamp experiments in the whole-cell configuration. Current injection in the current-clamp mode failed to elicit action potentials in any of the cells investigated (n=107; not shown) indicating that they were indeed glia or glial precursor cells, respectively. Throughout development, SR101-positive and SR101-negative cells differed significantly in their membrane properties. SR101-negative cells (n=13 at P3, n=5 at P15) generally had more depolarized membrane potentials, their membrane resistance was higher and their membrane capacity was lower than that of SR101-positive cells (Table I). We found no differences in these properties between P3 and P15 animals in SR101-negative cells, but observed developmental changes in SR101-positive cells. Whereas the membrane potential of SR101-positive cells was highly negative at all three stages investigated (-80 mV to -87 mV; Table I), their membrane resistance decreased from 94 MΩ at P3 (n=42) to 68 MΩ at P7 (n=6) and finally to 6 MΩ at P15 (n=37). At the same time, membrane capacity increased (from 69 to 120 to 139 pF, respectively; Table I). To reveal the functional expression of voltage-gated ion channels, cells were held in the voltage-clamp mode at -85 mV and then subjected to a rectangular voltage step protocol (from -150 to +50 mV, 10 mV increments). The voltage-step protocol induced large capacitive as well as passive currents (Fig. 3 A-C; insets). Leak subtraction (P/4) was performed to reveal voltage-gated currents activated by membrane depolarization (Fig. 3 A-C; insets; see also Fig. 4). The amplitudes of the leak-subtracted currents were measured at 8-10 ms after the start of the voltage step and current was plotted versus voltage (I/V-relationship, Fig. 3 A-C). Data were fit by a linear regression curve; the threshold for linearity of the I/V relation was set at a regression coefficient of $r^2 = 0.9983$. At P3, both SR101-positive (n=42) and SR101-negative (n=13) cells exhibited voltage-activated outward currents and only non-linear I/V relationships with a variable degree of outward rectification were found ("non-passive cells", nPC; Figs. 3 A, D and 4 A, B). In SR101-positive cells, outward-currents were non-inactivating (Fig. 3A), while in SR101-negative cells, the amplitude of outward currents decreased over time (Fig. 4A). At P7, SR101-positive cells exhibited non-linear I/V relationships with non-inactivating outward currents as well (n=6; Fig. 3B, D), whereas the majority (78%) of SR101-positive cells at P15 (n=38) did not exhibit voltage-gated currents and thus showed a linear I/V relationship ("passive cells", PC; Fig. 3 C, D and 4D). SR101-negative cells at P15 (n=5), in contrast, exclusively showed non-linear properties (Fig. 4C). To further characterize SR101-positive and negative cells, we examined which phenotype functionally expressed voltage-gated fast inward currents. To relieve inactivation of voltage-gated $Na^+$ channels, the voltage step protocol was extended by a hyperpolarizing preconditioning pulse to -120 mV. SR101-positive cells never expressed fast inward currents neither at P3 (n=42; Fig. 4B), nor at P15 (n=37; Fig.4D). In contrast, 4 out of 13 SR101-negative cells at P3 (Fig. 4A) and all SR101-negative cells at P15 (n=5) expressed voltage gated fast inward currents. Taken together, these results demonstrate that small-sized, SBFI-stained cells in the stratum radiatum represent glial cells that can be divided into two subtypes differing in their staining pattern with SR101 as well as in their passive and active membrane properties. At P15, the vast majority of SR101-positive cells show the typical electrophysio-

Table I. Membrane properties of SR101-positive and SR101-negative cells at P3, P7, and P15

| SR101 labeling | Age [pnd] | Membrane potential [mV] | Membrane resistance [MΩ] | Membrane capacity [pF] | n |
|---|---|---|---|---|---|
| SR- | P3 | -67 ± 17 | 353 ± 325 | 30 ± 30 | 13 |
| SR- | P15 | -77 ± 14 | 302 ± 202 | 27 ± 18 | 5 |
| SR+ | P3 | -83 ± 6 | 94 ± 52 | 69 ± 48 | 42 |
| SR+ | P7 | -80 ± 4 | 68 ± 32 | 120 ± 72 | 6 |
| SR+ | P15 | -87 ± 3 | 6 ± 5 | 139 ± 91 | 37 |

Significance levels: **: $\alpha = 0.01$; ***: $\alpha = 0.001$

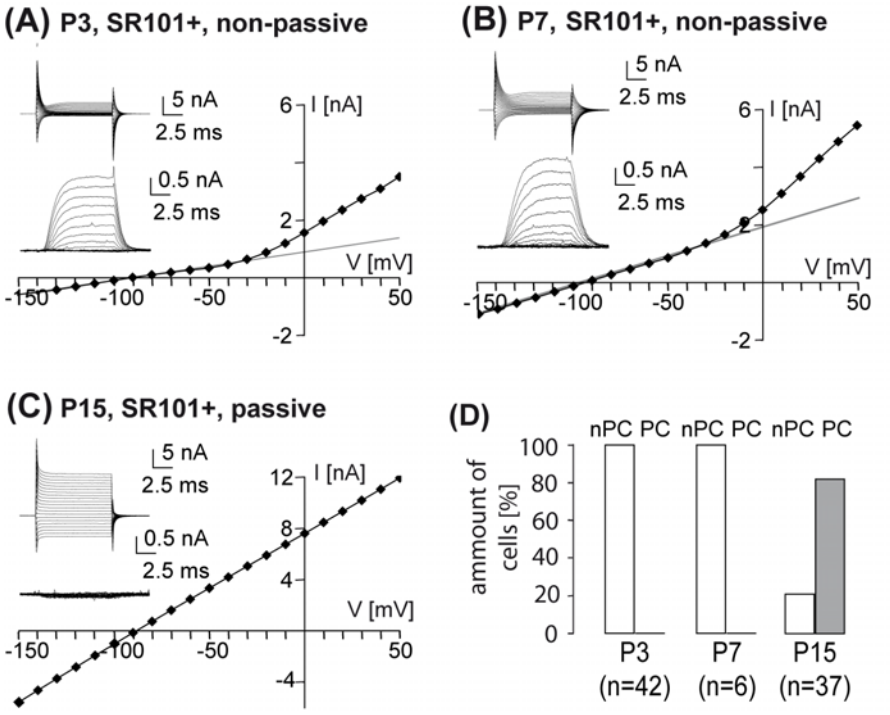


**Fig. 3**. I/V relationship of SR101-positive cells of P3 (A), P7 (B) and P15 (C) rats. Cells were held at -85 mV and subjected to 10 ms voltage steps ranging from –150 mV to +50 mV at 10 mV increments. The insets on the left side show the resulting membrane currents before (top) and after leak subtraction (bottom). The I/V plots depict the amplitudes of the resulting currents at 8-10 ms after the start of the voltage step of the same cells, the grey lines show the linear regression curves. Animals at P3 (A) and P7 (B) exclusively showed non-linear I/V relationships, in P15 animals (C), mostly linear I/V curves were found. (D) Quantification of the amount of cells with non-linear (non-passive cells, nPCs, white bars) or linear (passive cells, PCs, grey bars) I/V curves on the total number of SR101-positive cells at P3, P7 and P15.

logical properties of classical passive astrocytes (Bordey and Sontheimer, 2000; D'Ambrosio et al., 1998; Steinhauser et al., 1992; Zhou et al., 2006).

### 3.3. Immunohistochemical characterization of SR101-positive cells

To further establish the astrocytic identity of SR101-positive glial cells at P15, we immunohistochemically stained for GFAP. To this end, SR101-positive cells were first characterized electrophysiologically and in parallel filled with the fluorescent dye Alexa 488 via the patch pipette to enable their identification in the slices processed for immunohistochemistry. As described above, we found that all SR101-positive cells at P15 exhibited electrophysiological properties of classical astrocytes (n=26). The majority of these cells (n=23/26 cells) were also GFAP-positive, confirming their astrocytic identity (Fig. 5A). Three of 26 investigated SR101-positive cells were, however, GFAP-negative (Fig. 5B), indicating that GFAP only labels a subset of astroglial cells as reported earlier (Lee et al., 2006; Raponi et al., 2007).

### 3.4. ATP-induced $Ca^{2+}$ transients in SR101-stained slices

To validate the described double-staining protocol of SR101 and ion-selective dyes for physiological measurements, we performed dynamic fluorescence imaging in acute hippocampal slices at P15, employing the $Ca^{2+}$-sensitive dye Fura-2-AM (Fig. 6). We tested

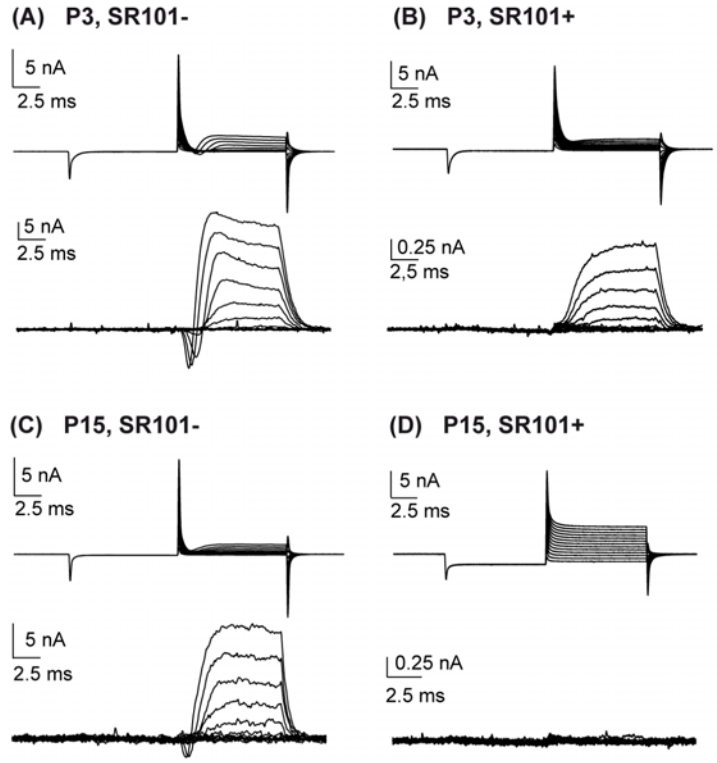


**Fig. 4**. Expression pattern of voltage-gated fast inward currents at P3 (A, B) and P15 (C, D). To relieve inactivation of voltage-gated Na+ channels, cells were held at -85 mV and subjected to a prepulse to -120 mV for 10 ms before stepping from -110 mV to +10 mV in increments of 10 mV. Shown are the resulting currents before (upper traces) and after (lower traces) leak subtraction. At both ages, fast voltage-gated inward currents were only observed in SR 101-negative (A, C), but not in SR101-positive (B, D) cells.

the responses of the cells to a focal pressure application of ATP (10µM, for 100ms), which has been shown to induce intracellular $Ca^{2+}$ transients in glial cells (Verkhratsky et al., 1998). Application of ATP resulted in a transient elevation of intracellular $Ca^{2+}$ concentration in SR101-positive as well as SR101-negative cells (n=6 experiments in 6 slices; Fig. 6). Thus, these measurements confirm that SR101 labeling of acute slices does not interfere with intracellular ion measurements using ion-selective fluorescent dyes (Jourdain et al., 2007; Nimmerjahn et al., 2004).

## 4. Discussion

In the present study, we describe a procedure for double-labeling of acute slice preparations of the early postnatal rat hippocampus with the fluorescent dye SR101 and AM-esters of the ion-selective fluorescent dyes SBFI or Fura-2. SR101 was introduced recently to selectively identify astrocytes in the neocortex of two to four week old rats (Nimmerjahn et al., 2004). It is a red fluorescent dye excited at 575 nm that can be combined with fluorescent dyes excited in the UV range such as Fura-2 or SBFI (this study), or excited at 400-500 nm such as Oregon Green (Nimmerjahn et al., 2004) or Alexa488 (this study, Nimmerjahn et al., 2004). In accordance with the latter study, we did not find any evidence for a distortion of induced intracellular $Ca^{2+}$ transients in cells that were both stained with SR101 and the ion-selective fluorescent dye. Astrocytes in situ are heterogeneous with respect to their physiological properties (D'Ambrosio et al., 1998; Grass et al., 2004; Matthias et al., 2003; Steinhauser et al., 1992; Steinhauser et al., 1994b; Zhou and Kimelberg, 2000, 2001) and undergo considerable changes in channel complement and passive membrane properties during early postnatal development (Bordey and Sontheimer, 1997; Kressin et al., 1995; Zhou et al., 2006). Thus, using whole-cell patch clamp, imaging techniques and immunohistochemistry, we characterized the properties of SR101-positive versus SR101-negative cells in the stratum radiatum at postnatal days 3, 7 and 15. Based on their electrophysiological properties, two basic types of astrocytes have been described in the hippocampus (Bordey and Sontheimer, 2000; D'Ambrosio et al., 1998; Kressin et al., 1995; Steinhauser et al., 1994b; Zhou and Kimelberg, 2001). One cell type, termed "outwardly rectifying" (Zhou and Kimelberg, 2000, 2001) or "complex" (Kressin et al., 1995; Steinhauser et al., 1994b) is mainly characterized by a membrane potential which is significantly more positive than the equilibrium potential for $K^+$, a high input resistance, and a low membrane capacity. Moreover, this cell type functionally expresses two types of $K^+$-outward currents, a delayed rectifier and a transient A-type current, as well as TTX-sensitive $Na^+$ channels. The hallmarks of the second type of astrocytes are a highly negative membrane potential, a low input resistance, and a high membrane capacity. Furthermore these cells lack voltage-gated $Na^+$ currents and show a largely symmetric expression of inward and outward $K^+$ currents that consist predominantly of ohmic currents with small contributions of delayed rectifier $K^+$ currents. Accordingly, this cell type was called "passive" (Kressin et al., 1995; Steinhauser et al., 1994a) or "variably rectifying" (Zhou and Kimelberg, 2000, 2001) astrocyte. In addition, both astrocyte types differ in their expression profile for ionotropic glutamate receptors and glutamate transporters. Whereas

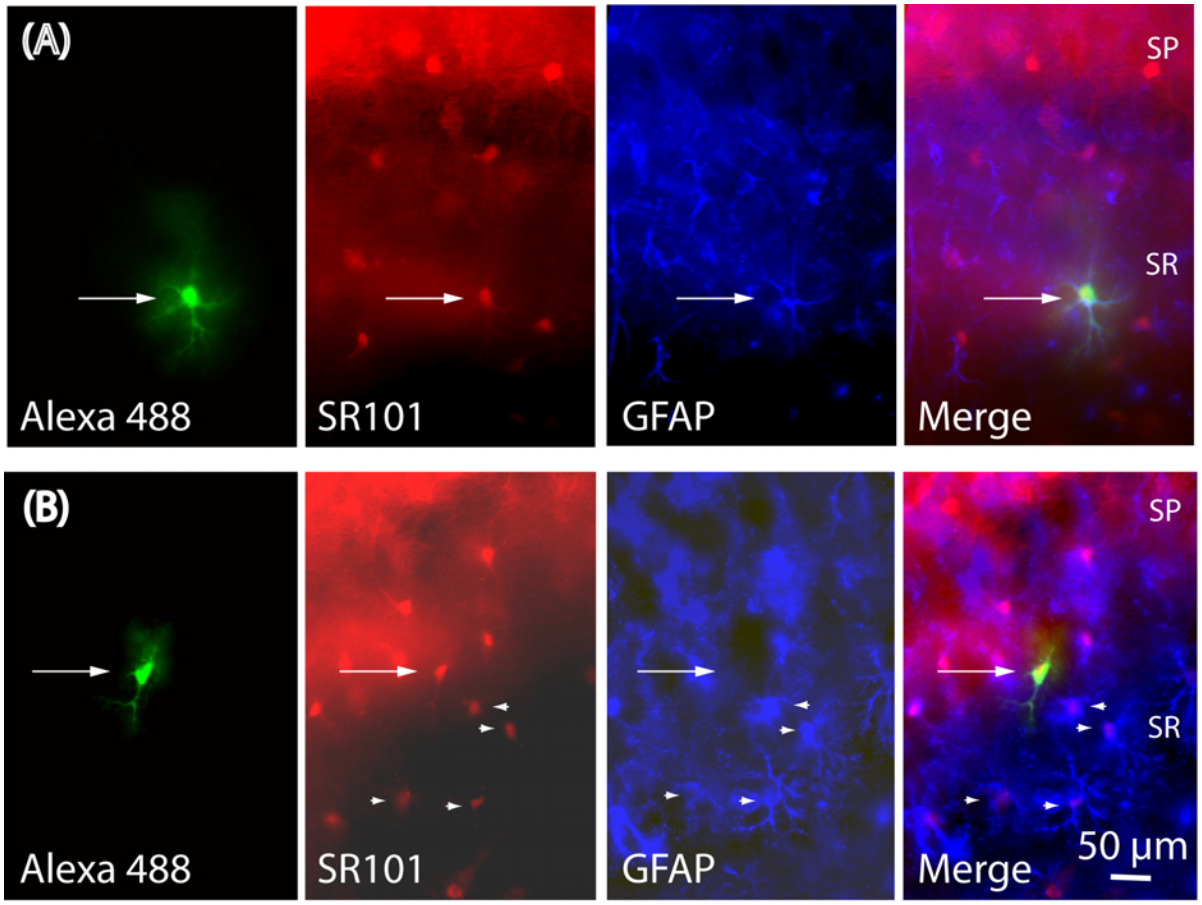


**Fig. 5.** Immunohistochemical characterization of SR101-positive cells at P15. (A) From left to right: Image of the staining pattern of SR101 in the stratum radiatum. Based on this staining, a SR101-positive cell was chosen (arrow) and characterized electrophysiologically while filling the cell with Alexa 488. In the subsequent immunohistochemical analysis, the same cell also showed immunoreactivity for GFAP. The merged picture of all three fluorescence images confirms the identity of the triple-labeled cell. (B) The same experimental design also identified a cell which was SR101-positive, electrophysiologically characterized as glial cell, but showed no immunoreactivity for GFAP (arrow). The arrowheads point to cells, which were double-labeled for SR101 and GFAP. SP: stratum pyramidale; SR: *stratum radiatum*.

the first type expresses ionotropic glutamate receptors and lacks glutamate transporter currents (Matthias et al., 2003; Zhou and Kimelberg, 2001), the second type lacks ionotropic glutamate receptors, but shows significant glutamate uptake currents (Matthias et al., 2003; Zhou and Kimelberg, 2001). Based on these differences, the second type ("passive" or "variably rectifying" astrocyte) is often regarded as the "classical" astrocyte, as it is capable to perform classical functions of astrocytes, such as the uptake of glutamate and potassium from the extracellular space (Matthias et al., 2003; Zhou and Kimelberg, 2001). Our results show that SR101-positive cells during the first two weeks of postnatal development display the electrophysiological properties typical for immature and mature classical astrocytes described above. The developmental profile of current expression of SR101-positive cells is in good agreement with earlier studies showing that the amount of outward rectification in such cells decreases with age (Steinhauser et al., 1992; Wallraff et al., 2004; Zhou et al., 2006). The electrophysiological properties of SR101-negative cells, in contrast, are reminiscent of the first type of astrocytes described above, but may also include a population of glial cells positive for the chondroitin sulphate proteoglycan NG2 and thus, may partly represent glial progenitor cells (Matthias et al., 2003; Zhou et al., 2006). Taken together, our data demonstrate for the first time that SR101, in contrast to conventional fluorescent ion-selective dyes such as Fura-2 or SBFI, selectively labels a subpopulation of glial cells in the early postnatal hippocampus that shows the typical developmental changes and characteristics of classical astrocytes. Staining with SR101 enables a direct and reliable identification of virtually all such astrocytes in acute brain slices for physiological measurements as well as immunohistochemical studies. Owing to its reliability and uncomplicated handling, we expect that this technique will be outstandingly helpful in future investigations studying the functions of astrocytes and neuron-glia interaction in the developing brain.

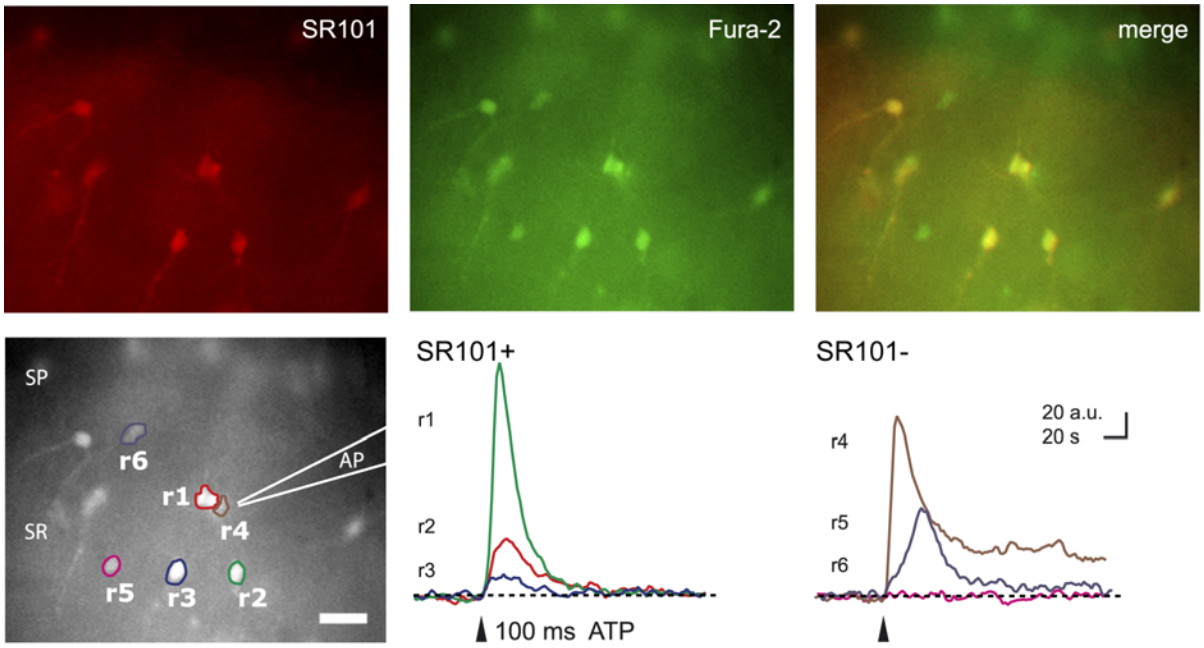


**Fig. 6**. ATP-induced $Ca^{2+}$ transients in SR101-positive and SR101-negative cells at P15. Top, left: Image of the staining pattern of SR101 in the stratum radiatum. Top, center and right: Staining pattern of the $Ca^{2+}$-sensitive dye Fura-2 and merged image. Bottom, left: Image of the Fura-2 fluorescence. The colored lines indicate the regions of interest (r1-r6) in which the $Ca^{2+}$-measurements were performed. The position of the application pipette (AP) is indicated schematically on the right. Bottom, right: Focal pressure application of 10 µM ATP for 100 ms induced $Ca^{2+}$ transients in both SR101-positive (left) and SR101-negative (right) cells. The experiment was performed using a widefield imaging system.

## Acknowledgements

We thank Simone Durry and Claudia Roderigo for expert technical assistance. This study was supported by the DFG.

## References

Araque A, Parpura V, Sanzgiri RP, Haydon PG. Tripartite synapses: glia, the unacknowledged partner. Trends Neurosci, 1999, 22(5):208-215.

Bordey A, Sontheimer H. Postnatal development of ionic currents in rat hippocampal astrocytes in situ. J Neurophysiol, 1997, 78(1):461-477.

Bordey A, Sontheimer H. Ion channel expression by astrocytes in situ: comparison of different CNS regions. Glia, 2000, 30(1):27-38.

D'Ambrosio R, Wenzel J, Schwartzkroin PA, McKhann GM, 2nd, Janigro D. Functional specialization and topographic segregation of hippocampal astrocytes. J Neurosci, 1998, 18(12):4425-4438.

Dallwig R, Deitmer JW. Cell-type specific calcium responses in acute rat hippocampal slices. J Neurosci Methods, 2002, 116(1):77-87.

Danbolt NC. Glutamate uptake. Prog Neurobiol, 2001, 65(1):1-105.

Fiacco TA, Agulhon C, Taves SR, Petravicz J, Casper KB, Dong X, Chen J, McCarthy KD. Selective stimulation of astrocyte calcium in situ does not affect neuronal excitatory synaptic activity. Neuron, 2007, 54(4):611-626.

Grass D, Pawlowski PG, Hirrlinger J, Papadopoulos N, Richter DW, Kirchhoff F, Hulsmann S. Diversity of functional astroglial properties in the respiratory network. J Neurosci, 2004, 24(6):1358-1365.

Haydon PG, Carmignoto G. Astrocyte control of synaptic transmission and neurovascular coupling. Physiol Rev, 2006, 86(3):1009-1031.

Hirrlinger PG, Scheller A, Braun C, Hirrlinger J, Kirchhoff F. Temporal control of gene recombination in astrocytes by transgenic expression of the tamoxifen-inducible DNA recombinase variant CreERT2. Glia, 2006, 54(1):11-20.

Jourdain P, Bergersen LH, Bhaukaurally K, Bezzi P, Santello M, Domercq M, Matute C, Tonello F, Gundersen V, Volterra A. Glutamate exocytosis from astrocytes controls synaptic strength. Nat Neurosci, 2007, 10(3):331-339.

Kafitz KW, Greer CA. Differential expression of extracellular matrix and cell adhesion molecules in the olfactory nerve and glomerular layers of adult rats [published erratum appears in J Neurobiol 1998 Apr;35(1):118]. J Neurobiol, 1998, 34(3):271-282.

Kafitz KW, Guttinger HR, Muller CM. Seasonal changes in astrocytes parallel neuronal plasticity in the song control area HVc of the canary. Glia, 1999, 27(1):88-100.

Kang J, Jiang L, Goldman S, Nedergaard M. Astrocyte-mediated potentiation of inhibitory synaptic transmission. Nature neurosci, 1998, 1:683-692.

Kimelberg HK. The problem of astrocyte identity. Neurochem Int, 2004, 45(2-3):191-202.

Kressin K, Kuprijanova E, Jabs R, Seifert G, Steinhauser C. Developmental regulation of $Na^+$ and $K^+$ conductances in glial cells of mouse hippocampal brain slices. Glia, 1995, 15(2):173-187.

Lee Y, Su M, Messing A, Brenner M. Astrocyte heterogeneity revealed by expression of a GFAP-LacZ transgene. Glia, 2006, 53(7):677-687.

Matthias K, Kirchhoff F, Seifert G, Huttmann K, Matyash M, Kettenmann H, Steinhauser C. Segregated expression of AMPA-type glutamate receptors and glutamate transporters defines distinct astrocyte populations in the

mouse hippocampus. J Neurosci, 2003, 23(5):1750-1758.

Meier SD, Kovalchuk Y, Rose CR. Properties of the new fluorescent $Na^+$ indicator CoroNa Green: comparison with SBFI and confocal $Na^+$ imaging. J Neurosci Methods, 2006, 155(2):251-259.

Metea MR, Newman EA. Glial cells dilate and constrict blood vessels: a mechanism of neurovascular coupling. J Neurosci, 2006, 26(11):2862-2870.

Mulligan SJ, MacVicar BA. Calcium transients in astrocyte endfeet cause cerebrovascular constrictions. Nature, 2004, 431(7005):195-199.

Nedergaard M. Direct signaling from astrocytes to neurons in cultures of mammalian brain cells. Science, 1994, 263(5154):1768-1771.

Newman EA, Volterra A. Glial control of synaptic function. Glia, 2004, 47(3):207-208.

Nimmerjahn A, Kirchhoff F, Kerr JN, Helmchen F. Sulforhodamine 101 as a specific marker of astroglia in the neocortex in vivo. Nat Methods, 2004, 1(1):31-37.

Nolte C, Matyash M, Pivneva T, Schipke CG, Ohlemeyer C, Hanisch UK, Kirchhoff F, Kettenmann H. GFAP promoter-controlled EGFP-expressing transgenic mice: a tool to visualize astrocytes and astrogliosis in living brain tissue. Glia, 2001, 33(1):72-86.

Parri HR, Gould TM, Crunelli V. Spontaneous astrocytic $Ca^{2+}$ oscillations in situ drive NMDAR-mediated neuronal excitation. Nat Neurosci, 2001, 4(8):803-812.

Parri R, Crunelli V. Astrocytes target presynaptic NMDA receptors to give synapses a boost. Nat Neurosci, 2007, 10(3):271-273.

Pascual O, Casper KB, Kubera C, Zhang J, Revilla-Sanchez R, Sul JY, Takano H, Moss SJ, McCarthy K, Haydon PG. Astrocytic purinergic signaling coordinates synaptic networks. Science, 2005, 310(5745):113-116.

Raponi E, Agenes F, Delphin C, Assard N, Baudier J, Legraverend C, Deloulme JC. S100B expression defines a state in which GFAP-expressing cells lose their neural stem cell potential and acquire a more mature developmental stage. Glia, 2007, 55(2):165-177.

Rose CR, Ransom BR. Intracellular $Na^+$ homeostasis in cultured rat hippocampal astrocytes. J Physiol, 1996, 491(2):291-305.

Rose CR, Ransom BR. Gap junctions equalize intracellular $Na^+$ concentration in astrocytes. Glia, 1997, 20:299-307.

Schipke CG, Kettenmann H. Astrocyte responses to neuronal activity. Glia, 2004, 47(3):226-232.

Serrano A, Haddjeri N, Lacaille JC, Robitaille R. GABAergic network activation of glial cells underlies hippocampal heterosynaptic depression. J Neurosci, 2006, 26(20):5370-5382.

Steinhauser C, Berger T, Frotscher M, Kettenmann H. Heterogeneity in the membrane current pattern of identified glial cells in the hippocampal slice. Eur J Neurosci, 1992, 4(6):472-484.

Steinhauser C, Jabs R, Kettenmann H. Properties of GABA and glutamate responses in identified glial cells of the mouse hippocampal slice. Hippocampus, 1994a, 4(1):19-35.

Steinhauser C, Kressin K, Kuprijanova E, Weber M, Seifert G. Properties of voltage-activated $Na^+$ and $K^+$ currents in mouse hippocampal glial cells in situ and after acute isolation from tissue slices. Pflugers Arch, 1994b, 428(5-6):610-620.

Stosiek C, Garaschuk O, Holthoff K, Konnerth A. In vivo two-photon calcium imaging of neuronal networks. Proc Natl Acad Sci U S A, 2003, 100(12):7319-7324.

Takano T, Tian GF, Peng W, Lou N, Libionka W, Han X, Nedergaard M. Astrocyte-mediated control of cerebral blood flow. Nat Neurosci, 2006, 9(2):260-267.

Verkhratsky A, Orkand RK, Kettenmann H. Glial calcium: Homeostasis and signaling function. Physiol Rev, 1998, 78(1):99-141.

Volterra A, Meldolesi J. Astrocytes, from brain glue to communication elements: the revolution continues. Nat Rev Neurosci, 2005, 6(8):626-640.

Wallraff A, Odermatt B, Willecke K, Steinhauser C. Distinct types of astroglial cells in the hippocampus differ in gap junction coupling. Glia, 2004, 48(1):36-43.

Wang X, Lou N, Xu Q, Tian GF, Peng WG, Han X, Kang J, Takano T, Nedergaard M. Astrocytic Ca(2+) signaling evoked by sensory stimulation in vivo. Nat Neurosci, 2006, 9(6):816-823.

Zhou M, Kimelberg HK. Freshly isolated astrocytes from rat hippocampus show two distinct current patterns and different [K(+)](o) uptake capabilities. J Neurophysiol, 2000, 84(6):2746-2757.

Zhou M, Kimelberg HK. Freshly isolated hippocampal CA1 astrocytes comprise two populations differing in glutamate transporter and AMPA receptor expression. J Neurosci, 2001, 21(20):7901-7908.

Zhou M, Schools GP, Kimelberg HK. Development of GLAST(+) astrocytes and NG2(+) glia in rat hippocampus CA1: mature astrocytes are electrophysiologically passive. J Neurophysiol, 2006, 95(1):134-143.

Zhuo L, Sun B, Zhang CL, Fine A, Chiu SY, Messing A. Live astrocytes visualized by green fluorescent protein in transgenic mice. Dev Biol, 1997, 187(1):36-42.

Zonta M, Angulo MC, Gobbo S, Rosengarten B, Hossmann KA, Pozzan T, Carmignoto G. Neuron-to-astrocyte signaling is central to the dynamic control of brain microcirculation. Nat Neurosci, 2003, 6(1):43-50.

## B.3 Bennay et al., J Neurosci, in Revision

### Sodium Signals in Cerebellar Purkinje Neurons and Bergmann Glial Cells Evoked by Glutamatergic Synaptic Transmission

Mustapha Bennay, Silke D. Meier, Karl W. Kafitz, Julia Langer and Christine R. Rose

My contributions:

- combined electrophysiological recordings and $Na^+$ imaging in the presence of TTX (experimental data for figures 2B (partially) and 2C)
- discussion of the manuscript

**Cellular/Molecular**

# Sodium signals in cerebellar Purkinje neurons and Bergmann glial cells evoked by glutamatergic synaptic transmission

**Mustapha Bennay, Silke D. Meier, Karl W. Kafitz, Julia Langer and Christine R. Rose**
Institute for Neurobiology, Geb. 26.02.00, Universitaetsstrasse 1, Heinrich Heine University of Duesseldorf, 40225 Duesseldorf, Germany

**In the brain, the extracellular concentration of glutamate is regulated by specific transporters, termed excitatory amino acid transporters 1-5 (EAAT 1-5). EAATs are electrogenic and mainly use the electrochemical gradient of sodium to transport glutamate into the cells. Glial cells predominantly express EAAT1 (GLAST) and EAAT2 (GLT-1), and play a central role in glutamate clearance by limiting glutamate diffusion. Using combined electrophysiological and quantitative imaging techniques in mouse cerebellar slices, we demonstrate that both exogenous application of glutamate as well as short burst synaptic activity induce sodium transients in the mM range in the processes of cerebellar Bergmann glial cells and Purkinje neurons. Glial sodium transients have rise times of several seconds and persist for tens of seconds. While activation of AMPA receptors accounts for part of the sodium signals in glial cells, the majority of sodium influx is caused by inward transport of glutamate. Sodium transients in dendrites of Purkinje neurons, in contrast, have much faster kinetics and are mainly caused by activation of AMPA receptors. Based on our findings, we present a model which indicates that sodium transients in Bergmann glial cells, in concert with a membrane depolarization and changes in the concentrations of other transported ions, result in a long-lasting reduction of the driving force for glial glutamate uptake at active synapses in the cerebellum. Sodium accumulation upon repetitive activity might thus provide a negative feedback mechanism on glutamate uptake promoting the diffusion of glutamate and the activation of extrasynaptic glutamate receptors.**

*Key words*: **Cerebellum, GLAST, SBFI, glutamate, parallel fiber, neuron-glia interaction**

## 1. Introduction

In the central nervous system, the extracellular concentration of glutamate is regulated by specific transporters that rapidly bind glutamate and move it inside cells. To date, five transporters, termed excitatory amino acid transporters 1-5 (EAAT 1-5), have been cloned. They are electrogenic and are mainly driven by the electrochemical gradient of sodium ($Na^+$) (Nicholls and Attwell, 1990; Anderson and Swanson, 2000; Danbolt, 2001; Maragakis and Rothstein, 2001; Schousboe, 2003). Glial cells predominantly express EAAT1 (GLAST) and EAAT2 (GLT-1). Their activation results in a fast decline of glutamate concentration in the synaptic cleft and shapes the time course of synaptic conductance (Barbour et al., 1994; Takahashi et al., 1995; Rothstein et al., 1996; Oliet et al., 2001; Bordey and Sontheimer, 2003; Takayasu et al., 2005). Furthermore, glial glutamate uptake moderates the activation of extrasynaptic receptors and limits spillover of glutamate to adjacent synapses (Asztely et al., 1997; Rusakov et al., 1999; Knopfel et al., 2000; Chen and Diamond, 2002; Clark and Cull-Candy, 2002; Huang and Bergles, 2004; Marcaggi and Attwell, 2004).

Bergmann glial cells of the cerebellum are specialized astrocytes. Their processes tightly enclose synapses of climbing and parallel fibers onto Purkinje cells and form microdomains that are virtually uncoupled from the rest of the cell (Grosche et al., 1999; Ito, 2000; Grosche et al., 2002). Bergmann cells express both a-amino-3-hydroxy-5-methyl-4-isoxazolepropionate (AMPA) receptors and glutamate transporters (GLAST, GLT-1; Danbolt, 2001). GLAST-deficient knockout mice suffer from impaired motor coordination, abnormal climbing fiber innervation and increased susceptibility to cerebellar injury (Watase et al., 1998 ), illustrating the vital role of glial glutamate uptake for cerebellar function.

Stimulation of glutamatergic inputs to Purkinje neurons evokes inward currents in adjacent Bergmann cells that result from activation of AMPA receptors and uptake of glutamate (e. g. Bergles and Jahr, 1997; Linden, 1997; Grosche et al., 1999; Kulik et al., 1999; Matyash et al., 2001; Bordey and Sontheimer, 2003; Bellamy and Ogden, 2005). Because both mechanisms involve inward movement of sodium, excitatory synaptic activity will be accompanied by $Na^+$ influx into Bergmann glia (Kirischuk et al. 2007). Furthermore, in hippocampal and cortical astrocytes, exogenous application of glutamate results in intracellular $Na^+$ transients (Rose and Ransom, 1996; Chatton et al., 2000; Magistretti and Chatton, 2005). An increased intracellular $Na^+$ concentration decreases the driving force for glutamate transport and might thus result in reduced uptake.

So far, no detailed description and analysis of activity-induced $Na^+$ transients in the processes of Bergmann glial cells has been performed. Therefore, we have performed quantitative $Na^+$ measurements in Bergmann glial cells and Purkinje neurons of acute cerebellar slices of the mouse. Our experiments demonstrate that application of glutamate as well as bursts of synaptic activity induce long-lasting $Na^+$ transients in the processes of Bergmann glial cells, which are mainly caused by the influx of $Na^+$ associated with glutamate uptake. $Na^+$ transients can reach several mM following short burst stimulation, suggesting that they provide a negative feedback on glutamate uptake by reducing its driving force at active synapses in the cerebellum.

## 2. Materials and Methods

*Tissue preparation and patch clamp recordings:* Experiments were carried out on acute tissue slices (300 µm) of mouse cerebellum (postnatal day 11-15) as described earlier (Barski et al., 2003). Animals were decapitated following anesthesia with $CO_2$ and the cerebella were rapidly removed. After sectioning, slices were kept in physiological saline composed of (in mM): 125 NaCl, 2.5 KCl, 2 $CaCl_2$, 1 $MgCl_2$, 1.25 $NaH_2PO_4$, 26 $NaHCO_3$ and 20 glucose, bubbled with 95% $O_2$ and 5% $CO_2$ until they were used for experiments. Experiments were performed at room temperature (22-24 ℃). When synaptic stimulation was performed, the slices were continuously perfused with saline containing 20 µM bicuculline methiodide to block transmission by GABAA receptors. All chemicals were purchased from Sigma, except for tetrodotoxin (purchased at Alomone Labs, Jerusalem, Israel and at Biotrend Chemicals, Cologne, Germany) and TBOA (threo-ß-benzyloxyaspartate; Tocris/BIOZOL Diagnostica Vertrieb GmbH, Eching, Germany).

Somatic whole-cell recordings were obtained with an EPC10 amplifier (HEKA Elektronik, Lambrecht, Germany); "PatchMaster"-software (HEKA Elektronik, Lambrecht, Germany) was used for data acquisition. The pipette solution contained (in mM): 148 potassium gluconate, 6 KCl, 10 HEPES (N-(2-Hydroxyethyl)piperazine-N'-(2-ethanesulfonic acid), 8 NaCl, 0.5 MgCl2, 4 Mg-ATP and 0.4 Na3-GTP, pH 7.3. Bergmann glial cells were generally held at membrane potentials of -80 mV, holding potential of Purkinje neurons was -70 mV; liquid junction potential was not corrected. For $Na^+$-imaging experiments, 1 or 2 mM SBFI (sodium-binding benzofuran isophthalate; Molecular Probes/Invitrogen, Karlsruhe, Germany) was added to the pipette solution. Glutamate, AMPA (α-amino-3-hydroxy-5-methyl-4-isoxazolepropionate), NMDA (N-methyl-d-aspartate) or D-aspartate were applied by a pressure application device (PDES-02D, NPI Electronic GmbH, Tamm, Germany) coupled to standard micropipettes (Hilgenberg, Waldkappel, Germany) placed at a distance of approximately 10-20 µm to a visible cellular process. All other drugs were applied with the bath perfusion.

Electrical stimulation of parallel fibers (PF) was performed by square pulses (150 µs duration) delivered at 50 Hz via a thin borosilicate glass pipette (Hilgenberg, Waldkappel, Germany) filled with saline which was placed in the molecular layer. For stimulation of climbing fibers (CF), the stimulation pipette was placed in the granular cell layer. The stimulus pulse amplitude was 20-50 V for PF stimulation and 50-90 V for CF stimulation.

*$Na^+$ imaging:* Conventional, wide-field fluorescence imaging was performed using a variable scan digital imaging system (TILL Photonics, Martinsried, Germany) attached to an upright microscope (Olympus BX51Wi, 60x water immersion objective, N.A. 0.90, Olympus Europe, Hamburg, Germany) and a CCD camera as sensor (TILL Imago VGA, TILL Photonics, Martinsried, Germany). Cells were loaded with the sodium-sensitive fluorescent dye SBFI via the patch-pipette. To ensure sufficient diffusion of the dye into distal branches, cells were filled with SBFI for at least 30 min before starting the recordings. In some experiments, cells were dye-loaded by bath application of the membrane permeable form of SBFI (SBFI-AM). For wide-field imaging with SBFI, background-corrected fluorescence signals (>410 nm) were collected from defined regions of interest after alternate excitation at 345 nm and at 385 nm, and the fluorescence ratio (F345/F385 nm) was calculated. Images were acquired at 2-5 Hz and analyzed off-line. Imaging and electrophysiological data were processed and analyzed by employing OriginPro (OriginLab Corporation, Northhampton, MA) or IGOR Pro Software (WaveMetrics, Inc., Lake Owego, OR).

In situ calibration of SBFI fluorescence in Bergmann glial cells and Purkinje neurons was performed as described earlier (Meier et al., 2006). In brief, cells were first loaded with SBFI via a patch pipette and then the pipette was carefully removed. Subsequently, slices were perfused with calibration solutions containing different concentrations of $Na^+$ and ionophores (gramicidin, monensin) to equilibrate extra- and intracellular sodium while recording the fluorescence emission of SBFI (Bergmann glia: n=8; Purkinje Neurons: n=4; Suppl. Fig. 1).

Unless otherwise specified, data are expressed as means ± s.e.m.. Data were statistically analyzed by a one-way-analysis of variance (Bonferroni-post-hoc test; significance level, $p<0.01$)

## 3. Results

### $Na^+$ transients induced by glutamate and glutamate agonists

In the cerebellum, synaptically released glutamate activates Purkinje neurons and adjacent Bergmann glial cells by binding to glutamate receptors and sodium-dependent glutamate transporters. Because both involve $Na^+$ influx, we first studied the effect of an exogenous application of glutamate or glutamate agonists on the intracellular $Na^+$ concentration of Purkinje neurons and Bergmann glia loaded with the sodium indicator dye SBFI. In parallel to the imaging of $Na^+$ transients in the cellular somata and/or processes, membrane currents were recorded at the cell bodies.

In Purkinje neurons, a focal pressure-application of glutamate (1 mM, 200 ms) in the presence of the $Na^+$ channel blocker tetrodotoxin (TTX; 0.5 µM) resulted in an inward current of -2.1±0.6 nA. This inward current was accompanied by an increase in the intracellular $Na^+$ concentration by 5.9±3.1 mM in cellular regions located in the vicinity of the application pipette (n=4; Fig. 1A).

Application of glutamate also caused inward currents and $Na^+$ transients in Bergmann glial cells (n=31; Fig. 1B). As observed for Purkinje neurons, Glutamate-evoked $Na^+$ transients in Bergmann glial cells were largest in processes close to the application pipette (Fig. 2A). Their maximal amplitude was linearly dependent on the peak current amplitude (n=5; Fig. 2B). On average, glutamate induced a maximal $Na^+$ increase of 2.4±0.3 mM, accompanied by a peak current of -125±3.6 pA. Glutamate-induced $Na^+$ transients and inward currents in Bergmann glial cells were not altered by TTX (0.5 µM; n=5; Fig. 2C), indicating that

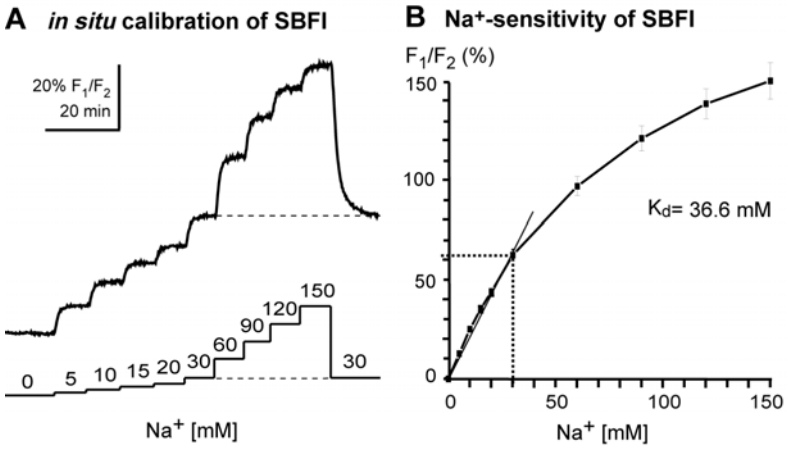


**Supplementary Figure 1.** In situ calibration of the sensitivity of SBFI to changes in $[Na^+]$ in Bergmann glial cells. **A**, In cells loaded with SBFI and perfused with a calibration cocktail containing 3 mM gramicidin D,10 mM monensin, and 100 mM ouabain to equilibrate extra- and intracellular sodium concentrations, stepwise changes in the extracellular Na+ concentration from 0 to 150 mM and back to 30 mM caused stepwise changes in the fluorescence ratio of SBFI (F1=345 nm/ F2=385 nm). **B,** Relationship between changes in fluorescence ratio and $[Na^+]_i$. Shown are mean values and S.E. (n=8). The curve reveals a nearly linear relationship between 0 and 30 mM sodium. Within this range, a 10% change in fluorescence emission corresponds to a change of about 4.8 mM sodium. The $K_d$ of about 37 mM was determined from a Lineweaver-Burk plot.

they were not induced by neuronal activity and transmitter release, but by direct action of glutamate onto Bergmann glial cells.

Bergmann glial cells predominately express ionotropic a-amino-3-hydroxy-5-methyl-4-isoxazolepropionate (AMPA) receptors; some studies reported the expression of ionotropic N-methyl-D-aspartate (NMDA) receptors (Verkhratsky et al., 1998; Verkhratsky and Steinhäuser, 2000). To analyze the effect of an activation of non-NMDA receptor channels, we locally applied AMPA (50 µM) for 100-3000 ms to Bergmann glial cells in the presence of TTX. AMPA application induced an inward current (Fig. 3A) that was completely and reversibly blocked by the AMPA receptor antagonist 6-cyano-7-nitroquinoxaline-2,3-dione (CNQX, 5 µM; n=9, not shown), confirming the presence of these receptors in Bergmann glial cells. Glutamate-evoked $Na^+$ transients in Bergmann glial cells were largest in processes close to the application pipette (Fig. 2A). Surprisingly, despite considerable AMPA-induced somatic inward currents, only small increases in $Na^+$ were detected, followed by a longer lasting decrease in the $Na^+$ concentration below baseline (n=10; Fig. 3A). This delayed $Na^+$ decrease might have been caused by reversed operation of $Na^+/Ca^{2+}$ exchange, and $Na^+$ export, following large AMPA-induced calcium influx (Kirischuk et al., 1997).

In contrast to AMPA, application of NMDA (1 mM) for 500-2000 ms failed to induce inward currents and $Na^+$ signals in Bergmann glial cells in the presence of TTX (n=7, Fig. 3B). This was observed both in regular saline at holding potentials between -85 and -20 mV and in $Mg^{2+}$ free saline, in which the voltage-dependent $Mg^{2+}$ block of NMDA receptor channels was relieved (n=7; not shown). These results are in line with other studies in which no evidence for a contribution of NMDA receptor activation to glutamate-induced signals in Bergmann glial cells was found (e.g. Kirischuk et al., 1999).

To study the effect of a selective activation of glutamate transport on the intracellular $Na^+$ concentration in Bergmann glial cells, D-aspartate, a competitive inhibitor of glutamate uptake, was applied in the presence of TTX. Because D-aspartate is also transported (Danbolt, 2001), this is expected to result in $Na^+$ transients and inward currents if functional transporters are expressed (Rose and Ransom, 1996; Chatton et al., 2001). Indeed, D-aspartate (1 mM, 200-500 ms) induced both a $Na^+$ signal and a somatic current (n=18; Fig. 3C) in Bergmann glial cells. D-aspartate-induced glial $Na^+$ signals were reduced by 70±3% in the presence of 200 µM threo-ß-benzyloxyaspartate (TBOA), which is a non-transported blocker of glutamate uptake, confirming that they were predominately induced by activation of glutamate uptake (n=6; not illustrated).

## Synaptically-induced $Na^+$ transients in Purkinje neurons

Each Purkinje cell receives local glutamatergic inputs from more than 100000 granule cells via their axons, the parallel fibers (Ito, 2000). Purkinje neurons respond to activation of parallel fibers by graded electrophysiological responses and localized dendritic $Ca^{2+}$ transients (Eilers et al., 1995a; Barski et al., 2003). A second powerful glutamatergic input derives from the inferior olive and is represented by the climbing fiber, that makes some 10.000's of synapses to a single Purkinje neuron. Climbing fiber activation results in a standard all-or-none electrical response, the so-called "complex spike", which results in a global dendritic calcium increase in Purkinje neurons (Eilers et al., 1995b). In addition, stimulation of parallel and climbing fibers activates AMPA receptors and uptake of glutamate in adjacent Bergmann glial cells (e. g. Bergles and Jahr, 1997; Linden, 1997; Grosche et al., 1999; Kulik et al., 1999; Matyash et al., 2001; Bordey and Sontheimer, 2003; Bellamy and Ogden, 2005).

To study synaptically-induced intracellular $Na^+$ transients, parallel fiber inputs were stimulated by current injection at 50 Hz for 100 ms (20-50 V) through a fine micropipette, which was positioned in the molecular layer above visible cellular processes of SBFI-filled cells. As reported previously (Lasser-Ross and Ross, 1992; Callaway and Ross, 1997; Kuruma et al., 2003), synaptic activity caused an inward current (peak am-

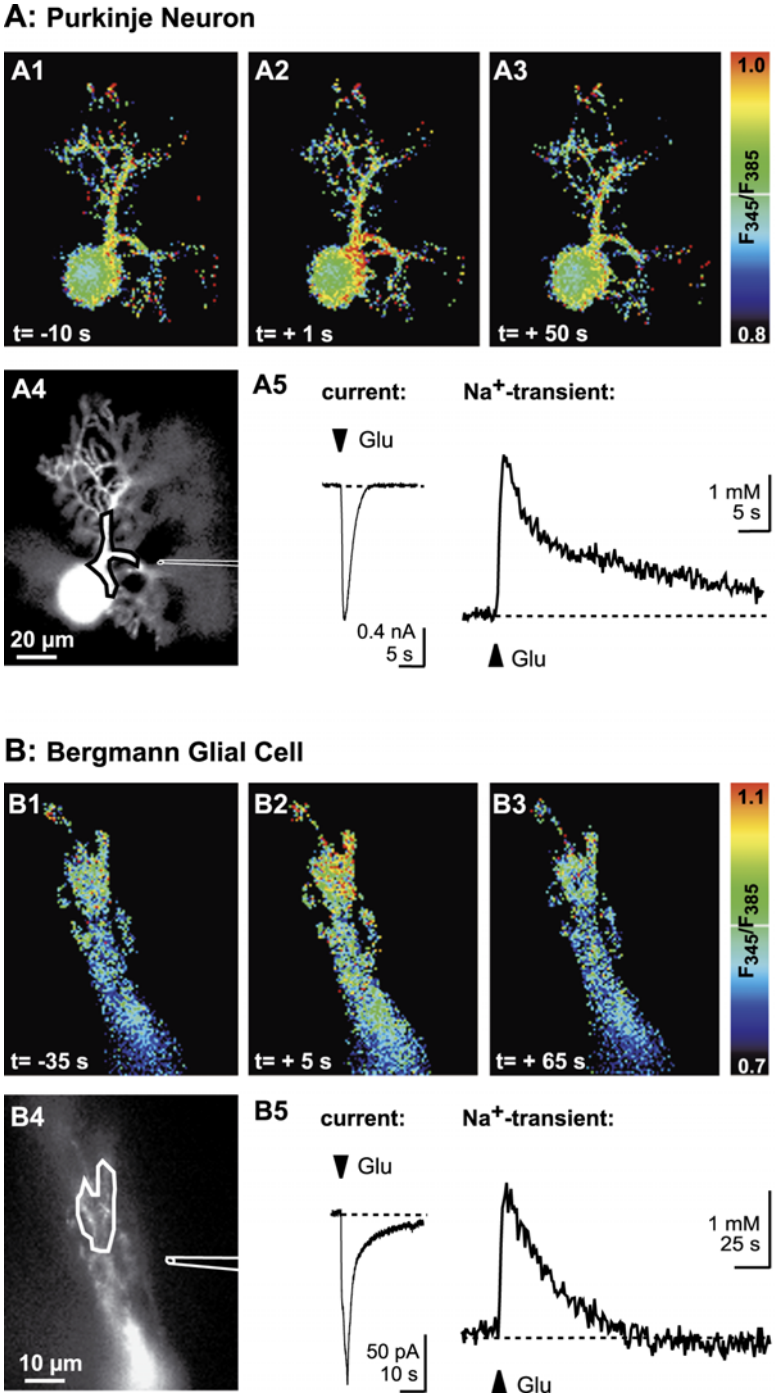


**Figure 1.** $Na^+$ transients induced by focal pressure application of glutamate. **A**, Purkinje neuron. **A1-A3**, Color-coded images of the ratio of SBFI fluorescence emission (345/385 nm), averaged from 3 consecutive images. Red indicates high, blue indicates low intracellular $Na^+$ concentration. At t=0 s, glutamate (1 mM) was applied for 200 ms; flow of perfusion was from bottom to top. **A4**, Image of the fluorescence emission of SBFI at 385 nm excitation. The application pipette is schematically shown on the right. The black line indicates the area in which the $Na^+$ measurement was performed. **A5**, Somatic current and $Na^+$ transient induced by the glutamate application. **B**, Bergmann glial cell. **B1-B3**, Color-coded images of the SBFI ratio as above. At t=0 s, glutamate (1 mM) was applied for 3 s; flow of perfusion was from bottom to top. **B4**, Image of the fluorescence emission of SBFI at 385 nm excitation. The application pipette is schematically shown on the right. The white line indicates the area in which the $Na^+$ measurement was performed. **B5**, Somatic current and $Na^+$ transient induced by the glutamate application.

plitude -1.8±0.2 nA) and dendritic $Na^+$ transients in Purkinje neurons (n=14; Fig. 4A). Glutamate-evoked $Na^+$ transients in Bergmann glial cells were largest in processes close to the application pipette (Fig. 2A). In accordance with these earlier studies, the rise time of dendritic $Na^+$ transients was less than a second (Fig. 4D). Based on our in situ calibration of SBFI fluorescence, we found that the amplitude of dendritic $Na^+$ transients induced by the synaptic stimulation protocol was 1.5±0.2 mM. $Na^+$ transients decayed with a monoexponential time course and a decay time constant of 13.1 s (n=5, Fig. 4D).

As expected (Callaway and Ross, 1997; Kuruma et al., 2003), $Na^+$ transients in Purkinje cell dendrites induced by short burst stimulation of parallel fibers were largely blocked by CNQX (10 µM), confirming that they are mainly caused by $Na^+$ influx through postsynaptic AMPA channels (n=9; Fig. 4B,C). The small CNQX-resistant currents and $Na^+$ transients (Fig. 4B,C) might reflect activation of metabotropic glutamate receptors (Knopfel et al., 2000) or postsynaptic uptake of glutamate (Otis et al., 1997; Brasnjo and Otis, 2001, 2004).

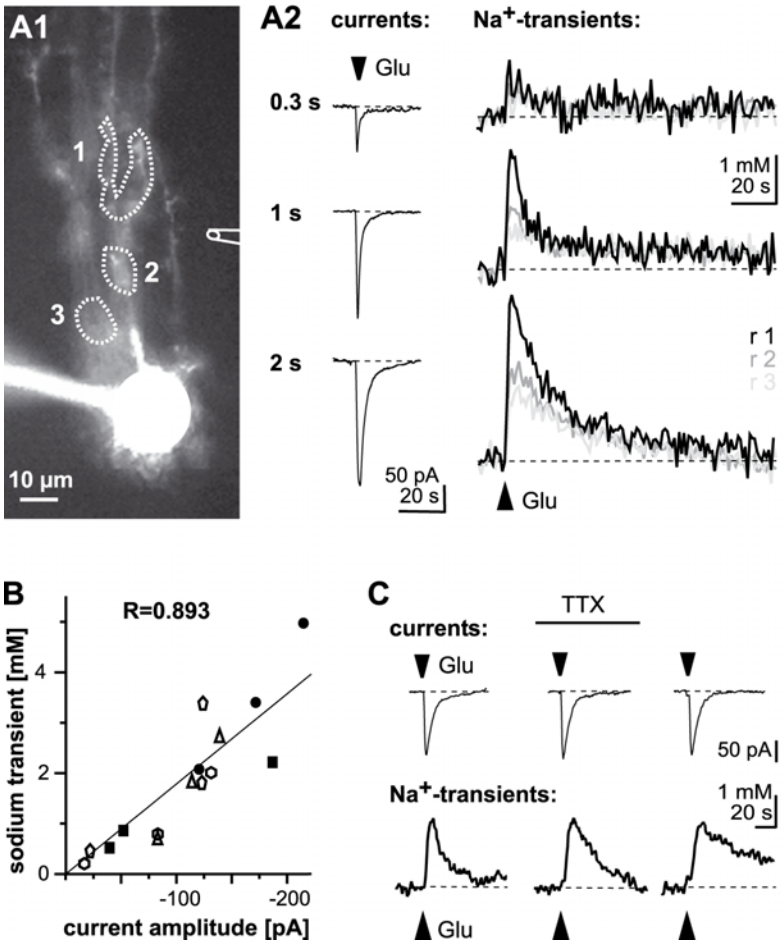


**Figure 2.** Glutamate-induced $Na^+$ transients in Bergmann glial cells. **A1**, Image of the fluorescence emission of a Bergmann glial cell excited at 385 nm. The application pipette is schematically shown on the right, flow of perfusion was from bottom to top. The patch pipette attached to the cell body can be seen on the lower left. The white dashed lines indicate the areas of interest which were analyzed. **A2**, somatic currents and $Na^+$ signals in the regions depicted in A1 following application of glutamate (1 mM) for 0.3, 1, and 2 s. **B**, Glutamate-evoked $Na^+$ increases plotted versus corresponding peak current amplitudes. Data points are from six different cells as indicated by the six different symbols. The straight line represents a linear fit (correlation coefficient R=0.893). C, Glutamate-induced inward currents and $Na^+$ transients in the absence and presence of TTX (tetrodotoxin, 0.5 µM)

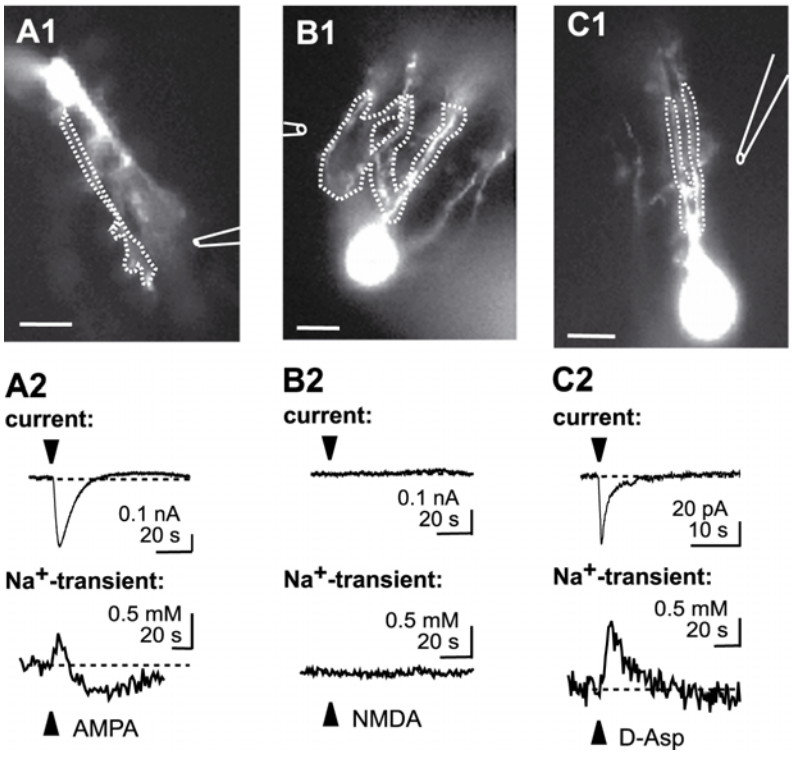


**Figure 3.** $Na^+$ transients evoked by glutamate agonists in Bergmann glial cells. **A**, Effect of AMPA. A1, B1, C1, Image of the fluorescence emission of the recorded Bergmann glial cell excited at 385 nm. The application pipette is schematically shown on the right. The white dashed line indicates the area of interest which was analyzed. A2, Local application of AMPA (50 µM, 3 s) induced an inward current that was accompanied by a biphasic $Na^+$ signal. **B**, Effect of NMDA. B2, Local application of NMDA (1 mM, 2 s) did not result in an inward current, nor in a $Na^+$ signal. **C**, Effect of D-aspartate. C2, Local application of D-aspartate (1 mM, 0.5 s) induced both a somatic inward current and a Na+ signal. All experiments were performed in the presence of 0.5 µM TTX to prevent neuronal action potentials. Scale bars are 10 µm.

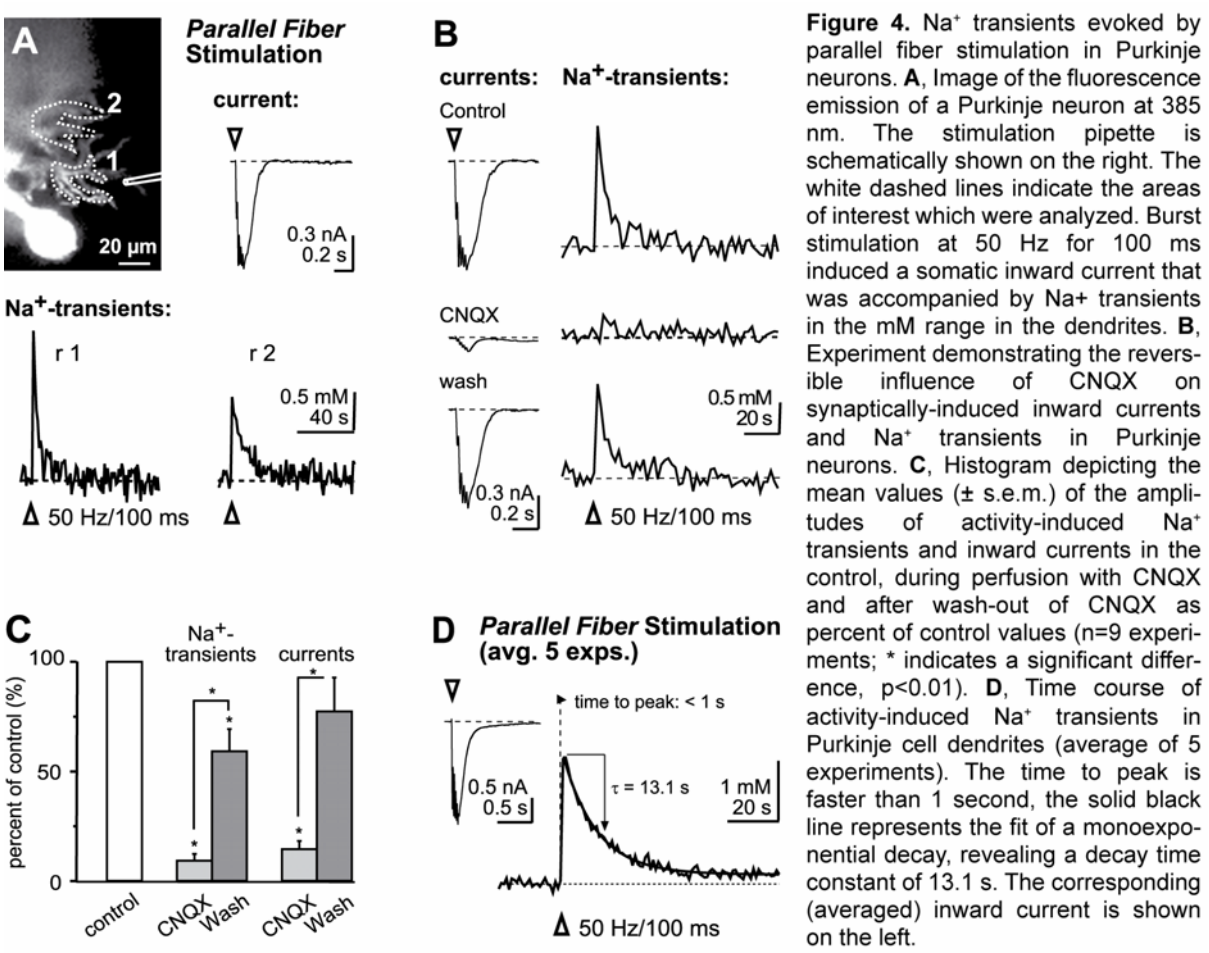


**Figure 4.** $Na^+$ transients evoked by parallel fiber stimulation in Purkinje neurons. **A**, Image of the fluorescence emission of a Purkinje neuron at 385 nm. The stimulation pipette is schematically shown on the right. The white dashed lines indicate the areas of interest which were analyzed. Burst stimulation at 50 Hz for 100 ms induced a somatic inward current that was accompanied by Na+ transients in the mM range in the dendrites. **B**, Experiment demonstrating the reversible influence of CNQX on synaptically-induced inward currents and $Na^+$ transients in Purkinje neurons. **C**, Histogram depicting the mean values (± s.e.m.) of the amplitudes of activity-induced $Na^+$ transients and inward currents in the control, during perfusion with CNQX and after wash-out of CNQX as percent of control values (n=9 experiments; * indicates a significant difference, $p<0.01$). **D**, Time course of activity-induced $Na^+$ transients in Purkinje cell dendrites (average of 5 experiments). The time to peak is faster than 1 second, the solid black line represents the fit of a monoexponential decay, revealing a decay time constant of 13.1 s. The corresponding (averaged) inward current is shown on the left.

### Synaptically-induced $Na^+$ transients in Bergmann glial cells

As described above for measurements in Purkinje neurons, parallel fiber inputs were stimulated by current injection through a micropipette positioned in the molecular layer above visible cellular processes of an SBFI-filled Bergmann glial cell. Because of increased scattering of the fluorescence signals from Bergmann glia processes with increasing depth, $Na^+$ measurements were usually restricted to a main process located near the surface of the slice.

Short burst stimulation of parallel fibers (50 Hz/100 ms) induced a somatic inward current with a characteristic biphasic decay time course as described earlier (Figs. 5A,C; 6A; Bergles et al., 1997; Clark and Barbour, 1997). Glutamate-evoked $Na^+$ transients in Bergmann glial cells were largest in processes close to the application pipette (Fig. 2A). Stimulation-induced inward currents were accompanied by clearly detectable, long lasting $Na^+$ transients (Figs. 5A,C; 6A). Both glial currents and $Na^+$ transients were absent during perfusion with TTX, confirming their synaptic origin (n=4; not shown). Increasing the stimulus intensity to raise the number of activated parallel fibers increased the amplitude of inward currents and $Na^+$ transients (n=9; Fig. 5A,B). For each of the experiments described in the following, the stimulation intensity was increased stepwise from 20 to up to 50V until maximal $Na^+$ signals were obtained in the analyzed process. These maximal $Na^+$ signals were associated with average somatic inward currents of 430±34 pA (n=36).

The peak amplitude of glial $Na^+$ signals ranged from about 0.5 mM to up to 9 mM (mean 2.7±0.3; n=36). The kinetics of these signals varied between different cells. Basically, two time courses, as well as intermediates between these two, were found. $Na^+$ increases of less than 2 mM (20 out of 36 cells; e. g. Fig. 8A) were usually characterized by rise times of 10 to more than 30 seconds and a broad peak ("slow $Na^+$ transients"). Moreover, the decay to baseline could not be fitted by a monoexponential decay time course (Fig. 5C). In contrast, $Na^+$ increases of more than 4 mM, detected in 9 out of 36 cells (mean 5.6±0.6 mM; e. g. Fig. 6A), had an average rise time of several seconds, a clearly defined peak and a strictly monoexponential decay to baseline with a time constant of about 90 seconds (Fig. 5C; "fast $Na^+$ transients").

These differences in kinetics were not only found when comparing different cells, but were also observed within a given cell when several main processes could be analyzed in parallel (n=10). Fig. 6A illustrates such a cell. Glutamate-evoked $Na^+$ transients in Bergmann glial cells were largest in processes close to the application pipette (Fig. 2A). The $Na^+$ signal was largest in the process that was located closest to the stimula-

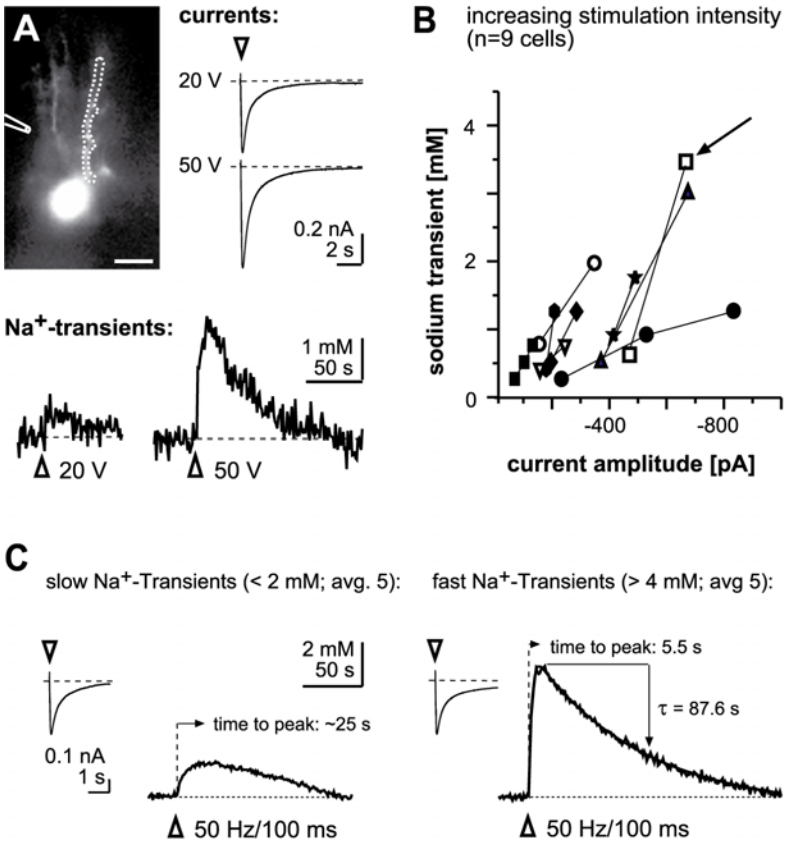


**Figure 5**. $Na^+$ transients evoked by parallel fibers stimulation in Bergmann glial cells. **A**, Image of the fluorescence emission of a Bergmann glial cell excited at 385 nm (Scale bar: 10 µm). The stimulation pipette is schematically shown on the left. The white dashed line indicates the area of interest which was analyzed. Parallel fibers stimulation (50 Hz/100 ms) induced somatic inward currents and Na+ signals in the main cellular processes. Increasing the stimulus intensity from 20V to 50V caused an increase in the amplitude of the resulting inward current, as well as an increase in the accompanying $Na^+$ transient. **B**, Plot showing the relationship between current amplitude and amplitude of the corresponding $Na^+$ transient obtained from 9 cells (indicated by the 9 different symbols) at different stimulation intensities. Data points from individual cells are connected. **C**, Left: Average of $Na^+$ transients smaller than 2 mM, taken from arbitrarily chosen cells. The rise time of this signal is about 25 s, the peak duration in the range of 20-30 seconds and the decay can not be fitted by a monoexponential decay time course. Right: Average of activity-induced $Na^+$ transients larger than 4 mM, taken from 5 different experiments. The solid black line represents the fit of a monoexponential decay, revealing a decay time constant of 87.6 s. The corresponding (averaged) inward current is shown on the left.

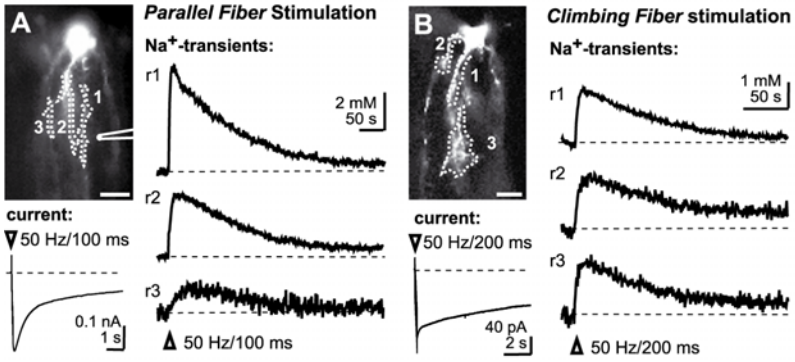


**Figure 6.** $Na^+$ transients in different processes during parallel versus climbing fibers stimulation. **A**, $Na^+$ signals following parallel fibers stimulation (50 Hz, 100 ms) were largest in processes that were located close to the stimulation pipette (r1 and r2). Note the change in kinetics of the $Na^+$ transients with increasing distance from the stimulation pipette. **B**, $Na^+$ transients following stimulation of climbing fibers (50 Hz, 200 ms) were not localized, but had comparable time courses and kinetics in different processes of a Bergmann glial cell (r1-r3). Scale bars are 10 µm.

tion pipette (region1). The maximal $Na^+$ transient was characterized by a fast rise time, defined peak and a monoexponential decay to baseline. In the process located furthest away from the stimulation pipette (region3), the amplitude of the $Na^+$ transient was much smaller and only reached many seconds later; furthermore this $Na^+$ signal was characterized by a markedly broadened peak. In the process located in between (region2), an intermediate time course and amplitude was detected. Based on these observations, we assume that processes, in which we detected $Na^+$ signals with a relatively fast rise time, a defined peak and a monoexponential decay to baseline in response to parallel fibers stimulation, were the site of main synaptic input and direct $Na^+$ influx.

In contrast to parallel fibers stimulation, burst stimulation of climbing fibers (50 Hz, 100-200 ms), resulted in global intracellular $Na^+$ transients with similar kinetics, amplitude and time course throughout the entire tree of processes of Bergmann glial cells (n=3, Fig. 6B). Thus, the spatial distribution of $Na^+$ transients induced by stimulation of the two different inputs, parallel and climbing fibers, followed the profile expected from measurements of calcium transients in the dendritic tree of Purkinje neurons (Eilers et al., 1995a; Eilers et al., 1995b).

To determine the membrane potential changes induced by the synaptic stimulation protocol, we performed experiments in which we first held the cells in the voltage-clamp mode and then switched to the current-clamp mode. The burst stimulation protocol resulted in an average inward current of -430±67 pA as

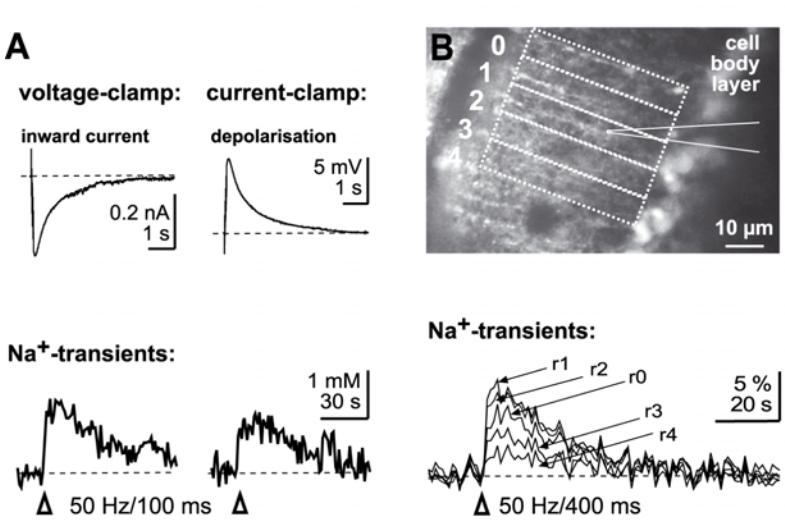


**Figure 7**. Synaptically-induced changes in membrane potential and spatial extend of glial $Na^+$ signals in the molecular layer. **A**, Switching from voltage-clamp into the current-clamp mode revealed that the burst stimulation of parallel fibers (50 Hz/100 ms) generated a membrane depolarisation by about 12 mV. The respective $Na^+$ transients are shown below. **B**, Top: Image of SBFI fluorescence (385 nm) of the cerebellar cortex after bath incubation with the dye. A band of Bergmann glial cell bodies is visible on the right, as well as numerous fine parallel processes that extend to the pia on the left. The stimulation pipette is schematically shown, as well as 5 rectangular areas (0-4) that indicate the regions of interest in which the fluorescence signals were analyzed. Bottom: Change in the fluorescence ratio of SBFI in the different regions (r0-r4) evoked by a burst stimulation (50 Hz/400 ms) of parallel fibers.

measured in the voltage-clamp mode, and a membrane depolarization of 11.8±2.3 mV when cells were held in the current-clamp mode (n=6, Fig. 7A). Glutamate-evoked $Na^+$ transients in Bergmann glial cells were largest in processes close to the application pipette (Fig. 2A). The amplitude of $Na^+$ transients was reduced by 22±11% in the current-clamp as compared to the voltage-clamp mode (Fig. 7A), indicating that the depolarization decreased the activity of electrogenic glutamate uptake.

$Na^+$ transients following stimulation of parallel fibers were not restricted to single cells. In slices loaded with the membrane permeable form of SBFI to stain a large population of cells, stimulus-induced $Na^+$ transients were observed in the processes of several Bergmann glial cells located to the left and to the right of the stimulation pipette (n=6; Fig. 7B). The amplitude of these $Na^+$ transients decreased with increasing distance from the stimulation pipette, indicating decreased parallel fiber activation (Fig. 7B).

### Origin of activity-induced glial $Na^+$ transients

To analyze the origin of $Na^+$ transients induced by glutamatergic transmission in Bergmann glial cells, we applied blockers of glutamate receptors and glutamate uptake. CNQX caused a reduction in the peak amplitude of the current induced by parallel fiber stimulation by 43±8%. At the same time, the peak $Na^+$ increase was reduced by 38±10

We next studied the role of sodium-dependent glutamate uptake. As reported by others (e. g. Bellamy and Ogden, 2005), application of CNQX together with the glutamate-uptake blocker TBOA (200 µM) blocked the glial inward current evoked by a single pulse stimulation of parallel fibers (n=4; not shown). Performing the burst stimulation protocol (5 pulses at 50 Hz/100 ms), however, yielded a different result. While TBOA reduced the peak amplitude of $Na^+$ transients evoked by burst stimulation by 64±6%, the amplitude of the glial inward current was increased to 177±16% of control (n=12; Fig. 8B,C). Glutamate-evoked $Na^+$ transients in Bergmann glial cells were largest in processes close to the application pipette (Fig. 2A). Concomitant application of both blockers, CNQX and TBOA, caused an virtually complete omission of the evoked $Na^+$ signals, while the peak current amplitude was reduced to 43±3% of control (n=4; not shown).

Taken together, these results demonstrate that the majority of glial $Na^+$ influx evoked by burst stimulation is caused by inward transport of $Na^+$ by glutamate uptake. Furthermore, inhibition of glutamate uptake by TBOA during repetitive synaptic stimulation causes the emergence of a large inward current in Bergmann glial cells. A potentiation of glial inward currents in the presence of glutamate uptake blockers following repetitive synaptic stimulation was also reported by Bellamy and Ogden (2005). It was proposed, that this current is due to AMPA-receptor-induced release of a paracrine messenger from neurons that activated a G-protein coupled receptor in Bergmann glia cells.

## 4. Discussion

Based on quantitative imaging measurements using the $Na^+$ indicator SBFI, the present study demonstrates that excitatory synaptic activity results in $Na^+$ transients in dendrites of Purkinje neurons and processes of Bergmann glial cells, which can reach several mM following short burst stimulation. $Na^+$ transients in dendrites of Purkinje neurons have much faster kinetics than glial $Na^+$ transients and are mainly caused by activation of AMPA receptors. Glial $Na^+$ transients have rise times of several seconds and persist for tens of seconds. While activation of AMPA receptors accounts for part of the $Na^+$ signals in glial cells, the majority of glial $Na^+$ influx is caused by glutamate uptake.

By providing information on the absolute amplitude of such $Na^+$ signals, our results extend earlier observations, which demonstrated that synaptically-induced $Na^+$ transients in dendrites of Purkinje neurons are

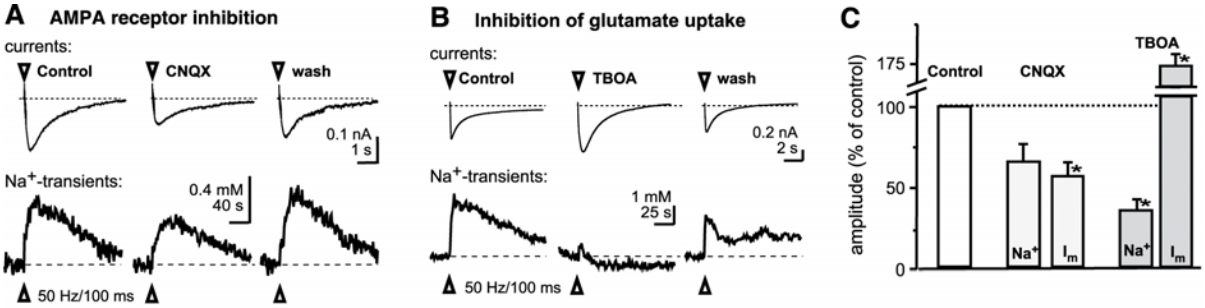


**Figure 8**. Pharmacological profile of synaptically-evoked signals in Bergmann glial cells. **A**, Blocking ionotropic non-NMDA receptors by application of CNQX (10 µM) while performing a burst stimulation of parallel fibers caused a reversible reduction in the peak current amplitude as well as in the peak $Na^+$ increase. **B**, TBOA, a transported blocker of glutamate uptake, strongly reduced the amplitude of $Na^+$ transients evoked by burst stimulation. At the same time, the amplitude of the inward current was increased. **C**, Histogram showing the mean values (± s.e.m.) of the amplitudes of activity-induced $Na^+$ transients and inward currents in the control and during perfusion with CNQX (n=7) and TBOA (n=12) as percent of control value (* indicates a significant difference, $p<0.01$).

mainly caused by AMPA-receptor opening (Lasser-Ross and Ross, 1992; Callaway and Ross, 1997; Kuruma et al., 2003). Activity-induced $Na^+$ transients in Purkinje cell dendrites amounted to about 1.5 mM. This is considerably lower than $Na^+$ accumulations in dendrites of CA1 pyramidal neurons, where a short burst of synaptic activity induced $Na^+$ transients of about 10 mM (Rose and Konnerth, 2001a). This difference may arise because synaptically-induced $Na^+$ transients in hippocampal neurons are largely mediated by NMDA receptors (Rose and Konnerth, 2001a), which are not expressed by Purkinje cells. Moreover, $Na^+$ spikes do not actively propagate into the dendrites of Purkinje cells and action potential generation itself does not cause dendritic $Na^+$ transients (Lasser-Ross and Ross, 1992; Callaway and Ross, 1997).

Our study also shows that short burst stimulation of parallel or climbing fibers evokes long lasting $Na^+$ transients in the processes of Bergmann glial cells. In agreement with a study published recently (Kirischuk et al., 2007), glial $Na^+$ transients were partially sensitive to CNQX and thus partly mediated by AMPA receptor activation. However, most of the $Na^+$ influx evoked by synaptic activity was sensitive to a blocker of glutamate uptake. Moreover, application of D-aspartate, a selective agonist of glutamate uptake, induced inward currents as well as $Na^+$ transients in Bergmann cell processes. This is consistent with earlier studies, in which $Na^+$ transients following activation of glutamate transport were reported from glial cells (Rose and Ransom, 1996; Chatton et al., 2000; Magistretti and Chatton, 2005, Kirischuk et al. 2007). Thus, glutamate uptake represents the predominant mechanism for activity-induced $Na^+$ influx into Bergmann glial cells.

Large synaptically-induced $Na^+$ transients in Bergmann glial cells, which presumably reflected $Na^+$ influx at the site of main synaptic input, had an amplitude of up to 9 mM, a rise time of 5-6 seconds and a decay time constant of about 90 s. The kinetics of $Na^+$ transients depend on several factors. In addition to diffusional processes, the rise time is mainly governed by the activity of glutamate uptake, whereas the decay is largely dependent on the $Na^+/K^+$-ATP'ase. Because transport systems are involved, kinetics also depend on the temperature, and both rise and decay time will be 2-3 times faster at physiological as compared to room temperature (e.g. Wadiche and Kavanaugh, 1998; Rose et al., 1999). Nevertheless, even when accelerated threefold, glial $Na^+$ signals will persist for tens of seconds. Such large decay time constants are in agreement with earlier studies demonstrating that $Na^+$ transients are less localized and decay much slower than calcium transients (e. g. Callaway and Ross, 1997; Regehr, 1997; Rose and Konnerth, 2001a; Grosche et al., 2002; Kuruma et al., 2003; Beierlein and Regehr, 2006; Piet and Jahr, 2007, Kirischuk et al., 2007).

Accumulation of $Na^+$ reduces the driving force for glutamate uptake (see below). Moreover, it might influence the recovery of calcium transients mediated by the $Na^+/Ca^{2+}$-exchanger (Kirischuk et al., 1997). A well documented consequence of glial $Na^+$ transients is increased ATP hydrolysis by the $Na^+/K^+$-ATP'ase. In astrocytes, this has been suggested to promote glycogen breakdown (Chatton et al., 2000; Voutsinos-Porche et al., 2003; Magistretti and Chatton, 2005). Thus, $Na^+$ accumulations might link increased neuronal activity and glial metabolism (Magistretti and Chatton, 2005).

## Consequences of $Na^+$ transients for the driving force of glial glutamate uptake

Because glutamate transport is coupled to the transport of three $Na^+$ ions, the inwardly directed $Na^+$ gradient provides its major driving force (Nicholls and Attwell, 1990; Levy et al., 1998; Danbolt, 2001; Maragakis and Rothstein, 2001); Fig. 9A). In addition, glutamate uptake is dependent on the electrochemical gradients for potassium, protons, and glutamate (Fig. 9A). Glutamate-evoked $Na^+$ transients in Bergmann glial cells were largest in processes close to the application pipette (Fig. 2A). Our experiments demonstrate that synaptic activation causes long-lasting $Na^+$ transients of up to 9 mM in processes of Bergmann glia. Earlier work has shown that neuronal activity is accompanied by additional changes in ion concentrations in the

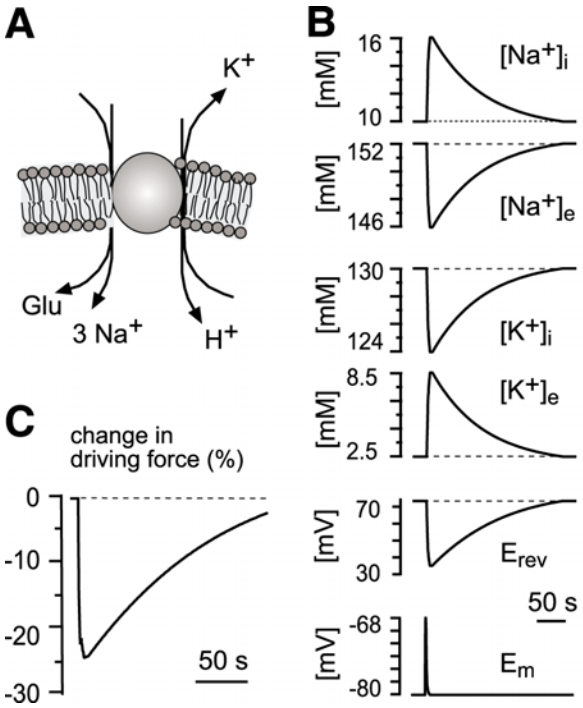


**Figure 9**. Consequences of activity-induced ion transients for the overall driving force of glutamate uptake. **A**, Model of the stoichiometry of glutamate uptake. The transport of glutamate is coupled to the antiport of one potassium ion and to the symport of three $Na^+$ ions and one proton. **B**, $[Na^+]_i$: fit of the averaged time course of large intracellular $Na^+$ transients (taken from Fig. 5C), assuming a baseline intracellular $Na^+$ concentration of 10 mM. This fit was used as matrix to model the time course of a decrease in the extracellular $Na^+$ ($[Na^+]_e$; baseline 152 mM), an increase in the extracellular potassium ($[K^+]_e$; baseline 2.5 mM), and a decrease in the intracellular potassium concentration ($[K^+]_i$; baseline 130 mM). $E_{rev}$: Time course of the change in the reversal potential for glutamate uptake during synaptic activity, calculated using the equation introduced by Zerangue (Zerangue and Kavanaugh, 1996). $E_m$: Average of 6 current clamp experiments (Fig. 7A), showing the membrane depolarization in Bergmann glial cells caused by synaptic activity. **C**, Change in the driving force for glutamate uptake, generated by adding the numerical values of changes in reversal potential ($E_{rev}$) and in membrane potential ($E_m$) and normalizing the resulting curve to baseline.

mM range: a decrease in the extracellular $Na^+$, an increase in the extracellular potassium, and a decrease in the intracellular potassium concentration (Sykova and Chvatal, 1993). Furthermore, both extracellular and intraglial pH increase with moderate synaptic stimulation (Chesler, 2003).

Based on these results, we estimated the consequences of activity-induced intracellular $Na^+$ signals for the driving force for glutamate uptake at active synapses. Thus, we first calculated the reversal potential of glutamate uptake (Erev) applying the equation introduced earlier ($E_{rev}$=(RT/F(n $_{Na}$ +$n_H$-$n_K$-$n_{Glu}$)) x ln ((([$Na_o$]/[$Na_i$])$^{nNa}$ x ([$Glu_o$]/[$Glu_i$])$^{nGlu}$ x ([$H_o$]/[$H_i$])$^{nH}$ x ([$K_i$]/[$K_o$])$^{nK}$)); Zerangue and Kavanaugh, 1996). To obtain a more realistic model, we not only incorporated our own experimental results, but also included changes in other ion concentrations. To this end, the fit of the averaged time course of fast intracellular $Na^+$ transients (Fig. 5C, peak amplitude 6 mM) served to generate time courses for assumed changes in extracellular $Na^+$, and intra- and extracellular potassium concentrations by the same value (Fig. 9B). Because moderate activity evokes alkalinizations in the extracellular space and in glial cells (Chesler, 2003), we assumed that there is no change in the overall proton gradient, and set intracellular and extracellular pH at fixed levels of 7.2 and 7.3, respectively (Chesler, 2003). Extracellular glutamate reaches levels close to baseline several orders of magnitudes faster than the rise time of $Na^+$ transients detected in the present study (Diamond and Jahr, 1997; Rusakov et al., 1999; Matsui et al., 2005). Thus, we chose to set extra- and intracellular glutamate concentrations at fixed values (0.1 µM and 0.5 mM, respectively). Solving the above mentioned equation for these ion concentrations over time revealed that synaptic activity causes a decrease in the reversal potential for glutamate uptake from +73 mV to +37 mV during the peak of the intracellular $Na^+$ increase (Fig. 9B).

Because glutamate uptake is electrogenic, its activity also depends on the membrane potential. Thus, we averaged the results of 6 current-clamp experiments (Fig. 7A), generating a time course of membrane potential changes (Em; Fig. 9B). Adding the numerical value of Em to Erev and normalizing the resulting curve to baseline, resulted in a curve reflecting the change in the driving force for glutamate uptake over time (Fig. 9C). Our model predicts that short burst synaptic activity reduces the driving force for glial glutamate uptake by about 20-25% for tens of seconds (Fig. 9C).

When looking at this number, one has to keep in mind that both rise and decay times of $Na^+$ transients will be increased by a factor of 2-3 at physiological temperature (e.g. Wadiche and Kavanaugh, 1998; Rose et al., 1999). Thus, whereas the actual decrease in driving force will not be as long-lasting as indicated in our model, a faster rise time of $Na^+$ signals will accelerate the decrease in Erev, and thus result in a larger maximal reduction in the driving force. In addition, $Na^+$ changes right underneath the plasma membrane are probably significantly higher and faster than those measured in the bulk cytosol, again arguing for a larger and faster reduction in driving force as predicted by our model. However, even with these limitations in mind, the model clearly indicates that following physiological activity, changes in ion gradients, and especially changes in the intracellular $Na^+$ concentration, will reduce the driving force for glial glutamate uptake for periods of at least several seconds.

Further studies on Bergmann glial cells are required to elucidate the physiological consequences of this activity-dependent reduction. A study by Diamond

and Jahr (Diamond and Jahr, 2000) on hippocampal astrocytes showed that high frequency stimulation does not overwhelm glutamate transporters at physiological temperature. In the cerebellum, it is well established that glutamate uptake moderates the activation of extrasynaptic receptors and limits spillover to adjacent synapses (Huang and Bergles, 2004). On the other hand, both processes play a functional role at cerebellar synapses (Clark and Cull-Candy, 2002; Huang and Bordey, 2004; Szapiro and Barbour, 2007), and are enhanced with intense activity. Activation of perisynaptic mGluRs and delayed synaptic calcium transients in Purkinje neurons that are observed with repetitive parallel fibers stimulation, are key events in LTD induction (Rose and Konnerth, 2001b). Thus, decreased glial glutamate uptake resulting from a $Na^+$ dependent reduction in its driving force could serve as a negative feedback mechanism promoting the diffusion of glutamate and the activation of extrasynaptic glutamate receptors as well as spillover following repetitive activity.

## Acknowledgements

We thank Claudia Roderigo and Simone Durry for expert technical help and Drs. Peter Hochstrate and Tony Kelly for critical discussion of the manuscript. The study was supported by the Deutsche Forschungsgemeinschaft (SPP 1172; Ro 2327/4-1,2).

## References

Anderson CM, Swanson RA (2000) Astrocyte glutamate transport: review of properties, regulation, and physiological functions. Glia 32:1-14.

Asztely F, Erdemli G, Kullmann DM (1997) Extrasynaptic glutamate spillover in the hippocampus: dependence on temperature and the role of active glutamate uptake. Neuron 18:281-293.

Barbour B, Keller BU, Llano I, Marty A (1994) Prolonged presence of glutamate during excitatory synaptic transmission to cerebellar Purkinje cells. Neuron 12:1331-1343.

Barski JJ, Hartmann J, Rose CR, Hoebeek F, Morl K, Noll-Hussong M, De Zeuww CI, Konnerth A, Meyer M (2003) Calbindin in cerebellar Purkinje cells is a critical determinant of the precision of motor coordination. J Neurosci 23:3469-3477.

Beierlein M, Regehr WG (2006) Brief bursts of parallel fiber activity trigger calcium signals in bergmann glia. J Neurosci 26:6958-6967.

Bellamy TC, Ogden D (2005) Short-term plasticity of Bergmann glial cell extrasynaptic currents during parallel fiber stimulation in rat cerebellum. Glia 52:325-335.

Bergles D, Jahr C (1997) Synaptic activation of glutamate transporters in hippocampal astrocytes.

Bergles D, Dzubay J, Jahr C (1997) Glutamate transporter currents in Bergmann glial cells follow the time course of extrasynaptic glutamate. Proc Natl Acad Sci U S A 94:14821-14825.

Bordey A, Sontheimer H (2003) Modulation of glutamatergic transmission by Bergmann glial cells in rat cerebellum in situ. J Neurophysiol 89:979-988.

Brasnjo G, Otis TS (2001) Neuronal glutamate transporters control activation of postsynaptic metabotropic glutamate receptors and influence cerebellar long-term depression. Neuron 31:607-616.

Brasnjo G, Otis TS (2004) Isolation of glutamate transport-coupled charge flux and estimation of glutamate uptake at the climbing fiber-Purkinje cell synapse. Proc Natl Acad Sci U S A 101:6273-6278.

Callaway JC, Ross WN (1997) Spatial distribution of synaptically activated sodium concentration changes in cerebellar Purkinje neurons. J Neurophysiol 77:145-152.

Chatton JY, Marquet P, Magistretti PJ (2000) A quantitative analysis of L-glutamate-regulated $Na^+$ dynamics in mouse cortical astrocytes: implications for cellular bioenergetics. Eur J Neurosci 12:3843-3853.

Chatton JY, Shimamoto K, Magistretti PJ (2001) Effects of glial glutamate transporter inhibitors on intracellular $Na^+$ in mouse astrocytes. Brain Res 893:46-52.

Chen S, Diamond JS (2002) Synaptically released glutamate activates extrasynaptic NMDA receptors on cells in the ganglion cell layer of rat retina. J Neurosci 22:2165-2173.

Chesler M (2003) Regulation and modulation of pH in the brain. Physiol Rev 83:1183-1221.

Clark BA, Barbour B (1997) Currents evoked in Bergmann glial cells by parallel fibre stimulation in rat cerebellar slices. J Physiol 502:335-350.

Clark BA, Cull-Candy SG (2002) Activity-dependent recruitment of extrasynaptic NMDA receptor activation at an AMPA receptor-only synapse. J Neurosci 22:4428-4436.

Danbolt NC (2001) Glutamate uptake. Prog Neurobiol 65:1-105.

Diamond JS, Jahr CE (1997) Transporters buffer synaptically released glutamate on a submillisecond time scale. J Neurosci 17:4672-4687.

Diamond JS, Jahr CE (2000) Synaptically released glutamate does not overwhelm transporters on hippocampal astrocytes during high-frequency stimulation. J Neurophysiol 83:2835-2843.

Eilers J, Augustine GJ, Konnerth A (1995a) Subthreshold synaptic $Ca^{2+}$ signalling in fine dendrites and spines of cerebellar Purkinje neurons. Nature 373:155-158.

Eilers J, Callewaert G, Armstrong C, Konnerth A (1995b) Calcium signaling in a narrow somatic submembrane shell during synaptic activity in cerebellar Purkinje neurons. Proc Natl Acad Sci U S A 92:10272-10276.

Grosche J, Kettenmann H, Reichenbach A (2002) Bergmann glial cells form distinct morphological structures to interact with cerebellar neurons. J Neurosci Res 68:138-149.

Grosche J, Matyash V, Möller T, Verkhratsky A, Reichenbach A, Kettenmann H (1999) Microdomains for neuron-glia interaction: parallel fiber signaling to Bergmann glial cells. Nat Neurosci 2:139-143.

Huang H, Bordey A (2004) Glial glutamate transporters limit spillover activation of presynaptic NMDA receptors and influence synaptic inhibition of Purkinje neurons. J Neurosci 24:5659-5669.

Huang YH, Bergles DE (2004) Glutamate transporters bring competition to the synapse. Curr Opin Neurobiol 14:346-352.

Ito M (2000) Mechanisms of motor learning in the cerebellum. Brain Res 886:237-245.

Jaffe DB, Johnston D, Lasser-Ross N, Lisman JE, Miyakawa H, Ross WN (1992) The spread of $Na^+$ spikes determines the pattern of dendritic $Ca^{2+}$ entry into hippocampal neurons. Nature 357:244-246.

Kirischuk S, Kettenmann H, Verkhratsky A (1997) $Na^+/Ca^{2+}$ exchanger modulates kainate-triggered $Ca^{2+}$ signaling in Bergmann glial cells in situ. Faseb J 11:566-572.

Kirischuk S, Kirchhoff F, Matyash V, Kettenmann H, Verkhratsky A (1999) Glutamate-triggered calcium signalling in mouse bergmann glial cells in situ: role of inositol-1,4,5-trisphosphate-mediated intracellular calcium release. Neuroscience 92:1051-1059.

Kirischuk S, Kettenmann H, Verkhratsky A (2007) Membrane currents and cytoplasmic sodium transients generated by glutamate transport in Bergmann glial cells. Pflugers Arch 454:245-25.

Knopfel T, Anchisi D, Alojado ME, Tempia F, Strata P (2000) Elevation of intradendritic sodium concentration mediated by synaptic activation of metabotropic glutamate receptors in cerebellar Purkinje cells. Eur J Neurosci 12:2199-2204.

Kulik A, Haentzsch A, Luckermann M, Reichelt W, Ballanyi K (1999) Neuron-glia signaling via alpha(1) adrenoceptor-mediated Ca(2+) release in Bergmann glial cells in situ. J Neurosci 19:8401-8408.

Kuruma A, Inoue T, Mikoshiba K (2003) Dynamics of $Ca^{2+}$ and $Na^{+}$ in the dendrites of mouse cerebellar Purkinje cells evoked by parallel fibre stimulation. Eur J Neurosci 18:2677-2689.

Lasser-Ross N, Ross WN (1992) Imaging voltage and synaptically activated sodium transients in cerebellar Purkinje cells. Proc Biol Sci 247:35-39.

Levy LM, Warr O, Attwell D (1998) Stoichiometry of the glial glutamate transporter GLT-1 expressed inducibly in a Chinese hamster ovary cell line selected for low endogenous $Na^{+}$-dependent glutamate uptake. J Neurosci 18:9620-9628.

Linden DJ (1997) Long-term potentiation of glial synaptic currents in cerebellar culture. Neuron 18:983-994.

Magistretti PJ, Chatton JY (2005) Relationship between L-glutamate-regulated intracellular $Na^{+}$ dynamics and ATP hydrolysis in astrocytes. J Neural Transm 112:77-85.

Maragakis NJ, Rothstein JD (2001) Glutamate transporters in neurologic disease. Arch Neurol 58:365-370.

Marcaggi P, Attwell D (2004) Role of glial amino acid transporters in synaptic transmission and brain energetics. Glia 47:217-225.

Matsui K, Jahr CE, Rubio ME (2005) High-concentration rapid transients of glutamate mediate neural-glial communication via ectopic release. J Neurosci 25:7538-7547.

Matyash V, Filippov V, Mohrhagen K, Kettenmann H (2001) Nitric oxide signals parallel fiber activity to Bergmann glial cells in the mouse cerebellar slice. Mol Cell Neurosci 18:664-670.

Meier SD, Kovalchuk Y, Rose CR (2006) Properties of the new fluorescent $Na^{+}$ indicator CoroNa Green: comparison with SBFI and confocal $Na^{+}$ imaging. J Neurosci Methods 155:251-259.

Nicholls D, Attwell D (1990) The release and uptake of excitatory amino acids. Trends Pharmacol Sci 11:462-468.

Oliet SH, Piet R, Poulain DA (2001) Control of glutamate clearance and synaptic efficacy by glial coverage of neurons. Science 292:923-926.

Otis TS, Kavanaugh MP, Jahr CE (1997) Postsynaptic glutamate transport at the climbing fiber-Purkinje cell synapse. Science 277:1515-1518.

Piet R, Jahr CE (2007) Glutamatergic and purinergic receptor-mediated calcium transients in Bergmann glial cells. J Neurosci 27:4027-4035.

Regehr WG (1997) Interplay between sodium and calcium dynamics in granule cell presynaptic terminals. Biophys J 73:2476-2488.

Rose CR, Ransom BR (1996) Mechanisms of H+ and $Na^{+}$ changes induced by glutamate, kainate, and D-Aspartate in rat hippocampal astrocytes. J Neurosci 16:5393-5404.

Rose CR, Konnerth A (2001a) NMDA receptor-mediated $Na^{+}$ signals in spines and dendrites. J Neurosci 21:4207-4214.

Rose CR, Konnerth A (2001b) Stores not just for storage: Intracellular calcium release and synaptic plasticity. Neuron 31:519-522.

Rose CR, Kovalchuk Y, Eilers J, Konnerth A (1999) Two-photon $Na^{+}$ imaging in spines and fine dendrites of central neurons. Pflugers Arch 439:201-207.

Rothstein JD, Dykes-Hoberg M, Pardo CA, Bristol LA, Jin L, Kuncl RW, Kanai Y, Hediger MA, Wang Y, Schielke JP, Welty DF (1996) Knockout of glutamate transporters reveals a major role for astroglial transport in excitotoxicity and clearance of glutamate. Neuron 16:675-686.

Rusakov DA, Kullmann DM, Stewart MG (1999) Hippocampal synapses: do they talk to their neighbours? Trends Neurosci 22:382-388.

Schousboe A (2003) Role of astrocytes in the maintenance and modulation of glutamatergic and GABAergic neurotransmission. Neurochem Res 28:347-352.

Sykova E, Chvatal A (1993) Extracellular ionic and volume changes: the role in glia-neuron interaction. J Chem Neuroanat 6:247-260.

Szapiro G, Barbour B (2007) Multiple climbing fibers signal to molecular layer interneurons exclusively via glutamate spillover. Nat Neurosci 10:735-742.

Takahashi M, Kovalchuk Y, Attwell D (1995) Pre- and postsynaptic determinants of EPSC waveform at cerebellar climbing fiber and parallel fiber to Purkinje cell synapses. J Neurosci 15:5693-5702.

Takayasu Y, Iino M, Kakegawa W, Maeno H, Watase K, Wada K, Yanagihara D, Miyazaki T, Komine O, Watanabe M, Tanaka K, Ozawa S (2005) Differential roles of glial and neuronal glutamate transporters in Purkinje cell synapses. J Neurosci 25:8788-8793.

Verkhratsky A, Steinhäuser C (2000) Ion channels in glial cells. Brain Res Rev 32:380-412.

Verkhratsky A, Orkand RK, Kettenmann H (1998) Glial calcium: Homeostasis and signaling function. Physiol Rev 78:99-141.

Voutsinos-Porche B, Bonvento G, Tanaka K, Steiner P, Welker E, Chatton JY, Magistretti PJ, Pellerin L (2003) Glial glutamate transporters mediate a functional metabolic crosstalk between neurons and astrocytes in the mouse developing cortex. Neuron 37:275-286.

Wadiche JI, Kavanaugh MP (1998) Macroscopic and microscopic properties of a cloned glutamate transporter/chloride channel. J Neurosci 18:7650-7661.

Watase K, Hashimoto K, Kano M, Yamada K, Watanabe M, Inoue Y, Okuyama S, Sakagawa T, Ogawa S-i, Kawashima N, Hori S, Takimoto M, Wada K, Tanaka K (1998) Motor discoordination and increased susceptibility to cerebellar injury in GLAST mutant mice. Eur J Neurosci 10:976-988.

Zerangue N, Kavanaugh MP (1996) Flux coupling in a neuronal glutamate transporter. Nature 383:634-637.

## B.4 Meier et al., J Neurosci Meth 155 (2006) 251-259.

### Properties of the New Fluorescent $Na^+$ Indicator CoroNa Green: Comparison with SBFI and Confocal $Na^+$ Imaging

Silke D. Meier, Yury Kovalchuk, and Christine R. Rose

My contributions:

- experimental design, together with C.R.R.
- all experimental data except for confocal imaging (figure 5) where Y.K. carried out the experiments according to my experimental design
- data analysis and first versions of illustrations
- revision of the manuscript, together with C.R.R.

ELSEVIER

Journal of Neuroscience Methods 155 (2006) 251–259

JOURNAL OF NEUROSCIENCE METHODS

www.elsevier.com/locate/jneumeth

# Properties of the new fluorescent $Na^+$ indicator CoroNa Green: Comparison with SBFI and confocal $Na^+$ imaging

Silke D. Meier [1], Yury Kovalchuk [2], Christine R. Rose *

*Physiologisches Institut, Ludwig-Maximilians-Universität München, Pettenkofer Strasse 12, D-80336 Munich, Germany*

Received 31 October 2005; received in revised form 13 January 2006; accepted 17 January 2006

**Abstract**

Neuronal activity causes substantial $Na^+$ transients in fine cellular processes such as dendrites and spines. The physiological consequences of such $Na^+$ transients are still largely unknown. High-resolution $Na^+$ imaging is pivotal to study these questions, and, up to now, two-photon imaging with the fluorescent $Na^+$ indicator sodium-binding benzofuran isophthalate (SBFI) has been the primary method of choice. Recently, a new $Na^+$ indicator dye, CoroNa Green (CoroNa), that has its absorbance maximum at 492 nm, has become available. In the present study, we have compared the properties of SBFI with those of CoroNa by performing $Na^+$ measurements in neurons of hippocampal slices. We show that CoroNa is suitable for measurement of $Na^+$ transients using non-confocal wide-field imaging with a CCD camera. However, substantial transmembrane dye leakage and lower $Na^+$ sensitivity are clearly disadvantages when compared to SBFI. We also tested CoroNa for its suitability for high-resolution imaging of $Na^+$ transients using a confocal laser scanning system. We demonstrate that CoroNa, in contrast to SBFI, can be employed for confocal imaging using a conventional argon laser and report the first $Na^+$ measurements in dendrites using this dye. In conclusion, CoroNa may prove to be a valuable tool for confocal $Na^+$ imaging in fine cellular processes.


*Keywords:* Sodium; Confocal imaging; Dendrite; Hippocampus; SBFI; CoroNa Green; Glutamate

## 1. Introduction

The inwardly directed $Na^+$ gradient energizes the vast majority of transport systems across the plasma membrane and is critical for homeostasis of intracellular ions such as $Ca^{2+}$ or protons and for reuptake of transmitters in the brain (Maragakis and Rothstein, 2004; Rose, 1997). Consequently, $Na^+$ entry is a significant factor in cellular brain damage observed following diverse pathological conditions (Pinelis et al., 1994; Pisani et al., 1998; Chen et al., 1999; Chatton et al., 2000; Sheldon et al., 2004b; Magistretti and Chatton, 2005). Moreover, $Na^+$ ions are the major charge carriers during action potentials and excitatory postsynaptic currents in most neurons. Besides their purely homeostatic function, several studies indicate that $Na^+$ ions have a signaling function and play a role in activity-dependent synaptic plasticity (Bouron and Reuter, 1996; Chatton et al., 2000; Chinopoulos et al., 2000; Linden et al., 1993; Rishal et al., 2003; Yu and Salter, 1998).

In contrast to large-volume fibers, in which electrical signaling requires only small ionic fluxes and does not change the intracellular $Na^+$ concentration ($[Na^+]_i$) significantly (e.g. Hodgkin and Huxley, 1952) activity-induced $Na^+$ accumulations have been reported from fine cellular processes such as dendrites (Callaway and Ross, 1997; Jaffe et al., 1992; Knöpfel et al., 2000; Lasser-Ross and Ross, 1992). In hippocampal neurons, synaptic stimulation causes $[Na^+]_i$ transients of about 10 mM in dendrites and of up to 35–40 mM in dendritic spines (Rose et al., 1999; Rose and Konnerth, 2001).

Many questions concerning the physiological consequences of $[Na^+]_i$ transients and the role of $Na^+$ ions in intracellular signaling are still open. Clearly, high-resolution $[Na^+]_i$ imaging close to synapses and in axons is necessary to answer these questions. In contrast to imaging intracellular $Ca^{2+}$ transients,

* Corresponding author. Present address: Institut für Neurobiologie, Universität Düsseldorf, Universitätsstrasse 1, D-40225 Düsseldorf, Germany. Tel.: +49 211 81 13416; fax: +49 211 81 13415.

*E-mail addresses:* s.meier@uni-duesseldorf.de (S.D. Meier), kovalchuk@lrz.uni-muenchen.de (Y. Kovalchuk), rose@uni-duesseldorf.de (C.R. Rose).

[1] Present address: Institut für Neurobiologie, Universität Düsseldorf, Universitätsstrasse 1, D-40225 Düsseldorf, Germany. Tel.: +49 211 81 13584.

[2] Present address: Institut für Neurowissenschaften, Technische Universität München, Biedersteiner Strasse 29, D-80802 Munich, Germany. Tel.: +49 89 4140 3350.

0165-0270/$ – see front matter © 2006 Elsevier B.V. All rights reserved.
doi:10.1016/j.jneumeth.2006.01.009

high-resolution $[Na^+]_i$ imaging has been, up to date, a rather tedious and difficult task. This is partly due to the scarcity of suitable fluorescent indicator dyes. Imaging with the sodium indicator Sodium Green, which has its absorption maximum around 488 nm, has been proven useful in a variety of studies (Friedman and Haddad, 1994; Senatorov et al., 2000; Winslow et al., 2002). However, interactions of this dye with cellular proteins can hinder reliable measurements (Despa et al., 2000). The best established $Na^+$-sensitive fluorescent dye, sodium-binding benzofuran isophthalate (SBFI) (Minta and Tsien, 1989), must be excited below 400 nm, and can only be employed in confocal imaging when special UV-lasers are used. Although conventional fluorescence imaging allows detection of $[Na^+]_i$ transients in dendrites (Callaway and Ross, 1997; Jaffe et al., 1992; Knöpfel et al., 2000; Lasser-Ross and Ross, 1992; Miyakawa et al., 1992; Ross et al., 1993; Tsubokawa et al., 1999), the analysis of the spatial distribution of $Na^+$ signals or measurements in fine dendrites and spines in the intact tissue with SBFI require two-photon imaging (Rose et al., 1999). This technique, however, is not applicable for many laboratories because of its high costs for purchase and maintenance.

Recently, a new, green-fluorescent $Na^+$ indicator dye, CoroNa Green (CoroNa), has become available (Invitrogen/Molecular Probes). The absorbance maximum of CoroNa is near 492 nm, which makes it suitable for excitation by argon lasers commonly used in confocal microscopy. According to the manufacturer (Invitrogen), CoroNa is brighter and exhibits larger changes in fluorescence after binding of sodium as compared to Sodium Green. In the present study, we compared the properties of CoroNa with those of SBFI to assess the suitability of the former for imaging of $[Na^+]_i$ transients in neurons in situ with both wide-field and high-resolution confocal imaging. We demonstrate that CoroNa is a suitable tool for measurement of $[Na^+]_i$ transients using conventional wide-field imaging and report the first confocal $[Na^+]_i$ measurements in fine dendrites in acute brain slices using this dye.

## 2. Methods

### 2.1. Tissue preparation and patch-clamp recordings

Balb/c mice (10–13 days old) were anesthetized and decapitated. Parasagittal hippocampal slices (250 μm) were prepared as described previously (Edwards et al., 1989). After sectioning, slices were kept in physiological saline for 30 min at 34 °C and then at 25 °C for up to 7 h. Standard techniques were used for somatic whole-cell patch-clamp recordings (Edwards et al., 1989). CA1 pyramidal cells were generally held at membrane potentials of −60 to −65 mV.

The intracellular solution for patch-clamp experiments contained: 120 mM K-gluconate, 10 mM Hepes, 32 mM KCl, 4 mM NaCl, 0.16 mM EGTA, 4 mM Mg-ATP, 0.4 mM Na-GTP, 0.5 mM SBFI (tetraammonium salt of sodium-binding benzofuran isophthalate; Molecular Probes/Invitrogen) or CoroNa Green (Molecular Probes/Invitrogen) and was titrated with KOH to a pH of 7.3. During experiments, slices were perfused with physiological saline containing: 125 mM NaCl, 2.5 mM KCl, 1.25 mM $NaH_2PO_4$, 26 mM $NaHCO_3$, 2 mM $CaCl_2$, 1 mM $MgCl_2$, 20 mM glucose; continuously bubbled with 95% $O_2$/5% $CO_2$ resulting in a pH of 7.4. Experiments were performed at room temperature (22–24 °C). α-Amino-3-hydroxy-5-methyl-4-isoxazolepropionate (AMPA) was applied by a picospritzer (Intracel) coupled to standard micropipettes placed at a distance of approximately 15 μm above the cell soma. Glutamate (50 or 100 mM) was applied iontophoretically with fine glass pipettes placed at a distance of 10–15 μm from a dendrite of interest.

### 2.2. $Na^+$ imaging

Conventional, wide-field fluorescence imaging was performed using a variable scan digital imaging system (TILL Photonics) attached to an upright microscope (Zeiss Axioskop, 40× water immersion objective) and a CCD camera as sensor (TILL Imago Super-VGA). Hippocampal CA1 pyramidal neurons were loaded with the fluorescent dye SBFI or CoroNa (CoroNa Green) either by injection of the membrane-permeable AM-form of the dye into the stratum radiatum as described earlier (Stosiek et al., 2003) or by direct intracellular loading through a patch-pipette. For wide-field imaging with SBFI, background-corrected fluorescence signals from the cell bodies (>410 nm) were collected after alternate excitation at 345 nm (isosbestic point) and at 385 nm ($Na^+$-sensitive wavelength), and the fluorescence ratio (345 nm/385 nm) was calculated. For wide-field imaging with CoroNa, cells were excited at 492 nm and background-corrected fluorescence above 515 nm was collected. CoroNa data were expressed as changes in fluorescence emission compared to baseline fluorescence ($\Delta F/F$) and SBFI measurements as changes in fluorescence ratio compared to baseline ratio ($\Delta R/R$) using Igor Pro software (Wavemetrics) for analyses, unless otherwise stated. Images were acquired at 1–2 Hz, except during calibration experiments, where images were taken every 5 or 10 s.

Confocal imaging was performed in combination with whole-cell recording using a confocal laser scanning microscope ("Oz", Noran, 488 nm argon-ion laser), attached to an upright microscope (Olympus, 60× water immersion objective). Fluorescence images were acquired at 30 Hz and imaging was started at least 30 min after establishing the whole-cell configuration. Full-frame images were analyzed off-line with custom-made software based on LABVIEW (National Instruments). $Na^+$-transients were recorded in regions of interest along secondary apical dendrites.

### 2.3. Calibration

For in vitro calibration of CoroNa, calibration solutions contained: 100 μM CoroNa, 170 mM $[Na^+]+[K^+]$, 30 mM $[Cl^-]$, 10 mM Hepes and 136 mM gluconate. Solutions were titrated to pH 7.3 with KOH. Background-corrected fluorescence excitation spectra for wavelengths between 400 and 509 nm were obtained for solutions with $Na^+$ concentrations of 0, 15, 30, 60, 90, 120, 150 or 170 mM using the TILL Photonics system.

In situ calibration of SBFI or CoroNa Green fluorescence was performed as described earlier (Rose et al., 1999; Rose

and Ransom, 1996, 1997b). Calibration solutions contained: 170 mM ($Na^+ + K^+$), 30 mM $Cl^-$, 136 mM gluconate, 10 mM Hepes, pH 7.3 and 3 μM gramicidin D, 10 μM monensin and 100 μM ouabain. For analysis of non-ratiometric experiments, we only included cells in which the fluorescence emission at 0 mM $Na^+$ at the start and the end of the experiment did not differ by more than 20%.

## 3. Results

SBFI (Minta and Tsien, 1989) is similar to the well-known ratiometric calcium-sensitive dye Fura-2 (Grynkiewicz et al., 1985). It is established for measurements of $[Na^+]_i$ in many cell types, and up to now, the most widely used fluorescent $Na^+$ indicator dye (Rose, 2003). The optimal $Na^+$-sensitive excitation wavelength of SBFI inside the cell is between 380 and 390 nm, whereas its isosbestic point is found near 345 nm. When $Na^+$ is bound to SBFI, its fluorescence quantum yield increases, its excitation peak narrows and its excitation maximum shifts to shorter wavelengths, causing a significant change in the ratio of fluorescence intensities excited at 345 nm/385 nm. In contrast, the recently developed $Na^+$-sensitive fluorescent dye CoroNa is a non-ratiometric green-fluorescent $Na^+$ indicator that exhibits an increase in fluorescence emission intensity upon binding $Na^+$, with little shift in wavelength. The in vitro absorption maximum of CoroNa is at 492 nm, which makes it suitable for excitation by argon lasers commonly used in confocal microscopy.

### 3.1. Intracellular dye loading

Use of membrane-permeant acetoxymethyl (AM) esters of fluorescent dyes is a convenient and non-invasive method which enables the loading of many cells at a time and allows both the study of single cells and of network activities (Peterlin et al., 2000; Rose and Ransom, 1997a; Stosiek et al., 2003). To test the suitability of CoroNa for this loading technique in comparison to SBFI, the AM forms of CoroNa or SBFI were injected into the stratum radiatum close to the pyramidal cell layer at a concentration of 0.8 mM using a micropipette coupled to a picospritzer as described earlier (Stosiek et al., 2003).

Injection of CoroNa–AM resulted in a rapid increase in the fluorescence emission of CA1 pyramidal neurons when excited at 492 nm. Fluorescence emission from cell bodies reached its maximum at about 5 min after injection, but then dropped to levels close to background within 90–120 min ($n = 4$; Fig. 1A). This drop was not due to dye bleaching, as it was not halted by switching off the excitation light (Fig. 1A, white box). In contrast, injection of SBFI–AM resulted in stable dye loading and fluorescence emission from cell bodies for several hours (excitation wavelength 385 nm; $n = 3$; Fig. 1A), as described previously for other fluorescent indicator dyes (Peterlin et al., 2000; Stosiek et al., 2003).

Including the membrane-impermeant form of either dye into a patch-pipette resulted in a maximal fluorescence emission from cell bodies within 2–5 min after establishing the whole-cell patch-clamp mode (CoroNa: $n = 5$, SBFI: $n = 3$; Fig. 1B). The emission of CoroNa stayed at this level for as long as the whole-cell configuration was maintained, but dropped steadily when the pipette was withdrawn from the cell ($n = 3$; not shown). In contrast, the fluorescence emission of SBFI-filled cells was stable for several hours even after removal of the patch-pipette ($n = 6$; not shown) as reported earlier (Rose et al., 1999).

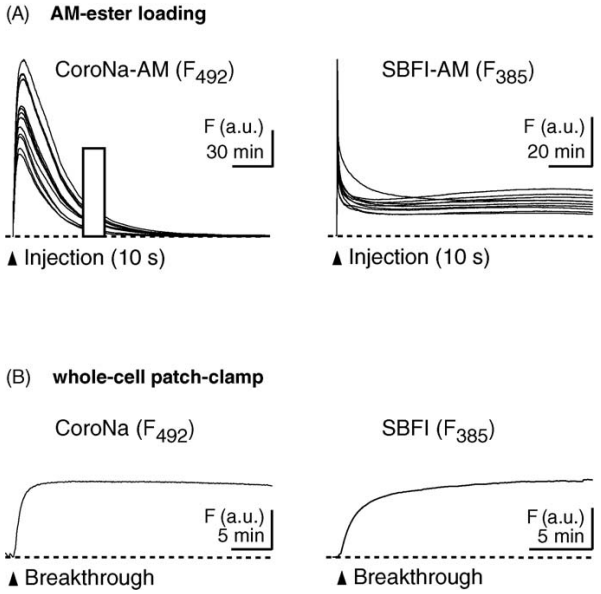


Fig. 1. Dye loading of CA1 pyramidal neurons in hippocampal slices. (A) Left panel: Fluorescence emission of CoroNa excited at 492 nm following an injection of the AM–ester form of the dye into the *stratum radiatum* for 10 s. Fluorescence emission from cell bodies increased rapidly after the injection, but then dropped again to levels close to background within 90–120 min. This drop continued while switching off the excitation light (white box). Right panel: Injection of SBFI–AM resulted in stable dye loading and fluorescence emission of cells (excitation wavelength 385 nm). (B) Delivery of either CoroNa or SBFI through the patch-pipette during whole-cell patch-clamp resulted in a stable fluorescence emission within a few minutes after breakthrough when excited at 492 and 385 nm, respectively. *F* (a.u.): fluorescence emission, depicted as arbitrary units.

These experiments demonstrate that CoroNa, in contrast to SBFI, is not suitable for conventional ester loading or brief loading through a patch-pipette because the dye is lost quickly from the intracellular compartment. Stable intracellular dye concentrations can, however, be obtained by constant delivery of the dye such as through a patch-pipette during whole-cell patch-clamp recordings.

### 3.2. $Na^+$-sensitivity of CoroNa and SBFI

According to the manufacturer, the $K_d$ of CoroNa in the test tube is around 80 mM. To determine the $Na^+$-sensitivity of CoroNa in our hands, we first performed an in vitro calibration. Fluorescence emission was measured above 515 nm for excitation wavelengths from 400 to 509 nm at $Na^+$ concentrations of 0, 15, 30, 60, 90, 120, 150 or 170 mM ($n = 3$; Fig. 2A). Fluorescence emission peaked at excitation wavelengths between 492 and 496 nm at all $Na^+$ concentrations, confirming the spectra given by the manufacturer. Plotting the difference in fluores-

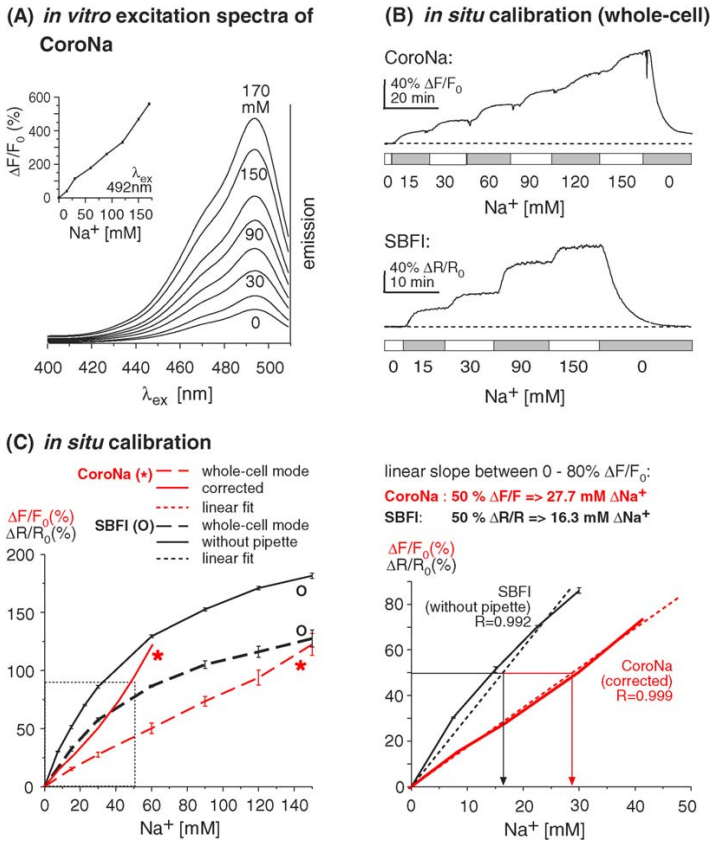


Fig. 2. Calibration of the sensitivity of CoroNa and SBFI to changes in $[Na^+]$. (A) For in vitro calibration of CoroNa, the background-corrected fluorescence emission above 515 nm was measured in a test chamber for excitation wavelengths ($\lambda_{ex}$) from 400 to 509 nm at $Na^+$ concentrations of 0, 15, 30, 60, 90, 120, 150 or 170 mM. In the inset, the change in fluorescence emission normalized to 0 mM $Na^+$ ($\Delta F/F_0$) is plotted against the $Na^+$ concentration, revealing a virtually linear relationship ($\lambda_{ex}$ 492 nm). (B) Calibration of the $Na^+$ sensitivity of CoroNa and SBFI in CA1 pyramidal cells. Cells were loaded through the patch-pipette and then objected to a calibration solution containing ionophores. Stepwise changes in the extracellular $Na^+$ concentration from 0 to 150 mM and back caused stepwise changes in the fluorescence emission of CoroNa ($\Delta F/F_0$) and fluorescence ratio of SBFI ($\Delta R/R_0$). (C) Left panel: Relationship between changes in fluorescence emission/ratio and $[Na^+]_i$. Shown are mean values ± S.E. Dashed black line: Calibration of SBFI with patch-pipette attached ($n = 5$); solid black line: SBFI with pipette withdrawn ($n = 4$). Dashed red line: CoroNa with pipette attached ($n = 5$); solid red line: corrected calibration curve for CoroNa, adjusted for the presumed inefficient equilibration of extra- and intracellular $Na^+$ (see text). Right panel: Regression lines for the calibration data of SBFI obtained without pipette (dotted black line) and the corrected CoroNa data (dotted red line) demonstrate a linear relationship between changes in fluorescence emission and $[Na^+]$ in the range between 0 and 80% $\Delta F/F_0$. The slopes reveal that, within this range, a 50% change in fluorescence emission corresponds to a change of about 16 mM $Na^+$ when determined with SBFI, and to a change of about 28 mM $Na^+$ when determined with CoroNa. (For interpretation of the references to colour in this figure legend, the reader is referred to the web version of the article.)

cence emission at 492 nm normalized to 0 mM $Na^+$ ($\Delta F/F_0$) against the $Na^+$ concentration revealed a basically linear relationship and no saturation in this concentration range (Fig. 2A). Although the in vitro $K_d$ could not be determined properly from these data, its apparent value is at least 80 mM. Calibration with higher $Na^+$ concentrations was not performed because this implied the use of solutions with higher (and therefore, unphysiological) osmolarity.

The spectral properties of SBFI when calibrated in a cell free system differ significantly from those in an intracellular environment (Harootunian et al., 1989; Rose and Ransom, 1996). Therefore, we also performed calibrations of the $Na^+$-sensitivity of CoroNa in situ and compared those with in situ calibrations of SBFI. For these experiments, CA1 pyramidal cells were loaded with either dye in the whole-cell patch-clamp mode. Subsequently, a calibration cocktail containing 3 μM gramicidin ($Na^+$ ionophore), 10 μM monensin ($Na^+/H^+$ carrier) and 100 μM ouabain ($Na^+/K^+$-ATPase blocker) to promote rapid exchange and equilibration of $Na^+$ across the plasma membrane was perfused (Rose et al., 1999; Rose and Ransom, 1996). Stepwise changes of the extracellular $Na^+$ concentration then resulted in stepwise changes in fluorescence (Fig. 2B). The change in fluorescence ratio of SBFI ($\Delta R$) at each $Na^+$ concentration was normalized to the emission ratio at 0 mM $Na^+$ ($\Delta R/R_0$). For measurements with CoroNa, changes in fluorescence emission ($\Delta F$) were normalized correspondingly ($\Delta F/F_0$). Calibration curves were then generated from these data (Fig. 2C). For these and all following experiments, CoroNa was excited at 492 nm, whereas SBFI was excited alternately at 345 nm (isosbestic point) and 385 nm ($Na^+$-sensitive wavelength) and the ratio in

SBFI's fluorescence emission (345 nm/385 nm) was calculated. For measurements with SBFI, increases in the $Na^+$ concentration are, therefore, reflected in increases in the fluorescence ratio (Fig. 2B).

To prevent a decrease in fluorescence due to loss of CoroNa from the cell during calibration (see above), the patch-pipette was kept attached to the cell body throughout the entire experiment ($n=5$). This approach not only guaranteed a stable intracellular dye concentration (Fig. 1B), but also caused diffusion of $Na^+$ between the pipette solution (containing 4 mM $Na^+$) and the cytosol during calibration. To estimate the error resulting from diffusion of $Na^+$ through the tip of the pipette, we compared calibration curves of SBFI in whole-cell mode ($n=5$; Fig. 2C, dashed black line) and with pipette withdrawn ($n=4$; Fig. 2C, solid black line). For both calibration curves, the relationship between SBFI fluorescence and $[Na^+]_i$ follows Michaelis–Menten kinetics, as demonstrated earlier (e.g. Donoso et al., 1992; Rose et al., 1999; Diarra et al., 2001). Plotting the data of SBFI's calibration without pipette in a Lineweaver–Burk diagram ($1/(\Delta R/R_0)$ versus $1/[Na^+]_i$) revealed a $\beta K_d$ (*apparent* $K_d$) of 51.54 mM and a $\beta$ (ratio of the fluorescence of the bound dye to the free (unbound) dye) of 2.36. According to the calibration equations established by (Grynkiewicz et al., 1985), this resulted in a $K_d$ of 21.8 mM, confirming values published earlier (e.g. Donoso et al., 1992; Rose et al., 1999; Diarra et al., 2001; Sheldon et al., 2004a). In contrast, the $K_d$ of SBFI appeared nearly twice as high when the pipette was still attached (Fig. 2C). We reasoned that the shift in calibration curves resulted from an incomplete equilibration of extra- and intracellular $Na^+$ concentrations, caused by the presence of the pipette (4 mM sodium). Given that each $\Delta R/R_0$ value of SBFI corresponds to a specific intracellular $Na^+$ concentration we used the SBFI calibration curve obtained without the pipette in order to determine the actual $Na^+$ concentrations inside the cell when the calibration was performed with the pipette attached. Under our experimental conditions (pipette resistances 4.6–4.9 MΩ, same perfusion velocity and ionophore concentrations) extracellular $Na^+$ concentrations of 15, 30, 60, 90, 120 and 150 mM resulted in intracellular concentrations of 8.2, 16.7, 29.9, 41.4, 50 and 60.7 mM, respectively, during the calibration with pipette attached. Based on these results we corrected the calibration curve of CoroNa (Fig. 2C, dashed red line) for the presumed incomplete equilibration of extra- and intracellular $Na^+$ concentrations. This correction resulted in a shift of the curve to the left and in a significant increase in its slope (Fig. 2C, solid red line). As for the in vitro calibration, the relationship between the measured $\Delta F/F_0$ and the presumed intracellular $Na^+$ concentration was linear and did not approach saturation up to the highest extracellular $Na^+$ concentration used (150 mM), precluding a proper determination of the apparent $K_d$ of CoroNa. However, the calibration data clearly show that the apparent $K_d$ of CoroNa is significantly higher than that of SBFI.

For both SBFI (without pipette) and the corrected CoroNa calibration data, the correlation between $\Delta F/F_0$ and the $Na^+$ concentration was linear up to about 80% $\Delta F/F_0$ (Fig. 2C, right panel). The linear regression lines revealed that within this range, a change in the fluorescence emission ($\Delta F/F$) of 50% corresponds to a $[Na^+]_i$ change of 16.3 mM when determined with SBFI, and to a $[Na^+]_i$ change of about 27.7 mM when determined with CoroNa.

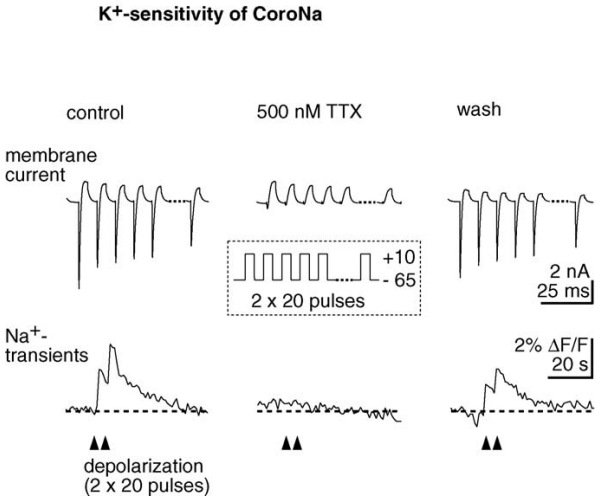


Fig. 3. Determination of CoroNa's sensitivity to discriminate between changes in $[Na^+]_i$ versus changes in $[K^+]_i$. A neuron was stimulated with two series (arrowheads) of 20 voltage steps from −65 to 10 mV (inset). This stimulation resulted in $Na^+$-currents followed by $K^+$-currents (upper traces show the first five and the last evoked current). The stimulation evoked a transient increase in the CoroNa-fluorescence in the cell body, which was reversibly blocked by 500 nM tetrodotoxin (TTX). Data are expressed as changes in fluorescence ($\Delta F$) divided by the baseline fluorescence before the stimulation ($F$).

To analyze a possible cross-sensitivity of CoroNa with $K^+$, voltage-clamped CA1 pyramidal neurons were depolarized by a series of voltage steps that induced sequences of $Na^+$-inward, followed by $K^+$-outward currents (Rose et al., 1999; Fig. 3, inset). This stimulation was accompanied by a transient increase in CoroNa emission from the cell body, indicating an increase in $[Na^+]_i$. During perfusion with tetrodotoxin, both the $Na^+$ currents and the increase in fluorescence were reversibly abolished, while the $K^+$-currents persisted ($n=4$; Fig. 3). As previously reported for SBFI (Rose et al., 1999), these results demonstrate that the sensitivity of CoroNa to changes in intracellular $[K^+]$ was negligible under our experimental conditions.

### 3.3. $Na^+$ transients induced by application of AMPA

To determine the suitability of CoroNa as compared to SBFI for measurement of agonist-induced $[Na^+]_i$ transients in intact cells, we performed experiments, in which the ionotropic glutamate receptor agonist AMPA was locally applied to cell bodies of hippocampal CA1 pyramidal neurons by pressure ejection from fine micropipettes. Fluorescence emission and membrane currents were recorded simultaneously from the cell bodies. For both dyes, increasing the duration of the AMPA application from 20 to 100 ms increased the membrane current as well as the amplitude of fluorescence changes, reflecting larger $[Na^+]_i$ transients with increasing currents through AMPA receptors ($n=4$ for CoroNa, $n=3$ for SBFI; Fig. 4A and B). As

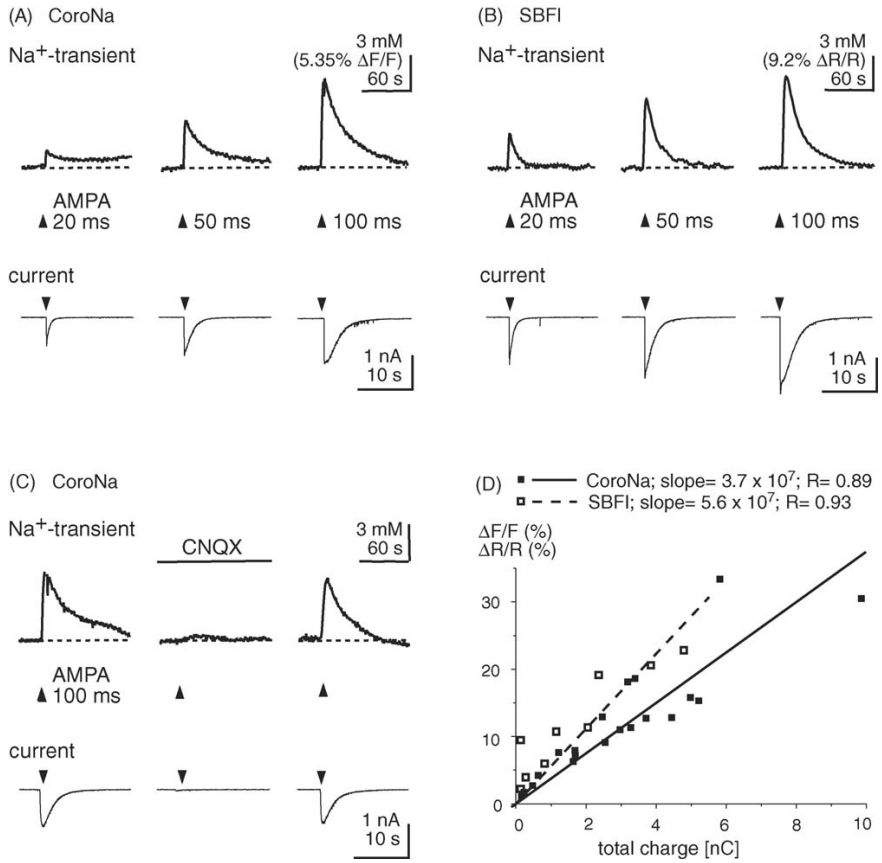


Fig. 4. AMPA-induced $Na^+$ transients. (A and B) Local pressure application of the non-NMDA receptor agonist AMPA for 20, 50 and 100 ms to cell bodies of CA1 pyramidal cells evoked both $Na^+$ transients and inward currents. (A) Measurements with CoroNa; (B) measurements with SBFI; (C) the AMPA-receptor blocker CNQX reversibly blocked AMPA-induced $Na^+$ transients, determined with CoroNa, and inward currents; (D) relationship between fluorescence transients ($\Delta F/F$ for CoroNa, filled squares; $\Delta R/R$ for SBFI, open squares) elicited by AMPA application and total charge of the corresponding inward currents, calculated from the area under the curve ($n = 3$ cells for SBFI; $n = 4$ cells for CoroNa). The slope of the linear regression line generated from these data was 1.5 times higher for SBFI (dashed line) than for CoroNa (solid line).

expected, the AMPA-induced $[Na^+]_i$ transients and inward currents were reversibly blocked by application of the AMPA receptor antagonist CNQX (6-cyano-7-nitroqionoxaline-2,3-dione, 10 μM) ($n = 3$, CoroNa; Fig. 4).

Calculation of absolute $Na^+$ concentrations based on the results of the in situ calibration (see Fig. 2C), revealed comparable $[Na^+]_i$ transients following AMPA-induced currents for measurements performed using CoroNa or SBFI. Moreover, the kinetics of AMPA-induced $[Na^+]_i$ signals did not substantially differ between the two dyes, despite their difference in molecular weight and $K_d$ values. However, as expected from the calibration, the $Na^+$-dependent changes in fluorescence emission differed significantly. To compare $Na^+$-dependent $\Delta F/F$ values of both dyes, we plotted their peak fluorescence amplitudes against the total charge of the corresponding inward currents, and corresponding $Na^+$-influx, respectively (Fig. 4D). The slope of the linear regression line generated from these data was 1.5 times higher for SBFI than for CoroNa. This result is in good agreement with the results obtained from the in situ calibration (Fig. 2C).

### 3.4. Confocal $Na^+$ imaging in dendrites using CoroNa

To test the suitability of CoroNa for confocal measurements in dendrites, CA1 pyramidal cells were filled with 0.5 mM CoroNa through the patch-pipette. Imaging experiments were started at least 30 min after rupturing the patch to ensure diffusion of the dye into the distal parts of the cell ($n = 4$). After this loading time, the entire dendritic tree of the cells was clearly visible when excited at 488 nm (Fig. 5A). A dendrite was chosen and a fine glass pipette was positioned in close proximity (10–15 μm) to this dendrite. Iontophoretic ejection of glutamate for a few milliseconds (3–10 ms) evoked an inward current and a local increase in the fluorescence emission of CoroNa, indicating a local $[Na^+]_i$ increase in the dendrite ($n = 6$; Fig. 5B).

Fig. 5B shows the $[Na^+]_i$ transients induced by glutamate, along different regions of a secondary apical dendrite of a CA1 pyramidal neuron. With increasing distance from the region of maximal response, presumably the site of activation of glutamate receptors, the peak amplitudes of the $[Na^+]_i$ transients declined and were reached at later time points. With glutamate

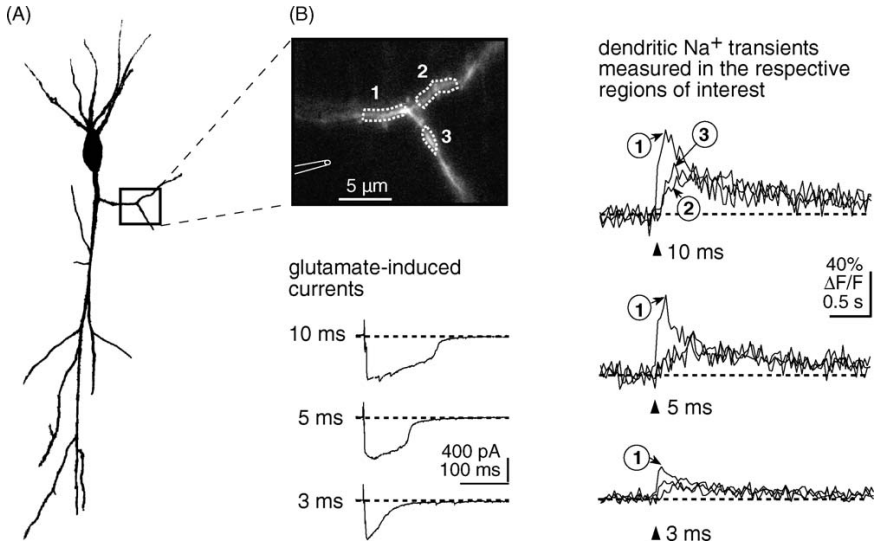


Fig. 5. Glutamate-induced $Na^+$ transients in dendrites of CA1 pyramidal cells revealed by confocal imaging. (A) Reconstruction of a CA1 pyramidal neuron filled with CoroNa. The box denotes the dendritic region where the experiments illustrated in (B) were performed. (B) Upper left: Image of the apical dendrite that was chosen for the glutamate application. The position of the application pipette is schematically indicated on the left. The numbered, dashed lines indicate the regions of interest in which the sodium transients were measured using CoroNa. Right: Dendritic $Na^+$ transients induced by glutamate applications (10, 5 or 3 ms). The $Na^+$ transient is largest in the dendritic region closest to the application pipette (region 1). Lower left: Corresponding currents (10, 5, 3 ms), recorded in the whole-cell voltage-clamp configuration at the cell soma.

applications of only 3 ms, dendritic $\Delta F/F$ values in the region of maximal response reached about 30%. If one assumed similar calibration properties of CoroNa for confocal and conventional imaging, this corresponded to a glutamate-induced $[Na^+]_i$ increase of about 17 mM in the dendrite.

Taken together, these results demonstrate that CoroNa is well suited for detection of local $[Na^+]_i$ transients that occur in dendritic domains near the site of activation of glutamate receptors.

## 4. Discussion

In this study, we compare the properties of CoroNa Green, a newly developed non-ratiometric sodium indicator, excited by green light of about 490 nm, with those of SBFI, which is a well-established ratiometric indicator excitable in the UV-range. Our comparison is based on experiments in CA1 pyramidal cells in acute slices of the mouse hippocampus performed with conventional epifluorescence wide-field microscopy. In addition, we tested CoroNa for its suitability for confocal imaging of $[Na^+]_i$ transients in dendrites using a confocal laser scanning microscope and excitation at 488 nm.

### 4.1. Basic properties of CoroNa as compared to SBFI

As established by many earlier studies (e.g. Jaffe et al., 1992; Rose et al., 1999; Rose and Ransom, 1996; Knöpfel et al., 1998; Chatton et al., 2000; Diarra et al., 2001), SBFI proved to be well suited for both passive AM–ester loading and for loading of single cells with a patch-pipette. In contrast, application of the AM–ester of CoroNa did not result in stable intracellular dye concentrations. Even loading of the presumably membrane-impermeable form of the dye into cells through a patch-pipette was followed by significant dye loss when the dye-containing pipette was removed from the cell. Significant decrease in fluorescence emission following intracellular injection of CoroNa was also observed in a recent study by Nikolaeva et al. (2005). Our study shows, however, that permanent dye delivery through a patch-pipette yields a constant basal fluorescence emission and dye concentration, respectively. Apparently, the molecular structure of CoroNa, comprising a fluorescein molecule linked to a crown ether, does not confer sufficient membrane impermeability to effectively trap the dye inside the cell. We conclude that quantitative determination of the $Na^+$ concentration using CoroNa, which requires stable intracellular dye concentrations, requires permanent dye delivery in the whole-cell patch-clamp mode or constant dye injection through an intracellular microelectrode.

Our calibration studies revealed a $K_d$ of SBFI of 21.8 mM, which is close to $K_d$ values reported earlier (e.g. Donoso et al., 1992; Rose et al., 1999; Rose and Ransom, 1996; Diarra et al., 2001), whereas the $K_d$ of CoroNa was considerably higher. $K_d$ values determined for Sodium Green are in the range of 21–30 mM (Despa et al., 2000, Invitrogen). Thus, CoroNa might be better suited than both SBFI and Sodium Green to accurately resolve very large $Na^+$ transients or $Na^+$ changes at high background $Na^+$ concentration.

The calibrations demonstrated that both SBFI and CoroNa reliably report $[Na^+]_i$ changes and are suited for the measurement of $[Na^+]_i$ alterations that are expected to occur during physiological conditions. However, both calibration experiments and local AMPA applications showed that CoroNa exhibits signif-

icantly smaller changes in the fluorescence emission ($\Delta F/F$) with changes in $[Na^+]_i$ between 0 and about 50 mM $[Na^+]_i$ than SBFI.

The molecular weight of CoroNa is roughly half that of SBFI (586 g/mol versus 907 g/mol), probably resulting in a faster intracellular diffusion. However, CoroNa and SBFI, despite their difference in molecular weight and $K_d$ values, reported similar amplitudes and kinetics for AMPA-induced $[Na^+]_i$ signals. A likely reason for this observation is that the dye concentration (0.5 mM) was small as compared to the baseline $[Na^+]_i$ (presumably 4 mM; intracellular pipette solution). Therefore, neither dye apparently distorted the $[Na^+]_i$ signals significantly due to their buffering of $Na^+$.

Taken together, we conclude that the use of SBFI is clearly advantageous when performing experiments with conventional epifluorescence systems. First, only SBFI is suitable for AM–ester loading and single intracellular dye injection. Second, SBFI allows ratiometric imaging, which renders measurements independent of the dye concentration. Finally, SBFIs smaller $K_d$ and larger $\Delta F/F$ values below 50 mM $Na^+$ result in a better resolution of small $[Na^+]_i$ transients within this range. Still, CoroNa might be the dye of choice for analyzing very large $Na^+$ elevations such as those reported during pathological conditions (e.g. Longuemare et al., 1999).

### 4.2. Confocal $Na^+$ imaging with CoroNa and fields of application

High-resolution $[Na^+]_i$ measurements in small cellular compartments in the intact, light-scattering tissue can be performed using two-photon imaging with SBFI (Rose et al., 1999; Rose and Konnerth, 2001). Although two-photon imaging is a technique that is more and more widely used, it is still a quite expensive and complex method not available to many laboratories. The present study shows that, in contrast to SBFI, CoroNa is suited for high-resolution confocal microscopy in dendrites in the intact tissue when combined with whole-cell patch-clamp recordings. Therefore, it represents an alternative to two-photon imaging for $[Na^+]_i$ measurements. Our confocal $[Na^+]_i$ measurements revealed that significant $[Na^+]_i$ accumulations occur in fine dendrites following local iontophoresis of glutamate, similar to the large $[Na^+]_i$ transients reported following synaptic stimulation (Rose and Konnerth, 2001).

Despite the apparent disadvantages of CoroNa as compared to SBFI, confocal imaging of $[Na^+]_i$ transients with CoroNa may prove to be a useful tool in the investigation of physiological properties of neurons and glial cells in fine cellular processes. Open questions that can be addressed using this technique are the consequences of activity-induced $[Na^+]_i$ transients in dendrites, spines and axons for synaptic transmission and signal propagation. Notably, $Na^+$ imaging allows to monitor excitatory synaptic activity without directly influencing $Ca^{2+}$-dependent processes, which is always a concern when $Ca^{2+}$-sensitive dyes are introduced into the cells (Regehr and Tank, 1992). Confocal $[Na^+]_i$ imaging will also allow to study the role of $Na^+$-dependent pumps and transporters in neuronal and glial signaling in fine processes and to take a detailed look on $[Na^+]_i$ transients in fine processes during pathological conditions to elucidate the mechanisms that cause cellular damage.

## Acknowledgments

We thank Arthur Konnerth, Knut Holthoff and Peter Grafe for valuable comments. This study was supported by a Heisenberg-Fellowship to C.R.R. and by the Deutsche Forschungsgemeinschaft.

## References

Bouron A, Reuter H. A role of intracellular $Na^+$ in the regulation of synaptic transmission and the turnover of the vesicular pool in cultured hippocampal cells. Neuron 1996;17:969–78.

Callaway JC, Ross WN. Spatial distribution of synaptically activated sodium concentration changes in cerebellar Purkinje neurons. J Neurophys 1997;77:145–52.

Chatton JY, Marquet P, Magistretti PJ. A quantitative analysis of L-glutamate-regulated $Na^+$ dynamics in mouse cortical astrocytes: implications for cellular bioenergetics. Eur J Neurosci 2000;12:3843–53.

Chen W-H, Chu K-C, Wu S-J, Wu J-C, Shui H-A, Wu M-L. Early metabolic inhibition-induced intracellular sodium and calcium increase in rat cerebellar granule cells. J Physiol 1999;515:133–46.

Chinopoulos C, Tretter L, Rozsa A, Adan-Vizi V. Exacerbated responses to oxidative stress by an $Na^+$ load in isolated nerve terminals: the role of ATP depletion and rise of $[Ca^{2+}]_i$. J Neurosci 2000;20:2094–103.

Despa S, Vecer J, Steels P, Ameloot M. Fluorescence lifetime microscopy of the $Na^+$ indicator sodium Green in HeLa cells. Anal Biochem 2000;281:159–75.

Diarra A, Sheldon C, Church J. In situ calibration and [H+] sensitivity of the fluorescent Na+ indicator SBFI. Am J Physiol Cell Physiol 2001;280:C1623–33.

Donoso P, Mill J, O'Neill S, Eisner D. Fluorescence measurements of cytoplasmic and mitochondrial sodium concentration in rat vertricular myocytes. J Physiol 1992;448:493–509.

Edwards FA, Konnerth ABS, Takahashi T. A thin slice preparation for patch clamp recordings from neurones of the mammalian central nervous system. Pfluegers Arch (Eur J Physiol) 1989;414:600–12.

Friedman J, Haddad G. Anoxia induces an increase in intracellular sodium in rat central neurons in vitro. Brain Res 1994;663:329–34.

Grynkiewicz G, Poenie M, Tsien R. A new generation of $Ca^{2+}$ indicators with greatly improved fluorescence properties. J Biol Chem 1985;260:3440–50.

Harootunian A, Kao JP, Eckert BK, Tsien RY. Fluorescence ratio imaging of cytosolic free $Na^+$ in individual fibroblasts and lymphocytes. J Biol Chem 1989;264:19458–67.

Hodgkin A, Huxley A. A quantitative description of membrane current and its application to conduction and excitation in nerve. J Physiol 1952;117:500–44.

Jaffe DB, Johnston D, Lasser-Ross N, Lisman JE, Miyakawa H, Ross WN. The spread of $Na^+$ spikes determines the pattern of dendritic $Ca^{2+}$ entry into hippocampal neurons. Nature 1992;357:244–6.

Knöpfel T, Guatteo G, Mercuri N. Hyperpolarization induces a rise in intracellular sodium concentration in dopamine cells of the substantia nigra pars compacta. Eur J Neurosci 1998;10:1926–9.

Knöpfel T, Anchisi D, Alojado ME, Tempia F, Strata P. Elevation of intradendritic sodium concentration mediated by synaptic activation of metabotropic glutamate receptors in cerebellar Purkinje cells. Eur J Neurosci 2000;12:2199–204.

Lasser-Ross N, Ross WN. Imaging voltage and synaptically activated sodium transients in cerebellar Purkinje cells. Proc R Soc Lond B 1992;247:35–9.

Linden DJ, Smeyne M, Connor JA. Induction of cerebellar long-term depression in culture requires postsynaptic action of sodium ions. Neuron 1993;11:1093–100.

Longuemare MC, Rose CR, Farrell K, Ransom BR, Waxman SG, Swanson RA. $K^+$-induced reversal of astrocyte glutamate uptake is limited by compensatory changes in intracellular $Na^+$. Neuroscience 1999;93:285–92.

Magistretti PJ, Chatton JY. Relationship between L-glutamate-regulated intracellular Na+ dynamics and ATP hydrolysis in astrocytes. J Neural Transm 2005;112:77–85.

Maragakis NJ, Rothstein JD. Glutamate transporters: animal models to neurologic disease. Neurobiol Dis 2004;15:461–73.

Minta A, Tsien RY. Fluorescent indicators for cytosolic sodium. J Biol Chem 1989;264:19449–57.

Miyakawa H, Ross WN, Jaffe D, Callaway JC, Lasser-Ross N, Lisman JE, et al. Synaptically activated increases in $Ca^{2+}$ concentration in hippocampal CA1 pyramidal cells are primarily due to voltage-gated $Ca^{2+}$ channels. Neuron 1992;9:1163–73.

Nikolaeva MA, Mukherjee B, Stys PK. $Na^+$-dependent sources of intra-axonal $Ca^{2+}$ release in rat optic nerve during in vitro chemical ischemia. J Neurosci 2005;25:9960–7.

Peterlin ZA, Kozloski J, Mao B-Q, Tsiola A, Yuste R. Optical probing of neuronal circuits with calcium indicators. Proc Natl Acad Sci USA 2000;97:3619–24.

Pinelis V, Segal M, Grennberger V, Khodorov B. Changes in cytosolic sodium caused by a toxic glutamate treatment of cultured hippocampal neurons. Biochem Mol Biol Int 1994;32:475–82.

Pisani A, Calabresi P, Tozzi A, Bernardi G, Knöpfel T. Early sodium elevations induced by combined oxygen and glucose deprivation in pyramidal cortical neurons. Eur J Neurosci 1998;10:3572–4.

Regehr WG, Tank DW. Calcium concentration dynamics produced by synaptic activation of CA1 hippocampal pyramidal cells. J Neurosci 1992;12:4202–5223.

Rishal I, Keren-Raifman T, Yakubovich D, Ivanina T, Dessauer CW, Slepak VZ, et al. $Na^+$ promotes the dissociation between Galpha GDP and Gbeta gamma, activating G protein-gated $K^+$ channels. J Biol Chem 2003;278:3840–5.

Rose CR. High resolution $Na^+$ imaging in dendrites and spines. Pfluegers Arch (Eur J Physiol) 2003;446:317–21.

Rose CR. Intracellular $Na^+$ regulation in neurons and glia: functional implications. Neuroscientist 1997;3:85–8.

Rose CR, Konnerth A. NMDA receptor-mediated $Na^+$ signals in spines and dendrites. J Neurosci 2001;21:4207–14.

Rose CR, Kovalchuk Y, Eilers J, Konnerth A. Two-photon $Na^+$ imaging in spines and fine dendrites of central neurons. Pfluegers Arch (Eur J Physiol) 1999;439:201–7.

Rose CR, Ransom BR. Intracellular $Na^+$ homeostasis in cultured rat hippocampal astrocytes. J Physiol 1996;491:291–305.

Rose CR, Ransom BR. Gap junctions equalize intracellular $Na^+$ concentration in astrocytes. Glia 1997a;20:299–307.

Rose CR, Ransom BR. Regulation of intracellular sodium in cultured rat hippocampal neurones. J Physiol 1997b;499:573–87.

Ross W, Miyakawa H, Lev-Ram V, Lasser-Ross N, Lisman J, Jaffe D, et al. Dendritic excitability in CNS neurons: insights from dynamic calcium and sodium imaging in single cells. Jpn J Physiol 1993;43:S83–99.

Senatorov VV, Stys PK, Hu B. Regulation of $Na^+$, $K^+$-ATPase by persistent sodium accumulation in adult rat thalamic neurones. J Physiol 2000;525(Pt 2):343–53.

Sheldon C, Cheng YM, Church J. Concurrent measurements of the free cytosolic concentrations of H(+) and Na(+) ions with fluorescent indicators. Pflugers Arch 2004a.

Sheldon C, Diarra A, Cheng YM, Church J. Sodium influx pathways during and after anoxia in rat hippocampal neurons. J Neurosci 2004b;24:11057–69.

Stosiek C, Garaschuk O, Holthoff K, Konnerth A. In vivo two-photon calcium imaging of neuronal networks. PNAS 2003;100:7319–24.

Tsubokawa H, Miura M, Kano M. Elevation of intracellular Na+ induced by hyperpolarization at the dendrites of pyramidal neurones of mouse hippocampus. J Physiol 1999;517:135–42.

Winslow JL, Cooper RL, Atwood HL. Intracellular ionic concentration by calibration from fluorescence indicator emission spectra, its relationship to the $K$(d), $F$(min), $F$(max) formula, and use with Na-Green for presynaptic sodium. J Neurosci Methods 2002;118:163–75.

Yu X-M, Salter MW. Gain control of NMDA-receptor currents by intracellular sodium. Nature 1998;396:469–74.

Die hier vorgelegte Dissertation habe ich eigenständig und ohne unerlaubte Hilfe angefertigt. Die Dissertation wurde in der vorgelegten oder in ähnlicher Form noch bei keiner anderen Institution eingereicht. Ich habe bisher keine erfolglosen Promotionsversuche unternommen.

Düsseldorf, den 25.09.2007

(Silke D. Meier)